Modeling Climate Change Effects on Chesapeake Water Quality Standards and Development of 2025 Planning Targets to Address Climate Change

Chesapeake Bay Program
Science, Restoration, Partnership

Chesapeake Bay Program
Science, Restoration, Partnership

About the CBP Modeling Workgroup

The Modeling Workgroup has a responsibility to the Chesapeake Bay Program Partnership to provide state-of-the-art decision-support modeling tools that are built through community and participatory principles. The responsible planning and management of resources to provide the best available decision-support modeling tools requires the Modeling Workgroup members and participants to adhere to the core values of:

- **Integration** - Integration of most recent science and knowledge in the atmosphere, watershed, and coastal waters to support ecosystem modeling for restoration decision making.
- **Innovation** - Embracing creativity and encouraging improvement in the development and support of transparent and robust modeling tools.
- **Independence** – Making modeling decisions on the basis of best available evidence and using the most appropriate methods to produce, run, and interpret models, independent of policy considerations.
- **Inclusiveness** - Commitment to an open and transparent process and the engagement of relevant partners, that results in strengthening the Partnership's decision-making tools.

To find out more about the CBP Modeling Workgroup please visit the website:
https://www.chesapeakebay.net/who/group/modeling_team

Publication Date: January 2021

CBPO Publication Number: 328-21

Suggested Citation:
Shenk, G. W., Bhatt, G., Tian, R., Cerco, C.F., Bertani, I., Linker, L.C., 2021. Modeling Climate Change Effects on Chesapeake Water Quality Standards and Development of 2025 Planning Targets to Address Climate Change. CBPO Publication Number 328-21, Annapolis, MD. 145 pp.

Cover photo credit: Thomas Point Shoal Light as seen on November 20, 2015, the 140th anniversary of its establishment. Photo by Will Parson/Chesapeake Bay Program.
https://www.chesapeakebay.net/discover/photos

Contents

1   Introduction

This report is the result of the work guided by the Modeling Workgroup in 2019. The Modeling Workgroup members approved certain sections of this documentation at the July 16-17, 2019 meeting with Virginia standing aside from all decisions. The Modeling Workgroup members unanimously approved the remaining sections of this document at the October 8-9, 2019 meeting. The July documentation was emailed to the Modeling Workgroup and Climate Resiliency Workgroup on June 28th. The October documentation was emailed to the same groups on September 24th.

Table 1-1: Approval status of documentation sections

Section	Topic	July Approval	October Approval	November Approval	Does Not Require Approval
1	Introduction				X
2	Meteorology and precipitation	X			
3.1	Atmospheric deposition		X		
3.2	Land use	X			
3.3	Agricultural inputs	X			
3.4	Direct loads	X			
4.1	CO2 concentration response	X			
4.2	Hydrology simulation	X			
4.3	Sediment loss simulation	X			
4.4	Nitrogen loss sensitivity		X		
4.5	Phosphorus loss sensitivity		X		
4.6	BMP effectiveness		X		
4.7.1	Nitrogen speciation		X		
4.7.2	Groundwater lag	X			
4.7.3	Delivery effects		X		
4.8	Watershed simulation results			X	
5.1.1	Wetlands losses and gains		X		
5.1.2	Wind effects	X			
5.1.3	Sea level rise	X			
5.1.4	Ocean boundary	X			
5.1.5	Tidal flooding loads		X		
5.2	Growth curve modification	X			
5.3	Validation of model response		X		
5.4	Estuarine simulation results			X	
6	Management effort adjustment				

1.1   Partnership Decision Context

The EPA and the Chesapeake Bay Program (CBP) partnership put in place the Chesapeake Bay TMDL in 2010, setting allocation limits on nitrogen, phosphorus, and sediment from each jurisdiction and major basin (U.S. EPA 2010). The modeling for the TMDL was performed using a hydrologic averaging period, 1991-2000, that was judged to represent long-term average

precipitation, temperature, and meteorology. The critical period for meeting dissolved oxygen water quality standards is a wetter period within that span, 1993-1995, representing a three-year period with a 10-year recurrence interval.

The averaging period and critical period represent long-term climate norms that will no longer be representative of average conditions or a 10-year recurrence interval condition. The strategy for incorporating estimated climate change as of 2025 is to examine the changes expected between 1995 and 2025. The 30-year change in climate is to be applied to the CBP modeling data sets and the environmental change assessed. For information and planning purposes, particularly to aid in developing a robust 2025 response to climate change risk, the partnership will also examine estimated future climate risk expected by 2035, 2045, and 2055. Ultimately the process of assessing future climate risk to the Chesapeake watershed and tidal waters will be an iterative process of reassessment over periods of about a decade reflecting changes in the science, analysis tools, and climate.

The CBP partnership's 2017 Midpoint Assessment process resulted in updates to nutrient and sediment planning targets consistent with the 2010 Chesapeake Bay TMDL allocations. The new planning targets were based on updates to the CBP's suite of models, accounting for the influence of the changing conditions in the Conowingo Reservoir, and consideration of future population and land use change. Consideration of the effects of climate change on the CBP partnership's ability to reach water quality goals in the Bay was part of the 2017 Midpoint Assessment process as well, however, the partnership decided to delay decisions until additional modeling could be completed.

The CBP's Principals' Staff Committee (PSC) met in March 2018 and agreed that the jurisdictions' Phase III Watershed Implementation Plans (WIPs) would address climate change narratively and numerically. Specifically, the WIPs would include a narrative strategy describing the jurisdictions' current action plans and strategies to address climate change. The partnership further committed to adopting numerical climate change targets by 2021 using the CBP's modeling tools. Initial estimates were that climate change effects on dissolved oxygen standards were equivalent to an increase of 9 million pounds of nitrogen and 0.5 million pounds of phosphorus. Jurisdictions may include numerical adjustments to account for climate change within their current WIPs if they choose.

The PSC agreed to refine the climate modeling and assessment framework based on improved understanding of the science of the impacts of climate change. Research needs will be identified, particularly with regard to a better understanding of BMP responses. New, enhanced, and resilient BMPs that better address climate change conditions such as increased storm intensity are a focus point.

In March 2021, the Partnership will consider results of updated methods, techniques, and studies and develop an estimate of pollutant load changes (nitrogen, phosphorus, and sediment) due to 2025 climate change conditions.   In September 2021 jurisdictions will account for additional nutrient and sediment pollutant loads due to 2025 climate change conditions in a Phase III WIP addendum and/or 2-year milestones beginning in 2022.   Starting with the 2022-2023 milestones, the Partnership will determine how climate change will impact the BMPs included in the WIPs

and address these vulnerabilities in the two-year milestones.   Figure 1-1 shows a simplified timeline of the climate analysis.

2018	2019	2020	2021
STAC Workshop

Partnership Decisions on schedule | The Modeling WG and Climate Resiliency WQ direct the Modeling team to develop climate change assessment for TMDL | Technical Review of Models | Climate change considerations will be implemented into the 2022-2023 milestones. |
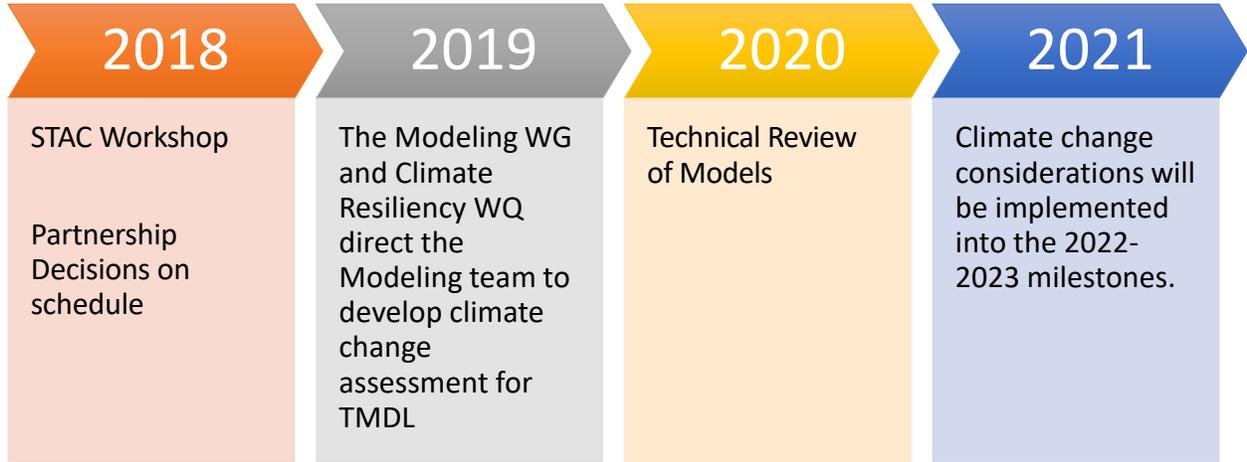
Figure 1-1: Climate assessment timeline

Oversight of the climate change assessment development process will be handled by groups within the CBP management structure. The management questions involving climate change will be articulated by the PSC, the Management Board (MB), and the Water Quality Goal Implementation Team (WQGIT). Technical direction for the climate change analysis will be handled by the Modeling Workgroup (MWG) and Climate Resiliency Workgroup (CRWG) of Scientific, Technical Assessment & Reporting (STAR). The MWG and CRWG will direct the CBPO's modeling team on technical issues of input data set and modeling response development with the advice of the Scientific and Technical Advisory Committee (STAC), and the direction the MB and WQGIT.

1.2   Modeling Framework

The CBP used a linked system of airshed, land use, watershed, and estuarine models for the 2010 TMDL (U.S. EPA 2010), the 2011 Phase II WIPs, and the 2017 Midpoint Assessment and associated Phase III WIPs. The CBP has used similar systems dating back to decisions in the 1980s and 1990s (Linker et al, 2002). Figure 1-2 shows a schematic of the system, which is designed to address questions of how Chesapeake Bay water quality will respond to changes in management actions. The CBP Land Use Change Model predicts changes in land use, sewerage, and septic systems given changes in land use policy. The Airshed Model, a combination of a regression model of National Atmospheric Deposition Program (NADP) data and a national application of the Community Multiscale Air Quality (CMAQ) Model, predicts changes in deposition of inorganic nitrogen due to changes in emissions. The Watershed Model combines the output of these models with other data sources, such as the US Census of Agriculture, and predicts the loads of nitrogen, phosphorus, and sediment that result from the given inputs. The estuarine Water Quality and Sediment Transport Model (WQSTM) predicts changes in Bay water quality due to the changes in input loads provided by the Watershed Model.
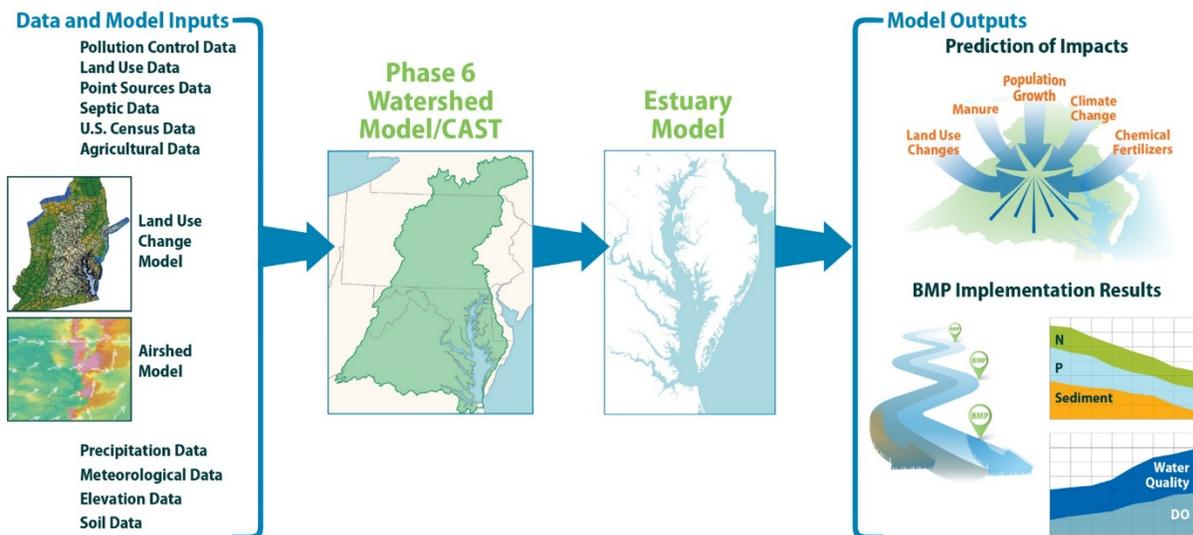
Figure 1-2: the Chesapeake Bay Program partnership's modeling system

The Phase 6 Watershed Model consists of two parallel models: a time-averaged model and a dynamic model, which is constrained to match the time-averaged model over the long term. The time-averaged model, known as the Chesapeake Assessment Scenario Tool (CAST) (Chesapeake Bay Program 2017) is used as the primary model for decision making. Stakeholders and other users can access CAST through a web interface at http://cast.chesapeakebay.net/. The dynamic model is used in calibration of the Phase 6 system, to translate CAST scenarios into hourly loads of nutrients and sediment for the estuarine model, and to perform research. For the climate change analysis, changes will be made to both CAST and the dynamic model. The dynamic model will run with projected precipitation and meteorology input data to predict changes in hydrology and sediment. These changes will be used in CAST, along with additional investigation using multiple lines of evidence, to predict changes in nitrogen and phosphorus loads delivered to large rivers. Finally, the modeling team will use the dynamic model to temporally disaggregate the predictions of CAST, simulate the effects in large rivers, and pass loads to the estuarine model. Further description of the Phase 6 Watershed Model is available on the CAST documentation page (http://cast.chesapeakebay.net/Documentation/ModelDocumentation). The relationship between CAST and the dynamic model is described in Section 1. The dynamic model is described in Section 10.

The modeling system used for all analyses December 2017 through July 2018 that resulted in the Phase III planning targets is in large part the same system used for the climate assessment. Some significant changes were made to accommodate climate-related analysis as detailed in this document.[1] Other minor changes such as the inclusion of new land use and BMP information for future scenarios may also be included per partnership decisions unrelated to climate change. Due to the changes made to the modeling system, the scenarios are not directly comparable to

---

[1] Other minor changes such as the inclusion of new land use and BMP information for future scenarios may also be included per partnership decisions unrelated to climate change.

scenarios that were run during the 2017 Midpoint Assessment. The climate change analysis will consist of new scenarios that will be compared to estimate the overall effect of climate change on water quality standards (U.S. EPA, 2010).

Models by their nature are imperfect representations of reality and are based on the best available data, knowledge, and computational power available at the time of their development and application. The analysis for the 2021 climate decisions will represent the current best estimate. It is anticipated that the CBP will reassess the TMDL progress relative to climate change and other factors in 2025 and later years in an iterative process.

1.3   Climate Effects Simulated
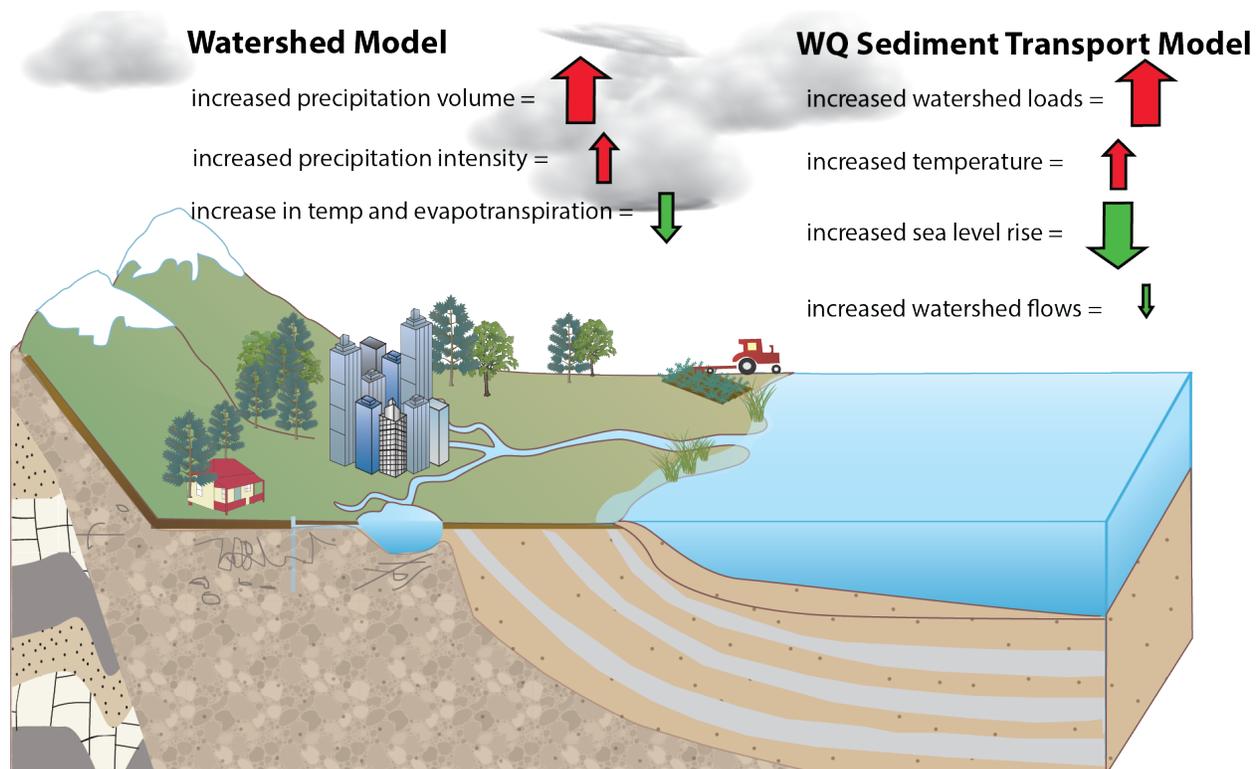
Figure 1-3: Simplified conceptual model of climate effects on dissolved oxygen water quality standards. Red arrows denote an increase in violation of standards. Green arrows denote a decrease.

Figure 1-3 illustrates the main effects of climate change on the dissolved oxygen in tidal waters. Increased precipitation volume is expected to increase the runoff of nitrogen, phosphorus, and sediment, which in isolation would lead to an increase in non-attainment of dissolved oxygen water quality standards. This is indicated in the figure by an upward facing red arrow. An increase in evapotranspiration caused by an increase in temperature will lead to a decrease in runoff, which in turn will lead to a decrease in nutrients and sediment and a decrease in non-attainment of dissolved oxygen standards, indicated by a downward facing green arrow. Increased precipitation intensity in isolation would cause an increase in sediment and particulate nutrient runoff leading to an increase in dissolved oxygen non-attainment. Increased temperatures in the Bay lowers the solubility of oxygen in water and increases respiration which has a negative effect on attainment. Sea level rise and increased watershed flows, in isolation, increase the circulation in the Bay, leading to improved attainment of standards.

10
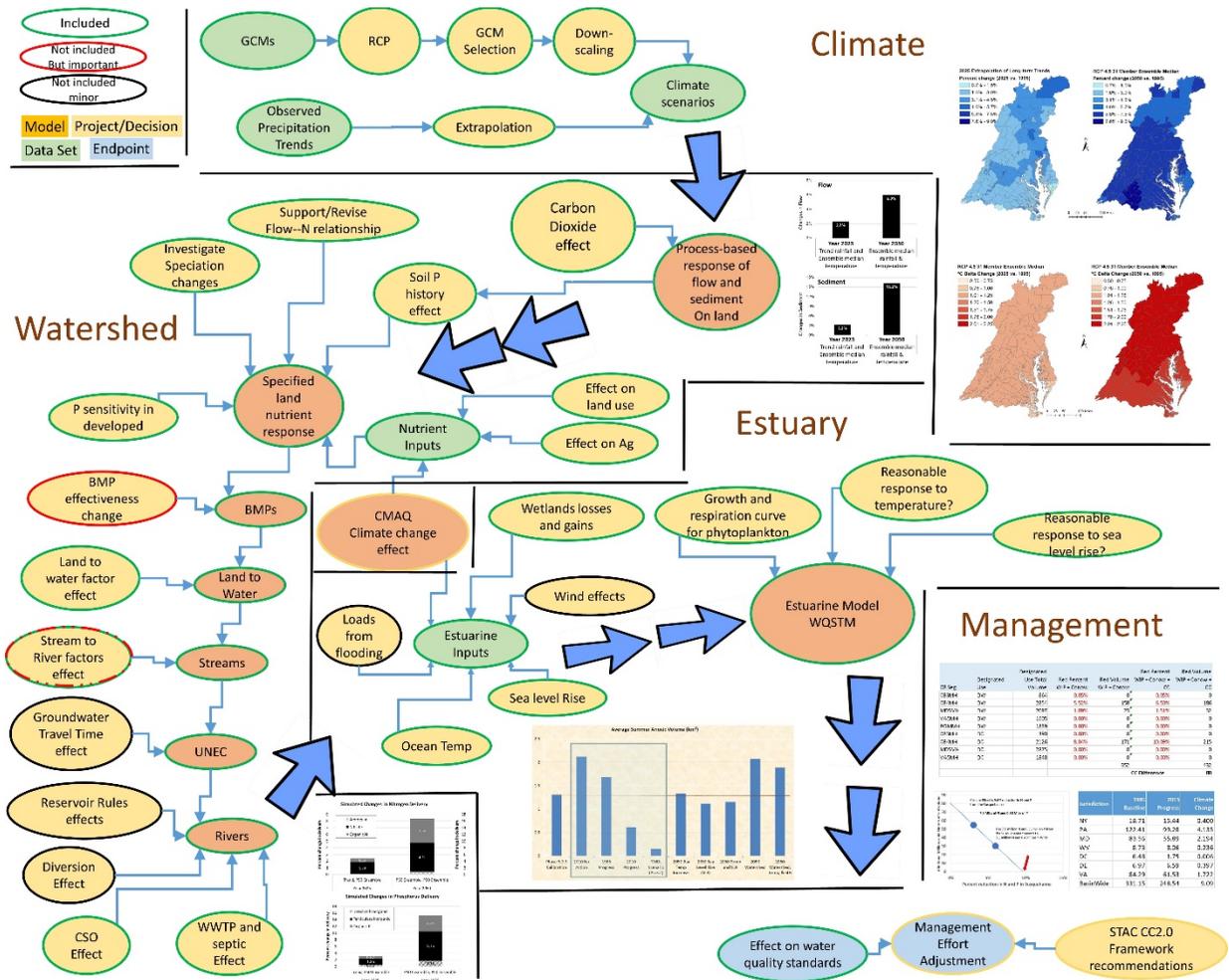
Figure 1-4: Detailed conceptual model of processes affecting dissolved oxygen water quality standards, indicating inclusion or non-inclusion in the CBP climate assessment

Figure 1-4 is a detailed conceptual model of the processes considered in the CBP climate assessment. The above figure was used to guide the CBP in determining the effects to directly include in the analysis. Climate change affects the majority of the inputs and processes in the modeling system. The CBP considered a wide array of effects and made decisions to include those processes which were both well understood and judged to have a significant effect on water quality standards. Some processes left out of the analysis could be important but are without sufficient data and understanding to include them.

For the assessment of climate change impacts in the Chesapeake watershed, the primary variables considered were precipitation volume, precipitation intensity, temperature, and evapotranspiration. Estimates of the influence of sea level rise, increased ocean inflow, air temperature, and tidal wetland loss were incorporated into the Water Quality and Sediment Transport Model (WQSTM) of the tidal Bay and are documented there (Cerco and Noel 2019).

1.4   Input from the CBP's Scientific and Technical Advisory Committee

The CBP's Scientific and Technical Advisory Committee (STAC) has conducted several assessments of climate science and has recommended processes for integrating consideration of climate change into the Bay Program's management framework. STAC proactively authored a report on

the likely effects of climate change (Pyke et al. 2008). STAC encouraged the CBP to consider the effects of sea level rise, temperature, and increasing variability of salinity and hydrology on hypoxia and on living resources including algal, submerged aquatic vegetation, and fish communities. STAC asked the CBP to understand the implications of climate change for important management decisions, update monitoring systems, and take action to mitigate the effects of climate change.

A 2011 STAC workshop on climate change (Pyke 2012; Pyke et al. 2012) produced a recommendation that climate change be embedded within the CBP decision-making structure. The response from the CBP (DiPasquale 2014) indicated that the CBP agreed and that a new climate resiliency position was being created and that the concept was consistent with the 2009 executive order (Office of the President, 2009) and the 2014 Bay Agreement (Chesapeake Executive Council 2014). The 2014 agreement explicitly called for climate change considerations to be part of all CBP goals and outcomes. STAC recommended focusing on specific problems, identified through assessments of vulnerability, and developing the technical capacity to address these issues. The inclusion of climate change in the 2017 Midpoint Assessment follows these principles. The recommendations were communicated to the CBP's Executive Council as well (STAC 2011).

A 2016 STAC workshop on climate projections assessed available climate data for use in the CBP decision process (Johnson et al. 2016; Wainger 2016). STAC recommended that the assessment should be as comprehensive as possible. Specific recommendations included the use of historical precipitation trends for 2025 while carefully considering evapotranspiration. For assessments after 2017, STAC recommended a 2050 time frame using multiple models to estimate response. The recommendations and guidance provided by the Chesapeake Bay Program's Climate Resiliency Workgroup (CRWG) (CBP 2016) rely heavily on the 2016 STAC workshop. A follow-up 2017 STAC workshop, not published as of this writing, generated specific near-term and long-term recommendations for watershed and estuarine modeling, and methods of model application.

2 Estimates of Changes in Meteorology and Precipitation

2.1 Climate Change Scenarios

Climate change assessments for the years 2025 and 2050 rely on robust estimates of changes in precipitation and temperature, and the CBP has utilized a combination of trend analysis and global climate models (GCMs) for these projections. The CBP's methods for developing the climate projections are based on recommendations provided by the 2016 STAC workshop *The Development of Climate Projections for Use in Chesapeake Bay Program Assessments* (Johnson et al. 2016). The recommendation of STAC was to use long-term observed precipitation trends instead of climate model projections to assess expected changes in precipitation for the year 2025, as the uncertainty of the models introduced more variability for this near future than extrapolation of the trend. For 2050 precipitation estimates, STAC recommended climate models used for assessing anticipated changes in precipitation that were based on the Coupled Model Intercomparison Project Phase 5 (CMIP5) set of Global Climate Models (GCMs) as outlined in the Intergovernmental Panel on Climate Change's Fifth Assessment Report (IPCC AR5, 2013). It was also recommended that these models be employed in the assessment of expected temperature change for both 2025 and 2050, as the model projections of temperature change are much less variable for both the short and long-term projections. Decisions by the Chesapeake Bay Program's Modeling Workgroup on 4/2/2019 affirmed the recommendations of the STAC workshop (Johnson et al, 2016).

Subsequent to the STAC workshop, the years 2025, 2035, 2045, and 2055 were selected for the climate change impacts assessment by the Modeling Workgroup rather than 2025 and 2050. The Phase 6 Watershed Model was used to assess expected changes in 2025 precipitation based on historical observed trends within the watershed. Climate models were used precipitation in 2050 and beyond, while 2035 and 2045 were interpolated between the two approaches. Expected changes in 2025, 2035, 2045, and 2055 temperatures were extracted from the models

The GCM projections of rainfall and temperature changes used in the assessment were based on the Representative Concentration Pathway (RCP) 4.5. Forcing for the GCMs were determined by the RCPs, which are each characterized by potential future socio-economic and natural conditions. The RCPs are defined according to the additional radiative forcing generated by the year 2100 measured in watts per square meter (W/m^2); for example, RCP 4.5 projects an increase in radiative forcing of 4.5 W/m^2. Additional analyses based upon RCP 2.6 and RCP 8.5 could be used to further develop the assessment to include a range of potential future climates. However, due to computational and analysis constraints only a limited number of key climate scenarios were simulated with the linked watershed and estuarine models to quantify the range of climate change impacts.

2.1.1 Long-term Observed Trends in Precipitation

The STAC Workshop Report, "The Development of Climate Projections for Use in the Chesapeake Bay Program Assessments" (Johnson et al. 2016), recommends using long-term observations to estimate the 30-year (1995 - 2025) change in precipitation volume that can be attributed to climate change. Precipitation trends for model land segments (counties) were developed by analyzing Parameter-elevation Relationship on Independent Slope Model (PRISM, Daly et al.

2008) rainfall data. A linear trend analysis was conducted with annual PRISM rainfall data as recommended by Jason Lynch, EPA, and Karen Rice, USGS. The PRISM dataset is a reanalysis product that uses point data measurements at rain gauges and incorporates a conceptual framework to address spatial variably in rainfall due to orographic and other processes. The long-term PRISM dataset (1895-1980) is modeled at 30 arc second (approx. 800 m) grid cell resolution but then upscaled to provide monthly total rainfall at 2.5 arc minute (approx. 4-km) grid cell resolution for the conterminous U.S. The annual PRISM dataset for the years 1927 to 2014 (i.e. 88 years) were used in the linear regression trend analysis. The selection of the 88-year period was made because of easy accessibility of the dataset. For the analysis, gridded PRISM data were first spatially aggregated to each Phase 6 land segment, and then for each segment, a linear trend line was fitted to the annual rainfall data.

Figure 2-1 shows the regression analysis for two counties, where the linear slopes indicate 2.67% and 3.14% increases in average annual rainfall volumes as compared to the reference 1991-2000 conditions. Since regression analysis was done for annual rainfall volumes, the resulting linear slope does not provide information on changes at monthly or seasonal time scale. Therefore, the percent change in average annual rainfall was used for every month. Figure 2-15 shows the increase in annual rainfall over the 30-year period between 1995 and 2025 estimated using the trends for the land segments in the Chesapeake Bay watershed.

CENTRE, PA	
Slope (mm/yr)	0.9367
2025 Projection mm (%)	28.10 (+2.67%)

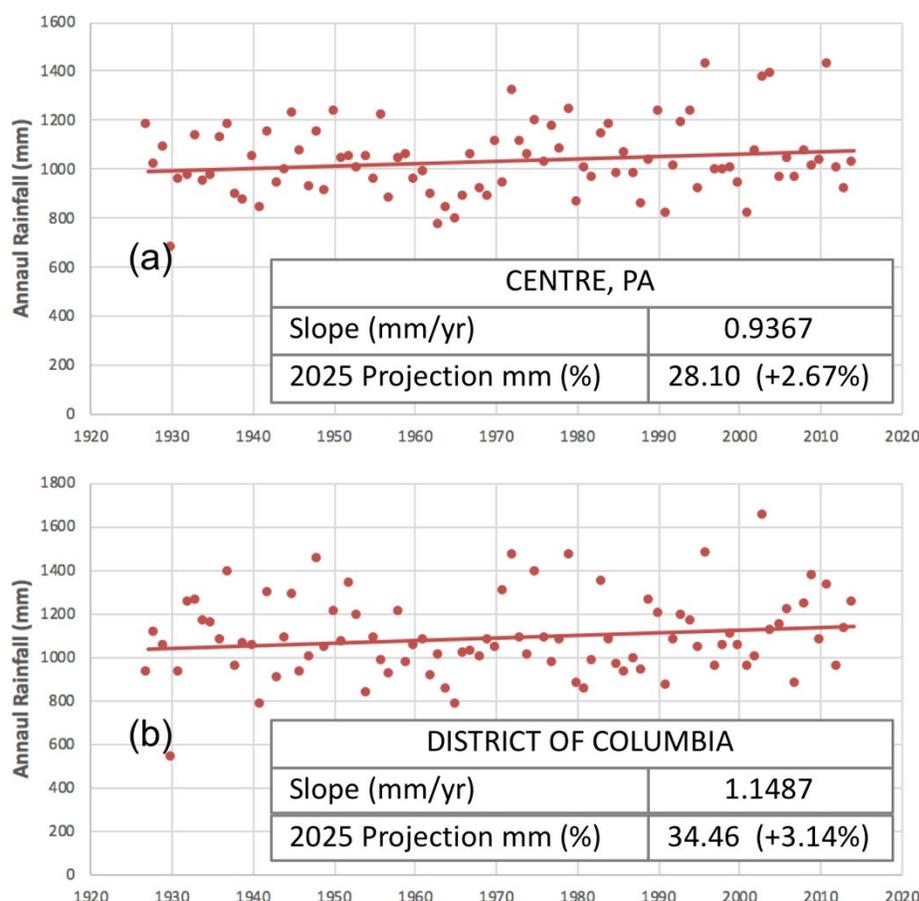| DISTRICT OF COLUMBIA	
Slope (mm/yr)	1.1487
2025 Projection mm (%)	34.46 (+3.14%)

Figure 2-1: Annual rainfall volumes for the 88-year period linear regression lines are shown in red for the two land segments (counties) – (a) Centre County in Pennsylvania and (b) District of Columbia. The values for the slope of the regression lines, and the corresponding 30-year projections in the rainfall volume (1995 to 2025) are also shown.

Trend information derived from a short-term (e.g. 30 years) rainfall dataset may be influenced by decadal-scale variations in climate as well as weather anomalies. The influence of such variations can be more easily detected and reduced using longer-term data, however, it was not clear if the use of an 88-year record would be sufficient for overcoming such decadal-scale variabilities. The CBPO modeling team conducted an analysis of long-term rainfall data to investigate this. Different lengths of historical observations were used for estimating the linear trend and the corresponding percent change in annual rainfall over a 30-year period. A total of 59 sets ranging between most recent 30 years to 88 years of historical observations were analyzed. The goal was to test the influence of number of years on the linear trend estimate, and on how the decadal and natural variabilities impacted the resulting trend. A set of same color dots in Figure 2-2 shows the estimated percent change in annual rainfall volume for 30 years based on linear trends calculated from those 59 sets for a land segment (or county). The analysis was repeated for several counties (Figure 2-2). It was found that, although not perfect, the 88-year record came pretty close to overcoming cyclical climatic variabilities as the estimated percent change became more stable. It is noted that for a given county the estimated change varied quite a bit when data for 30 to 60 years were selected but became stable for greater numbers of years, as shown in Figure 2-2.
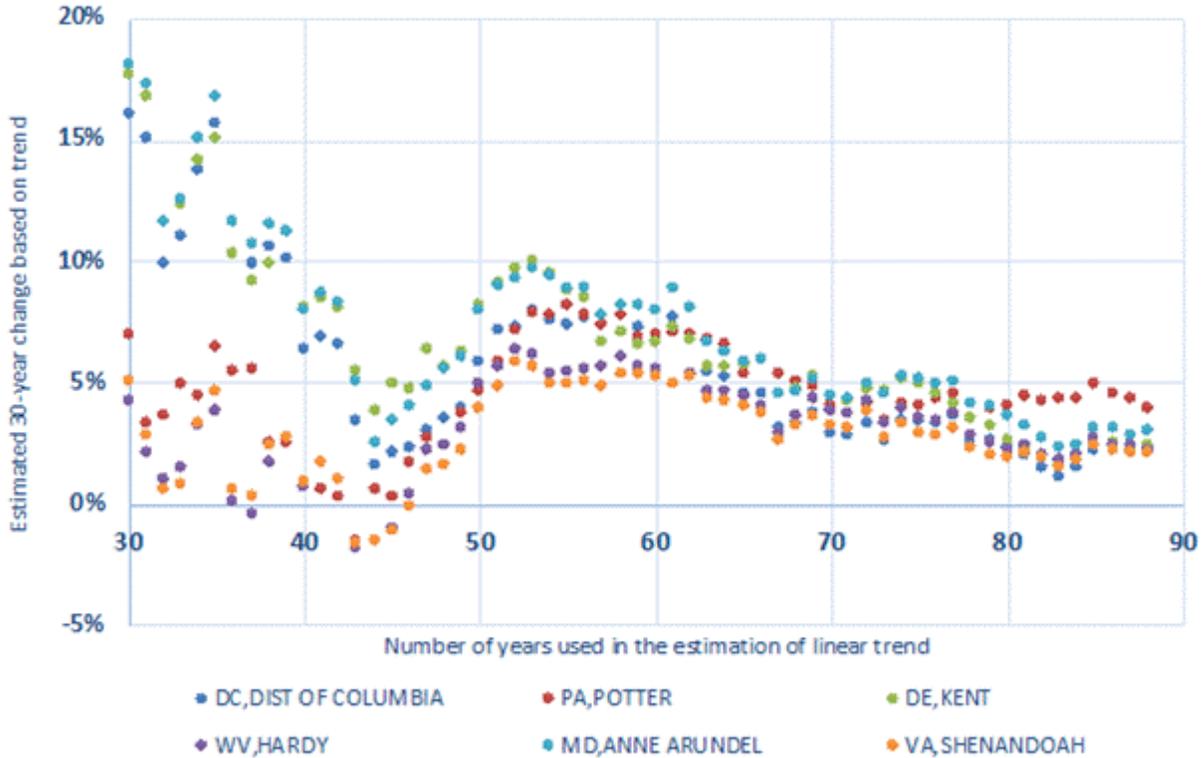
Figure 2-2: Estimated change in rainfall based on the extrapolation of linear trends are shown. For the estimation of linear trends historical observations ranging between last 30 to 88 years used. It was shown that a level of consistency was achieved after more than 80 years of observations were used in the estimation of linear trend.

2.1.2 General Circulation Models and Representative Concentration Pathways

General circulation models (GCMs) included in the most recently completed Coupled Model Intercomparison Project Phase 5, CMIP5 (Taylor et al. 2012) were used for the rainfall and temperature projections. As compared to CMIP3, the CMIP5 dataset provides incrementally refined climate projections that include more comprehensive models with a broader set of

experiments, higher spatial resolution for models, and an expanded set of output variables for both the near-term (decadal predictions) and long-term (century time scale). The list of GCMs and model runs included in the CMIP5 is provided in Table 2-1.

The set of climate models in the U.S. Climate Resilience Toolkit (CRT) (NOAA 2014) (accessed 2016) were used in the development of climate scenarios for the Phase 6 application except that the CBP did not use the BNU-ESM model, which was unavailable for download. Statistically downscaled climate models and corresponding realizations were retrieved from an online archive accessed through the Geo Data Portal (Bureau of Reclamation, 2013). The decision to use an existent downscaled dataset rather than either developing or applying a tailored statistical climate downscaling process was based upon the recommendations of the STAC workshop (Johnson et al. 2016). The Bias Corrected Spatial Disaggregation (BCSD) downscaling methodology was chosen for the assessment because of its commonality among numerous datasets including the U.S. Climate Resilience Toolkit and the NASA Earth Exchange (NEX) Downscaled Climate Projections (NEX-DCP30), its extensive review in peer-reviewed literature in comparison with other downscaling methodologies (Gutmann et al. 2014; Mizukami et al. 2016), and its relative ease of access and flexibility in choosing models and realizations to be incorporated into analyses. The downscaled dataset was among the ones recommended by the data.gov climate data catalog. Still, it may benefit future regional climate assessment to consider other datasets based on downscaling techniques that are also capable of producing reliable correlations with observed precipitation and temperature such as the Multivariate Adaptive Constructed Analogs (MACA) or Localized Constructed Analogs (LOCA) methodologies (Demirel and Moradkhani 2016; Pierce and Cayan 2015).

The GCMs utilize forcings based on potential future socio-economic and natural scenarios defined as Representative Concentration Pathways (RCPs). The RCPs are categorized according to the additional radiative forcing generated by the year 2100 relative to pre-industrial values as measured in Watts per square meter (Wm^{-2}). The additional radiative forcing is a measure of the cumulative impact of future anthropogenic greenhouse gas emissions. The four RCPs, RCP 2.6, RCP 4.5, RCP 6.0, and RCP 8.5 were adopted by the IPCC in its Fifth Assessment Report (AR5) to represent possible future trajectories of greenhouse gas concentrations. These concentration pathways are used in the climate model simulations to estimate four possible climate futures. However, it has been shown that the spread across RCPs in the near term for a single climate model is typically smaller than the difference between climate models under a single RCP scenario (Kirtman et al. 2013).

Table 2-1: A multi-model ensemble of statistically downscaled CMIP5 projections was used. "Downscaled CMIP3 and CMIP5 Climate and Hydrology Projections" archive at http://gdodcp.ucllnl.org/downscaled_cmip_projections was used for obtaining rainfall and temperature projections that were statistically downscaled using Bias Corrected Spatially Disaggregated method (Maurer et al. 2007). The symbol "Y" represents the member "model-runs" that were included as the ensemble analysis, whereas "x" indicates data for the model-run that were available but not included, and "o" indicates data for the model-run that were unavailable.

WCRP CMIP5 Modeling Workgroup	WCRP CMIP5 Climate Model	Model Run											
		R1	R2	R3	R4	R5	R6	R7	R8	R9	R10	R11	R12
	ACCESS1-0	Y	o	o	o	o	o	o	o	o	o	o	o

Commonwealth Scientific and Industrial Research Organization and Bureau of Meteorology, Australia	ACCESS1-3	x	o	o	o	o	o	o	o	o	o	o	o
Beijing Climate Center, China Meteorological Administration	BCC-CSM1-1	Y	o	o	o	o	o	o	o	o	o	o	o
	BCC-CSM1-1-M	Y	o	o	o	o	o	o	o	o	o	o	o
College of Global Change and Earth System Science, Beijing Normal University	BNU-ESM	o	o	o	o	o	o	o	o	o	o	o	o
Canadian Centre for Climate Modelling and Analysis	CanESM2	Y	x	x	x	x	o	o	o	o	o	o	o
National Center for Atmospheric Research	CCSM4	Y	x	x	x	x	o	o	o	o	o	o	o
Community Earth System Model Contributors	CESM1-BGC	Y	o	o	o	o	o	o	o	o	o	o	o
	CESM1-CAM5	Y	x	x	o	o	o	o	o	o	o	o	o
Centro Euro-Mediterraneo per I Cambiamenti Climatici	CMCC-CM	Y	o	o	o	o	o	o	o	o	o	o	o
Centre National de Recherches Météorologiques/ Centre Européen de Recherche et Formation Avancée en Calcul Scientifique	CNRM-CM5	Y	o	o	o	o	o	o	o	o	o	o	o
Commonwealth Scientific and Industrial Research Organization, Queensland Climate Change Centre of Excellence	CSIRO-Mk3-6-0	Y	x	x	x	x	x	x	x	x	x	x	x
EC-Earth consortium, representing 22 academic institutions and meteorological services from 10 countries in Europe	EC-EARTH	o	Y	o	o	o	o	o	x	o	o	o	x
Laboratory of Numerical Modeling for Atmospheric Sciences and Geophysical Fluid Dynamics, Institute of Atmospheric Physics, Chinese Academy of Sciences, and Center for Earth System Science, Tsinghua University	FGOALS-g2	Y	o	o	o	o	o	o	o	o	o	o	o
Laboratory of Numerical Modeling for Atmospheric Sciences and Geophysical Fluid Dynamics, Institute of Atmospheric Physics, Chinese Academy of Sciences	FGOALS-s2	o	x	o	o	o	o	o	o	o	o	o	o

Institute	Model												
The First Institute of Oceanography, State Oceanic Administration, China	FIO-ESM	Y	x	x	o	o	o	o	o	o	o	o	o
NOAA Geophysical Fluid Dynamics Laboratory	GFDL-CM3	Y	o	o	o	o	o	o	o	o	o	o	o
	GFDL-ESM2G	Y	o	o	o	o	o	o	o	o	o	o	o
	GFDL-ESM2M	Y	o	o	o	o	o	o	o	o	o	o	o
NASA Goddard Institute for Space Studies	GISS-E2-H-CC	x	o	o	o	o	o	o	o	o	o	o	o
	GISS-E2-R	Y	x	x	x	x	o	o	o	o	o	o	o
	GISS-E2-R-CC	x	o	o	o	o	o	o	o	o	o	o	o
Met Office Hadley Centre (additional HadGEM2ES realizations contributed by Instituto Nacional de Pesquisas Espaciais)	HadGEM2-AO	Y	o	o	o	o	o	o	o	o	o	o	o
	HadGEM2-CC	Y	o	o	o	o	o	o	o	o	o	o	o
	HadGEM2-ES	Y	x	x	x	o	o	o	o	o	o	o	o
Institute for Numerical Mathematics	INM-CM4	Y	o	o	o	o	o	o	o	o	o	o	o
Institut Pierre-Simon Laplace	IPSL-CM5A-LR	Y	x	x	x	o	o	o	o	o	o	o	o
	IPSL-CM5A-MR	Y	o	o	o	o	o	o	o	o	o	o	o
	IPSL-CM5B-LR	Y	o	o	o	o	o	o	o	o	o	o	o
Japan Agency for Marine-Earth Science and Technology, Atmosphere and Ocean Research Institute (The University of Tokyo), and National Institute for Environmental Studies	MIROC-ESM	Y	o	o	o	o	o	o	o	o	o	o	o
	MIROC-ESMCHEM	Y	o	o	o	o	o	o	o	o	o	o	o
Atmosphere and Ocean Research Institute (The University of Tokyo), National Institute for Environmental Studies, and Japan Agency for Marine-Earth Science and Technology	MIROC5	Y	o	o	o	o	o	o	o	o	o	o	o
Max-Planck-Institut für Meteorologie (Max Planck Institute for Meteorology)	MPI-ESM-LR	Y	x	x	o	o	o	o	o	o	o	o	o
	MPI-ESM-MR	Y	o	o	o	o	o	o	o	o	o	o	o
Meteorological Research Institute	MRI-CGCM3	Y	o	o	o	o	o	o	o	o	o	o	o
Norwegian Climate Centre	NorESM1-M	Y	o	o	o	o	o	o	o	o	o	o	o
	NorESM1-ME	x	o	o	o	o	o	o	o	o	o	o	o

2.1.3 Bias Correction and Downscaling of the Climatic Projections

The Bias Corrected and Spatially Disaggregated (BCSD) statistically downscaled CMIP5 climate projections were downloaded from the "Downscaled CMIP3 and CMIP5 Climate and Hydrology Projections" archive available at http://gdo-dcp.ucllnl.org/downscaled_cmip_projections/ (Maurer et al. 2007; Reclamation 2013). The online data archive provides output of GCMs that were statistically downscaled using the BCSD methodology that employed a quantile mapping technique for several GCMs. The archive also included several "model-runs" or "realizations" for a number of GCMs. The "model-runs" incorporate perturbations of initial conditions to provide a spread of possible outcomes. However, the selection of several GCMs over several model-runs for a particular GCM provides wider variability that enables an ensemble analysis to capture a fuller range of uncertainties in model projections (Pierce et al. 2009). In addition, selecting one realization per model constrains biases for models with more realizations. Subsequently, 31 GCMs that were included in the ensemble analysis are shown in Table 2-1. The selection was based on models used by the U.S. Climate Resiliency Toolkit (which itself relies upon the NASA NEX-DCP30 database) and the recommendation of the Chesapeake Bay Program's Climate Resiliency Workgroup.

Bias correction methods remove systematic climate model errors at regional scales, whereas the downscaling methods resolve finer scale climatological features, providing an improved dataset for applications in local scale impact analyses. The bias corrected data for every GCM are is forced to match the monthly cumulative density functions of observed rainfall at the regional scale. This is shown in Figure 2-3, where the dashed black lines represent the observed data, the red lines represent the hindcast simulations for the period 1950-1999 simulated by GCMs at a spatial grid of 2°, and the green lines represent the bias corrected dataset for all GCMs. The green line for all of the GCMs and the observations are situated on top of one another demonstrating that the bias corrected GCMs match the observed distributions. The quantile maps, which establish a tabular relationship between the rank probability and bias in the hindcast dataset, were applied to the future projections. This approach preserves the same relative changes projected by the GCMs in mean, variance, and other statistical moments of the data.

Dynamical downscaling, which involves the use of a finer scale regional climate model (RCM), offers a better representation of a local study area nested within a GCM domain and can simulate local fine-scale feedback processes that are not anticipated by statistical downscaling. However, for hydrological applications, statistically downscaled climate projections using the BCSD method have been shown to exhibit comparable fidelity as compared to other statistical and dynamical methods (Wood et al. 2004). Moreover, the climate change projections obtained using BCSD have been found to provide similar strengths and weaknesses as compared to Bias Correction Constructed Analogues, BCCA, and Multivariate Adaptive Constructed Analogues (MACA) (Maurer et al. 2010; Abatzoglou and Brown 2011).
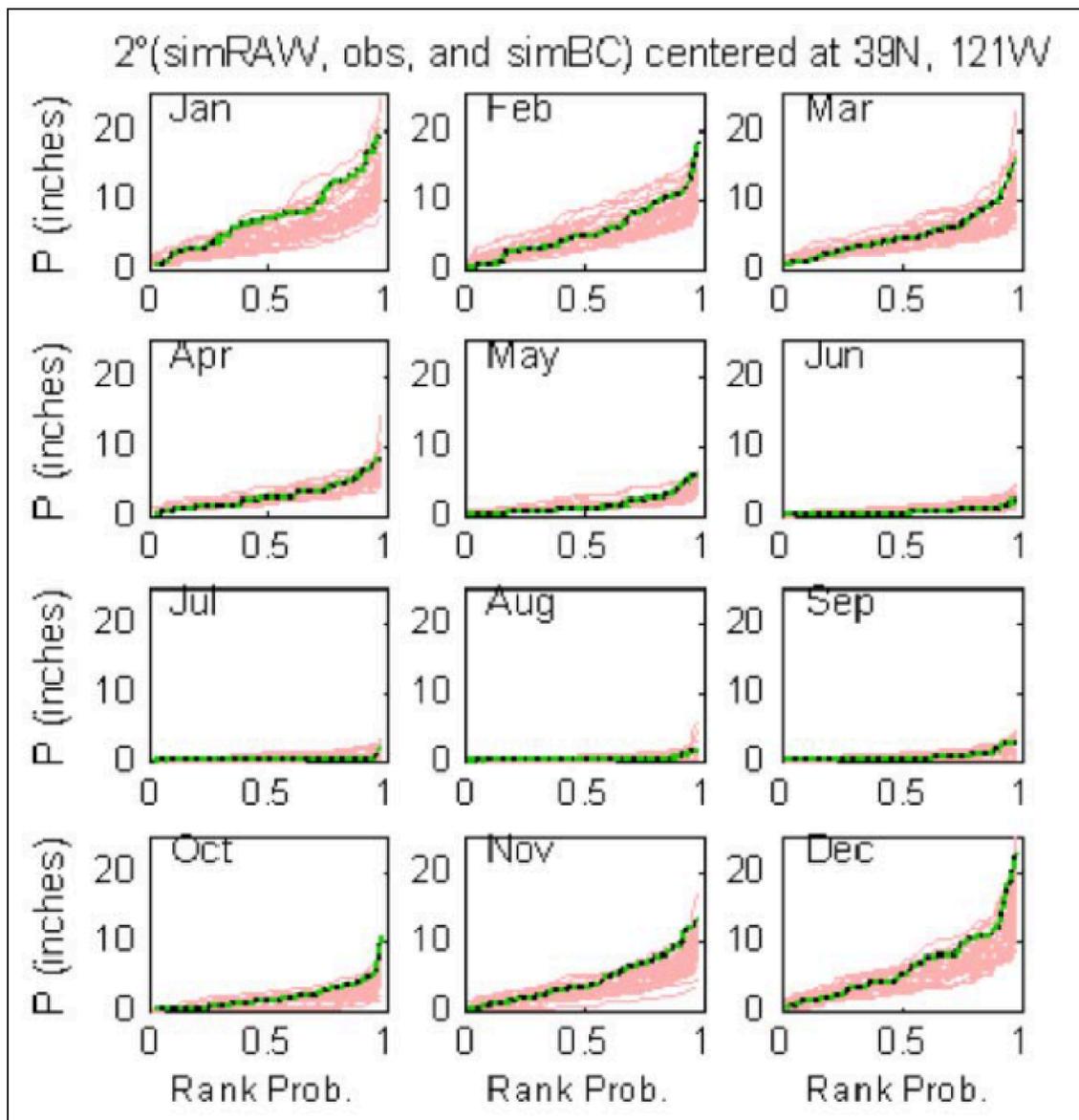
Figure 2-3: Bias corrected GCM outputs. Monthly bias corrections of rainfall data using a quantile mapping technique are shown (from Reclamation, 2013). Red lines show model output, dashed black lines show observations, and the green lines show the bias corrected GCM outputs.

2.1.4 The Ensemble Analysis

A widely used technique in climate change assessments involving the use of projections from multiple climate models is to combine ensembles of predictions from a collection of models. This approach allows increasing the sampling of both initial conditions and model properties in the subsequent climate change assessment. Furthermore, it has been shown that multi-model ensemble means generally exhibit higher skill, e.g., in capturing Atlantic Multi-decadal Variability, as compared to a single-model projection (Garcia-Serrano and Doblas-Reyes 2012; Kim et al. 2012; Kirtman et al. 2013).

Figure 2-4 shows monthly percent changes in rainfall volume and temperature changes in degrees Celsius for the 31-member ensemble described in Table 2-1. The modeled change between the years 2050 (2036-2065) and 1995 (1991-2000) are shown. The median change of the ensemble members for each month are also shown. For the ensemble median scenario, changes in monthly

rainfall volume and temperature for each land segment were applied to the 1991-2000 rainfall and temperature dataset, respectively.
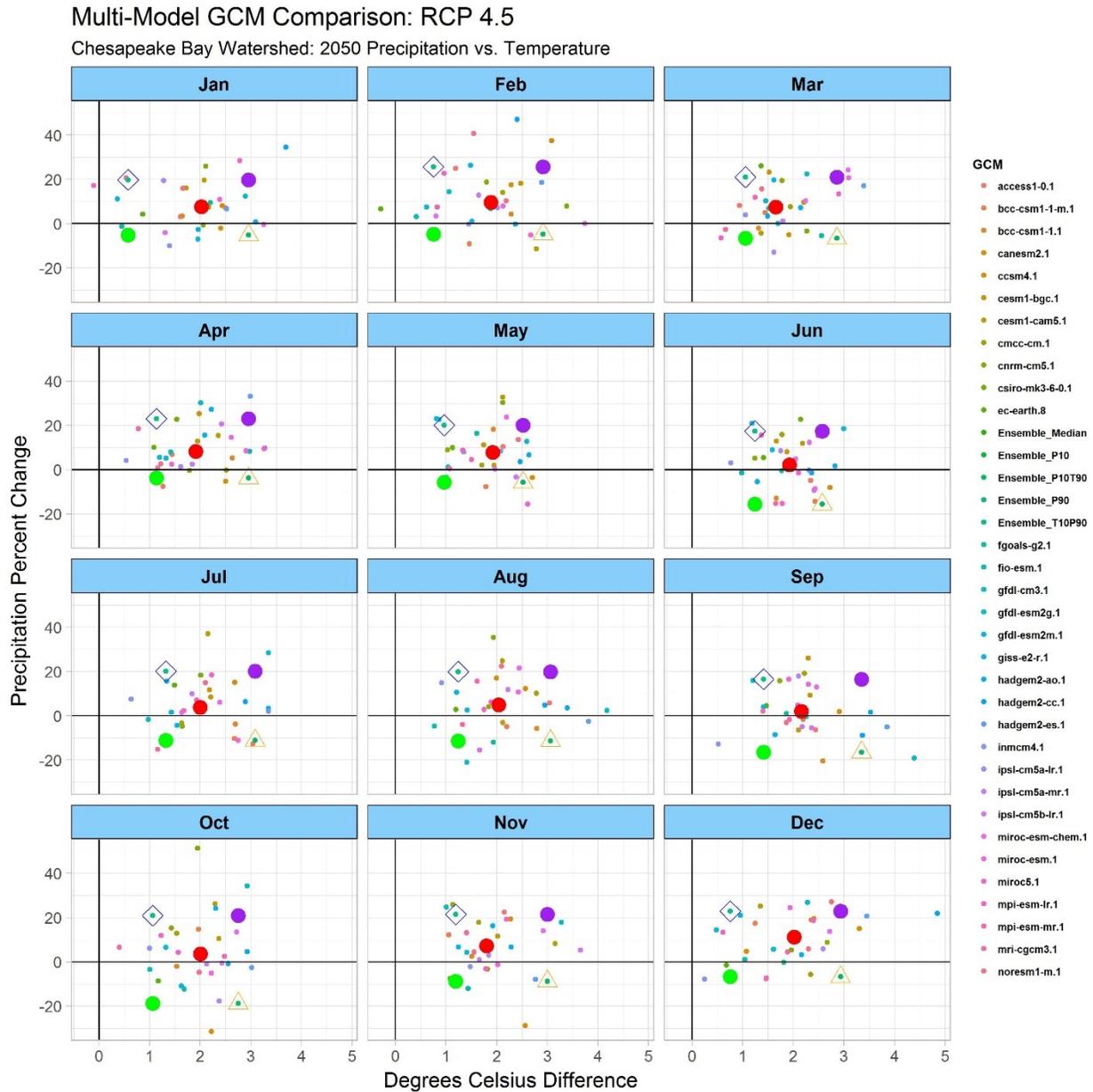

Figure 2-4: The monthly percent change in rainfall volume and degrees Celsius difference for the 31-member ensemble of the RCP 4.5 scenario are shown. Each data point represents the monthly difference between the average monthly temperature and precipitation volume between the periods 2036-2065 and 1981-2010. For year 2050, monthly median ensembles were used as the central tendency for the climate change assessment, whereas the 10th and 90th percentiles were used for uncertainty quantification.

Figure 2-5 and Figure 2-6 show the spatially averaged changes in precipitation and temperature, respectively, for the Chesapeake Bay watershed. Projected changes are compared for the years 2025 and 2050 relative to 1995 for three emission scenarios RCP 2.6, RCP 4.5, and RCP 8.5. The box plots show the ensemble distribution of projected change based on the ensemble of GCMs. Figure 2-5 shows that, for precipitation, the ensembles medians of different RCPs are similar and that the range between the 10th and 90th percentiles of RCP 4.5 includes the interquartile ranges

of RCP 2.6 and RCP 8.5 for both 2025 and 2050. Figure 2-6 shows that, for temperature change between 1995 and 2025, the 10th, 50th, and 90th percentiles for the three emission scenarios are all similar. Projections for the year 2050 show large differences in ensemble medians for the emission scenarios, however the uncertainty range for RCP4.5 considerably overlaps the RCP 2.6 and RCP 8.5 range. For both precipitation and temperature, and in both 2025 and 2050, the variability due to model selection is greater than the variability due to emission scenarios and therefore the RCP 4.5 is used for the CBP climate projections for 2025, 2035, 2045, and 2055.
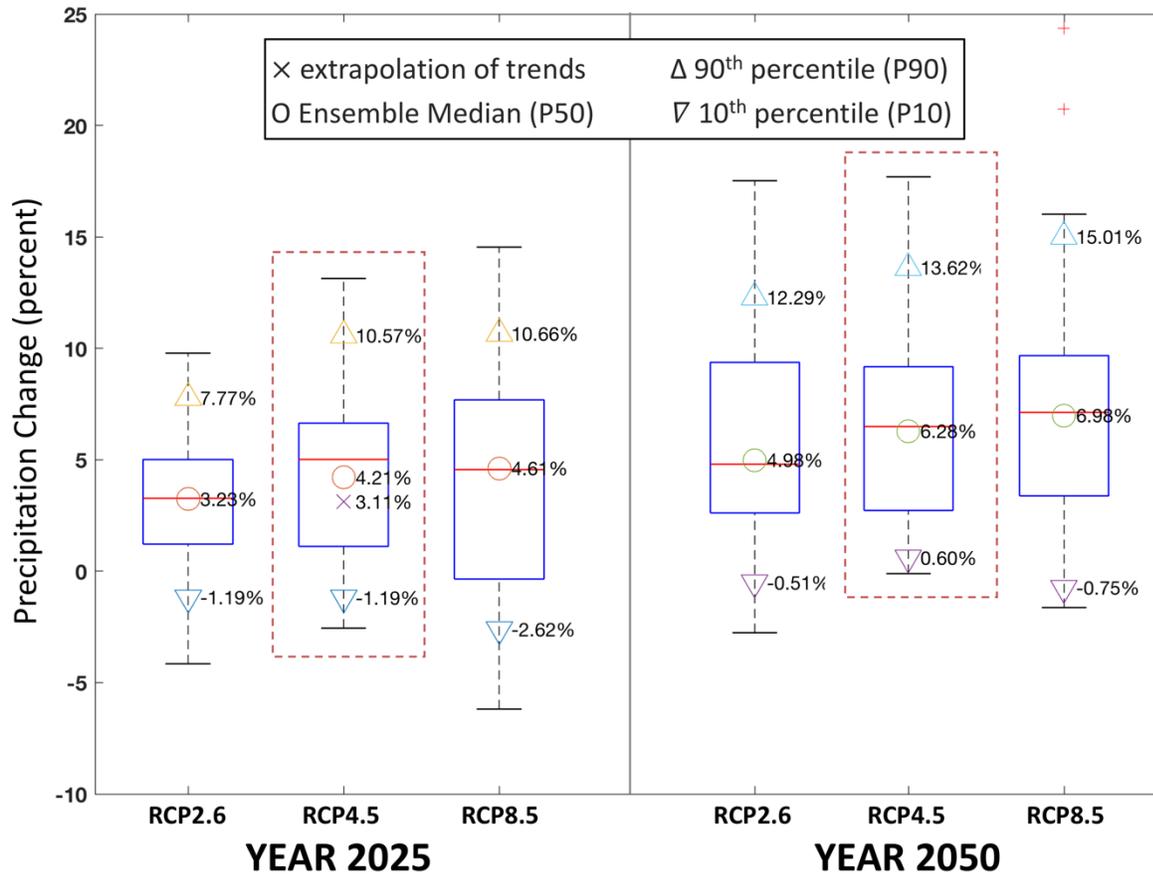

Figure 2-5: Percent change in rainfall volume for the Chesapeake Bay watershed for the years 2025 and 2050 relative to 1995 are shown. Box plots show variability in the ensemble of GCM projections. Ensemble median (circles) and 10th and 90th percentile (triangles) range are shown.
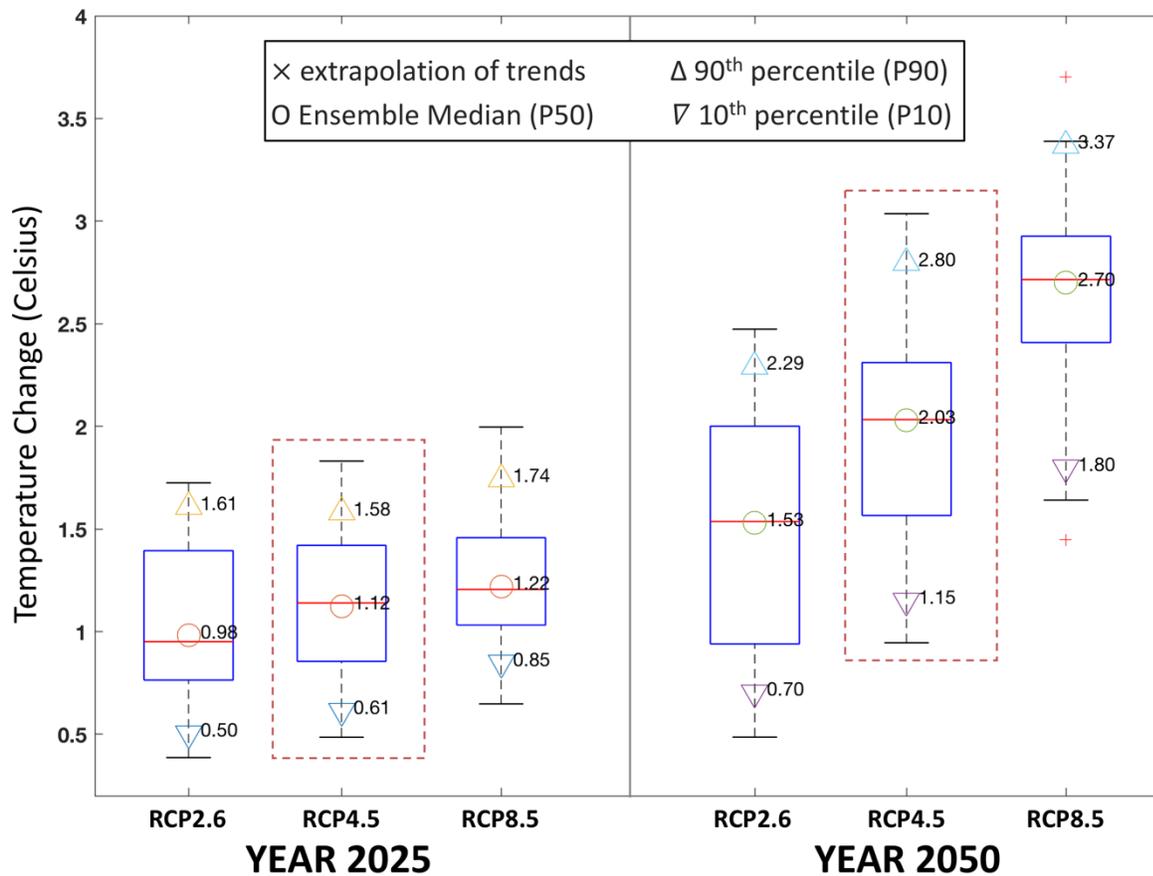
Figure 2-6: Percent change in temperature for the Chesapeake Bay watershed for the years 2025 and 2050 relative to 1995 are shown. Box plots show variability in the ensemble of GCM projections. Ensemble median (circles) and 10th and 90th percentile (triangles) ranges are shown.

2.1.5 Projected Changes in Precipitation Intensity

The capability to change precipitation by deciles was incorporated into the analysis. Changes in rainfall volume were divided among intensity deciles based on documented changes in intensity and frequency of precipitation events using a century of observations (Groisman et al. 2004; Groisman et al. 2001; Karl and Knight 1998, Gordon et al. 1992). The observed increases in larger precipitation events (Groisman et al. 2004) was the basis for assigning the total percent change in precipitation volume disproportionately to intensity deciles. Following Groisman et al. (2004), the larger share of the increase in estimated precipitation volume due to climate change was placed in the highest decile (90 to 100 percent) of intensity (Figure 2-7).

For comparison, a model sensitivity scenario was also developed that applied a uniform distribution for the increased rainfall volume estimate due to climate change among intensity deciles. In future, further analysis of rainfall intensity should explore the alteration of precipitation intensities based upon different downscaled projections and its subsequent impacts on the watershed responses.
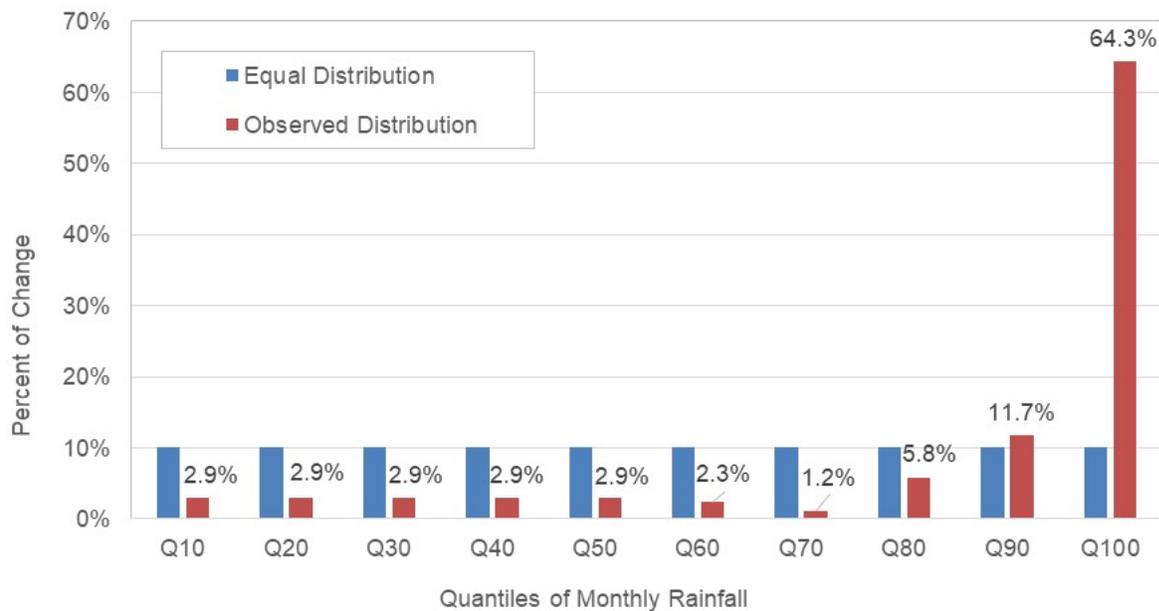
Figure 2-7: Observed changes in rainfall intensity over the last century (based on Figure 10 in Groisman et al. 2004). The equal allocation distribution (blue) is contrasted with the distribution obtained based on observed changes (red).

2.1.6   Application of the Delta Method

For hydrological applications and the impact analysis of linked natural systems, it is critical to maintain physically plausible spatial and temporal relationships between rainfall and other meteorological variables. Therefore, it is important that multiple variables are simultaneously downscaled at the regional scale. However, these relationships are not maintained by most of the statistical downscaling methods. The delta method is the creation of future meteorological time series by starting with a historical observed time series and applying change factors calculated from a modeled or statistical estimate of the effects of climate change. The use of a delta change method preserves the spatial and temporal relationship between the rainfall and meteorological variables in the observed reference data that was used for model calibration.

The Phase 6 Watershed Model was calibrated to the rainfall and meteorological data obtained from the NLDAS-2 database (Xia et al. 2012). Monthly changes to the NLDAS temperature data for future climate scenarios were calculated based on the median change in the model ensemble as described in Section 2.1.4. Monthly changes to the NLDAS precipitation data for the 2050 climate scenarios were calculated based on the median change in the model ensemble as described in Section 2.1.4. Monthly changes to the NLDAS precipitation for 2025 were based on long-term trends as described in Section 2.1.1. Changes in the precipitation data for the years 2035 and 2045 were interpolated between the two methods.

An appropriate selection of time-disaggregation procedures is needed for the application of monthly delta change to the reference dataset. For the time-disaggregation of monthly rainfall change, the monthly change in volume was divided into 10 rainfall intensity deciles based on an *a priori* distribution (Figure 2-7). Two methods were used for the quantile distributions (Figure 2-7). In the first method, additional precipitation volume was divided equally among the 10 quantiles, whereas in the second method the documented changes in observed rainfall intensities over the

24

last century were used. As a result, the second method allocates more rainfall volume to the 10th decile (largest 10% events) of rainfall in the average hydrology period from 1991-2000 (Figure 2-8). In both methods, the change in rainfall is applied as a monthly factor multiplying each hour of rainfall. For all scenarios, the change in temperature is applied as a monthly-varying additive value.
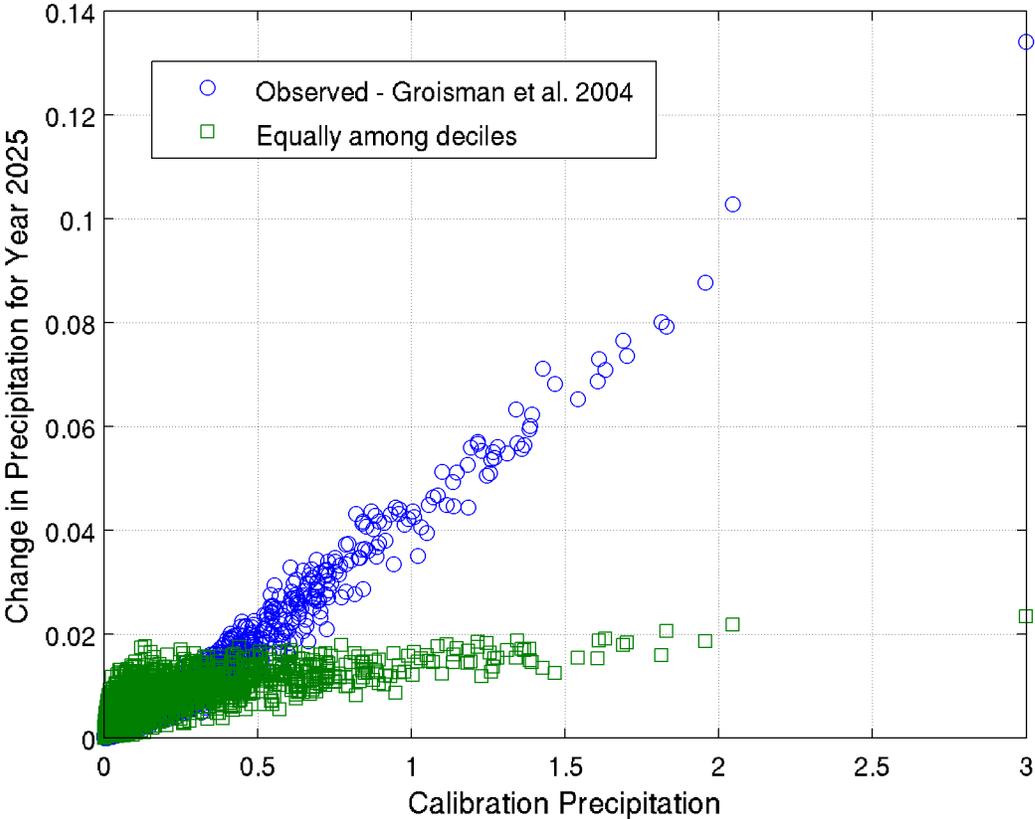
Figure 2-8: Additional rainfall added to the baseline daily rainfall over the 10-year period for a Phase 6 land segment (Potter, PA) is shown. In the method based on observed intensity trends, more volume is added to 10th decile resulting in higher intensity events become stronger.

2.1.7   Altered CO_2 Concentrations

Anticipated values of carbon dioxide concentrations were compiled from the IPCC's 5th Assessment Report for different emission scenarios (Figure 2-9). Carbon dioxide concentration levels of approximately 423 ppm and 487 ppm were obtained for the Representative Concentration Pathway (RCP) 4.5 for 2025 and 2050, respectively (IPCC, 2013: Annex II, Table AII.4.1). This is compared to 363 ppm for the average concentration for the years 1991-2000. Going forward, modifications to CO_2 concentrations based upon different RCP scenarios could also be simulated, depending upon the year and scenario of choice.
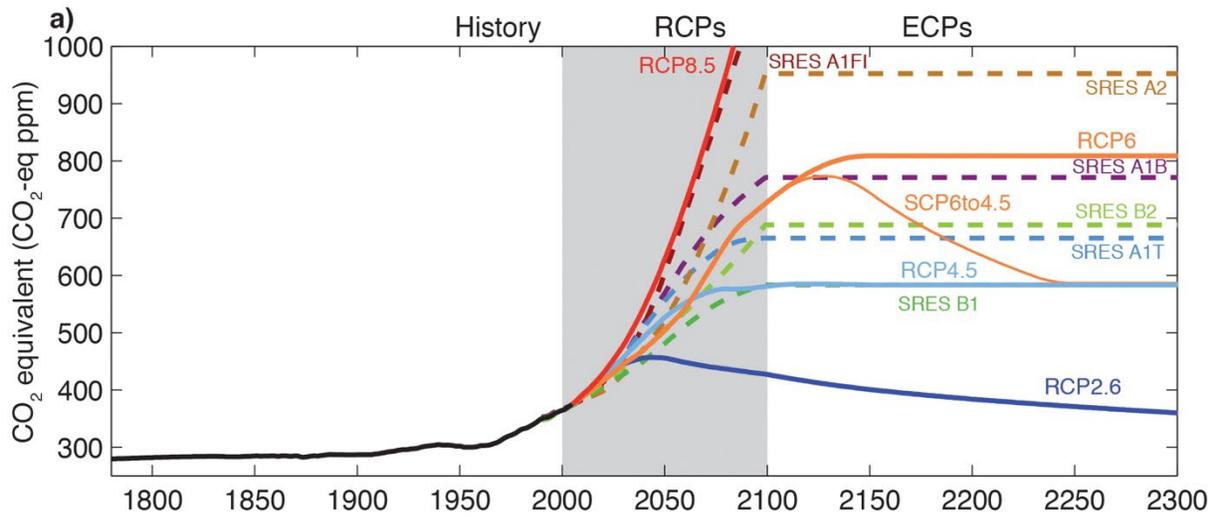
Figure 2-9: Equivalent CO2 concentration from IPCC 5 Worgking Group 1 report (Cubasch et al. 2013)

Table 2-2: CO_2 abundance table All.4.1 of IPCC, 2013: Annex II: Climate System Scenario Tables In: Climate Change 2013: The Physical Science Basis

Year	Observed	RCP2.6	RCP4.5	RCP6.0	RCP8.5
PI	*278 ± 2*	*278*	*278*	*278*	*278*
2011 obs	*390.5 ± 0.3*				
2000		368.9	368.9	368.9	368.9
2005		378.8	378.8	378.8	378.8
2010		389.3	389.1	389.1	389.3
2020		412.1	411.1	409.4	415.8
2030		430.8	435.0	428.9	448.8
2040		440.2	460.8	450.7	489.4
2050		442.7	486.5	477.7	540.5
2060		441.7	508.9	510.6	603.5
2070		437.5	524.3	549.8	677.1
2080		431.6	531.1	594.3	758.2
2090		426.0	533.7	635.6	844.8
2100		420.9	538.4	669.7	935.9

2.1.8 Estimates of Potential Evapotranspiration

Potential evapotranspiration (PET) is generally estimated as a function of temperature, dew point temperature, wind speed, stomatal resistance, and other factors. The Phase 6 Model calibration uses the Hamon method for the estimation of PET (Equation 2-1). In the early development stages of the Phase 6 Model, the Hamon method was used for estimating changes in PET with climate change, specifically in response to changes in temperature, which was consistent with methods of climate change assessment in the Phase 5 Model. In response to the climate change simulation of Phase 5 Model as well as some of the early assessment using Phase 6 Model, STAC recommended careful considerations of the PET methods (Johnson et al. 2016).

$$Hamon\ Daily\ PET\ =\ 0.0055 \times VD_{sat} \times \left(Daily\ light\ hours/12\right)^2$$

$$VD_{sat} = 216.7 \times \frac{VP_{sat}}{\left(T_{avg} + 273.3\right)}$$

$$VP_{sat} = 6.108 \times e^{\frac{17.26939 \times T_{avg}}{T_{avg}+237.3}}$$

Where:

PET = potential evapotranspiration, mm/day

VDsat = saturated vapor density, gram/m^3

Tavg = average daily temperature, degree Celsius

VPsat = saturated vapor pressure, millibars

To a large extent the simulated impact of climate change on the water budget of the watershed relies on the estimated PET. Therefore, the selection of PET method plays a very critical role. The Hamon method relies upon the temperature, the saturated water vapor density (also a function of temperature), and the number of daylight hours as inputs in calculating PET (Equation 2-1). As a result, the estimation of climate effects on PET in the Hamon method is solely a function of temperature. Milly (2016) showed an analysis of different PET methods, which demonstrated that Hamon method overestimated the impact of temperature change on the PET as compared to other methods, including Penman-Monteith (Figure 2-10). The Penman-Monteith equation is frequently relied upon for the estimation of PET in several watershed models for its more physically based approach. However, the Penman-Monteith equation requires several additional meteorological variables which are often hard to obtain. That was particularly the case for the downscaled climate change inputs that were available. The Hargreaves-Samani approach (Equation 2-2), on the other hand, uses readily available parameter variables as with Hamon but provides an estimated relationship of PET with temperature more similar to Penman-Monteith (Figure 2-10). For that reason, the Hargreaves-Samani method was used for estimating the change in PET. The estimated daily change was added as a factor to the hourly reference PET dataset. The Phase 6 Model simulation showed improved simulation results that were more consistent with streamflow trends (U.S. EPA. 2016a; Rice et al. 2017) when the change in PET was estimated using Hargreaves-Samani method rather than Hamon, which produced unrealistically drier conditions due to higher sensitivity to temperature.

Equation 2-2: Hargreaves-Samani PET equation

$$H\_S\ Daily\ PET = 0.0135 \times R_s \times (T_{avg} + 17.8)$$

$$R_s = KT \times R_a \times T_{del}^{1/2}$$

$$T_{del} = T_{max} - T_{min}$$

$$KT = 0.00185 \times T_{del}^2 - 0.0433 \times T_{del} + 0.4023$$

Where:
PET = potential evapotranspiration, mm/day
Rs = solar radiation, mm/day
KT = empirical coefficient
Ra = Extraterrestrial radiation, mm/day
Tdel = maximum minimum temperature difference, degree Celsius
Tmax = maximum daily temperature, degree Celsius
Tmin = minimum daily temperature, degree Celsius
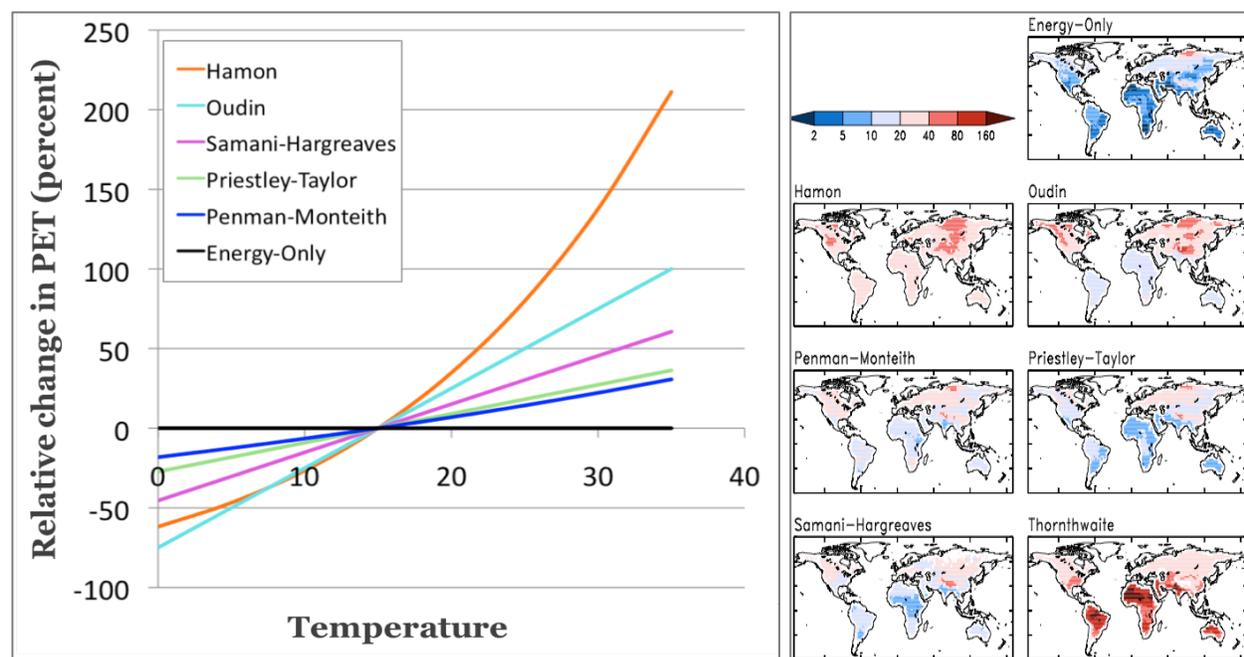Tavg = average daily temperature, degree Celsius

Figure 2-10: (a) Relative change in estimated change in potential evapotranspiration due to change in temperature is shown from different methods. It shows temperature alone can introduce considerable differences in estimation of potential evapotranspiration with the selection of method. (b) Estimate percent changes in potential evapotranspiration using different methods for RCP 8.5 for the late 21st century are shown (adapted from Milly 2016).

Both the Hamon and Hargreaves-Samani PET methods were evaluated for estimating change in potential evapotranspiration (PET). The average annual changes in PET over the watershed for the years 2025 and 2050 using the two methods are shown in Figure 2-11. The ensemble median of the change for the potential evapotranspiration data for short reference cover from the downscaled datasets are also shown, which is based on the Penman-Monteith equation. Short reference is defined as a hypothetical reference vegetative cover with an assumed height of 0.12 m, a fixed surface resistance of 70 s/m and an albedo of 0.23. Due to the similarities between estimated changes produced by the Hargreaves-Samani and

Penman-Monteith methods, along with guidance provided by CBP STAC, and the recommendation of the Modeling Workgroup, Hargreaves-Samani was used for the CBP climate simulations. It is noted that estimated change using Hargreaves-Samani method falls between the estimated changes for open water and short reference.
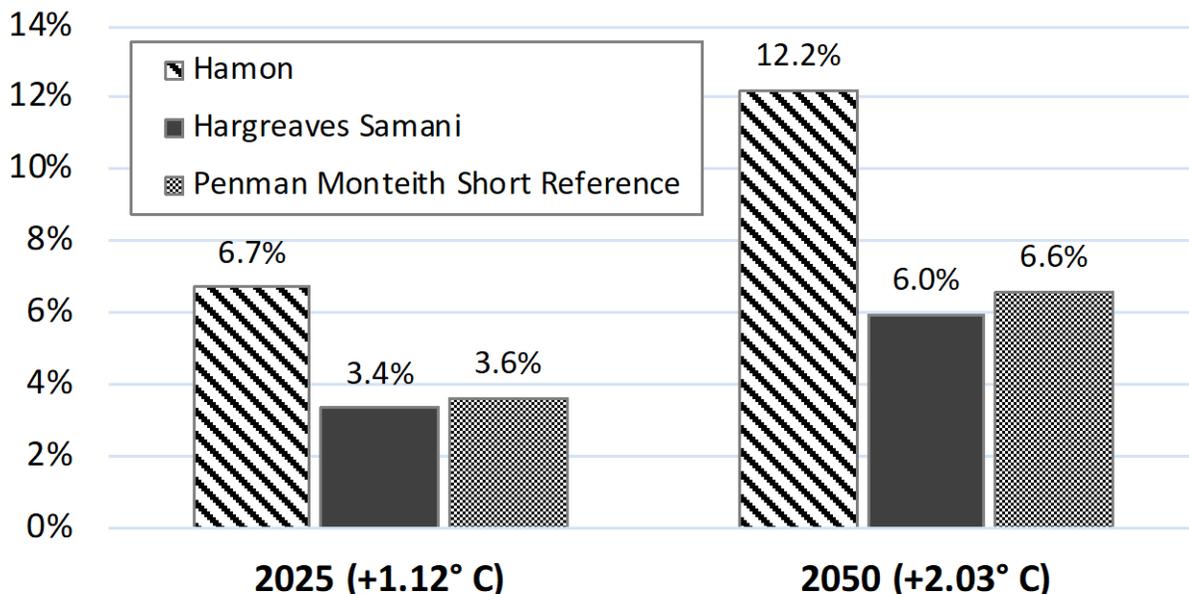

Figure 2-11: The relative difference in PET produced by using either the Hamon or Hargreaves-Samani methods are shown here. In 2025 projections produced by the WSM, the Hamon method simulated an increase in PET that was 3.36 percent greater than that simulated with the Hargreaves-Samani method. The change was more pronounced in 2050 simulations where the Hamon method outpaced the PET rate of Hargreaves-Samani by 6.26 percent.

2.2   Climate Scenario Input Summary

2.2.1   2025, 2035, 2045, and 2055 Temperature

Temperature change projections for 2025, 2035, 2045, and 2055 were obtained from an ensemble of statistically downscaled GCMs and were incorporated using the delta method (Section 2.1.6). For each model land segment, the average monthly change in temperature (in degree Celsius) was calculated for the GCMs, and the median change for each month was used as the central tendency of the projected future. Estimates for the 10th and 90th percentiles were also developed to define the range of uncertainty in projected future. As per the 31-member ensemble median for the RCP 4.5 scenario, the average annual increase in temperature for the Chesapeake Bay watershed in 2025, 2035, 2045, and 2055 were 1.12°C, 1.45°C, 1.84°C, and 2.12°C respectively. Spatial variability in average annual change for the land segments within the Chesapeake Bay watershed is shown in Figure 2-12. An elevation gradient in temperature increase is apparent for all scenarios, i.e. increases in air temperature are relatively lower at lower elevations. Figure 2-13 shows the ranges for monthly change in temperature averaged over the watershed from 31 GCMs for the RCP 4.5 scenario. The black line in the figure shows the spatial aggregation of the land segment ensemble median (P50) of monthly temperature changes. It shows a gradual increase in air temperature between 2025 to 2055 from 1.12°C to 2.12°C, where the increase in air temperature is almost the same across all months.
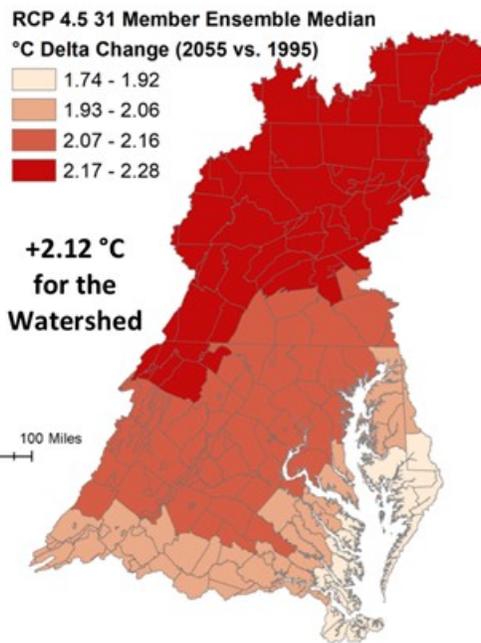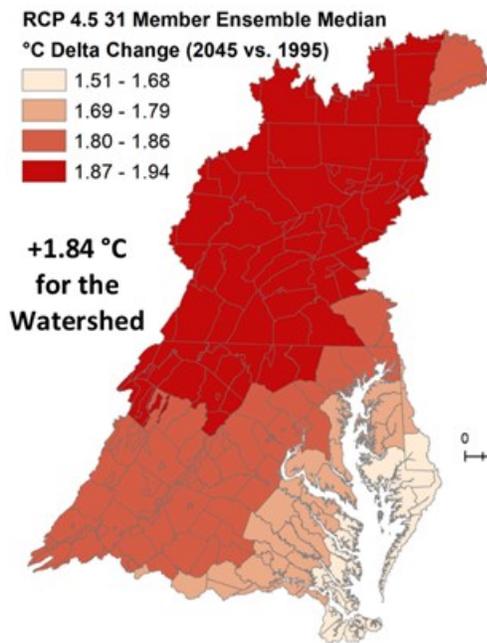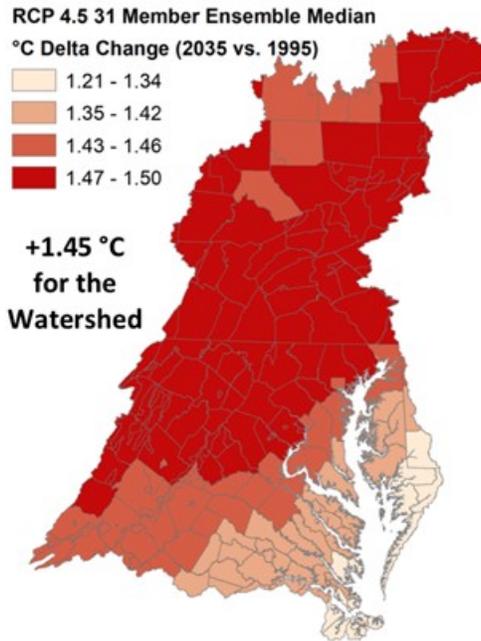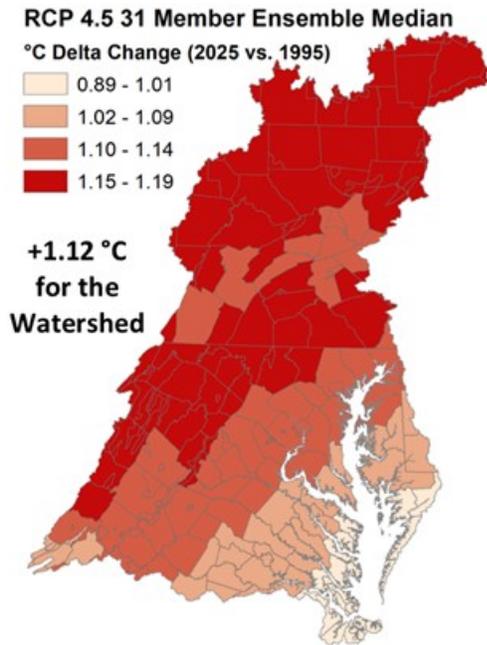
Figure 2-12: Estimated average annual change in temperature (°C) for the land segments (counties) in the Chesapeake Bay watershed are shown for 2025 (top-left) 2035 (top-right), 2045 (bottom-left) and 2055 (bottom-right). The change in temperature with respect to 1995 are based upon 31-member ensemble median of downscaled Global Climate Models for RCP 4.5 scenario.

Figure 2-13: Monthly change in temperature for the Chesapeake Bay watershed is shown. Box plots show the projected monthly change based on 31-member ensemble of downscaled Global Climate Models for RCP 4.5 for the years 2025, 2035, 2045 and 2055. Additional three markers show 10th percentile (P10), ensemble median (P50), and 90th percentile (P90) range for the spatially aggregated land segment data. The black line is spatial aggregation of the ensemble median (P50) of the RCP 4.5 GCMs for the land segments.

2.2.2   2025, 2035, 2045, and 2055 Precipitation

Precipitation change projections for 2025, 2035, 2045, and 2055 were developed using long-term rainfall trends and the ensemble of statistically downscaled GCMs and incorporated using the delta method (Section 2.1.6). For each land segment, the average monthly change in precipitation was calculated for each GCM, and the median change for each month was used as the central tendency of the projected future. Estimates for the 10th and 90th percentiles were also developed to define the range of uncertainty in projected future. The trend and GCM projections were reconciled using a hybrid approach, where the weight for trend varied linearly from 1 to 0 between 2025 and 2050, and weight for the GCM varied linearly from 0 to 1 between 2025 and 2050. As a result, rainfall projection for 2025 was entirely based on the extrapolation of rainfall trends, 60/40 hybrid of trend and GCMs for 2035, 20/80 hybrid of trend and GCMs for 2045, entirely based on GCMs for 2055. During the weighted averaging of trend and ensemble median of GCMs additional considerations were given to the seasonality. As discussed previously, information regarding seasonality was not directly available since rainfall trends were assessed using annual data. Therefore, before the trend data were combined with the ensemble median, the monthly percent change for trend data were calculated such that percent change in annual volume estimated by trend remained unchanged while the seasonal variability as seen in the ensemble median data was incorporated. As per these selections, the average annual increases in precipitation volume for the Chesapeake Bay watershed in 2025, 2035, 2045, and 2055 were 3.11%, 4.21%, 5.34%, and 6.91% respectively. Spatial variability in average annual change for the land segments within the Chesapeake Bay watershed is shown in Figure 2-15. Although the increase in rainfall gradually increases between 2025 and 2055 the spatial variability in rainfall do not show a consistent pattern. Figure 2-14 show an incremental increase in rainfall volume across all months between 2025 and 2055. Also, a relatively greater percent increase in rainfall during winter months (December to March) is evident as compared to July to September. Nonetheless, the representative scenario that is shown using the black line has an increase in rainfall volume for all months. The range or variability in monthly projections for rainfall change between the GCMs is considerably higher (Figure 2-14) as compared to variability seen for the changes in air temperature (Figure 2-13).
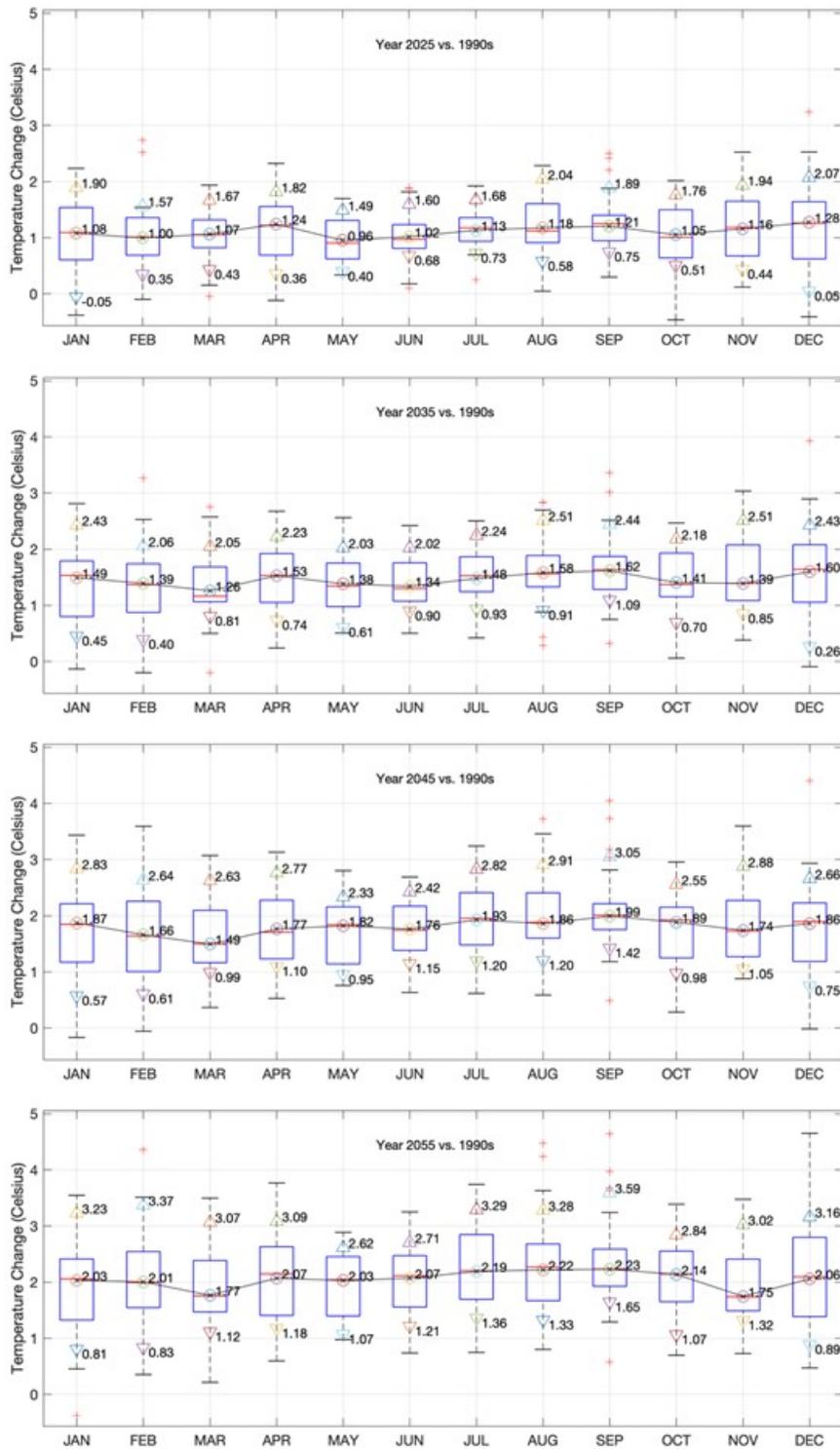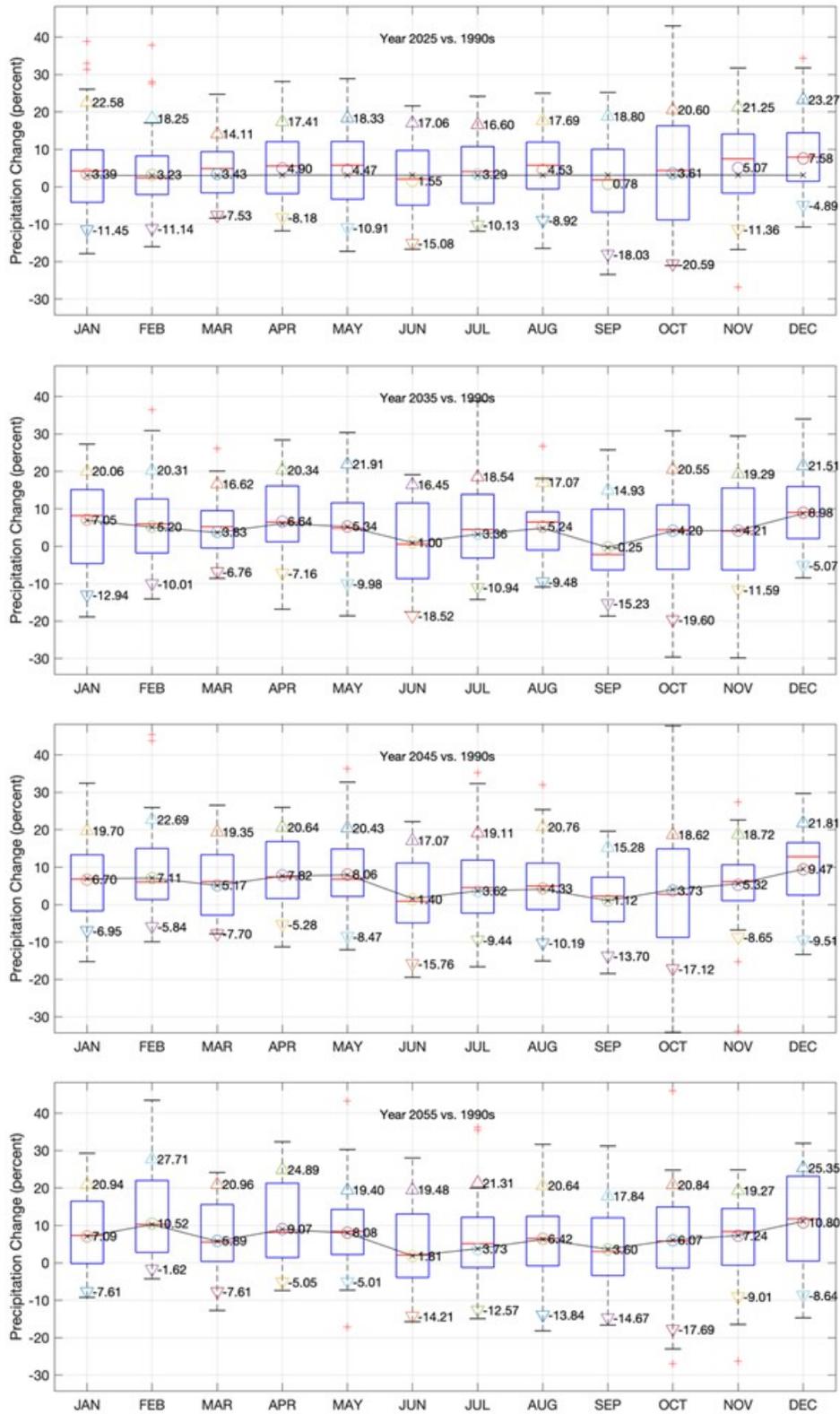
Figure 2-14: Monthly change in precipitation volume for the Chesapeake Bay watershed is shown. Box plots show the projected monthly change based on 31-member ensemble of downscaled Global Climate Models for RCP 4.5 for the years 2025, 2035, 2045 and 2055. Additional three markers show 10th percentile (P10), ensemble median (P50), and the 90th percentile (P90) range for the spatially aggregated land segment data. The black lines show the monthly change after the estimated change from trend and GCMs were reconciled.

2025 Extrapolation of Long-term Trends
Percent change (2025 vs. 1995)
- 0.7% - 2.0%
- 2.1% - 2.8%
- 2.9% - 3.6%
- 3.7% - 4.6%
- 4.7% - 5.7%

+3.11 %
for the
Watershed

2035 Hybrid of Extrapolation and GCMs
Percent change (2035 vs. 1995)
- 2.4% - 3.3%
- 3.4% - 3.9%
- 4.0% - 4.5%
- 4.6% - 5.3%
- 5.4% - 6.3%

+4.21 %
for the
Watershed

2045 Hybrid of Extrapolation and GCMs
Percent change (2045 vs. 1995)
- 4.3% - 4.7%
- 4.8% - 5.1%
- 5.2% - 5.5%
- 5.6% - 5.9%
- 6.0% - 6.6%

+5.34 %
for the
Watershed

RCP 4.5 31-Member Ensemble Median
Percent change (2055 vs. 1995)
- 5.0% - 5.7%
- 5.8% - 6.5%
- 6.6% - 7.2%
- 7.3% - 8.0%
- 8.1% - 8.8%

+6.91 %
for the
Watershed

Figure 2-15: Estimated average annual change in precipitation volume (as percent change) for the land segments (counties) in the Chesapeake Bay watershed are shown for 2025 (top-left), 2035 (top-right), 2045 (bottom-left) and 2055 (bottom-right). The change in rainfall volume with respect to 1995 are based on a specified combination of extrapolation of long-term trends and 31-member ensemble median of downscaled Global Climate Models for RCP 4.5 scenario.

2.2.3   2025, 2035, 2045, and 2055 Potential Evapotranspiration (PET)

Estimates for PET changes for 2025, 2035, 2045, and 2055, as discussed in Section 2.1.8, were developed using the Hargreaves Samani method and the temperature change from statistically downscaled GCMs (Section 2.1.6) that were incorporated using the delta method with the NLDAS temperature. Daily factor change in PET was calculated using Hargreaves Samani method and applied to the hourly calibration PET data. For each model land segment, the monthly median

change in temperature was used as the central tendency of the projected future in the estimation of PET. Estimates for the 10th and 90th percentiles were also developed to define the uncertainty in projected future. As per the 31-member ensemble median for the RCP 4.5 scenario, the average annual increase in PET for the Chesapeake Bay watershed in 2025, 2035, 2045, and 2055 were 3.36%, 4.43%, 5.54%, and 6.35%, respectively. Spatial variability in average annual change for the land segments within the Chesapeake Bay watershed is shown in Figure 2-18. An elevation gradient in estimated changes in PET is seen across the watershed same as for the changes in air temperature. Figure 2-16 and Figure 2-17 show monthly changes in PET using Penman Monteith method from Variable Infiltration Capacity (VIC) hydrologic simulations using 31-member ensemble of downscaled GCMs for RCP 4.5 for the years 2025, 2035, 2045 and 2055. The changes in PET corresponding to the ensemble median temperature estimated using Hargreaves Samani method.
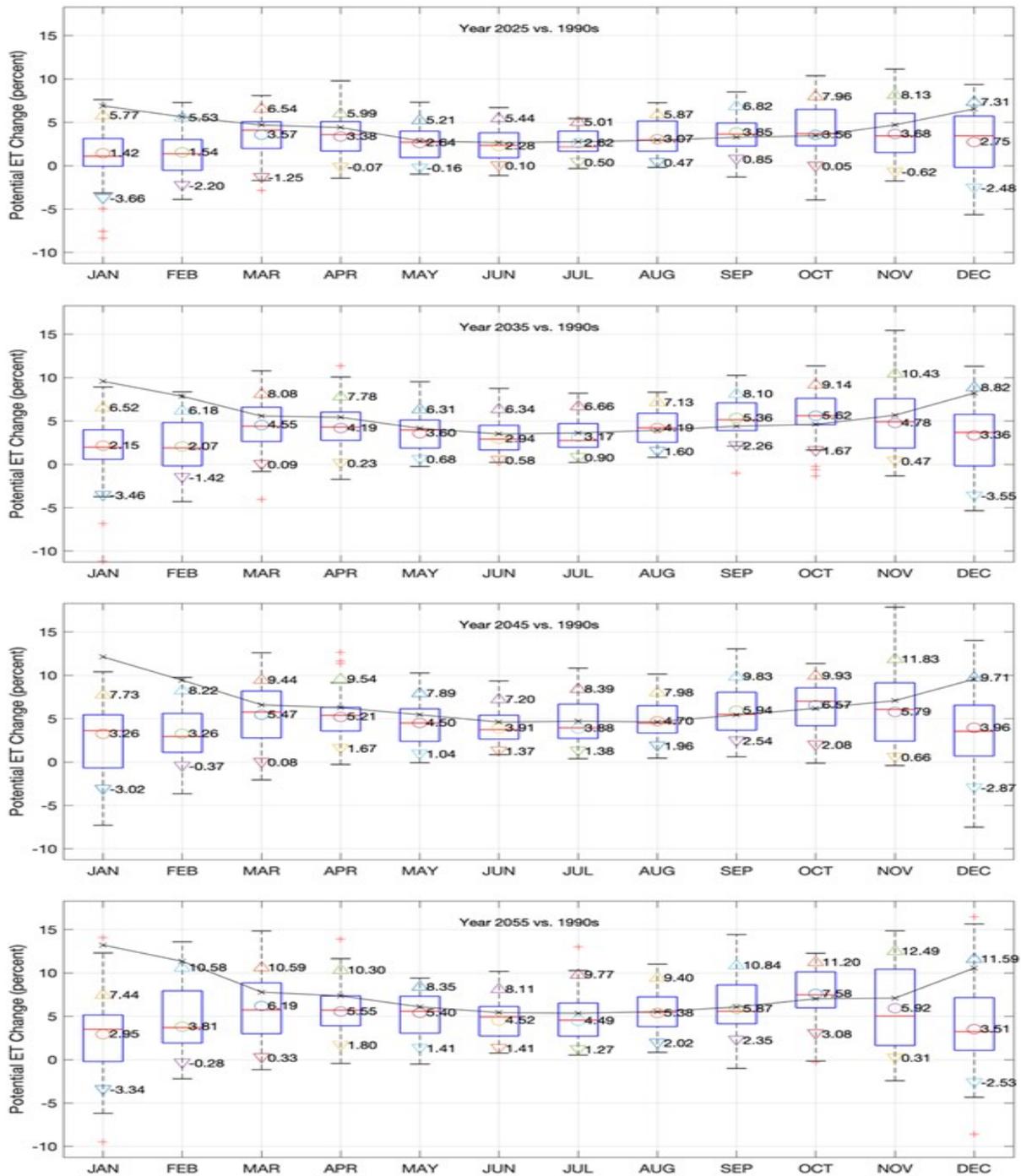
Figure 2-16: Monthly change in potential evapotranspiration for the Chesapeake Bay watershed is shown. Box plots show the estimated monthly change using Penman Monteith method from VIC hydrologic simulation using 31-member ensemble of downscaled Global Climate Models for RCP 4.5 for the years 2025, 2035, 2045 and 2055. Additional three markers show 10th percentile (P10), ensemble median (P50), and 90th percentile (P90) range for the spatially aggregated land segment data. The black lines show the changes in PET estimated using the Hargreaves Samani method using the ensemble median (P50) temperature change.
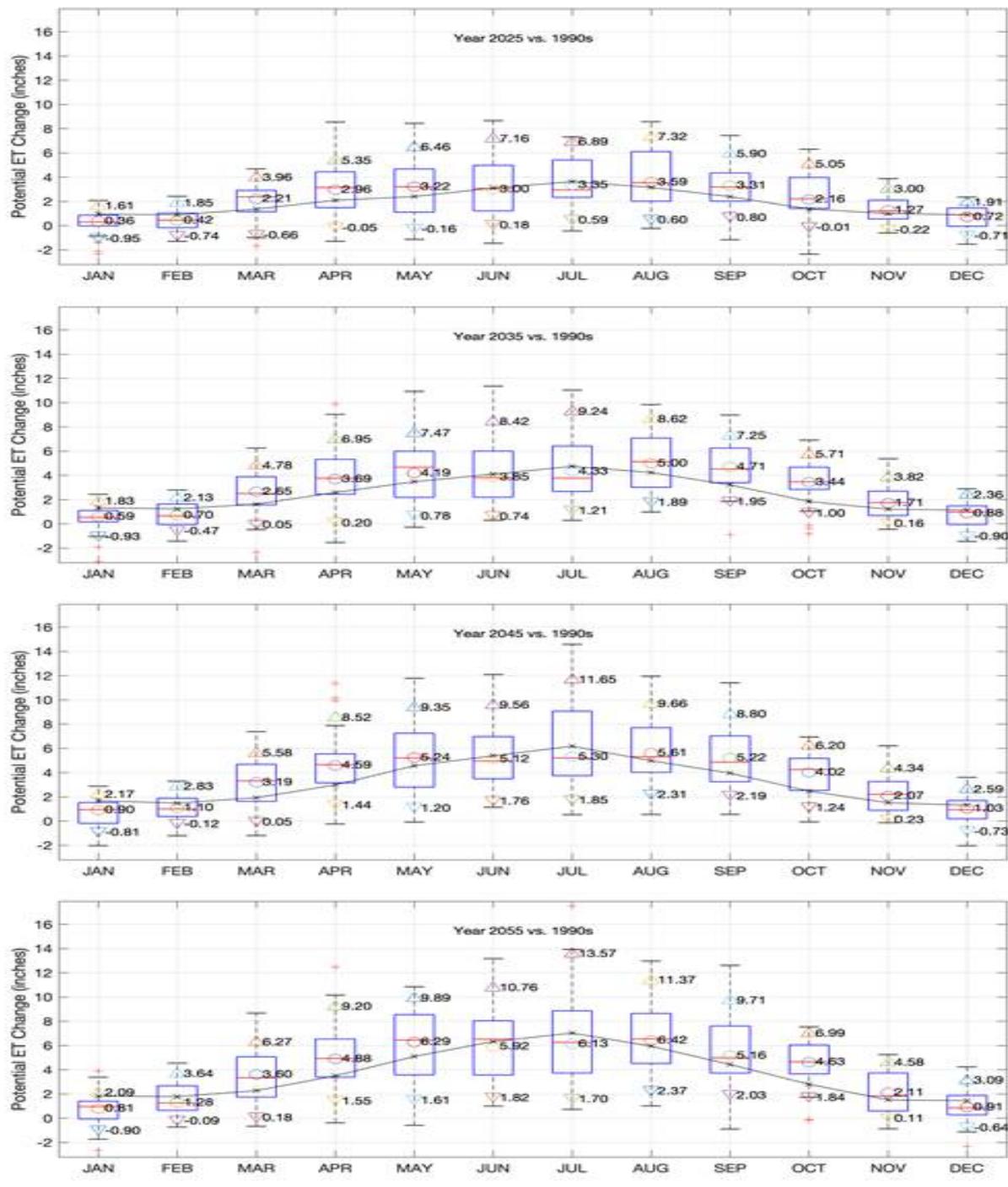
Figure 2-17: Monthly change in potential evapotranspiration for the Chesapeake Bay watershed is shown. The data are the same as in Figure 2-16 except the vertical axis is in inches rather than percent. Large percent differences during winter months are small absolute differences.
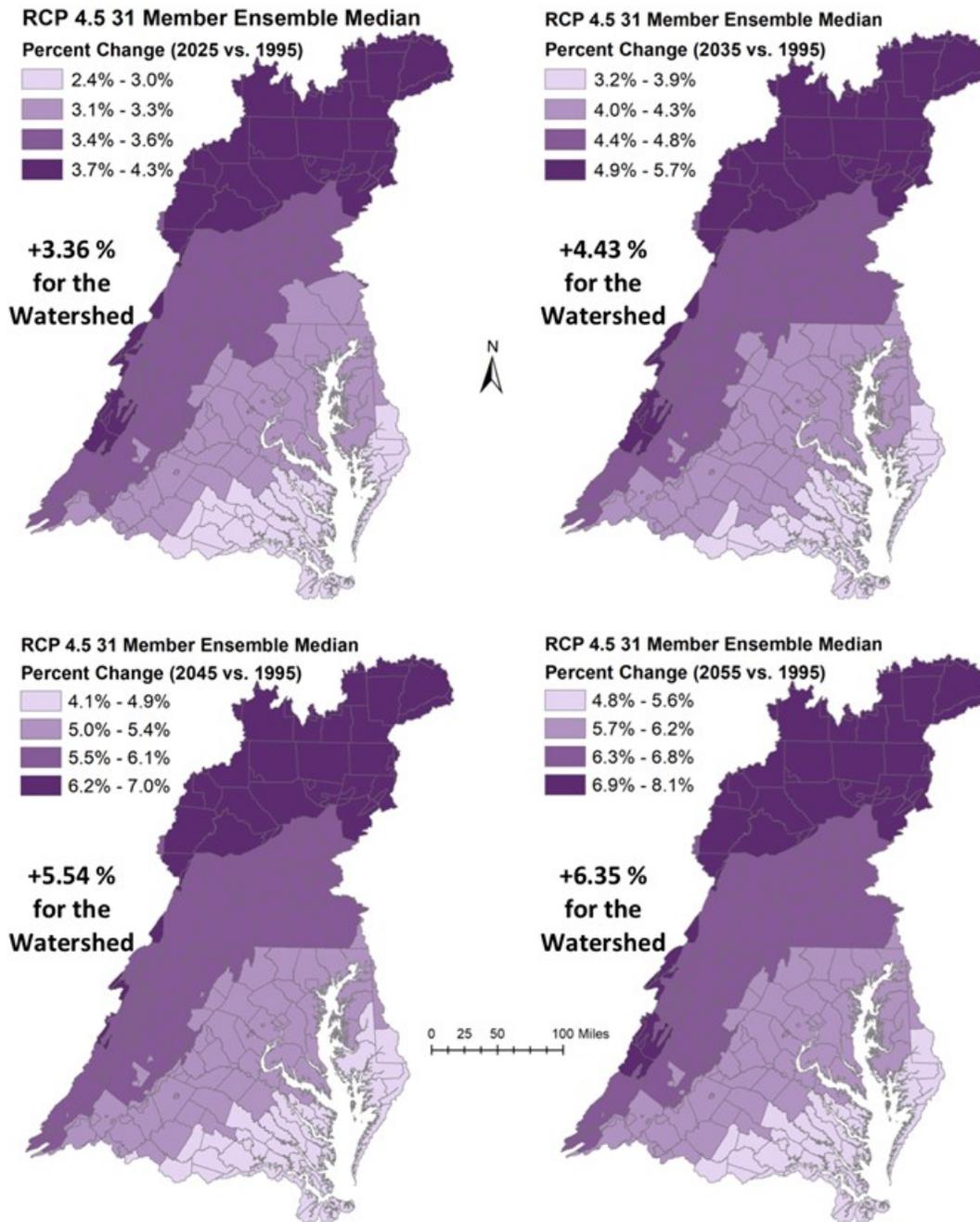
Figure 2-18: Estimated average annual change in potential evapotranspiration (as percent change) for the land segments (counties) in the Chesapeake Bay watershed are shown for 2025 (top-left), 2035 (top-right), 2045 (bottom-left) and 2055 (bottom-right). The change in potential evapotranspiration with respect to 1995 are based on a Hargreaves-Samani Method and 31-member ensemble median temperature change of downscaled Global Climate Models for RCP 4.5 scenario.

3 Nutrient Inputs Response to Climate Change

3.1 Atmospheric Deposition

Multiple data sources of the Chesapeake Bay watershed atmospheric nitrogen (N deposition) as well as analysis methods were used for investigating if and how atmospheric N deposition loads varied with changes in rainfall. Simple linear regressions were used for developing relationships (sensitives) that could be then applied for adjusting existing 1991-2000 atmospheric N deposition data to account for the effects of rainfall volume changes in climate change scenarios.

Atmospheric deposition is among the largest nitrogen inputs to the Chesapeake Bay watershed. The Community Multiscale Air Quality (CMAQ) model, which is the airshed model for Phase 6 Chesapeake Bay Program (CBP) modeling, and the National Atmospheric Deposition Program / National Trend Network (NADP/NTN) are some of the best available datasets for atmospheric N deposition. The Phase 6 estimations of atmospheric N deposition is a combination of a statistical regression model of wet N deposition (Grimm and Lynch 2000; 2005; Grimm 2016) and a continental-scale CMAQ Model application for estimates of dry N deposition (Bash et al., 2013). The daily precipitation nitrate and ammonium concentration models were developed using a linear least-square regression approach and single-event precipitation chemistry data from 85 NADP/NTN sites and Pennsylvania Atmospheric Deposition Monitoring (PADM) stations. The most significant variables in both models included precipitation volume, the number of days since the last event, seasonality, latitude, and the proportion of land within 8-km covered by forest or transportation and industry.

CMAQ data show an overall decreasing trend in total nitrogen deposition to the Chesapeake Bay Watershed (Figure 3-1). The proportion of dry and wet deposition of nitrate has decreased, whereas the proportion of dry and wet deposition of ammonium has increased. In Figure 3-1, the estimated total nitrogen deposition for 2002-2012 is based on CMAQ simulation using historical meteorology and emissions data. The current federal and state regulations are reflected in the projected regional emission in the CMAQ simulations and in the estimated N deposition for 2017, 2023, and 2028.

Campbell et al. (2019) evaluated the relative impacts of emission and climate changes on atmospheric nitrogen deposition for a recent historical period and a future period centered around 2050. Based on these historical and future simulations, they found that the climate influence on atmospheric nitrogen deposition was much smaller than the reductions due to emissions reductions. With the widespread decreases in anthropogenic nitrogen oxide and sulfur oxide emissions from combustion sources (de Gouw et al. 2014), and relatively constant ammonia emissions from agricultural and livestock sources (Li et al. 2016), the total average annual nitrogen deposition is estimated to decrease by 21% for the year 2050 as compared to that in 2011, where the oxidized nitrogen deposition decreased by 44% and reduced nitrogen deposition increased by 10% in the Chesapeake Bay watershed.
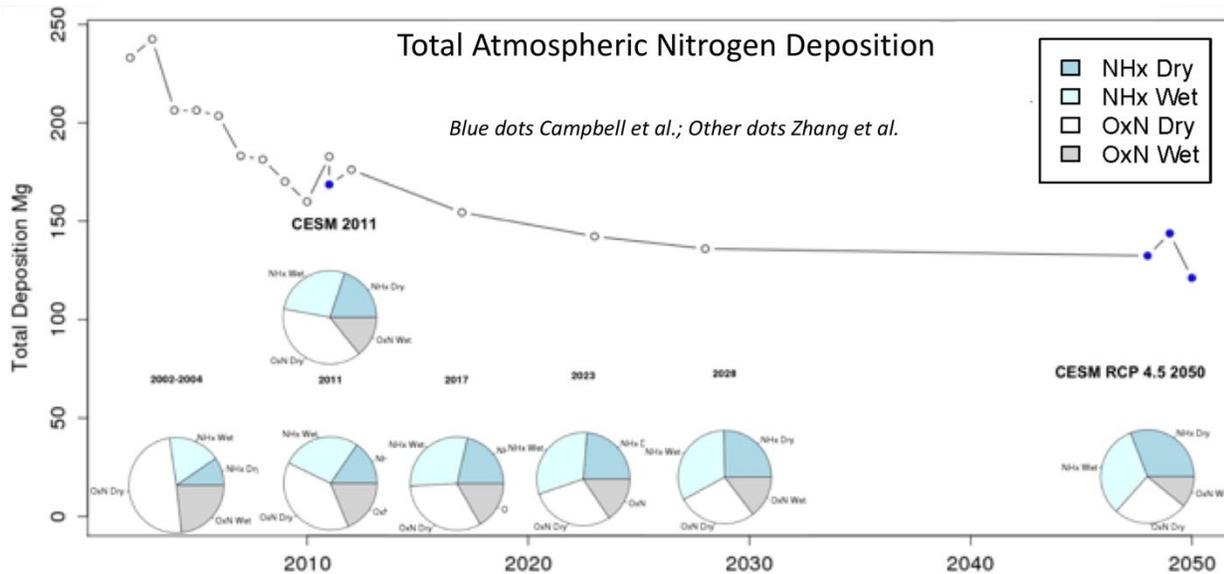
Figure 3-1: CMAQ estimated atmospheric N deposition and composition of wet and dry oxidized (OxN) and reduced (NHx) components. 2002-2011 is the historical CMAQ simulation, whereas estimates for 2017, 2023, and 2030 are based on "on the books" emission projections without considering any changes in climate. Blue dots show estimated total N deposition based on CESM dynamically downscaled meteorological data (adapted from Campbell et al., 2019).

Although the degree of change between the three climate conditions around 2050 were small, the CMAQ simulation results showed relatively lower N deposition for the dry condition (year) as compared to average (year), and more N deposition for the wet condition, suggesting changes in N deposition with climate and the degree of change in rainfall volume.

Encouraged by this CMAQ model response, detailed analyses of multiple data sources were performed to estimate the sensitivity of different atmospheric N deposition components with rainfall.

3.1.1 CMAQ – 2050 climate scenarios

Campbell et al. (2019) used climate projections from the Community Earth System Model (CESM) under the Representative Concentration Pathway 4.5 (RCP 4.5) scenario for simulating the atmospheric deposition under future climate with CMAQ. The climate projections where dynamically downscaled using the Weather Research Forecasting (WRF) Model. A linked system of WRF-CMAQ was used that features improved modeling of dry deposition. The emissions for the 2050 future scenario were based on federal and state regulations and measures for the year 2040 reference case (2040ref), which represent the impact of current "on-the-books" regulations without implementation of the heavy-duty vehicle greenhouse gas Phase 2 rule (EPA 2016c). The WRF-CMAQ model also featured a linkage with Environmental Policy Integrated Climate (EPIC) model for improved simulated changes to N deposition due to agricultural cropping management and soil biogeochemical processes. Estimated 2050 loads for the Chesapeake Bay watershed show a continued increase in the proportion of reduced N deposition driven by increases in ammonia emissions with temperature increase as well as decrease in oxidized nitrogen and sulfur dioxide emissions that lead to decreases in atmospheric aerosol causing faster deposition velocities for reduced ammonia. This change in reduced nitrogen deposition is due to the higher deposition rate for gaseous ammonia, which increased due to a lower atmospheric concertation of aerosols relative to particulate ammonium.

CMAQ 2050 simulations provide monthly estimates of N deposition loads and CESM rainfall for three years characterizing responses for average/moderate (2048), high/wet (2049), and low/dry (2050) climatic conditions (Figure 3-1). The monthly N deposition loads includes components of both wet and dry deposition for oxidized and reduced nitrogen forms.

Percent change were computed for N deposition and rainfall for the wet (2049) and the dry (2050) annual data with respect to that for the moderate (2048) year. The percent change in wet and dry deposition for nitrate and ammonium were plotting against percent change rainfall for all 235 counties in the Chesapeake Bay watershed as shown in Figure 3-2. Black lines connecting the wet and dry responses for different counties show a similar linear slope for both wet nitrate and wet ammonium deposition with rainfall. However, dry nitrate and dry ammonium deposition remained almost constant and did not show any sensitivity to changes in rainfall, suggesting climate alone did not have much of an impact on dry deposition.
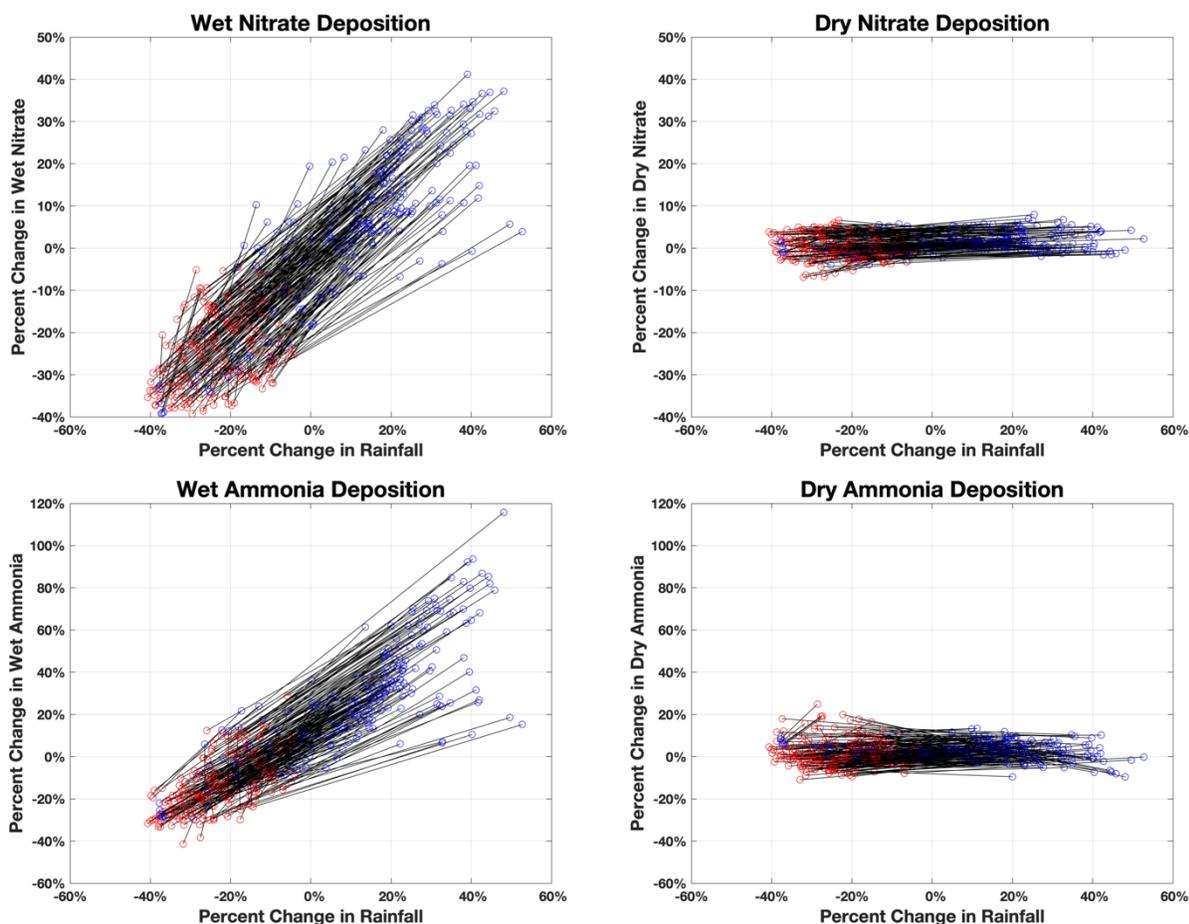
Figure 3-2: Percent change in N deposition with percent change in rainfall – (a) wet nitrate, (b) dry nitrate, (c) wet ammonium, and (d) dry ammonium. Pair of blue and red dots show percent change for a county in N deposition and rainfall for the high (2049) in blue and low (2050) in red annual data with respect to that for the average (2048) year. Black line

Although slope for changes in wet deposition with rainfall varied somewhat between counties but it did not show any specific spatial pattern across the watershed (Figure 3-3), suggesting that for most part the amount of change in wet deposition was similar throughout the watershed and primarily a function of changes in rainfall volume. The differences in the slope seen between the counties could be due to interaction of several factors including differences in precipitation intensity and seasonality, wind and storm patterns, distance from the emission sources (primarily

ammonia, sulfur oxide, and nitrate), scavenging and its impact on downwind availability of nutrients in the atmosphere.
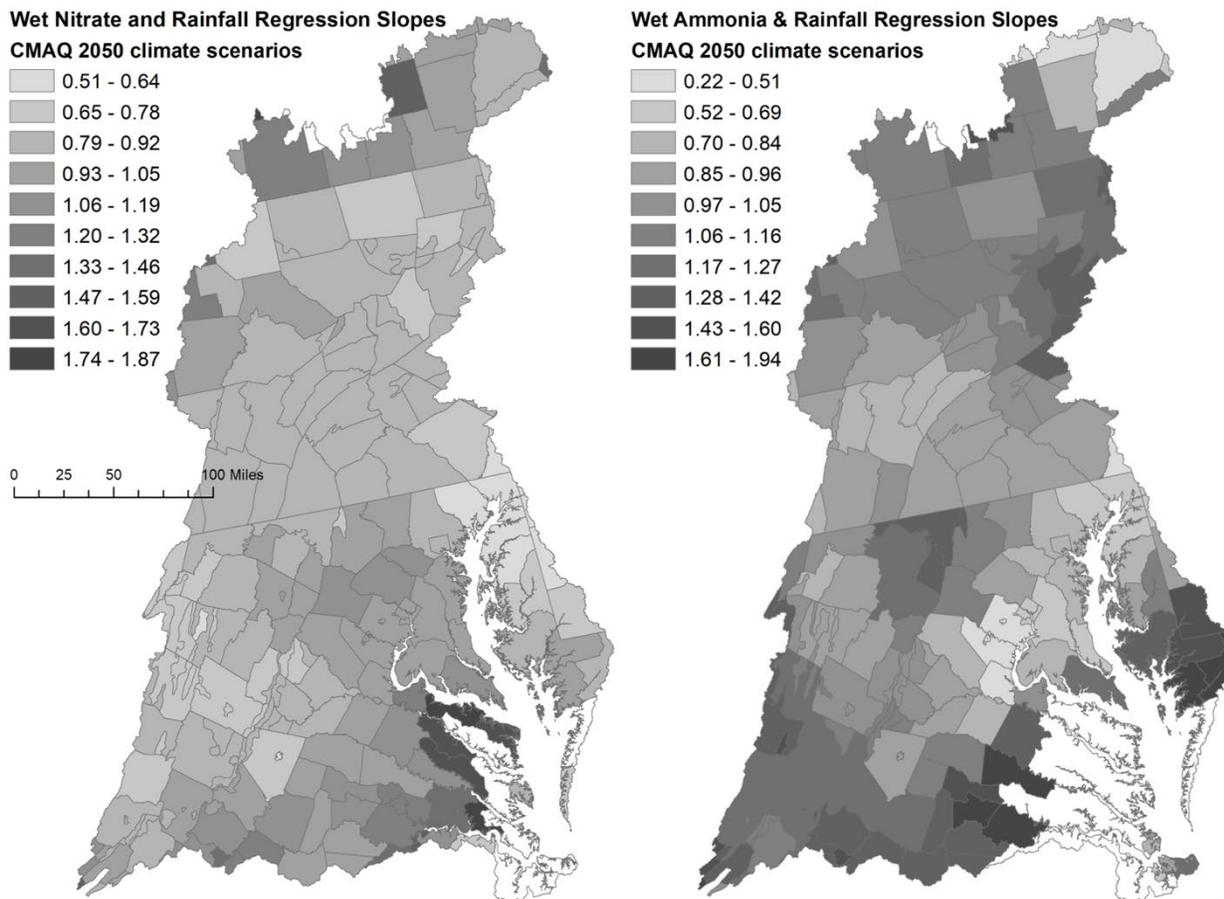
Figure 3-3: Percent change in wet N deposition with percent change in rainfall volume for the land segments . Although the slope varied with land segments it did not show any specific spatial pattern.

Boxplots in the Figure 3-4 show the distribution of slopes between 235 Chesapeake Bay watershed counties for the wet nitrate and ammonium deposition. Higher rates of wet deposition require the colocation of high atmospheric concentration from high emissions and high precipitation events. The differences in the slopes are likely due to differences in the seasonality and intensity of the projected precipitation changes and the spatial and temporal distribution of emission sources in the watershed counties. The median slope for the percent change in wet nitrate and wet ammonium with percent change in rainfall volume were 0.901 and 1.096, respectively.
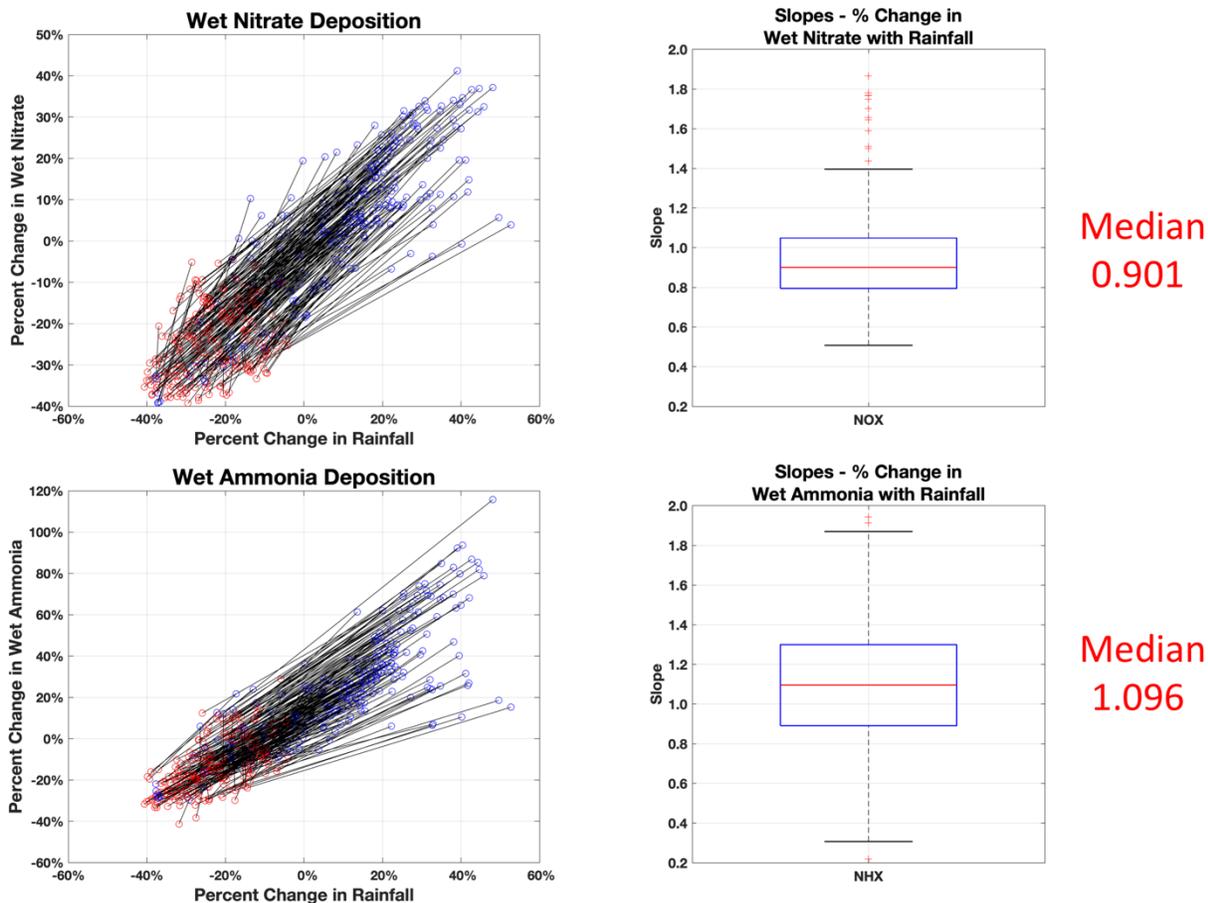
Figure 3-4: Percent change in wet nitrate and wet ammonium with changes in rainfall volume. Box plots show distribution of slopes for 235 counties in the Chesapeake Bay watershed. Median slopes were 0.901 and 1.096 for wet nitrate and wet ammonium respectively.

3.1.2   Phase 6 Chesapeake Bay Program Airshed Model

Wet atmospheric deposition data estimates from Phase 6 Chesapeake Bay Program airshed model were analyzed in two phases. As shown in Figure 3-5, Phase 6 atmospheric deposition data were available in two different forms – (a) an N deposition time series that included interannual variability in deposition due to both climate as well as emissions – i.e. non-detrended data, and (b) an N deposition time series where annual trends due to emissions were removed and therefore included the variability due climate alone – i.e. detrended data. These two Phase 6 data products are used in the Chesapeake Bay Program modeling for different purposes.

In the first phase, similar to the 2050 CMAQ data analysis, both non-detrended and detrended Phase 6 data were analyzed in pairs of 3 consecutive annual data points. Consecutive years were selected to minimize any differences in non-detrended data due to changes in emissions. Four different periods were selected where the differences in annual rainfall were sufficient and appropriate enough to categorize them as average (moderate), high (wet), and low (dry) years. Median slopes for wet nitrate and ammonium for these periods have shown in Table 3-1. All four periods showed a positive relationship for wet nitrate and wet ammonium with changes in rainfall. Although median slopes in Table 3-1 for both non-detrended and detrended data are similar to ones obtained earlier from the 2050 CMAQ data but it indicated that the median slope

varied with the selection of period, potentially due to drivers such as wind and atmospheric chemistry among others.
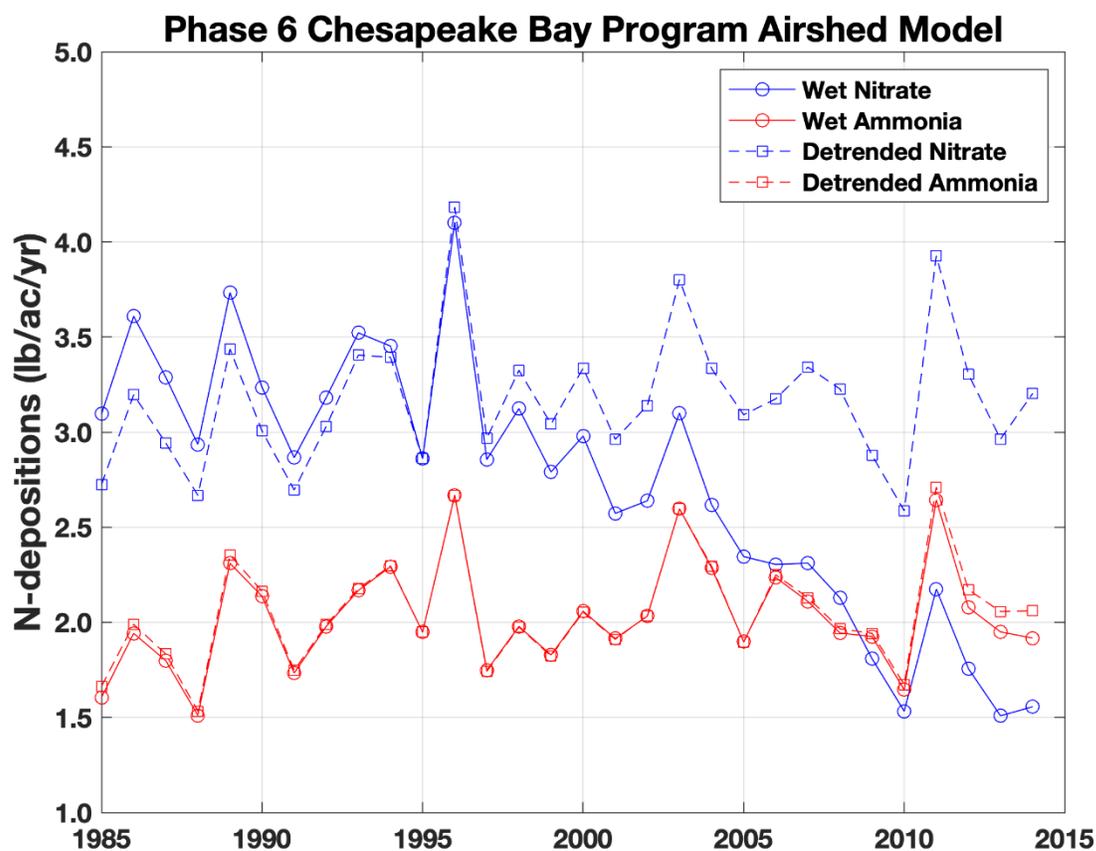
Figure 3-5: Phase 6 Chesapeake Bay Program Airshed Model estimates of wet deposition of nitrate and ammonium to the Chesapeake Bay watershed. Data shown with solid lines include interannual variability due to both climate and emissions, whereas the influence of emissions trends were removed in the ones shown with dotted lines.

Table 3-1: Median slopes for wet nitrate and wet ammonium deposition for the 235 counties in the Chesapeake Bay watershed.

Dry-Avg-Wet Years	Non-detrended		Detrended	
	Nitrate	Ammonium	Nitrate	Ammonium
1988-1987-1989	0.946	2.070	0.977	2.005
1995-1993-1994	0.854	0.748	0.781	0.763
2001-2002-2003	0.341	0.559	0.442	0.569
2010-2009-2011	1.322	2.547	1.773	2.580
Average	0.866	1.481	0.993	1.479

In the second phase, analysis was conducted using the detrended Phase 6 atmospheric deposition data for a longer 10-year period. As mentioned earlier the effect of changes in emissions were removed in detrended data therefore the variability in interannual loads were primarily due to annual rainfall. Furthermore, it was presumed that the longer period will overcome some of the limitations and anomalies in the previous analyses based on data for just 3 years. Percent change in 1991 to 2000 annual wet nitrate and ammonium data for the land segments (counties) with respect to average annual data are shown in Figure 3-6. Linear regression lines for every county based on 10 annual data points are also shown. Similar to the CMAQ data regression analysis described earlier, the detrended Phase 6 data showed some degree of variability in slopes between counties, with median slopes of 0.770 and 0.837 for wet nitrate and ammonium, respectively. It is noted that these median slopes are smaller as compared to that obtained from the CMAQ 2050 data. The longer-term second phase results were used in the final recommendation in Section 3.1.5 rather than the shorter-term results as more comprehensive and robust findings.
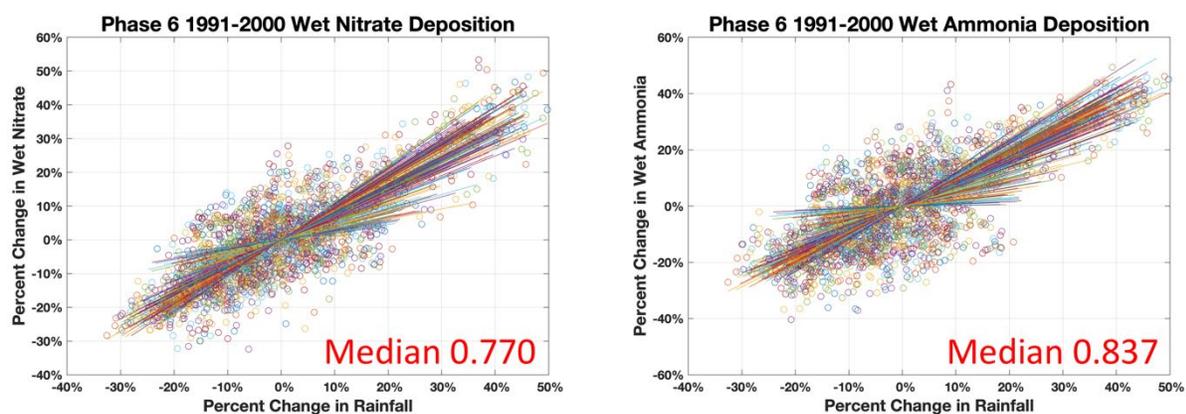
Figure 3-6: Percent change in wet nitrate and wet ammonium with changes in rainfall volume for 235 counties in the Chesapeake Bay watershed based on Phase 6 annual detrended data for 1991-2000. Median slopes of 0.770 and 0.837 for wet nitrate and wet ammonium respectively were smaller than that from CMAQ 2050 data.

3.1.3   NADP wet deposition estimates

National Atmospheric Deposition Program (NADP) is a network of monitoring stations across that United States where long term precipitation chemistry data is collected. The program provides one of the best available sources of observation-based data for amount, trends, and geographic variability in precipitation chemistry data (acids, base cations, and nutrients).

Time series data for rainfall and precipitation chemistry data for a total of 322 NADP/NTN stations were obtained (http://nadp.slh.wisc.edu/data/ntn/). Wet nitrate and wet ammonium data for a total of 25 NADP monitoring stations in the Chesapeake Bay watershed, and 70 NADP monitoring stations in the Chesapeake Bay airshed were analyzed (Figure 3-7).
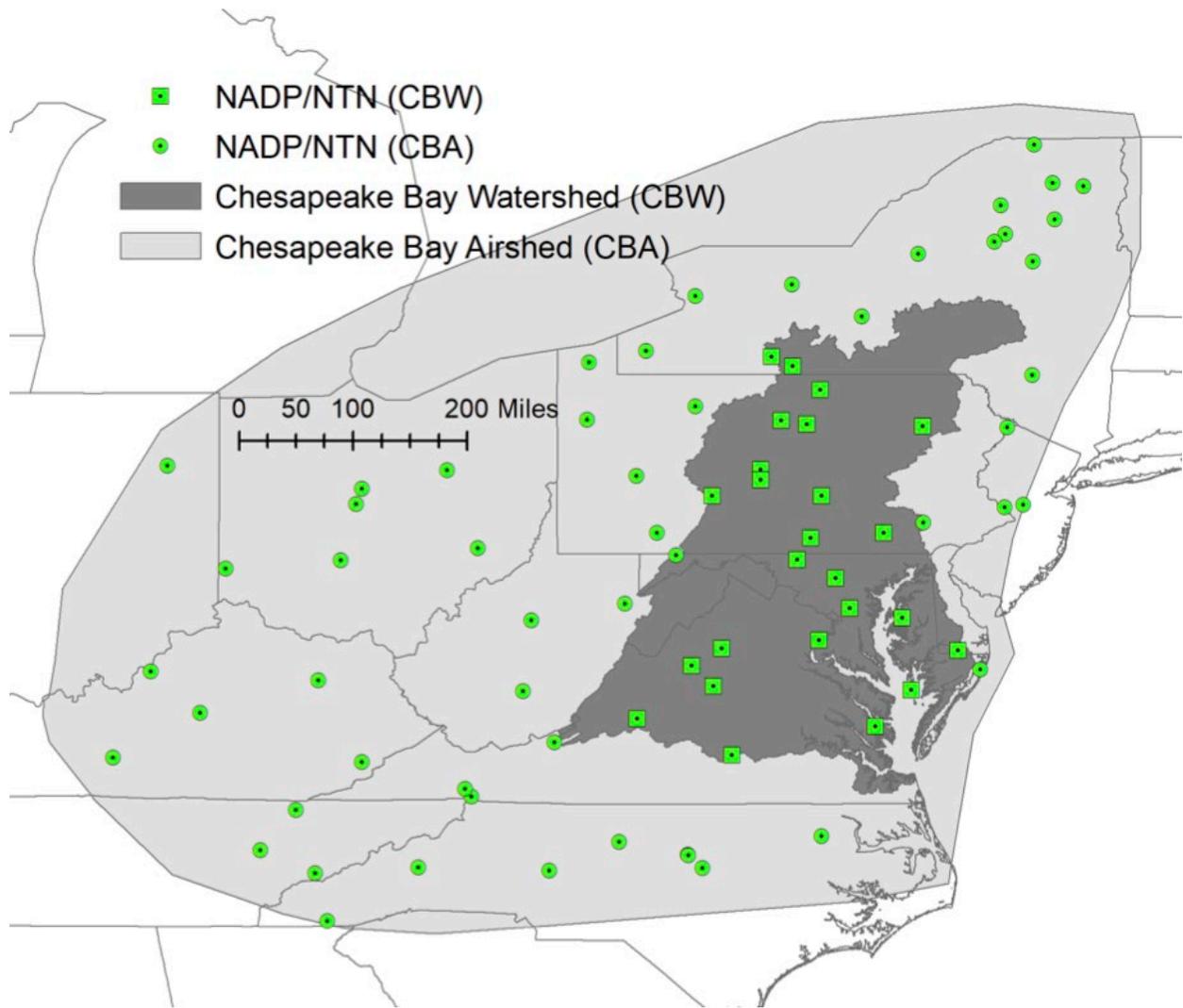
Figure 3-7: NADP monitoring stations in the Chesapeake Bay watershed and Chesapeake Bay airshed that were analyzed.

Available rainfall, wet nitrate, and wet ammonium data were pre-processed and aggregated at annual time step for the analysis. Annual data for the station with respect to station specific long-term average have been shown in the Figure 3-8 and Figure 3-9 for the 25 monitoring stations in the Chesapeake Bay watershed and 79 stations in the airshed, respectively. The median slopes obtained based on the stations in watershed and in airshed were almost the same (Figure 3-8 and Figure 3-9).
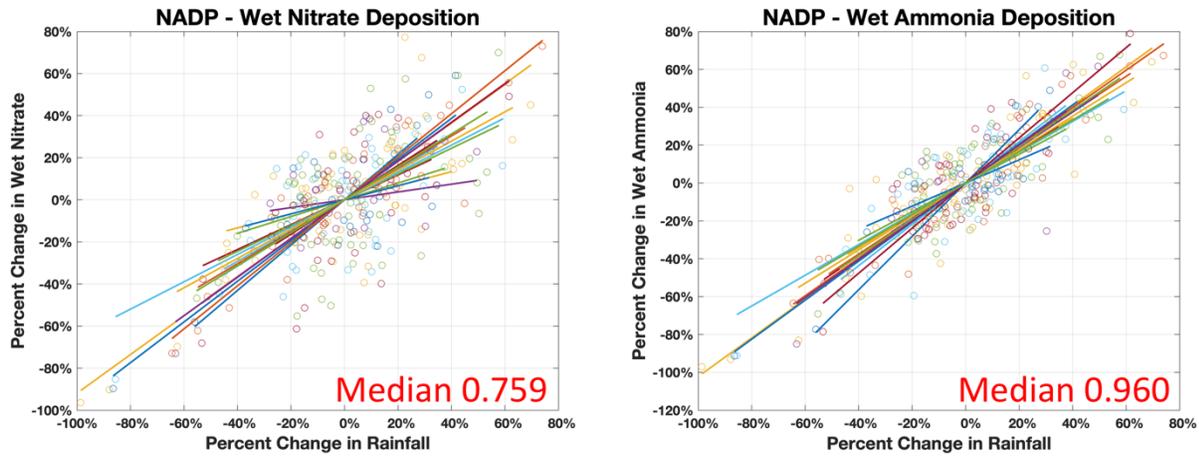
Figure 3-8: Percent change in wet nitrate and wet ammonium with changes in rainfall volume based on 25 NADP monitoring stations in the Chesapeake Bay Watershed. A specific color represents one of the 25 monitoring stations, where dots of same color show annual data points.
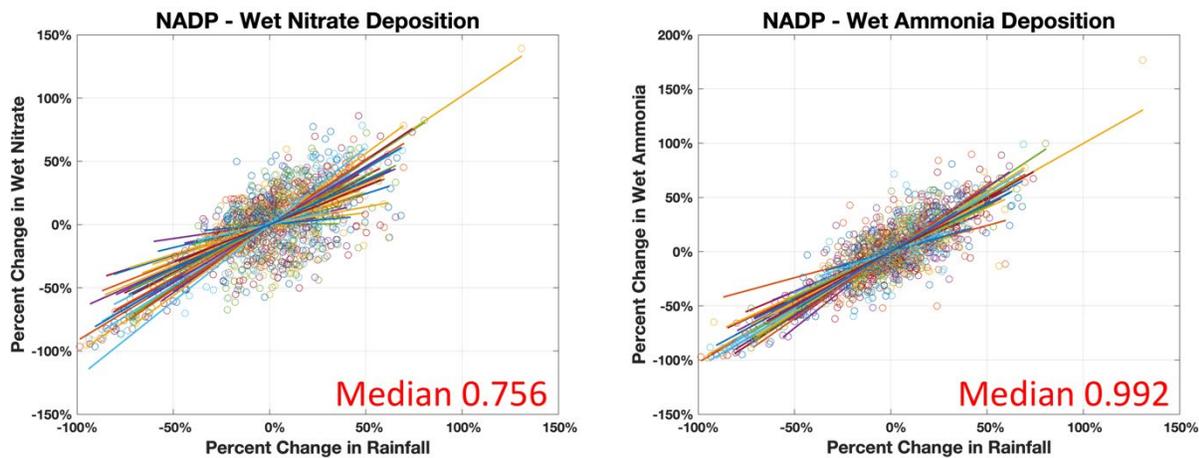
Figure 3-9: Percent change in wet nitrate and wet ammonium with changes in rainfall volume based on 79 NADP monitoring stations in the Chesapeake Bay Airshed. A specific color represents one of the 79 monitoring stations, where dots of same color show annual data points.

3.1.4   Organic nitrogen

Phase 6 airshed model uses 0.080 mg/l for spring (April, May, and June), and 0.040 mg/l for non-spring months as the organic nitrogen concentrations in the precipitation. The organic nitrogen is only deposited to the water bodies in the watershed. Due to the lack of any additional information, the same concentrations are used for the climate change scenarios, which would result in a proportional increase in loads from the water load sources with increase in rainfall volume and vice versa.

3.1.5   Summary and synthesis

Multiple data sources of atmospheric N deposition were analyzed from a physically-based CMAQ 2050 climate simulation, a statistical model-based Phase 6 data set, and observation-based estimates for NADP monitoring stations. Wet deposition of nitrate and ammonium showed a positive linear relationship with rainfall and dry deposition did not show much sensitivity to

rainfall. The slope of a linear regression between percent change in wet deposition and percent change in rainfall volume showed some variability between land segments (counties) but a clear spatial pattern was not found.

Table 3-2: Median sensitivity slopes for percent change in wet nitrate and wet ammonium with percent change in rainfall volume from multiple data sources including physics based model, statistical model, and observations.

Data Source	Wet Nitrate	Wet Ammonium
CMAQ 2050 Simulation	0.901	1.096
Phase 6 CBP Airshed Model	0.770	0.837
NADP Wet deposition – Chesapeake watershed	0.759	0.960
NADP Wet deposition – Chesapeake airshed	0.756	0.992
Rounded Average	**0.8**	**1.0**

The median sensitivity slopes from the analyses are summarized in Table 3-2. The median slope of wet ammonium was higher than the median slope of wet nitrate (Table 3-2). Some plausible drivers for this behavior could be (a) differences in the seasonality of nitrate and ammonium, where ammonium wet deposition peaks in the spring while nitrate wet deposition peaks in Mid-Summer; (b) feedbacks between cropping system ammonia and nitrate emissions and precipitation, though these are small as compared to other sectors, e.g., animal and mobile sources.

By suggestion of the Modeling Workgroup, the rounded average of the median slopes obtained from the analyses of different data sources was adopted as the *sensitivity* of wet deposition and used for adjusting wet deposition to the watershed and estuarine open waters with changes in rainfall volume (Table 3-2). The sensitivity (i.e. percent change in wet deposition with percent change in rainfall volume) of less than 1, 0.8 for wet nitrate deposition, suggests an overall decrease in concentration with increase in rainfall volume and vice versa. This is expected due to the scrubbing of the atmosphere from precipitation events, e.g. a wetter year will remove more nitrate mass from the atmosphere than a dry year, and the emissions are relatively constant year to year for the largest emission sectors.

3.2   Land Use

Climate and land use are linked in complex ways – land use choices have effects on the release of greenhouse gasses, climate trends can affect human choices about land cover and land use, and both can be driven by the same societal choices.

Climate change may result in a change in the frequency and severity of droughts, heat waves, tropical storms and other weather hazards which may affect the patterns of development. Additionally, agriculture will react by planting a different combination of crops more suited to the future weather patterns. (Grimm, et al 2013, Brown, et al 2014, Kutta and Hubbart, 2019)

Climate and land use are both changing through time; however, they are not the primary drivers of each other at the scale of the Chesapeake watershed. Land use changes in the watershed would have a small effect on the global carbon budget and the primary drivers of land use change within the Chesapeake are based on the local economy, regulation, conservation, and other factors that are not primarily driven by climate change.

Although the climate effect on land use change is likely small, the effect is already subsumed within the land use data set that has been developed by the CBP land data team detailed in Section 5 of the CAST documentation (CBP 2017). The land use data set is provided from 1985 through 2017 and projected through 2025 using trends and population projections that are based on observations occurring during a period of climate change, and therefore climate-induced changes in land use are already included in the data set. Climate effects are not separable from land use changes from other drivers, however. Land use projections will be provided through 2050. Climate effects will be included in these estimates to the extent that they are a continuation of current trends in land use.

3.3   Agricultural Inputs

Agricultural practices are highly dependent on expected weather and therefore will change in response to climate trends. Alterations in production due to climate have already occurred and have been estimated in the literature (e.g. Gammas et al, 2017). The National Climate Assessments (Hatfield et al, 2014, Gowda, et al, 2018) found that increased climate stressors such as droughts, extreme precipitation, and extreme temperatures will likely have negative effects on production systems. Other studies have found beneficial effects of increased carbon dioxide concentrations (e.g. Deryng et al, 2016). Meanwhile adaptations in cropping methods and technologies tend toward increasing agricultural yields in the Chesapeake region.

The CBP uses data from the census of agriculture (e.g. USDA-NASS 2014) and other sources (CBP 2017, Section 3) to estimate changes in production systems, animal populations, and yields through years of interest. The 2017 census of agriculture will be projected through 2022 and held constant for future years according to methods approved by the CBP partnership (CBP 2017, Section 3). The observed changes to agriculture in the census include changes due to climate, although the CBP does not break out agricultural change due to climate specifically. Currently, no method has been identified to include climate influences in land use or agricultural projections to 2035, 2045, and 2055. In their July 16, 2019 meeting, The Modeling Workgroup encouraged further work by the partnership for 2035, 2045, and 2055.

3.4   Direct Loads

3.4.1   Combined Sewer Overflows

Changes in Combined Sewer Overflow (CSO) volumes expected because of climate change were obtained by first estimating the expected changes in rainfall volume and intensity under a set of climate change scenarios and then using an empirical regression between rainfall and daily CSO volume. This regression was developed by Tetra Tech and previously used to estimate CSO inputs for the Phase 6 Watershed Model (see Section 8 of the Phase 6 CAST and Watershed Model documentation, Chesapeake Bay Program 2017).

Projected changes in average monthly volumes of rainfall for different climate change scenarios (2025, 2035, 2045 and 2055) were obtained through a combination of observed long-term historical trends in local rainfall and results from climate models as described in detail in Section 2.1. For each climate change scenario, the overall change in rainfall volume projected in each month was distributed across the historical (1991–2000) daily precipitation events exceeding 0.01 inches occurring in that month. As described in more detail in Section 2.1, the projected change in rainfall volume was not distributed uniformly across all daily precipitation events. Instead, the set of precipitation events > 0.01 inches occurring in each month was divided into deciles, and precipitation events falling into the highest deciles were assigned a larger fraction of the overall rainfall change projected for that month. For example, if a climate change scenario predicted a 3% increase in rainfall volume for the month of March and the observed rainfall volume for March in 1991-2000 was 7 inches, then 7 inches x 3% = 0.21 inches of total rainfall volume should be added to March rainfall. This added volume is distributed unevenly across rainfall deciles, with events falling in the highest decile of the distribution for March precipitation events receiving around 65% of 0.21 inches, events falling in the second highest decile receiving around 10% of 0.21 inches and events falling in smaller deciles receiving the remaining amount of volume. This approach was designed to account for the fact that previous literature has shown uneven increases in precipitation events in this area, with larger rainfall events increasing more compared to smaller ones (Groisman et al. 2004). As described in Section 2.1, climate-driven changes in monthly rainfall volumes vary geographically, and as a result, CSO service areas received somewhat different projected rainfall changes depending on their location in the watershed.

After generating new time series (1991–2000) of daily precipitation events for each CSO service area and for each climate change scenario, an empirical regression between CSO volume and rainfall previously developed by Tetra Tech (Figure 8-5 in Section 8 of the Phase 6 CAST and Watershed Model documentation, Chesapeake Bay Program 2017) was applied to obtain projected CSO volumes under each climate change scenario. For four CSO communities, historical CSO volumes in 1991-2000 were not originally estimated using the Tetra Tech regression because those facilities submitted their own volume data. For these communities, site-specific empirical regressions were developed that captured the relationship between CSO volume and rainfall (*Figure 3-10*), and these site-specific regressions were used instead of the Tetra Tech regression to estimate predicted CSO volumes under climate change scenarios. The four communities for which this approach was used were Washington DC (DC0021199), Lynchburg, VA (VA0024970), Richmond, VA (VA0063177) and Alexandria, VA (VA0087068).
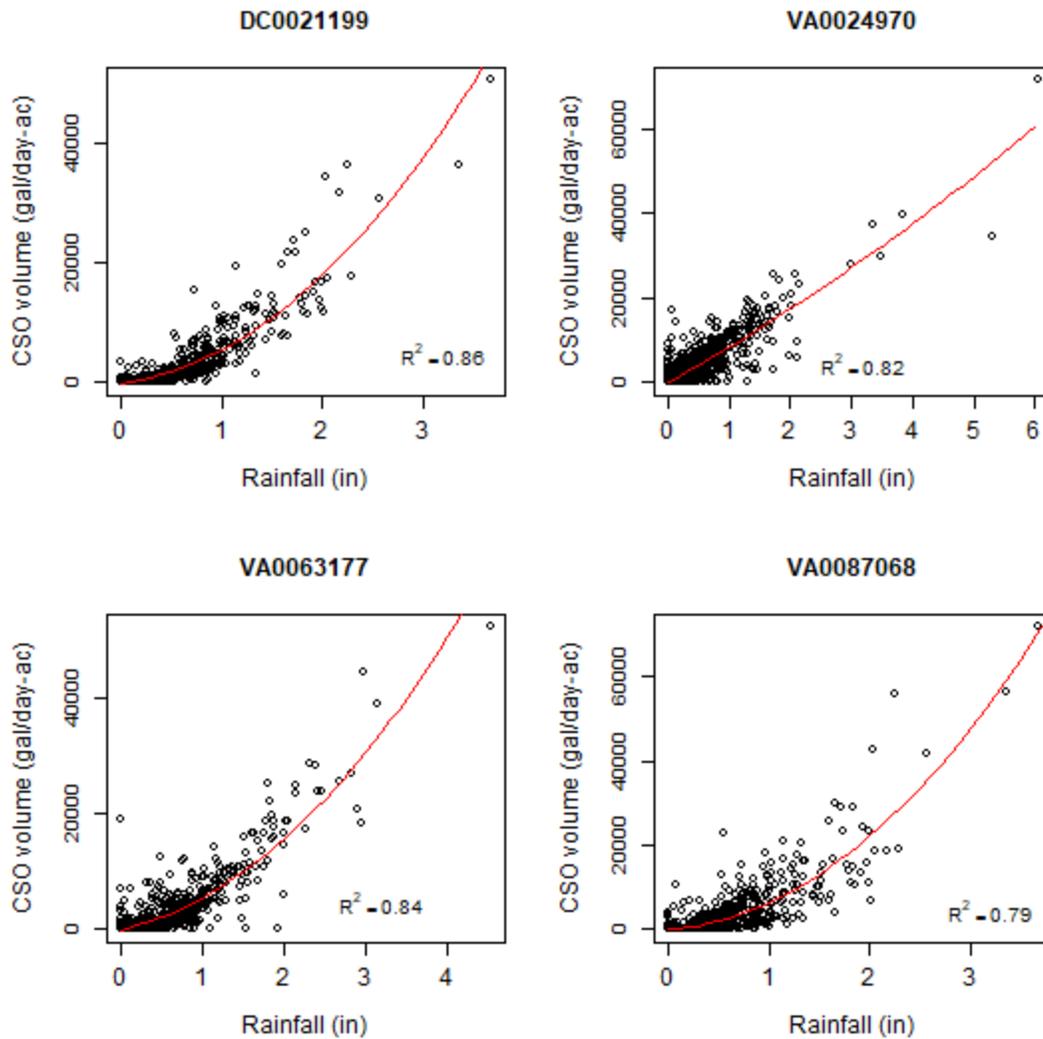
Figure 3-10 Relationship between daily CSO volume per unit area and rainfall at four communities that provided CSO volume data over the period 1991-2000. DC0021199: Washington, DC; VA0024970: Lynchburg, VA; VA0063177: Richmond, VA; VA0087068: Alexandria, VA

Loads of constituents were calculated by multiplying CSO volumes by event mean concentrations (EMC) derived from observations or literature as described in Section 8.5 of the Phase 6 CAST and Watershed Model documentation. Note that because constituent loads are estimated by multiplying CSO volumes by fixed EMC values, for each service area percent changes of constituent loads are identical to percent changes of CSO volumes.

With respect to the 1991-2000 reference period, the estimated average annual percent change in precipitation volume across all CSO service areas was 2.91% under 2025 conditions (estimated through extrapolation of long-term trends), and 4.09, 5.02 and 6.24% under 2035, 2045 and 2055 conditions, respectively (estimated from an ensemble of GCMs).

The corresponding estimated percent changes in average annual CSO volume are reported in *Figure 3-11*. *Figure 3-12* shows time series of total annual CSO volumes estimated for the period 1991-2000 and used for model calibration, together with the corresponding annual values

projected under different climate change scenarios. Finally, *Table 3-3* and *Table 3-4* summarize estimated CSO-derived TN and TP loads under different climate change scenarios broken down by state.

Figure 3-11 Estimated percent change in total CSO volume under different climate change scenarios. Reference period: 1991 – 2000

Figure 3-12 Time series of total annual CSO volume across all 64 communities in the Chesapeake Bay watershed. The darkest green line corresponds to CSO volumes 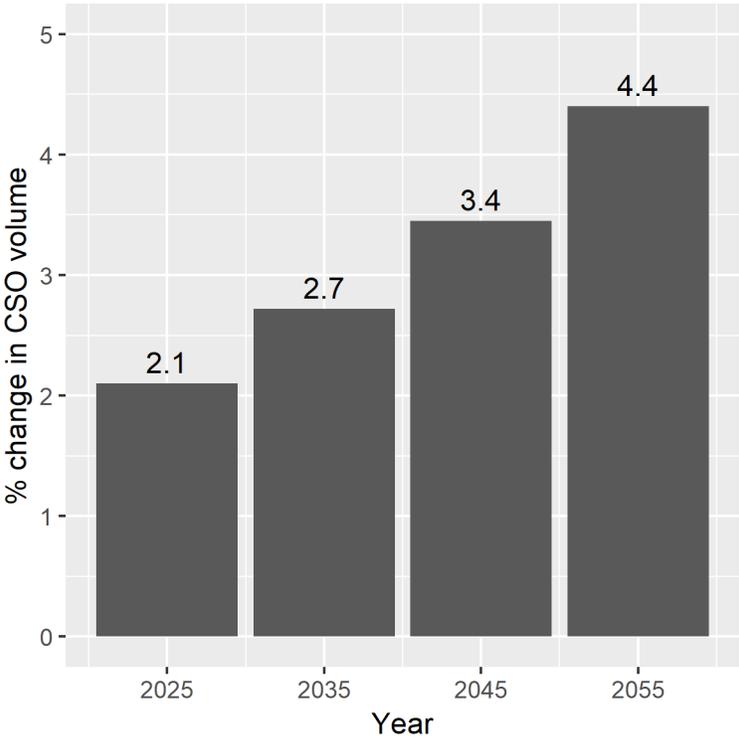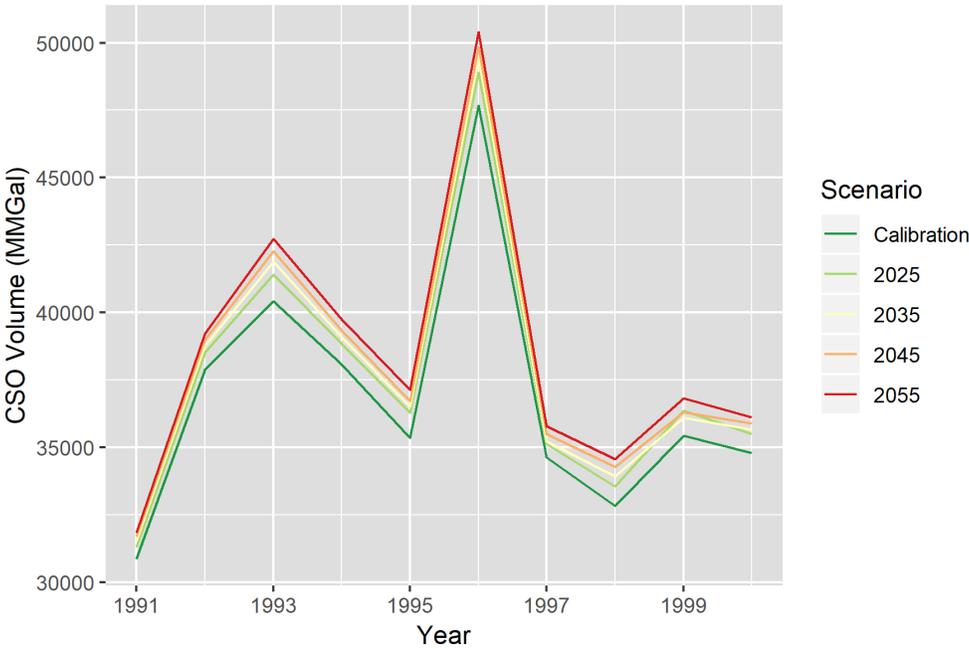used during model calibration, while other lines illustrate the estimated CSO volumes under different climate change projection years

Table 3-3 Mean annual TN loads (Lbs/yr) from CSOs estimated for the historical period 1991-2000 and a set of climate change scenarios

State	# Facilities	1991 – 2000	2025	2035	2045	2055
DC	1	87,414	92,182	93,453	94,890	97,651
DE	1	2,318	2,348	2,350	2,375	2,411
MD	10	31,072	31,675	31,828	32,035	32,465
NY	3	212,015	216,215	217,159	217,419	217,976
PA	40	1,629,861	1,657,892	1,664,987	1,671,681	1,682,526
VA	4	307,901	317,311	322,045	329,372	335,453
WV	5	62,752	63,879	64,317	64,888	65,570

Table 3-4 Mean annual TP loads (Lbs/yr) from CSOs estimated for the historical period 1991-2000 and a set of climate change scenarios

State	# Facilities	1991 – 2000	2025	2035	2045	2055
DC	1	18,599	19,613	19,884	20,189	20,777
DE	1	290	293	294	297	301
MD	10	3,609	3,680	3,698	3,722	3,772
NY	3	26,502	27,027	27,145	27,177	27,247
PA	40	257,694	261,753	262,907	264,028	265,594
VA	4	38,532	39,711	40,303	41,220	41,982
WV	5	7,844	7,985	8,040	8,111	8,196

It can be shown from the data in Table 3-3 and Table 3-4 that DC and VA have a higher sensitivity to climate based on this calculation. It should be noted that the estimates from DC and VA are based on much better data than other jurisdictions and it should not be interpreted to mean that climate change effects are worse in DC and VA. The estimates from other jurisdictions would likely benefit from better data collection.

3.4.2   Other direct loads

Wastewater treatment plants (WWTPs) may experience operational changes due to climate change. Changes in water use and supply may have an effect on the influent concentrations expected. Increases in influent temperature lead to increased reaction rates associated with biological nutrient removal. However, operators of plants are largely able to control effluent concentrations by altering their processes to meet permit limits. Given the existing permit limits that are expressed in the WIPs, it is unlikely that climate change will have an effect on the effluent of WWTPs in the Chesapeake. Moreover, any changes in wastewater loads due to climate change are already factored into the data supplied to the CBP from 1985 through 2017. Similarly, data for septic systems, rapid infiltration basins, and diversions are inclusive of the period 1985 through the mid-2010s, capturing most of the effects of climate change through 2025. No method has been determined to project climate effects on these systems through 2050.

4 Watershed Model Response to Climate Change

Section 2 discussed the calculation of precipitation, temperature, and carbon dioxide changes between the Chesapeake TMDL averaging period of 1991-2000 and future climate scenarios centered around 2025 and 2050. Section 3 discussed changes in nutrient inputs and land use changes. This section discusses simulated watershed responses to the climate-modified inputs. Watershed responses are represented in Figure 4-1 as sensitivities, BMPs, and the three watershed delivery factors – Land to Water, Stream Delivery, and River Delivery.

4.1 Simulation of CO_2 Concentration Response

The HSPF model structure does not provide a direct mechanism for simulating the impact of CO_2 on water budget through stomatal resistance and decreased plant evapotranspiration. However, Butcher et al. (2014) documents necessary adjustments to HSPF LZETP parameter that can

Figure 4-1: Phase 6 model structure

be used for the simulation of CO2 effects on plant stomatal resistance in HSPF and subsequently on the lower vadose zone evapotranspiration. Accordingly, the monthly LZETP parameter was modified to simulate the effect of increasing CO_2 concentrations as a result of continuing projections of atmospheric contributions from anthropogenic sources.

PETfactor = AET_1 / AET_0

Where,

PETfactor = ratio of actual ET (AET) under new CO2 level and reference

For HSPF: $PETfactor = \frac{1/(1-LZETP_1)}{1/(1-LZETP_o)}$

$LZETP_1$ = Max { $1 - (1 - LZETP_0)$ / PETfactor, 0.01 }

Equation 4-1

Where,

LZETP = HSPF lower zone ET parameter

For Penman Monteith: $PETfactor = \frac{1/\{\Delta+\gamma(1+r_{s1}/r_a)\}}{1/\{\Delta+\gamma(1+r_{s0}/r_a)\}}$

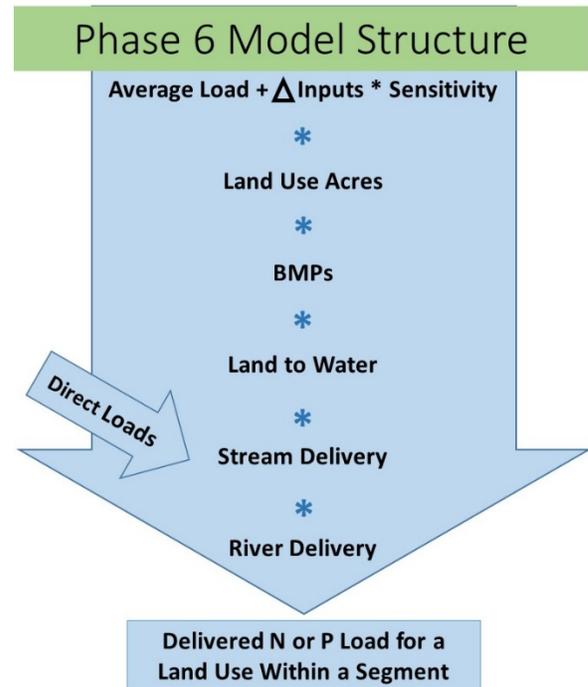$$PETfactor = \frac{(\Delta + \gamma)r_a + \gamma r_{s0}}{(\Delta + \gamma)r_a + \gamma r_{s1}}$$

$$\Delta = \frac{4098 \times \left[0.6108\, exp\left(\frac{17.27T}{T + 273.3}\right)\right]}{(T + 273.3)^2}$$

$$\gamma = 0.673645 \left(\frac{293 - 0.0065z}{293}\right)^{5.26}$$

T = air temperature (monthly), °C

z = elevation, meter

$$r_{s0} = \frac{r_l}{.5\, LAI} = \frac{100}{.5 \times 24 \times 0.12} = 70$$

$$r_{s1} = \frac{r_l}{.5\, LAI \left(1.4 - 0.4\frac{CO_2}{330}\right)} = \frac{100}{.5 \times 24 \times 0.12 \left(1.4 - 0.4\frac{CO_2}{330}\right)} = \frac{70}{\left(1.4 - 0.4\frac{CO_2}{330}\right)}$$

$$r_a = \frac{208}{u}$$

u = wind velocity (monthly), m/s

4.2 Simulation of Hydrology

A new set of precipitation, temperature, potential evapotranspiration, and modified LZETP parameters are inputs for the climate change scenarios. The impact of these climate change variables on the hydrologic response is simulated by the HSPF PWATER, IWATER, SNOW, and HYDR modules for the Phase 6 model. This approach is same as the one used in Phase 5 climate change simulation.

HSPF hydrologic simulation for climate change respond to changes in (a) rainfall volume and rainfall intensity, (b) potential evapotranspiration, (c) CO_2 level, and (d) temperature inputs. Changes in temperature inputs influence snow hydrology by introducing changes in the amount of snow and energy balance for the snowpack. Changes in potential evapotranspiration and adjustments for CO2 level influence the evapotranspiration calculations, subsequently impacting the simulated water budget.

4.3 Simulation of Sediment Loss

The impact of climate change on the sediment transport is simulated by HSPF SEDMNT, SOLIDS, and SEDTRN modules subroutines for the Phase 6 model. This approach is same as the one used in Phase 5 climate change simulation.

HSPF uses a process-based approach for the production and removal of sediment. The land surface erosion of sediment includes processes for detachment by net rainfall, attachment on days without rainfall, and removal by surface outflow.

As shown in Equation 4-2, the detachment of sediment particles (DET) is simulated due to kinetic energy of falling rain ($RAIN$), which are then available for transport. Changes in rainfall volume and intensity due to climate change will therefore directly impact the net sediment transport. The CR terms in the Equation 4-2 represent the fraction of land covered include coverage by snow. Therefore, any changes in the snow hydrology will also have direct impact on detachment of sediment particles.

$$DET = (1 - CR) \times SMPF \times KRER \times (RAIN)^{JRER}$$

<div align="right">Equation 4-2</div>

Where:
DET =   Detachment of particles
CR =   fraction covered by vegetation or snow
SMPF =   management practice factor (set to 1 for CBP purposes)
KRER =   soil detachment coefficient (complex units)
RAIN =   Precipitation (inches per hour)
JRER =   soil detachment exponent (complex units)

As shown in Equation 4-3, the transport (WSSD) of the detached sediment and the scour of soil is simulated based on surface outflow (SURO) and surface water storage (SURS). The detached sediment storage (DETS) and sediment removal capacity (STCAP) also control the amount of sediment transport. The climate change stressor would impact the surface outflow and surface water storage, and therefore the transport of sediment.

$$WSSD = (DETS \text{ or } STCAP) \times {SURO}/{(SURS + SURO)}$$

<div align="right">Equation 4-3</div>

Where:
WSSD =   Sediment Washoff (tons/acre/hour)
DETS =   Storage of detached sediment (tons/acre)
STCAP =   Sediment removal capacity
SURO =   Surface runoff (inches/acre/hour)
SURS =   Surface water storage

4.4   Nitrogen Loss Sensitivity to Climate Change

Time-averaged response of nitrogen does not have sensitivity to changes in hydrology and sediment in the Phase 6 Watershed Model. Nitrogen loads for a land use are determined by nutrient inputs as discussed in Section 4 and watershed characteristics as discussed in Section 7. Nitrogen loads would be affected by climate change and so additional sensitivities to inputs must be included.

4.4.1   Analyses Used in 2017 Climate Assessment

Using the framework of multiple lines of evidence, the modeling team analyzed percent change in nitrogen delivery relative to percent change in flow. Using the Phase 5.3.2 Watershed Model, this ratio was determined to be 0.643 as illustrated in Figure 4-2. In the '20 watersheds' study (U.S. EPA 2013), HSPF and SWAT were used to simulate the effect of climate change on 20 watersheds

across the contiguous U.S (Butcher et al. 2014, U.S. EPA 2013) and Figure 4-3 shows the simulated responses . This analysis simulated changes in flow (Table 7-7 U.S. EPA 2013) and total nitrogen delivery (Table 7-14 U.S. EPA 2013) in response to the changes in climatic inputs obtained from a set of six downscaled climate model projections. The findings suggest a ratio of 1.14 for the simulated changes in nitrogen load delivery with respect to changes in flow. For the Susquehanna, the only watershed situated in the Chesapeake Bay watershed, the ratio was 7 with a 49 percent increase in TN for a 7 percent increase in flow. However, this ratio was an outlier among the 20 watersheds. Given the wide variability in outcomes a ratio of 1 was selected for initial study with additional input being sought for future refinements. This is equivalent to an assumption of no changes in flow-weighted nitrogen concentrations with changes in flow or a proportional change in nitrogen load to a change in flow.

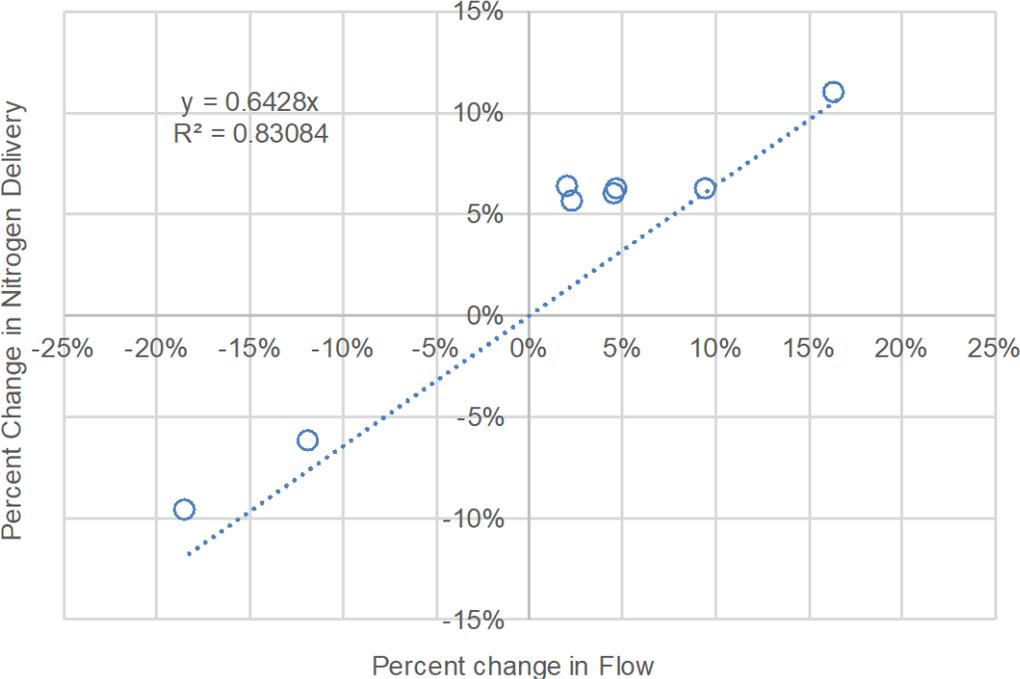Figure 4-2: Simulated responses for flow and nitrogen from the Phase 5.3.2 Chesapeake Bay Watershed Model. Climate change simulations included in the analysis were based on a CMIP3 ensemble of 6 downscaled Global Circulation Models for the years 2025 and 2050. Six additional sensitivity simulations for rainfall, temperature and potential evapotranspiration, and carbon dioxide were also included.
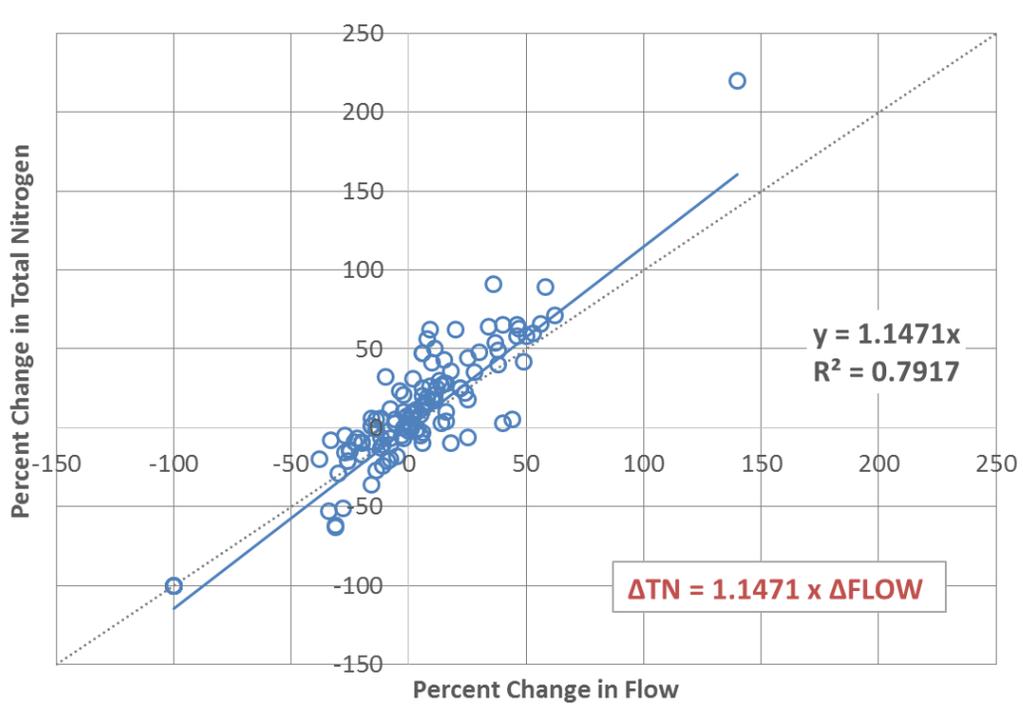
Figure 4-3: The sensitivity of nitrogen load delivery with changes in flow under a wide range of climate change scenarios. The simulated response for 20 watersheds under the climate change scenarios is shown (From U.S.EPA 2013).

4.4.2   Extended literature review

An additional, more extensive literature review was carried out in 2019 to validate or revise the proportional relationship between changes in streamflow and changes in TN load used in the 2017 Climate Assessment. A total of 27 studies carried out in 40 watersheds were found that used either an empirical or a process-based modeling approach to predict changes in flow and TN load under climate change scenarios (Table 4-1). To investigate whether watersheds characterized by different dominant land uses tended to exhibit different responses to climate change scenarios, the 40 watersheds were divided into three broad categories based on the land use data reported in each study: 1) "Agricultural/Developed" watersheds, where >60% of the watershed area was characterized as agricultural, pasture and/or developed; 2) "Mixed" watersheds, where neither anthropogenic (agricultural, pasture and/or developed) nor more natural (forested) land uses occupied >60% of the land; and 3) "Forested" watersheds, where >60% of the watershed area was forested (Table 4-1). For each study, average streamflow and either TN or NO3 load estimated under climate change conditions were expressed as percent change from their corresponding historical baselines. Percent changes in TN load were then regressed against percent changes in streamflow separately for the three broad land use categories identified above (Figure 4-6 through Figure 4-6). A hierarchical modeling approach was used, where the regression slope and intercept were assumed to derive from a common hyperdistribution and were allowed to vary across studies.

All studies conducted in predominantly agricultural or developed watersheds show a remarkable level of agreement in indicating an approximately 1:1 relationship between climate change-driven changes in flow and corresponding changes in TN load (Figure 4-6). Although studies conducted in mixed and forested watersheds appear to slightly deviate from a 1:1 relationship, they are

characterized by substantially larger variability when compared to results from agricultural/developed sites, and the 95% confidence intervals of the mixed and forested regression slopes overlap with the mean slope estimated for the agricultural/developed watersheds (Figure 4-6 through Figure 4-6). Due to the larger level of uncertainty associated with mixed and forested sites, robust conclusions on whether different land uses may be characterized by different TN-flow responses are not warranted based on this dataset, and results from this literature review *generally indicate support for the adoption of a 1:1 relationship for TN load sensitivity to changes in flow*.

Table 4-1 Main characteristics of the studies used to assess the impact of climate change-driven changes in hydrology on N loads. The column "Model" provides the modeling tool used either to simulate N loads in the study area or to analyze observed load data. The column "Land use gr." reports the broad land use categories used to divide watersheds into groups with relatively homogeneous land use characteristics (1: "Agricultural/Developed"; 2: "Mixed"; 3: "Forested"; see main text for explanation).

Reference	River	State/ Country	Area (km²)	Model	Land use	Land use gr.
Alam 2015	Eno	NC	364	SWAT	56% forest; 25.5% pasture; 11% developed; 2%agricultural; 2% grassland; 2% scrub; 2% open water	2
Alamdari et al 2017	Difficult Run	VA	150	SWMM	57% urban development; 8% commercial/industrial; 11% transportation; 24% open space	1
Arheimer et al 2005	Ronnea	Sweden	1900	SOILNDB + HBV-N	46.5% forest; 32.3% agricultural; 3.2% urban; 3% water	2
Bosch et al 2014	Maumee	OH/MI	17030	SWAT	76% crop; 5% hay; 11% urban; 8% forest	1
Bosch et al 2014	Sandusky	OH	3455	SWAT	80% crop; 3% hay; 9% urban; 8% forest	1
Bosch et al 2014	Raisin	OH/MI	2784	SWAT	53% crop; 19% hay; 11% urban; 16% forest	1
Bosch et al 2014	Grand	OH	1896	SWAT	27% crop; 10% hay; 10% urban; 52% forest	2
El Khoury et al 2015	South Nation	Ontario, Canada	3858	SWAT	57.8% agricultural; 41.03% forest	2
Ficklin et al 2013	San Joaquin	CA	14983	SWAT	2/3 agricultural	1
Ficklin et al 2013	Sacramento	CA	23300	SWAT	62% rangeland; 33% agricultural; 5% urban, waterways and forested	1
Hanratty & Stefan 1998	Cottonwood	MN	3400	SWAT	52% rangeland; 46% crop	1
Khoi and Thang 2017	3S	Laos/ Cambodia /Vietnam	78500	SWAT	78.76% forest; 13.2% agricultural; 1.32% urban	3

Lee et al 2018	Tuckahoe	MD	220.7	SWAT	54% agricultural; 8.4% pasture; 4.2% urban; 32.8% forest; 0.6% water	1
Lee et al 2018	Greensboro	MD/DE	290.1	SWAT	48% forest; 36.1% agricultural; 9.3% pasture; 5.6% urban; 0.7% water	2
Me et al 2018	Puarenga	New Zealand	77	SWAT	47% exotic forest; 26% farmland; 11% mixed scrub; 9% indigenous forest	2
Mehdi et al 2015a	Pike	Québec/ VT	629	SWAT	22% hay; 20% corn; 8% cereal; 2% soybean; 2% orchard; 40% forest; 5% water; 1% urban	2
Mehdi et al 2015b	Altmuhl	Germany	980	SWAT	60% agricultural; 30% forest; 5% urban	1
Nguyen et al 2019	Torrens	Australia	200	SWAT	100% urbanized	1
Park et al 2011	Chungju	South Korea	6642	SWAT	82.3% forested; 12.2% cultivated	3
Riverson et al 2013	Lake Tahoe Watershed	CA/NV	1298	LSPC	65.7% conservation; 22.4% recreation; 10.3% residential; 1.1% commercial; 0.5% tourist	3
Ross 2014	Woonasqua tucket-Moshassuck	RI/MA	192.6	SWAT	38.2% developed; 49.1% forest; 4.5% agricultural; 2% water; 6.2% wetland	2
Ross 2014	Ten Mile	RI/MA	143.6	SWAT	40.9 developed; 46.2% forest; 4.5% agricultural; 2% water; 6.3% wetland	2
Ross 2014	Taunton	RI/MA	1250	SWAT	Upper Taunton: 36% developed; 50.5% forest; 1.1% agricultural; 2.9% water; 9.5% wetland; Mid Taunton: 17.6% developed; 62.8% forest; 4.7% agricultural; 6.3% water; 8.7% wetland; Lower Taunton: 24.6% developed; 56.4% forest; 3.4% agricultural; 7.5% water; 8.0% wetland;	2
Ross 2014	Pawtuxet	RI/MA	599.6	SWAT	18.2% developed; 67% forest; 4.4% agricultural; 4.6% water; 5.6% wetland; 0.2% bare rock	3
Ross 2014	Blackstone	RI/MA	1229	SWAT	Upper Blackstone: 28.7% developed; 53.1% forest; 6.1% agricultural; 4.7% water; 7.3% wetland; 0.1% bare rock; Lower Blackstone: 14.6% developed; 70.2% forest;	3

|					6.5% agricultural; 2.3% water; 6.3% wetland;	
Sebestyen et al 2009	Sleepers	VT	0.41	Regression	100% forested	3
Shrestha et al 2011	Upper Assiniboine	Canada	13500	SWAT	55% cropland; 40% forest	2
Shrestha et al 2016	Onkaparinga	Australia	317	SWAT	49.5% pasture; 17% grazing; 19.5% bushland; 8.2% urban; 1.8% horticulture; 4% orchards	1
Tong et al 2007	Little Miami	OH	5840	SWAT	56.2% agricultural; 23.7% forest; 17.8% urban; 0.97% water; 0.38% other	1
Trang et al 2017	3S	Laos/ Cambodia /Vietnam	78500	SWAT	78.76% forest; 13.2% agricultural; 1.32% urban	3
Tu 2009	Aberjona (W4)	MA	64.7	AVGWLF	18.8% forest, 69.1% developed; 1.4% agricultural	1
Tu 2009	Old Swamp (W6)	MA	11.5	AVGWLF	42.5% forest; 49.6% developed; 0.1% agricultural	2
Tu 2009	Saugus (W3)	MA	63.4	AVGWLF	32.2% forest; 56.6 developed; 0.3 agricultural	2
Tu 2009	Neponset (W5)	MA	90.1	AVGWLF	43.9% forest; 31.0% developed; 3.5% agricultural	2
Tu 2009	Ipswich (W2)	MA	92.8	AVGWLF	44.7% forest; 42.5% developed; 0.8% agricultural	2
Tu 2009	Stillwater (W1)	MA	77.1	AVGWLF	75.2% forest; 3.7% developed; 8.1% agricultural	3
Tu 2009	Wading (W7)	MA	104.9	AVGWLF	63.6% forest; 17.2% developed; 3.5% agricultural	3
Verma et al 2015	Maumee	OH/MI	17030	SWAT	76% crop; 5% hay; 11% urban; 8% forest	1
Wagena et al 2018	WE-38 (sub-watershed of Mahantango Creek)	PA	7.3	SWAT	44.5 agricultural; 38.8% forest; 3.5 pasture; 6.2% developed; 2.2 plantations; 0.9% fallow and grassland; 3.1 conservation	2
Wang and Kalin 2018	Wolf Bay	AL	126	SWAT	1.2% water; 26.4% urban; 20.9% forest; 9.7% pasture; 29.9% cropland; 11.9% wetland	1
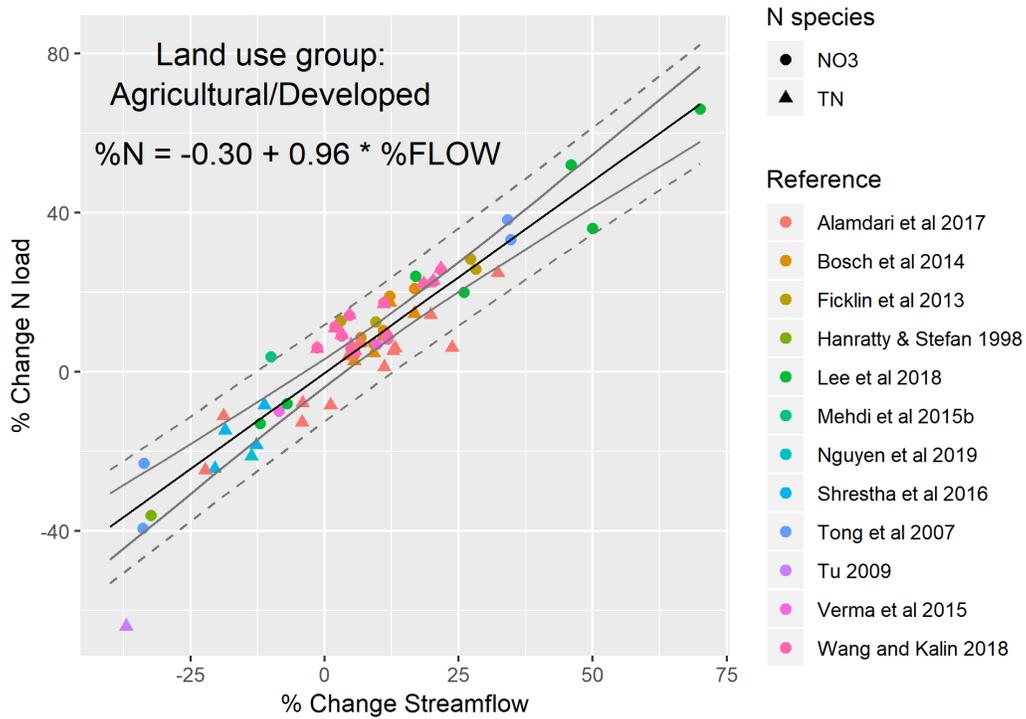
Figure 4-4: Relationship between percent change in N load and percent change in streamflow across climate scenarios in "agricultural/developed" watersheds. The black line is the average fitted line (equation shown in the figure) while the grey lines represent 95% confidence (solid) and prediction (dashed) intervals.
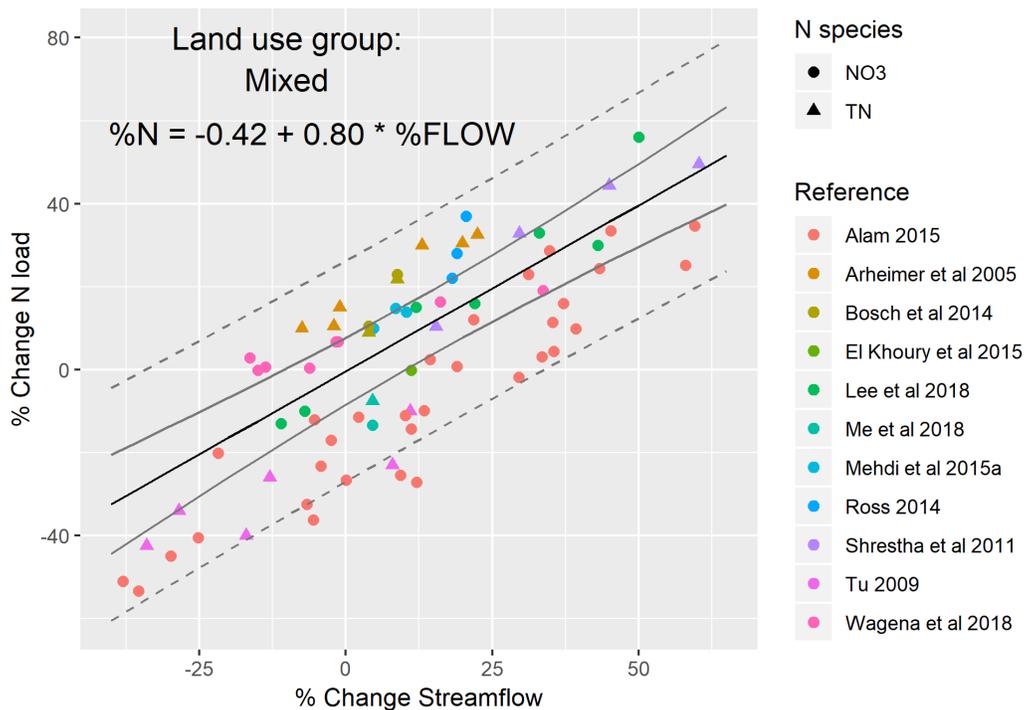
Figure 4-5: Relationship between percent change in N load and percent change in streamflow across climate scenarios in "mixed" watersheds. The black line is the average fitted line (equation shown in the figure) while the grey lines represent 95% confidence (solid) and prediction (dashed) intervals.

Figure 4-6: Relationship between percent change in N load and percent change in streamflow across climate scenarios in "forested" watersheds. The black line is the average fitted line (equation shown in the figure) while the grey lines represent 95% confidence (solid) and prediction (dashed) intervals.
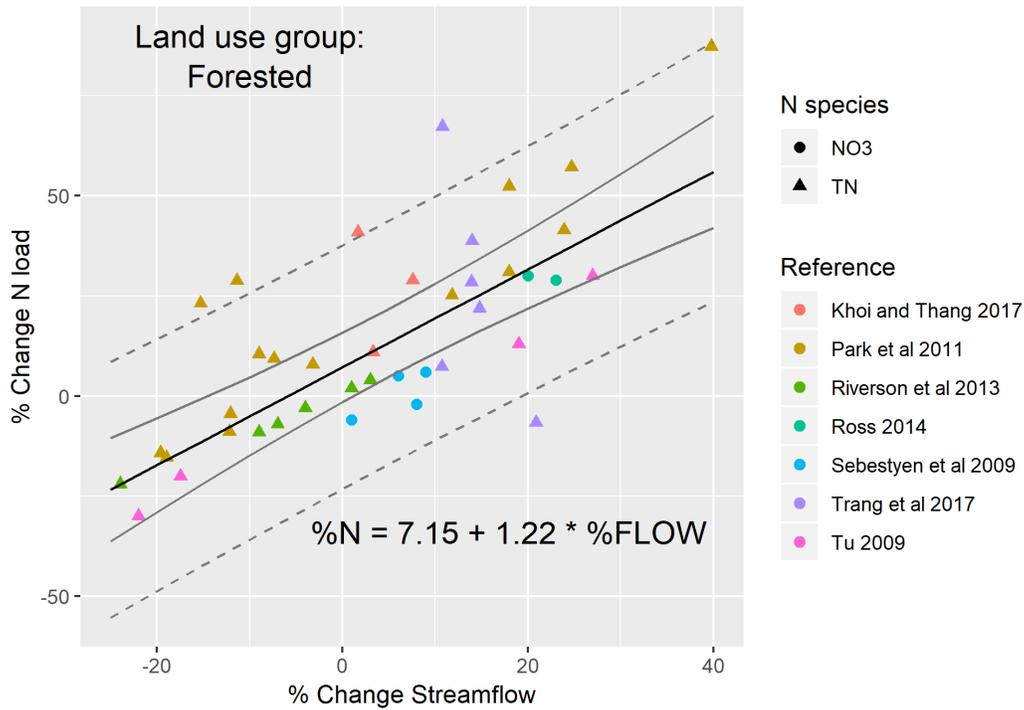
4.4.3 Analysis of data from Chesapeake Bay Nontidal Network stations

In addition to the literature review described above, we carried out an empirical analysis of the long-term flow and TN loads estimated at nontidal USGS stations across the Chesapeake Bay watershed to look for evidence of different responses to variability in hydrology as a function of spatially varying watershed characteristics.

Flow and TN loads estimated at 101 Chesapeake Bay Nontidal Network stations over 1985-2017 were retrieved from the USGS (https://doi.org/10.5066/F7RR1X68). To characterize the sensitivity of TN loads to inter-annual changes in flow at each station, annual flow and TN loads were expressed as percent change from the corresponding long-term average estimated at that station. Subsequently, for each station the annual percent change in TN load (from the long-term average) was regressed against the corresponding annual percent change in flow, thereby providing an estimate of the slope of the relationship between percent change in TN and percent change in flow at each station. Slopes near 1 would indicate agreement with the overall findings of the literature review and data presented in previous sections, while slopes that significantly deviate from 1 would suggest differences across stations in their behavior in terms of TN sensitivity to inter-annual variability in flow. Because the relationship between % change TN and % change flow showed substantial uncertainty for stations with sparse data (< 10 years), only stations with >10 years of data were retained for this analysis, leaving a total of 81 stations out of the original 101.

Although most of the stations had a slope close to 1, a non-negligible number of stations exhibited a slope >1 (Figure 4-7), with a relatively clear spatial pattern in the distribution of the slopes (Figure 4-8).
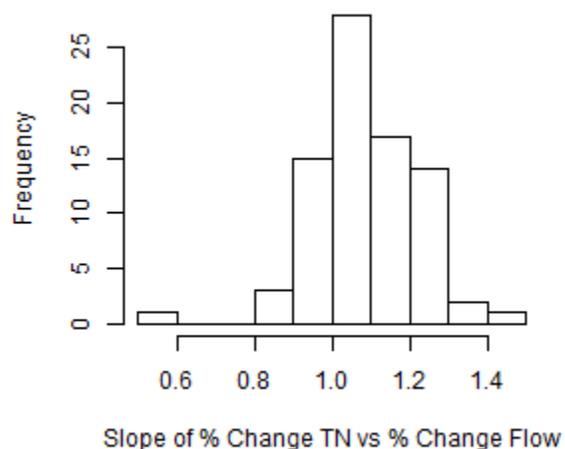

Figure 4-7: Distribution of the station-specific slopes that quantify the relationship between percent change in WRTDS-estimated TN load and percent change in flow calculated from annual data at 81 Chesapeake Bay nontidal stations with >10 years of data. Annual percent changes are calculated as difference from the corresponding long-term mean.
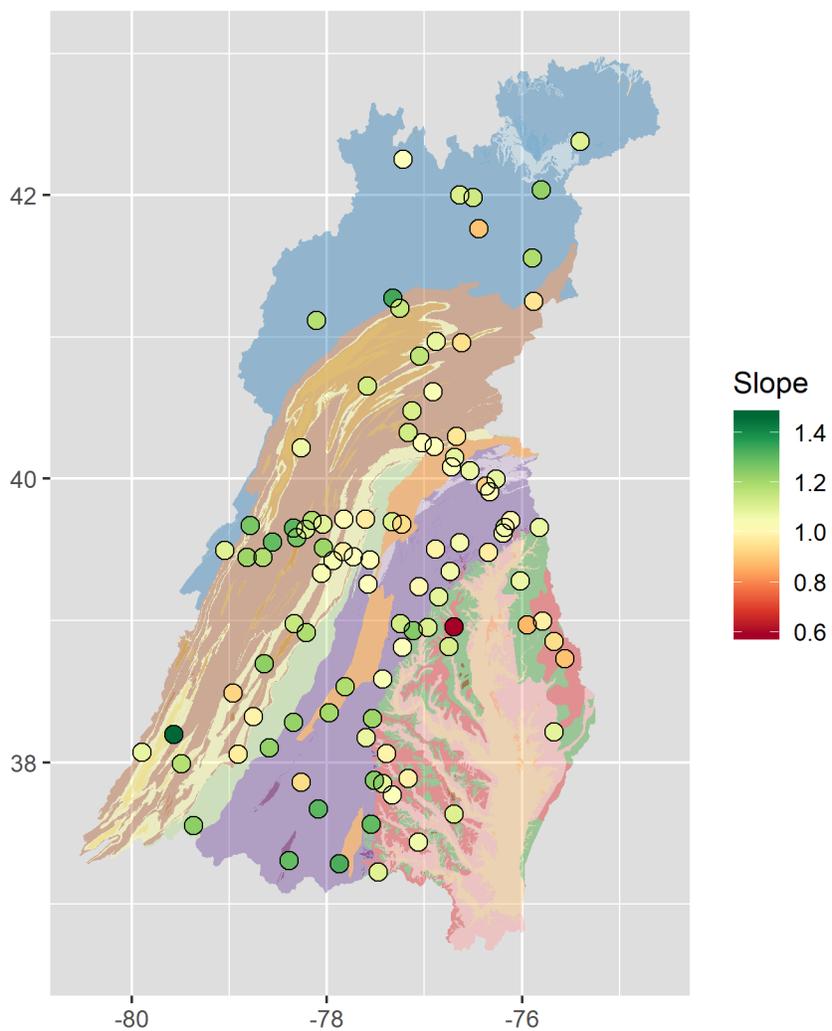
To investigate potential drivers of the observed spatial pattern in %TN-%FLOW slopes across the watershed, a set of available candidate covariates was considered that represent landscape, physiographic, land use and climatic characteristics hypothesized to influence TN sensitivity to hydrology (Table 4-2). As a first exploratory analysis, a Principal Component Analysis (PCA) was carried out to visualize the ordination of station-specific TN sensitivity slopes with respect to candidate covariates. All variables were standardized before analysis. The ordination biplot indicates a tendency of stations with higher %TN-%FLOW slopes to cluster along the right hand side of the first principal component (PC1), with a large portion of the stations with lower slopes clustering at the opposite end of the first axis (Figure 4-10). The first axis is most strongly correlated to variables related to land-use and amount of N input (Table 4-2), with stations with higher N sensitivities to flow tending to be associated with high percentages of forested areas in the upstream catchment and conversely lower percentages of agricultural areas and lower average TN loads and concentrations.

Table 4-2 Candidate covariates considered in exploring potential drivers of spatial variability in TN sensitivity to changes in flow at Chesapeake Bay nontidal stations. Columns "PC1" and "PC2" provide PCA loadings of individual variables quantifying the standardized correlation of each variable to each of the first two PCA axes in Figure 4-9. Variables are sorted in order of decreasing absolute correlation with respect to the first ordination axis (PC1).

Variable	Description	PC1	PC2
[TN]	Long-term average annual TN concentration	-0.368	0.0341
TN_load/ac	Long-term average annual TN load	-0.3677	0.0837
%C	Fraction of drainage area occupied by agricultural land uses	-0.3231	0.0231
DVF_rch	SPARROW Delivery Variance Factor related to groundwater recharge	-0.2658	0.2501
BI	Long-term average baseflow index	-0.2524	-0.0156
NOx/TN	Long-term average annual NOx/TN ratio	-0.2425	0.2928
%N	Fraction of drainage area occupied by non-forest natural land uses	-0.2002	-0.1273
DVF_pca	SPARROW Delivery Variance Factor related to Piedmont carbonate	-0.1907	0.0231
Pcp	Long-term average annual rainfall across the drainage area	-0.1834	-0.2048
Q/ac	Long-term average annual flow normalized by drainage area	-0.1779	0.3121
DVF_evi	SPARROW Delivery Variance Factor related to enhanced vegetation index	-0.1773	0.2237
%D	Fraction of drainage area occupied by developed land uses	-0.1755	-0.151
DVF_S2R	SPARROW average stream to river Delivery Variance Factor	-0.076	0.116
T	Long-term average annual air temperature across the drainage area	-0.0348	-0.4632
Q	Long-term average annual flow	0.0461	0.3023
WA	Station total drainage area	0.0544	0.2934

%P	Fraction of drainage area occupied by pasture	0.1061	-0.0245
DVF_awc	SPARROW Delivery Variance Factor related to soil available water capacity	0.1509	0.3292
Med_slo	Median slope across the drainage area	0.2311	0.2918
%F	Fraction of drainage area occupied by forests	0.3583	0.1192
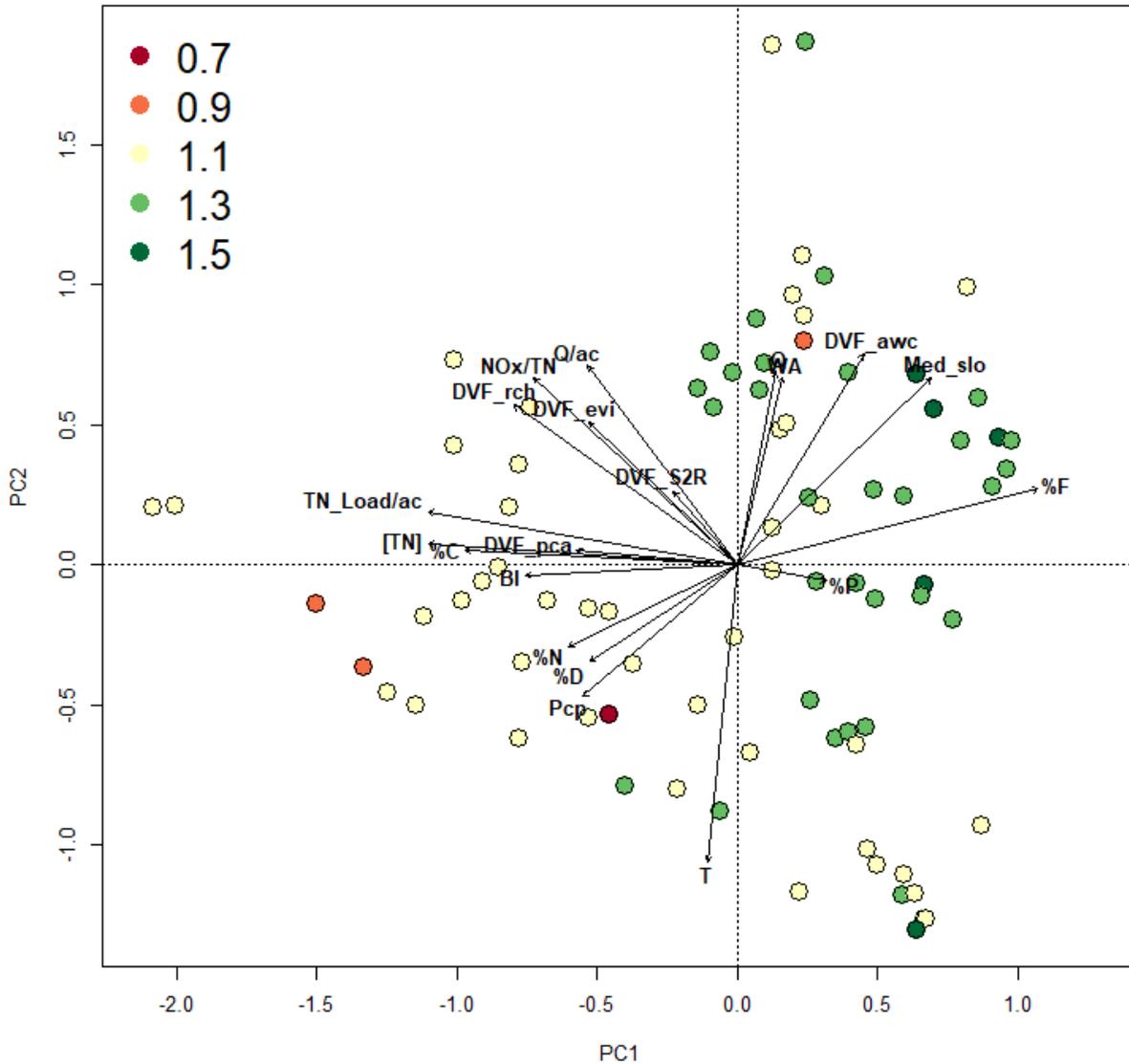
Figure 4-10: PCA biplot of station-specific slopes of the relationship between percent change in TN and percent change in flow. Each circle represents a station colored according to the respective slope value: 0.7: slopes < 0.7; 0.9: 0.7 ≤ slopes < 0.9; 1.1: 0.9 ≤ slopes < 1.1; 1.3: 1.1 ≤ slopes < 1.3; 1.5: 1.3 ≤ slopes < 1.5. For an explanation of variable symbols, see Table 4-2.

We also explored a multiple linear regression approach to identify the set of covariates that best explain the observed variability in %TN-%FLOW slopes. We built regression models using station-specific %TN-%FLOW slopes as the response variable and using all possible combinations of the variables listed in Table 4-2 as candidate predictors. We excluded models including both TN concentration and TN load as predictors, because these two variables had the highest degree of

collinearity and can be considered as largely representing the same underlying driving process (N input). We only considered regression models with up to four predictors to prevent overfitting and we selected the best performing model based on the Bayesian Information Criterion (BIC), which evaluates models in terms of both goodness of fit and number of estimated parameters (i.e., models are increasingly penalized as the number of predictors increases and, as a result, more parsimonious models tend to be preferred over more complex models when explanatory power is similar).

We found that a model with TN concentration and median drainage area slope as the two only predictors provided the optimal combination of explanatory power and parsimony among all possible combinations tested:

$$Y = 0.99 - 0.07 * \log([TN]) + 0.07 * \log(Med\_slo) \qquad R^2 = 0.40$$

Model parameter estimates indicate that stations with lower TN concentrations and higher median upstream catchment slopes tend to have higher %TN-%FLOW slopes. Stations with lower TN concentrations and higher median catchment slopes generally correspond to sites characterized by a high fraction of forested area in their upstream catchments, as also suggested by the PCA ordination plot and confirmed by the relatively high correlation of %F (percentage of forested area in the upstream catchment of each station) with both $\log([TN])$ ($r = -0.82$) and $\log(Med\_slo)$ ($r = 0.75$). Overall, these results suggest that stations characterized by relatively high N inputs and largely agricultural or developed watersheds tend to show an approximately 1:1 relationship between % change in TN and % change in flow at the inter-annual scale, in agreement with results of the literature review presented in Section 4.4.2 while relatively less impacted catchments exhibit a higher sensitivity of TN load to changes in flow (Figure 4-11).

Additional work is needed to fully explain this behavior, which could be due to differences in the combination of one or more of watershed's geospatial physical setting, land use composition, nutrient inputs and legacy storage, and management practices as well as combination of one of these factors. However, it is likely that this difference in behavior across a land-use and anthropogenic impact gradient may be the result of the different relative contribution of rainfall-related changes in atmospheric N deposition in higher- vs. lower-load areas. Specifically, in high rainfall years an increase in both flow-related N delivery and wet N atmospheric deposition is expected, but the relative contribution of the atmospheric deposition component is expected to be higher in areas characterized by relatively lower land-derived N inputs. As a result, the overall percent change in TN for a given percent change in flow is expected to be higher in areas where atmospheric deposition represents only to a non-negligible portion of the overall N inputs.

To assess the ability of atmospheric N-deposition to explain this behavior, we calculated the ratio of the percent change in TN due to the atmospheric deposition component alone over the percent change in flow estimated by the watershed model at each land segment when comparing the 2025 climate change scenario to 1995 conditions. The effect of atmospheric deposition was then plotted against the average TN load estimated at each land segment (Figure 4-12). Model-generated data at the land segment scale show a remarkably similar pattern to the variability in the %TN-%FLOW slope observed at the nontidal stations, with land segments characterized by lower average loads exhibiting a higher relative contribution of atmospheric deposition to the overall sensitivity of TN to changes in flow. These results, together with the literature review

described above, generally provide evidence in favor of maintaining a 1:1 relationship to capture the sensitivity of TN load to changes in flow, with the positive deviations observed in progressively less impacted watersheds being largely explained and accounted for by predicted changes in wet atmospheric deposition with rainfall (see Section 3.1). While accounting for the increase in TN transport due to changes in wet atmospheric deposition *in addition* to the predicted 1:1 response of TN load to flow provides a means to capture the higher sensitivity to hydrology observed in predominantly forested areas, this might result in double counting in largely agricultural areas, where an approximately 1:1 relationship between TN load and flow was found based on empirical data that should already include the influence of changes in atmospheric deposition. However, in predominantly agricultural areas N load from atmospheric deposition represents a substantially lower fraction of the overall N inputs compared to largely forested areas (Figure 4-13), so that the potential effect of double counting is assumed to be negligible.
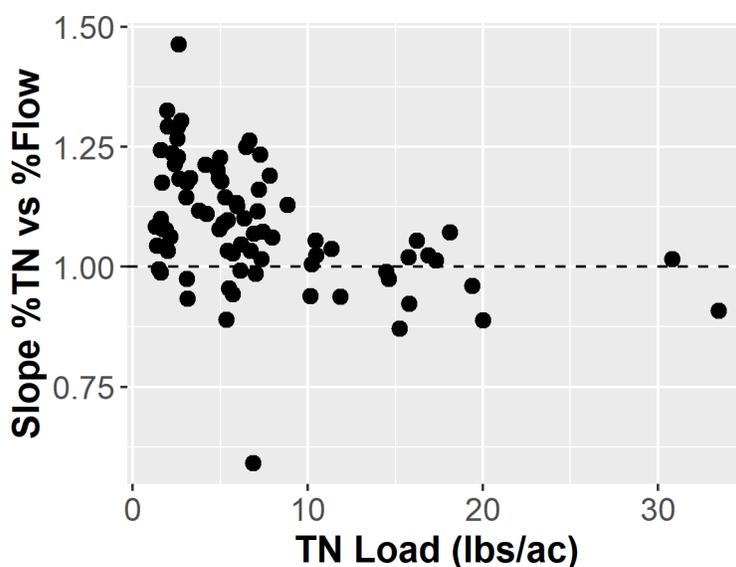

Figure 4-11: Variability in station-specific %TN-%FLOW slopes as a function of the long-term average TN load at each station.
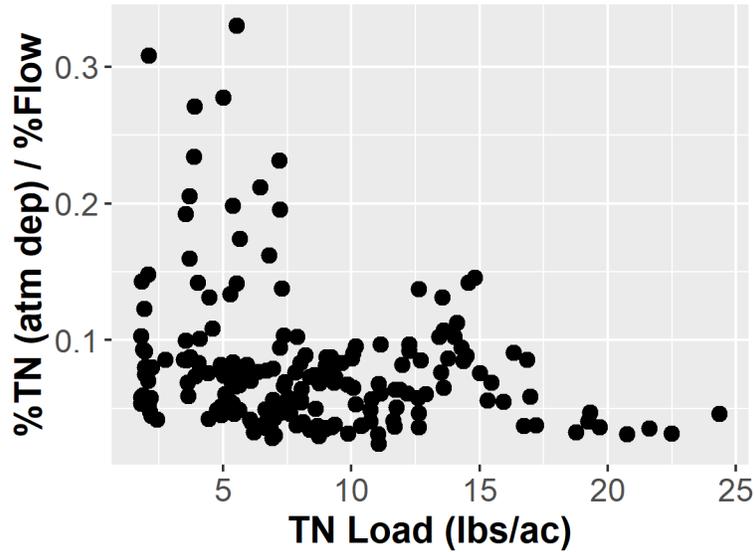
Figure 4-12: Variability in the relative contribution of rainfall-driven changes in wet N atmospheric deposition to the overall ratio of percent change in TN over percent change in flow estimated by the P6 watershed model at each land segment when comparing 2025 vs. 1995 conditions. The relative contribution of atmospheric deposition is plotted against the average TN load estimated at each land segment.
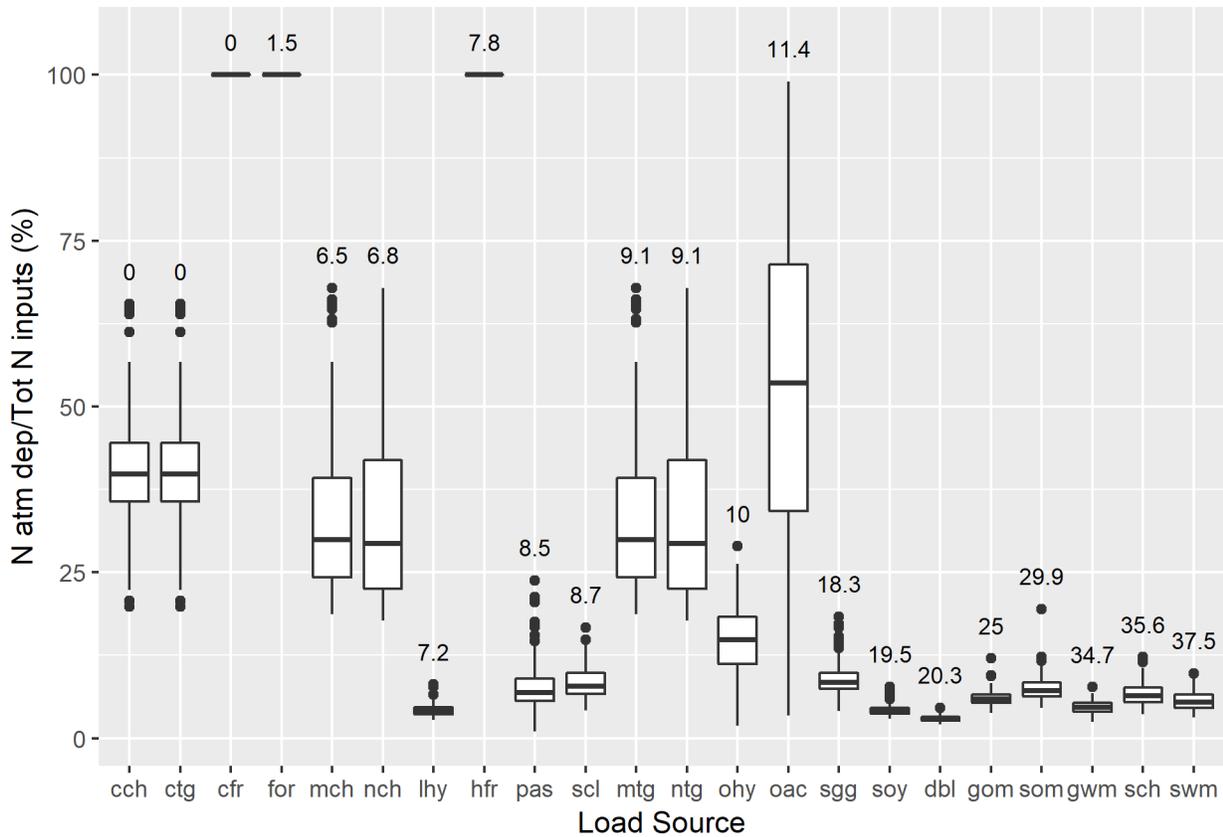
Figure 4-13: Fraction of overall N inputs represented by atmospheric deposition for each load source. Boxes and whiskers represent variability across land segments (one data point per land segment and load source combination) and the numbers above each box provide the watershed-wide average edge-of-stream TN load (lbs/acre) for each load source. Load source abbreviations: cch: CSS Tree Canopy over Turf Grass; ctg: CSS Turf Grass; cfr: CSS Forest; for: True Forest; mch: MS4 Tree Canopy over Turf Grass; nch: Non-regulated Tree Canopy over Turf Grass; lhy: Legume Hay; hfr: Harvested Forest; pas: Pasture; scl: Specialty Crop Low; mtg: MS4 Turf Grass; ntg: Non-regulated Turf Grass; ohy: Other Hay; oac: Other Agronomic Crops; sgg: Small Grains and Grains; soy; Full

To assess whether the patterns in TN sensitivity to flow observed at the nontidal stations may be substantially confounded by long-term changes in atmospheric deposition or changes due to long-term management efforts, we used two approaches: 1) we estimated the slopes of the relationship between percent change in TN and percent change in flow using progressively more recent subsets of data (last 20 years, last 15 years and last 10 years); 2) we used WRTDS flow-normalized TN loads as a proxy for long-term changes in N inputs at each station. Specifically, at each station we fitted a linear regression using flow-normalized TN load as the dependent variable and time (years) as the independent variable. We then used the slope of the regression to de-trend the time series of "actual" (not flow-normalized) TN loads at each station. Finally, we used this de-trended TN load time series to calculate the annual percent change in TN load and regress it against the annual percent change in flow at each station as described above. We thus obtained station-specific slopes of the relationship between de-trended percent change in TN and percent change in flow. Although there are limitations to both these approaches and more sophisticated and comprehensive analyses are warranted in the future to effectively disentangle the influence of multiple confounding factors that act over long-term time scales, we found no evidence of strong differences in the variability of %TN-%FLOW slopes when considering different portions of the available time series or accounting for estimated long-term changes in flow-normalized loads (Figure 4-14). **Therefore, the results of the analysis of observed data, consistent with the extended literature review in Section 4.4.2, indicates support for the adoption of a 1:1 relationship for TN load sensitivity to changes in flow.**
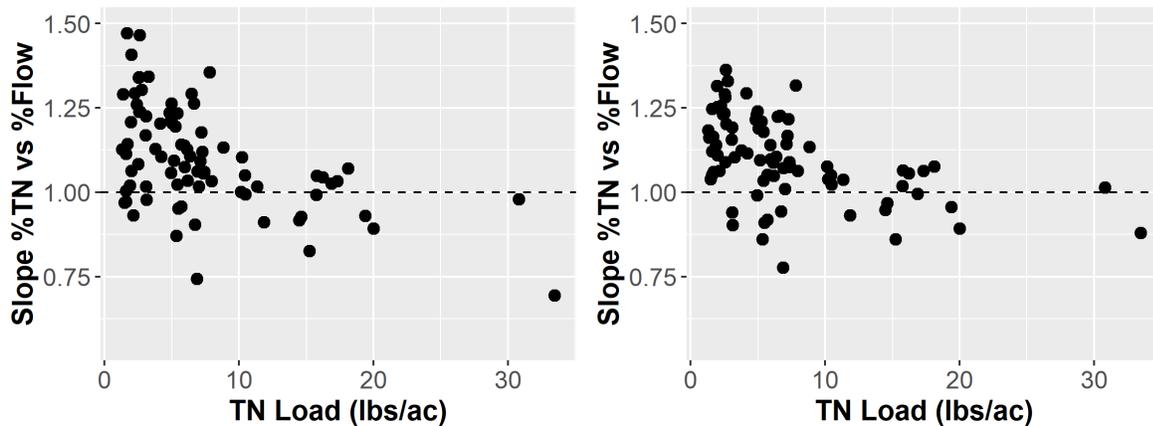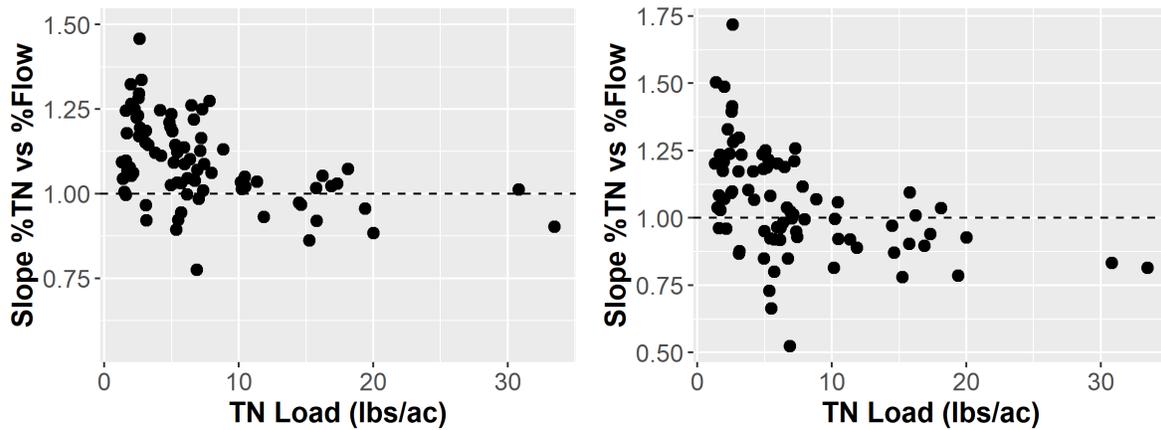
Figure 4-14: Variability in station-specific %TN-%FLOW slopes as a function of the long-term average TN load at each station. Slopes are estimated using only the last ten years (upper right panel), 15 years (upper right panel), and 20 years (lower left panel) of data and de-trending the time series of TN loads based on estimated long-term trends in flow-normalized TN loads at each station (lower right panel).

4.5 Phosphorus Loss Sensitivity to Climate Change

4.5.1 Agricultural and Natural Land

Phosphorus transport from land segments and land uses is a function of stormflow, sediment transport, soil phosphorus concentration, and applied water extractable phosphorus as described in Section 4.   Soil concentrations and applications are not altered in a climate change scenario, but stormflow and sediment transport are affected as described above. Stormflow is defined as the sum of HSPF simulated *Surface* and *Interflow outflows*. The time-averaged changes in stormflow and sediment transport for climate change scenarios are estimated using the HSPF simulation. The time-averaged model uses simulated time-averaged changes in stormflow and sediment transport for the estimation of time-averaged changes in phosphorus transport. The sensitivity coefficients for phosphorus transport are based on results from the Annual Phosphorus Loss Estimator (APLE) model. The detailed derivations of these sensitivities are described in Section 4. Table 4-3 provides a brief summary of phosphorus sensitivities to stormflow and sediment losses for major land uses. The sensitivities show changes in phosphorus transport in pounds per acre corresponding to changes in stormflow (inches/acre) and sediment washoff (tons/acre). These sensitivities are additive.

Table 4-3: Time-averaged phosphorus sensitivities (pounds/acre) of major land uses for stormflow (inches/acre) and sediment washoff (tons/acre). If applicable, the range shows minimum, mean and maximum sensitivity values for the land uses within each category.

Land use Category	Flow Sensitivity Range	Sediment Sensitivity Range
Natural	0.007, 0.019, 0.042	0.012, 0.031, 0.067
Pasture	0.080	0.126
Cropland	0.041	0.121

4.5.1.1 *Soil P history*

The CBP's Scientific and Technical Advisory Committee (STAC) strongly recommended the primacy of soil P as a determinant of P export in Staver et al. 2014. Section 4.4 of the Phase 6 Watershed Model documentation (Chesapeake Bay Program 2017) further describes the dominant influence of soil phosphorus concentration on the export of phosphorus from agricultural land uses based on evidence from the literature and tests of the mass-balance-based Annual Phosphorus Loading Estimator (APLE) model (Vadas, 2014).

Section 3.9 of the Phase 6 Watershed Model documentation describes the method of calculation for county-wide averages of soil P concentrations from 1984 through 2015 using a Bayesian model that combines point observations of soil P and runs of the APLE model. These soil P estimates were used in calibration runs of the Phase 6 Watershed Model. For scenario operations, the CBP partnership decided to simulate the long-term effects of a given state of management actions. The soil P used for scenarios is the initial estimate for the scenario year with an estimate of the change in soil P given 25 years of the same land management. For example, the soil P used for the 1995 scenario is the 1995 best estimate plus or minus the buildup or drawdown in soil P that would occur under 25 years of constant 1995 management. If the base year for the scenario is 2014 or after, 2014 is used as the staring point for the 25-year simulation of change in soil P. Section 3.9.3.2 describes the development of an APLE Emulator Model (Equation 4-4) with the coefficients in Table 4-4. The APLE Emulator Model is used to estimate the soil P as a result of holding the management specified in a given scenario constant for 25 years.

Equation 4-4: APLE Emulator Model

$$M_{i+1} = M_i + \left(\sum_{n=1}^{Nfactors} (Factor * Coefficient) \right) * (1 - 0.95 * \log_{75} i)$$

Table 4-4: Factors used in the APLE Emulator Model

Factor	unit	Coefficient
Solid Manure	pound/acre/year TP	0.151
Liquid Manure	pound/acre/year TP	0.154
Fertilizer	pound/acre/year TP	0.0559
Biosolids	pound/acre/year TP	0.00463
Uptake	pound/acre/year TP	-0.159
Sediment Loss	ton/acre/year	-0.208
Stormflow	inches/year	-0.0355
Percent Incorporation	percent	0.0479
Percent Mixing	percent	-0.0508
Depth of Incorporation	inches	0.183
Precipitation	inches/year	-0.00152
Clay percent	percent	Clay > 15: 0.160
		Else: 0.000

Factor	unit	Coefficient	
Organic Matter	percent	Clay >15:	-0.549
		Else:	0.000
Local Adjustment	ppm Mechlich 3	Varies	

Inspection of Table 4-4 shows that three of factors have predicted changes due to climate change. Precipitation, stormflow, and sediment loss all contribute to the evaluation of soil P levels. Higher values for each of these parameters would tend to deplete the soil phosphorus faster as more phosphorus is transported away from the soil. The negative coefficients in Table 4-4 indicate that there is an inverse relationship between future soil P levels and precipitation, runoff, and sediment loss. The depletion of the soil is caused by the increased phosphorus loads which are predicted by CAST due to increases in stormflow and sediment.

The depletion of the soil P lessens the total impact of climate change. Using the sensitivities for stormflow, sediment and soil phosphorus in Section 4 of the Phase 6 documentation, the values in Table 4-4, and Equation 4-4, it can be calculated that the increase in load due to the increase in sediment loss is about 20% lower due to the inclusion of soil P depletion. The increase in load due to additional precipitation is about 12% lower due to the inclusion of soil P depletion, assuming that 50% of the additional precipitation is converted to runoff.

4.5.2   Developed Land

Two sources of information were considered to assess the impact of climate change-driven changes in hydrology on TP loads from developed land uses: 1) a literature review of small-scale studies that have simulated flow and TP loads under climate change scenarios in predominantly developed watersheds; and 2) an empirical analysis of data from the National Stormwater Quality Database (Maestre and Pitt, 2005). The results of the analysis indicate that a slope of 1 between percent TP change and percent flow change is appropriate for developed land, reflecting no change in average concentration of TP as flow changes. This result is compared to other land uses for context in Section 4.5.2.3

4.5.2.1   *Literature review*

To assess the impact of potential climate change-driven changes in hydrology on TP loads from developed land uses, a review of the relevant literature was carried out. To be included in this review a study must have either been conducted in a watershed/site where > 50% of the study area was defined as urban/developed or, if conducted in predominantly agricultural watersheds, reported results of climate change-driven changes in TP loads separately for developed land uses. Both empirical and modeling studies were considered. A total of six studies were found that matched these criteria (Table 4-5), and a brief description of each study`s main characteristics and methods is provided in the following paragraphs.

Alamdari et al. (2017) used EPA`s Storm Water Management Model (SWMM) to assess the impacts of climate change on runoff and water quality in the urbanized Difficult Run watershed (Fairfax, VA). The SWMM model was calibrated and verified to observations from two USGS stream gauges in the watershed. Historical (1971–1998) and future (2041–2068) precipitation and temperature projections from the North American Regional Climate Change Assessment Program

(NARCCAP) were used to run the model and compare historical vs. climate change-driven flow and constituent loads. Climate change projections were based on only one of the NARCCAP products (MM51-CCSM, greenhouse gas scenario A2), which was selected based on historical model performance in the study area.

Xiang (2017) quantified the effects of climate change on streamflow and nutrient loads in the suburban Wilde Lake watershed (Columbia, MD) using the Soil and Water Assessment Tool (SWAT). Data from one USGS gauging station were used to calibrate and validate the model, and six downscaled and bias-corrected CMIP5 climate models were selected based on their predictive accuracy over the eastern United States and their representativeness of a broad range of future climates. Predictions corresponding to up to four RCP scenarios were used for each climate model. The SWAT model was run using: 1) precipitation and temperature time series hindcasts of 1965–2015 from each climate model and 2) precipitation and temperature predicted by each climate model x RCP scenario combination for the future period 2016–2099. For each climate model and RCP scenario, annual streamflow and load values averaged over 2080–2090 at the watershed outlet were compared to values averaged over 1970–1989.

Pyke et al. (2011) simulated changes in annual runoff and constituent loads under five precipitation-change scenarios and three hypothetical land use scenarios designed for the redevelopment of a former military base near Boston, MA. Of the three land use scenarios (one representative of low-intensity suburban development, one representative of a mixed-use configuration and one representative of an undeveloped site), only results from the first two scenarios were considered in this review, because the third scenario was more representative of natural rather than developed land use. Precipitation scenarios were developed using an observed historical time series (1996–2005) of daily precipitation from a local NOAA weather station. Specifically, five hypothetical future change scenarios were obtained by applying the delta change factor approach. Of the five precipitation change scenarios presented in the manuscript, only three were retained in this review because the other two did not entail a change in precipitation volume but rather only a change in the distribution of precipitation across events with different magnitudes. The three scenarios retained here corresponded to a 20% increase in rainfall volume, a 20% decrease in rainfall volume and a 3% increase in rainfall volume distributed unevenly across rainfall events that ultimately resulted in a 10% increase in the proportion of annual precipitation occurring in the 5% largest events. Potential future changes in temperature were not considered during simulations, which were performed with EPA`s Smart Growth Water Assessment Tool for Estimating Runoff (SG WATER). SG WATER is a simplified stormwater modeling tool designed to provide coarse exploratory information on possible impacts of development scenarios on runoff quantity and quality. It is important to note that, as the authors of the study indicate, "*SG WATER is not calibrated or validated against observed stormwater runoff values, and it is therefore appropriate only for evaluating relative changes resulting from different scenarios and not for providing absolute, quantitative predictions or comparing to simulations from other hydrologic models*".

The work by Munson et al. (2018) differs substantially from the studies mentioned above in that it uses a data-driven approach to estimate the sensitivity of TP loads from an urban stream to changes in a set of variables, including temperature and precipitation. Rather than simulating projected changes in climate variables, the authors used a multivariate regression approach to

model the "elasticity" of historical (2007–2014) monthly TP loads estimated at a USGS gauging station to simultaneous changes in observed monthly precipitation, temperature, streamflow and number of CSO events. Elasticity is defined in the manuscript as the relative change in loads divided by the relative change in each of the predictors that are simultaneously included in the regression model. The work was conducted in the Alewife Brook, a heavily urbanized watershed near Boston, MA. As the authors of the study recognize, this approach has some obvious limitations, including the lack of incorporation of potentially important explanatory variables in the empirical model, such as changes in land use or population growth, or the level of correlation among predictors that makes the separation of their individual effects challenging.

Tong et al. (2006) used EPA`s Better Assessment Science Integrating Point and Nonpoint Sources (BASINS) model to estimate climate-driven changes in runoff quantity and quality in the Lower Great Miami River Basin in southwest Ohio. Although the watershed is predominantly agricultural, results specific to urban land use areas are provided in the manuscript. The watershed model was calibrated over the period 1975–1984 and validated over the period 1985–1994 using data from a USGS gauging station. Observed precipitation and temperature time series were modified to simulate four different future scenarios using delta change factors based on projected climate-related changes from two GCMs (IPCC and UK Hadley Centre`s climate model). The manuscript provides percent changes in TP loads associated with select percent changes in precipitation but does not provide the corresponding percent changes in flow.

Fischbach et al. (2015) used the Chesapeake Bay Phase 5.3.2 Watershed Model to simulate the impact of different future climate scenarios on streamflow and TP loads from urban land uses within the Patuxent River watershed. The watershed model was run using 1) observed historical (1984–2005) precipitation and air temperature data and 2) downscaled temperature and precipitation projections from six IPCC GCMs, three emission scenarios and two future time periods (2035–2045 and 2055–2065), thereby resulting in a total of 36 climate-altered hydrology projections. Authors of the study kindly provided average annual streamflow and TP load data estimated for the observed historical period and the 36 climate scenarios.

For each study, average flow and TP load estimated under climate change conditions were expressed as percentage change from their corresponding historical baselines. Percentage changes in TP load across all studies were then regressed against percentage changes in flow (Figure 4-15). A hierarchical modeling approach was used, where the regression slope and intercept were assumed to derive from a common hyperdistribution and were allowed to vary across studies, thereby accounting for intra-class correlation arising because observations within each study are not independent.

Although only a limited number of studies were found, they span a relatively broad range in terms of size of the study area, land use characteristics and level of complexity of the modeling approach adopted (Table 4-5). Despite this large inter-study variability, all studies appear to indicate that a linear relationship exists between climate-driven changes in flow and corresponding changes in TP load, with a 1% change in flow corresponding to an approximately 1% change in TP load when averaging across studies (Table 4-5).

Table 4-5: Main characteristics of the studies used to assess the impact of climate change-driven changes in hydrology on TP loads from developed land uses. The column "Model" provides the modeling tool used either to simulate TP loads in the study area or to

analyze observed load data. The column "Climate simulation approach" reports the method adopted to simulate expected changes in climate variables (Delta change factor: one or more multipliers were applied to historical time series of climate variables to generate modified time series that represent expected future changes; GCM: hourly or daily precipitation and temperature data predicted by one or more GCMs were directly used as input to a watershed model to generate loads expected under future climate scenarios). The column "T change" provides the range of projected temperature increases/decreases that were considered in each study.

| Reference	Site	Area (km²)	Land use	Model	Climate simulation approach	T change
Pyke et al. 2011	Naval Air Station, MA	5.7	Built environment with 64-71% open space	SG WATER	Delta change factor	Not assessed
Alamdari et al. 2017	Difficult Run watershed, VA	150	57% urban development; 8% commercial/industrial; 11% transportation; 24% open space	SWMM	GCM	-1.2/+4.1 °C
Munson et al. 2015	Alewife Brook watershed, MA	22	61% residential; 11% commercial; 11% open land; 17% other	Multiple regression	Analysis of historical climate variability	+1/+5%
Tong et al. 2006	Lower Great Miami watershed, OH	3600	71% agricultural; 17% forest; 12% urban	BASINS	Delta change factor	+2/+4 °C
Xiang, 2017	Wilde Lake watershed, MD	4.9	Fully built out, 32% impervious	SWAT	GCM	-0.2/+7.2 °C
Fischbach et al. 2015	Patuxent River watershed, MD	2479	22% developed; 18% agricultural; 9% grassland; 50% forest	CBP 5.3.2	GCM	+0.7/+2.8 °C
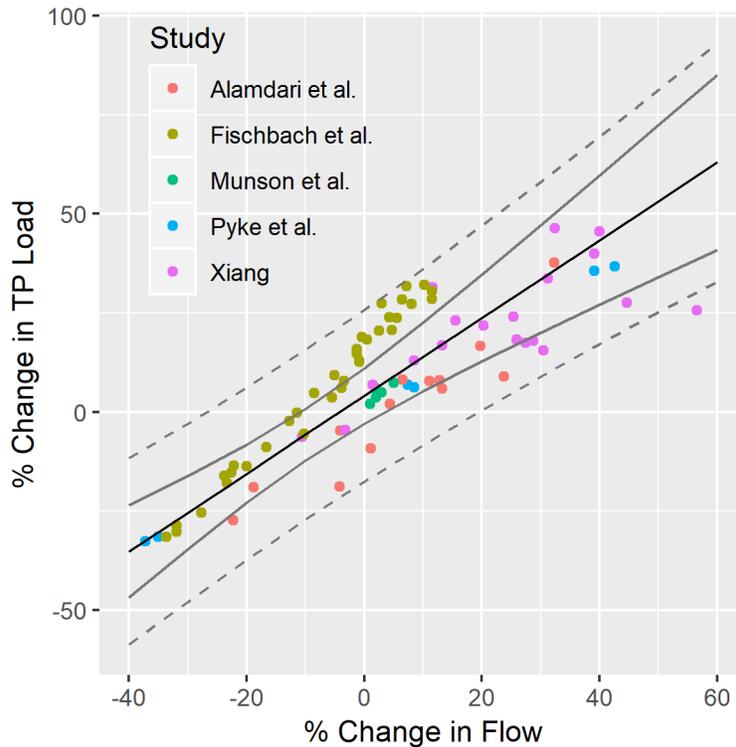
*Figure 4-15: Relationship between % Change in TP Load and % Change in Flow across a set of independent studies. The black line is the average (population-level) fitted line resulting from a hierarchical linear regression where intercept and slope are allowed to vary across studies. The grey lines represent 95% confidence (solid) and prediction (dashed) intervals. Note that results from Tong et al. are not included in this regression because that study reported % changes in rainfall but not % changes in flow. The equation of the population-level regression is: %TP = 4.07 + 0.98 * %FLOW, and the standard errors associated with the intercept and slope estimates are 3.59 and 0.16, respectively.*

4.5.2.2 Analysis of National Stormwater Quality Data

The National Stormwater Quality Database (NSQD) contains data on stormwater runoff quantity and quality collected in urban areas throughout the US (Maestre and Pitt, 2005). The most updated version of the dataset (Version 4.02, last updated in January 2015 and available at http://www.bmpdatabase.org/nsqd.html) contains data on a total of 9051 storm events from 594 sampling locations across 87 counties in 30 states. Sampling years range from 1977 to 2013 and only samples collected at drainage system outfalls are included in the database.

For this analysis, we retained only storm events that have paired data on runoff TP concentration and precipitation depth, leaving a total of 4419 samples from 351 sampling locations across 57 counties in 22 states. We then regressed TP concentration against precipitation depth to investigate how urban runoff TP concentration may change as a function of increasing rainfall. To account for the potential impact of different types of urban land use on the relationship between TP concentration and rainfall depth, we grouped sampling locations based on the principal land use reported in the database and estimated one regression per group. We found that the majority of land uses exhibit a regression slope that is not significantly different from zero (Figure 4-16), suggesting no significant changes in runoff TP concentration with increasing rainfall and therefore generally corroborating the findings from the literature review presented above.
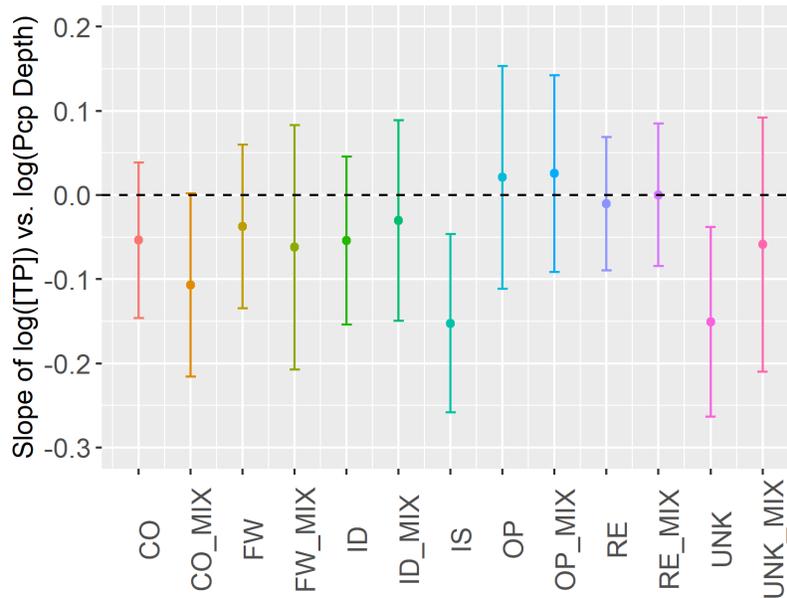
Figure 4-16: Mean and 95% confidence intervals estimates for the slopes of the relationship between log(TP concentration) (mg/L) and log(Precipitation depth) (in) estimated from National Stormwater Quality data. Slopes are estimated for sites characterized by different dominant urban land use types. CO: Commercial; ID: Industrial; RE: Residential; IS: Institutional; FW: Highways and/or Freeways; OP: Open Space; UNK: Unknown. If there is more than one principal use, it is considered a mix and indicated with the suffix _MIX after the dominant land use.

Despite the relatively large uncertainties and prevailing lack of statistical significance, most of the land uses do tend to exhibit a negative mean slope (Figure 4-16). To estimate the effect of adopting a negative slope consistent with results shown in Figure 4-16 on the sensitivity of developed TP loads to climate change, we compared the changes in TP load predicted under 2055 climate conditions following two contrasting assumptions: a) a 1% increase in flow results in a 1% increase in TP load, with TP concentrations remaining constant across climate change scenarios, and b) both flow and TP concentrations are varied across climate change scenarios, with TP concentrations changing as a function of future rainfall according to the mean of the slopes in Figure 4-16 (-0.05 in log-log space). We performed this comparison for an example land segment in the watershed model domain (Fairfax County, land segment ID: N51059) and separately for two types of developed land uses, an impervious land use (MNR - MS4 Buildings and Other) and a pervious one (MTG - MS4 Turf Grass). Specifically, for each land use we estimated two sets of daily TP concentrations predicted under 2055 climate conditions: a) one set was estimated by scaling the time series of daily 1991-2000 TP concentrations by a constant factor to ensure a match between average annual % change in TP load and average annual % change in flow under the no-change-in-concentration assumption, and b) another set was estimated by modifying the scaled 1991-2000 daily TP concentrations according to the mean of the slopes in Figure 4-16 (-0.05 in log-log space) and the expected mean change in rainfall between 1995 and 2055, with appropriate back-transformation to the original, unlogged scale. Both sets of daily TP concentrations were then multiplied by predicted 2050 daily flow values to obtain two sets of future TP loads. Results of these calculations (Table 4-6) indicate that adopting a negative TP-rainfall slope that is consistent with our analyses of the NSQD data has a largely negligible effect on predicted changes in TP loads on developed land resulting from climate change. We interpret

these results as further corroboration for the adoption of a 1:1 relationship as our current best estimate of the response of TP load to climate change-driven changes in flow on developed land.

Table 4-6: Comparison of predicted % changes in flow and TP load on two developed land uses in Fairfax County, VA when comparing 2055 and 1995 climate conditions. Percent changes are calculated on an average annual scale. The Load factor column reports the multiplicative load factor necessary to convert the estimated % change in TP load under a constant concentration assumption to the % change in TP load expected when TP concentration varies as a function of rainfall according to a slope of -0.05 in the log-log space. MNR: MS4 Buildings and Other; MTG: MS4 Turf Grass.

Land use	% change flow	% change TP load under constant concentration assumption	% change TP load under varying concentration assumption	Load factor
MNR	7.13	7.13	6.74	0.95
MTG	8.24	8.24	7.78	0.94

4.5.2.3 Comparison of results from literature review with TP load sensitivities used in the Phase 6 Watershed Model for non-developed land uses

To compare the proposed 1:1 relationship between percent change in TP load and percent change in flow on developed land uses with TP sensitivities that are described for the Phase 6 model in Section 4.5.1 for other land uses or sectors, percent changes in TP load and flow predicted for a few example non-developed land uses under 2025 climate conditions were estimated with respect to 1995 climate conditions. When comparing responses of developed vs. non-developed land uses, it is critical to distinguish between stormflow and total flow. While on impervious land stormflow and total flow essentially represent the same quantity, in pervious land stormflow is only a portion of total flow, and model results indicate that overall percent changes in total flow generally represent only a fraction of the corresponding percent changes in stormflow on pervious land (Figure 4-17). As a result, when regressing percent changes in TP load against percent changes in flow, the slope of the relationship will be different, and generally lower, when considering stormflow rather than total flow in pervious land uses. The difference between stormflow and total flow is attenuated in developed land uses, which are typically made up of a mix of pervious and impervious surfaces. To offer an appropriate comparison of TP sensitivities across land uses with different fractions of impervious surfaces and thus different ratios of stormflow to total flow, percent changes in TP load are expressed with respect to percent changes in both stormflow and total flow. Percent changes in flow obtained from published studies were converted to approximate percent changes in stormflow using output from the Phase 6 Watershed Model. Specifically, output from the 2025 and 1995 climate scenarios was used to estimate the ratio between percent change in stormflow and percent change in total flow over developed areas in each land segment. That ratio varies across the land segments with the fraction of impervious area (Table 4-7), and the estimated median, 5%, and 95% percentile values of that ratio were used to convert the TP load sensitivity to total flow estimated from published studies to a corresponding approximate range of sensitivities to stormflow (Table 4-8).
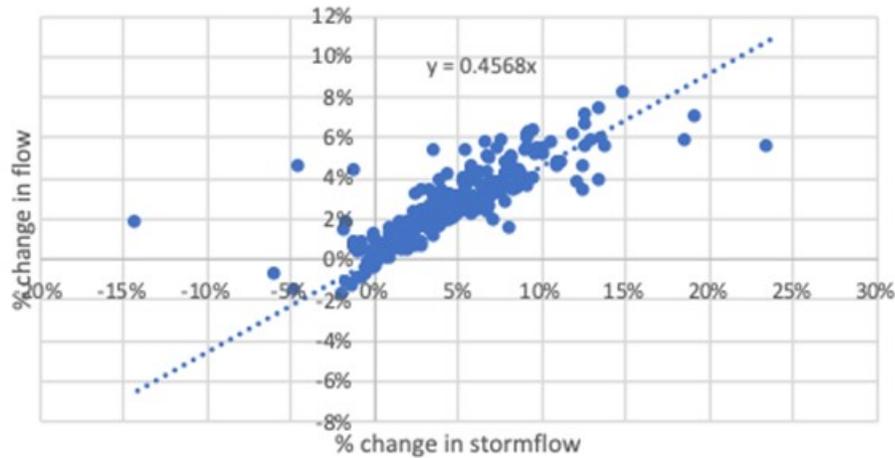
Figure 4-17: Example of relationship between percent change in total flow and corresponding percent change in stormflow estimated by the Phase 6 Watershed Model at each land segment on a pervious land use (grain with manure) when comparing 2025 and 1995 climate scenarios.

Table 4-7 Characteristics of the distribution of the fraction of impervious area, percent change in total flow and percent change in stormflow estimated by the Phase 6 Watershed Model at each land segment when comparing 2025 and 1995 climate conditions. Land segments with higher fractions of impervious area tend to exhibit a larger ratio of percent change in stormflow/percent change in flow.

Percentile	% Impervious Area	% Change in Flow	% Change in Stormflow	% Change in Stormflow / % Change in Flow
95%	55%	5.4%	7.0%	2.70
75%	39%	3.6%	5.2%	1.69
50%	32%	2.6%	4.0%	1.50
25%	27%	1.7%	2.8%	1.32
05%	22%	0.8%	1.5%	1.15

Table 4-8 TP load sensitivities to changes in total flow and stormflow estimated by the Phase 6 Watershed Model for a few example load sources and land uses when comparing 2025 and 1995 climate conditions. The last row of the table provides the TP load sensitivity to changes in flow proposed after a review of published small-scale studies.

Load Sources	% Change in TP Load per Unit % Change in Flow	% Change in TP Load per Unit % Change in Stormflow
Grain with Manure	1.54	0.86
Full Season Soybeans	1.72	0.97
Pasture	0.96	0.42
Forest	1.41	0.49
Crops	1.41	0.79
Pasture & Hay	1.16	0.51
Natural	1.27	0.49
Developed	**1.00**	**0.67 (0.37 – 0.87)***

*Values estimated by dividing the TP sensitivity to changes in total flow (1.00) by the median (5-95% percentiles) ratios of percent change in stormflow/percent change in total flow estimated by the Phase 6 Watershed Model across land segments when comparing 2025 and 1995 climate change scenarios

4.6   BMP effectiveness change

As climate change alters the intensity of storm events the effectiveness of BMPs will likely change, particularly for those BMPs that control nutrients and sediment by controlling flow. Studies have found decreasing BMP effectiveness under future climate scenarios using process-based models. For example, Bosch et al. 2014 and Woznicki and Nejadhashemi 2011, modeled agricultural BMPs and Fischbach et al, 2014 modeled developed BMPs. However, the CBP partnership has determined that, while acknowledging the likelihood of decreased BMP performance, there is not sufficient information available to model the effect at this time.

The CBP's Principals' Staff Committee (PSC) gave specific direction to the CBP partnership at their December 2017 meeting to "… develop a better understanding of the BMP responses, including new or other emerging BMPs, to climate change conditions". The PSC gave instructions to the Management Board to develop a multiyear prototype science and technical program on new stormwater management and BMPs responsive to the new climate reality of increased flow volumes and intensities is recommended using available annual funding. The prototype program is suggested to run until 2025, and if successful, the CBP partnership could decide to continue the program. The program would be specific and directed toward the specific CBP partnership applied scientific needs. The Climate Resiliency Workgroup and the WQGIT will examine the top tier agricultural/urban BMPs and actions in the WIP3s that are vulnerable to future climate risk, with initial emphasis on multi-year BMPs that contribute substantially to WIP nutrient and sediment reductions and/or are structural in nature or persist longer in the landscape.

4.7   Landscape processing effects

4.7.1   Changes in speciation

An empirical relationship between WRTDS-estimated Total Nitrogen (TN) and Nitrate (NO_3) per acre loads from the Chesapeake Bay Nontidal Network stations is currently used in the Phase 6 Watershed Model to estimate the fraction of the annual edge-of-river TN load that is NO_3 at each river segment (Figure 4-18; Section 10.5.2.1.1 CAST 2017).

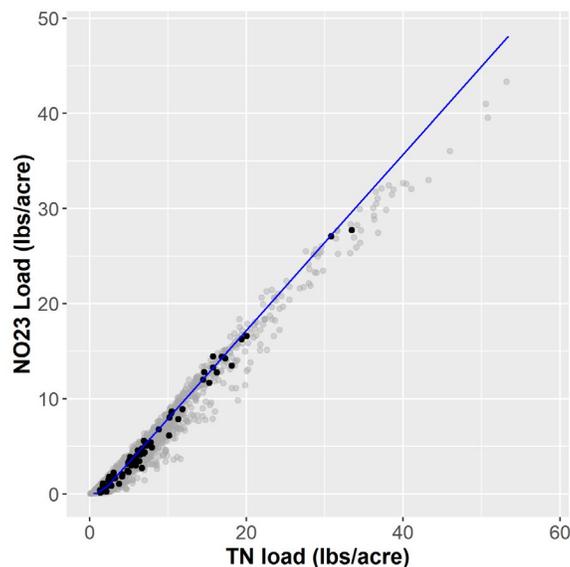*Figure 4-18: Relationship between NO₃ and TN load per acre obtained from Chesapeake Bay Nontidal stations and used in the Phase 6 Watershed Model to estimate edge-of-river annual NO₃ loads at each river segment (for more information, see Section 10 of the Phase 6 CAST and Watershed Model documentation, Chesapeake Bay Program 2017). Black circles represent the long-term average annual TN and NO₃ loads estimated at each nontidal station, while gray circles represent annual TN and NO₃ loads.*

This relationship was also used for preliminary climate change scenario development to predict the response of N speciation, hereby characterized as the ratio of NO_3/TN, to climate change-driven changes in hydrology and TN loads. However, during the 2018 Chesapeake Bay Program Climate Change Modeling 2.0 Workshop which is not yet published, members of the watershed breakout group suggested that this empirical relationship might be primarily driven by spatial differences in land use across stations and may therefore not be representative of the expected response of N speciation to climate change-driven changes in hydrology. To address these concerns, long-term time series of TN and NO_3 loads available at Chesapeake Bay Nontidal stations (https://doi.org/10.5066/F7RR1X68) were further analyzed to explore differences in N speciation responses due to between-station changes in long-term average N loads, a proxy for long-term average N inputs and thus level of anthropogenic impact, and within-station inter-annual variability in hydrology. A review of process-based studies that quantified changes in both organic and inorganic N species under climate change scenarios was also carried out in the spirit of a "multiple lines of evidence" approach.

4.7.1.1   Literature review

We found six modeling studies that compared changes in NO_3 and organic nitrogen (ON) loads under climate change scenarios, all of which were based on SWAT simulations (Table 4-9). The limited number of studies did not warrant any consideration of potential differences in responses across land uses or other gradients of watershed characteristics, and an overall linear regression was fit across all six studies to quantify the relationship between expected percent changes in NO_3 and percent changes in ON loads (Figure 4-19). Although results from the linear regression appear to suggest a relatively lower increase in NO_3 associated with climate change-driven increases in ON, resulting in an overall decrease in the $NO_3/(ON+NO_3)$ ratio, the limited number of studies and substantial uncertainty in the estimated relationship prevent from drawing reliable conclusions on the relative response of inorganic and organic N forms to climate change impacts.

Table 4-9: Main characteristics of the studies used to assess the relative response of NO₃ and organic nitrogen (ON) loads to climate change scenarios.

Reference	River	State/ Country	Watershed Area (km²)	Model	Land use
El Khoury et al 2015	South Nation	Ontario, Canada	3858	SWAT	57.8% agricultural; 41.03% forest
Hanratty & Stefan 1998	Cottonwood	MN	3400	SWAT	52% rangeland; 46% crop
Moshtaghi et al 2018	Golgol	Iran	280	SWAT	27% cultivated
Ross 2014	Woonasquatucket-Moshassuck	RI/MA	192.6	SWAT	38.2% developed; 49.1% forest; 4.5% agricultural; 2% water; 6.2% wetland

| Reference	River	State/Country	Watershed Area (km^2)	Model	Land use
Ross 2014	Ten Mile	RI/MA	143.6	SWAT	40.9 developed; 46.2% forest; 4.5% agricultural; 2% water; 6.3% wetland
Ross 2014	Taunton	RI/MA	1250.2	SWAT	Upper Taunton: 36% developed; 50.5% forest; 1.1% agricultural; 2.9% water; 9.5% wetland; Mid Taunton: 17.6% developed; 62.8% forest; 4.7% agricultural; 6.3% water; 8.7% wetland; Lower Taunton: 24.6% developed; 56.4% forest; 3.4% agricultural; 7.5% water; 8.0% wetland
Ross 2014	Pawtuxet	RI/MA	599.6	SWAT	18.2% developed; 67% forest; 4.4% agricultural; 4.6% water; 5.6% wetland; 0.2% bare rock
Ross 2014	Blackstone	RI/MA	1228.5	SWAT	Upper Blackstone: 28.7% developed; 53.1% forest; 6.1% agricultural; 4.7% water; 7.3% wetland; 0.1% bare rock; Lower Blackstone: 14.6% developed; 70.2% forest; 6.5% agricultural; 2.3% water; 6.3% wetland
Tong et al 2007	Little Miami	OH	5840	SWAT	56.2% agricultural; 23.7% forest; 17.8% urban; 0.97% water; 0.38% other
Wang and Kalin 2018	Wolf Bay	AL	126	SWAT	1.2% water; 26.4% urban; 20.9% forest; 9.7% pasture; 29.9% cropland; 11.9% wetland
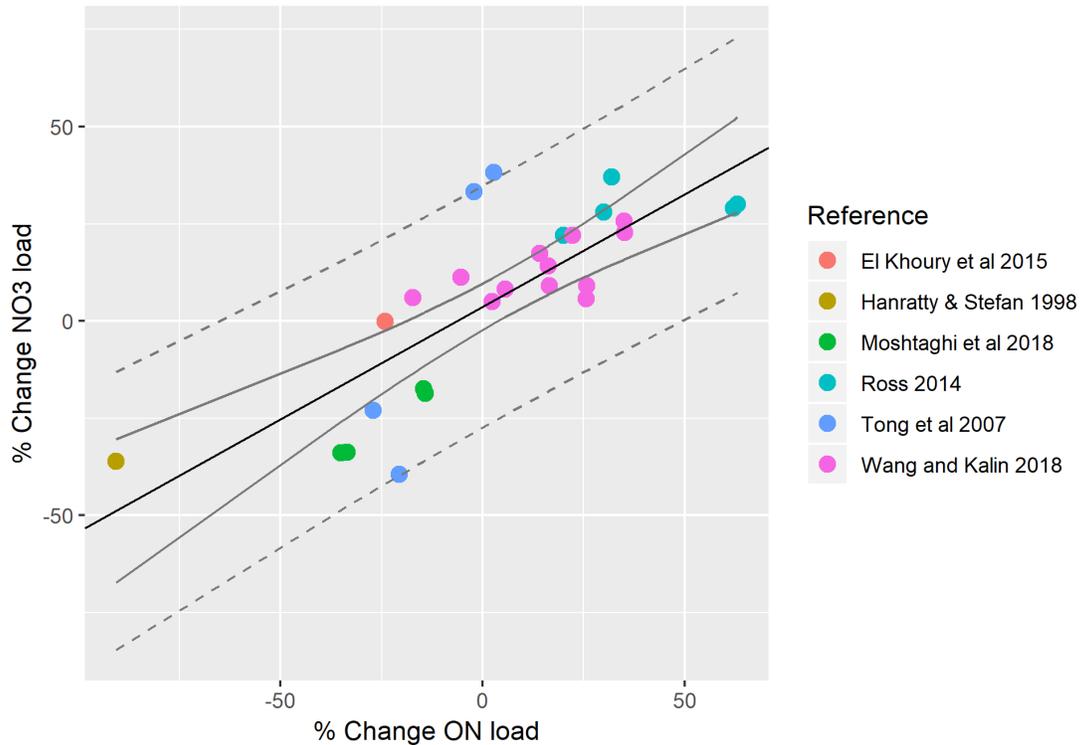
Figure 4-19: Relationship between percent change in NO$_3$ load and percent change in ON load under climate change scenarios from six published studies. The grey lines represent 95% confidence (solid) and prediction (dashed) intervals. The equation of the mean regression is: **%NO$_3$ = 3.67 + 0.58 * %ON** *(intercept standard error = 2.89, slope standard error= 0.09).*

4.7.1.2 Analysis of data from Chesapeake Bay Nontidal Network stations

The relationship found between NO$_3$ and TN loads when pooling data across all stations (either individual annual loads or long-term average annual loads; Figure 4-18) implies that an increase in TN load will result in an increase in the NO$_3$/TN ratio (Figure 4-20). This type of response is often expected as a result of land-use and/or management-driven changes in N loads, with several studies showing that predominantly agricultural watersheds tend to exhibit higher NO$_3$/TN ratios compared to more pristine regions characterized by relatively lower anthropogenic N inputs (Scott et al., 2007; Sponseller et al., 2014). However, when looking at the inter-annual response of the NO$_3$/TN ratio within individual stations, several stations appear to show an opposite pattern, with increasing TN loads being associated with lower NO$_3$/TN ratios (Figure 4-21, right panels). To simultaneously model the different response of the NO$_3$/TN ratio to changes in TN load at different scales (*across-stations*, where spatial differences in land use and watershed characteristics may play a critical role, and *within-stations*, where inter-annual variability in hydrology represents an important driver), we expanded the Phase 6 linear regression through a hierarchical modeling approach. Hierarchical models are especially well suited to model data that are structured into distinct groups, such as samples collected at different sites (Gelman and Hill, 2007) and they offer several benefits, including the ability to: 1) simultaneously take advantage of all available data, 2) improve estimates of model coefficients for groups with lower sample size and/or higher variability by "borrowing strength" from groups with larger sample size and higher strength of information, 3) better account for different sources of uncertainty across the levels of the model hierarchy, and 4) incorporate predictors that act at different levels of the hierarchy, thereby simultaneously modeling variation at the individual data-level and at the group-level

(Cressie et al., 2009; Gelman and Hill, 2007; Qian and Shen, 2007; Stow et al., 2009). In this work, we built a model that quantifies the relationship between annual NO_3 and TN loads, where the coefficients that characterize that relationship vary by station.

After several tests, we found that a non-linear formulation of the functional relationship between annual NO_3 and TN loads better fitted the observed data and offered a more realistic representation of the behavior of NO_3/TN dynamics near the edges of the range of observed TN loads. The deterministic form of the model is thus a non-linear regression between WRTDS-estimated annual NO_3 loads per acre (response variable) and annual TN loads per acre (individual-level predictor) at each station. In its basic form, the chosen non-linear functional form, a modification of Holling`s Type III functional response widely used in animal ecology, has the same number of parameters (2) of a linear regression (α and β in Eq. 2). The hierarchical model formulation can be represented as follows. Each individual observation (annual nitrate for year i at a station j, $NO3_{i,j}$) is modeled as arising from a normal distribution with mean $\hat{y}_{i,j}$ and standard deviation σ (Eq. 1), where $\hat{y}_{i,j}$ represents the mean deterministic model prediction for the individual observation $NO3_{i,j}$ as a function of the predictor $TN_{i,j}$ (Eq. 2). The two parameters that quantify the functional relationship between $NO3_{i,j}$ and $TN_{i,j}$ are allowed to vary across stations, i.e. instead of estimating one single value of α and β for the whole dataset, as is typically done in a classical regression approach, different α_j and β_j values are estimated for each station j and these station-specific α_j and β_j values are themselves modeled as random variables arising from probability distributions. As mentioned above, the hierarchical structure of the model allows for the incorporation of station-level covariates that may help explain the between-station variation in model coefficients. We then modeled both sets of parameters as arising from normal distributions whose respective means are estimated as a linear function of the long-term average TN load per acre estimated at each station ($\overline{TN_j}$) (Eqs. 3 and 4).

$$NO3_{i,j} \sim Normal(\hat{y}_{i,j}, \sigma) \hspace{4cm} \text{Eq. 1}$$

$$\hat{y}_{i,j} = \frac{\alpha_j * TN_{i,j}}{\sqrt{\beta_j^2 + TN_{i,j}^2}} \hspace{4cm} \text{Eq. 2}$$

$$\alpha_j \sim Normal(a_0 + a_1 * \overline{TN_j}, \sigma_\alpha) \hspace{2.5cm} \text{Eq. 3}$$

$$\beta_j \sim Normal(b_0 + b_1 * \overline{TN_j}, \sigma_\beta) \hspace{2.5cm} \text{Eq. 4}$$

where:

$NO3_{i,j}$:   WRTDS-estimated NO3 load (lbs/ac) in year i at station j

$\hat{y}_{i,j}$:   mean deterministic model prediction for $NO3_{i,j}$

$TN_{i,j}$:   WRTDS-estimated TN load (lbs/ac) in year i at station j

$\overline{TN_j}$:   long-term average TN load (lbs/ac) at station j

α_j, β_j: station-specific coefficients quantifying the non-linear relationship between NO_3 and TN at each station

a_0, a_1, b_0, b_1:   coefficients quantifying the relationship between station-specific model coefficients and $\overline{TN_j}$.

σ, σ_α, σ_β: within- and across-station variances

Model parameters` posterior distributions were estimated within a Bayesian framework using a Markov Chain Monte Carlo (MCMC) algorithm implemented in the software JAGS (Plummer, 2003) interfaced with R (R Core Team, 2015) through the R package rjags (Plummer, 2015). We ran three parallel MCMC chains with 50,000 iterations, a burn-in period of 25,000 iterations, and a thinning factor of 100 to reduce auto-correlation. We considered the chains to have converged when R̂<1.1 for all model parameters.

Model parameter estimates are provided in Table 4-10. The flexible hierarchical formulation allows for the estimation of an overall average regression, but also of station-specific regressions, whose parameters can be estimated for new stations outside of the current dataset as linear functions of the average long-term TN load at each station (Figure 4-22). The overall average regression is very close to the Phase 6 regression (Figure 4-22), while the station-specific regressions appear to better capture the observed response of the NO_3/TN ratio to inter-annual variability in hydrology. The hierarchical model developed and parametrized using the network of monitoring data and the formulation described above (Eqs. 1-4) can be applied for estimating the mean N speciation response of a specific catchment (or river segment) J in the watershed model using Eq. 5:

$$NO3_{i,j=J} = \frac{(a_o+a_1\overline{TN}_{j=J})\times TN_{i,j=J}}{\sqrt{(b_o+b_1\overline{TN}_{j=J})^2+TN_{i,j=J}^2}}$$ Eq. 5

This revised regression is used in the model for estimating the edge-of-river N speciation response. The revised regression aids in the quantification of two different components of a watershed N speciation response – the *average annual* response where speciation changes are due to drivers such as land use, nutrient inputs, watershed characteristics, and management practices, and the *annual* response where speciation changes annually with TN due to hydrologic drivers (Table 4-11). Specifically, when estimating changes in N speciation due to annual variability in hydrology and climate change at catchment J, the long-term average TN load for that catchment ($\overline{TN}_{j=J}$ in Eq. 5) is held constant. On the other hand, when estimating changes in the average NO_3/TN ratio due to differences in land-use, nutrient inputs and management practices, $\overline{TN}_{j=J}$ is varied, causing catchment J to shift position along the red line in Figure 4-22. For a climate change scenario application, $\overline{TN}_{j=J}$ is the long-term average annual TN estimated for catchment J under that specific scenario but before accounting for the impact of climate change. For all other scenario applications, $\overline{TN}_{j=J}$ is the long-term average annual TN estimated for catchment J for each specific scenario that changes with land-use, nutrient inputs, and management practices. Once the average component of the speciation response ($\overline{TN}_{j=J}$) is varied for a given land-use or management scenario, it is assumed that the average watershed response does not change across years, and interannual variability is primarily due to hydrology, even when land-use and/or management may change within the simulation period.

It is recognized that this empirical approach has some obvious limitations, such as, among others: 1) uncertainty associated with WRTDS load estimates, b) uncertainty related to the extrapolation of observed responses to inter-annual variability in hydrology to approximate the expected response to long-term, gradual changes in hydrology due to climate change, and 3) uncertainty in

the potential influence of multiple confounding factors at several spatial and temporal scales in determining N loads ultimately observed at the nontidal stations. Nonetheless, we think that this revised regression represents an improvement over the previous formulation especially in its ability to better differentiate between N speciation responses to large-scale spatial patterns vs. more local variability in hydrology.
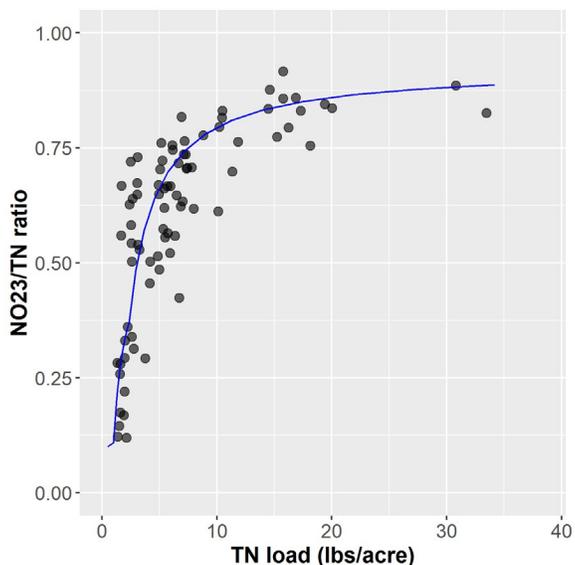

Figure 4-20: Same regression as in Figure 4-18 but here the y-axis represents the NO₃/TN ratio rather than the NO3 load per acre. Just like in Figure 4-18, black circles represent the long-term average annual TN and NO₃ loads estimated at each nontidal station.
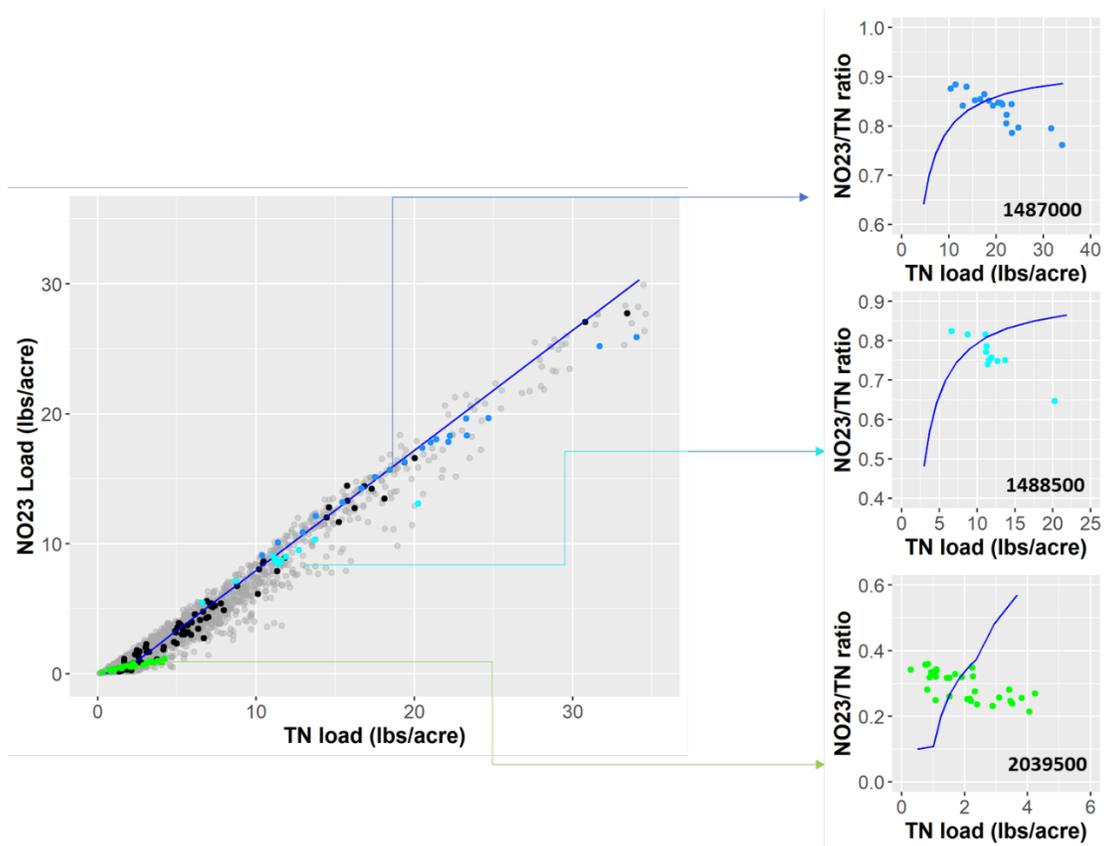

Figure 4-21: Example of inter-annual variability in the NO3/TN ratio as a function of annual TN load at individual nontidal stations. Annual NO3 and TN loads for three exemplary stations are highlighted with different colors in the main figure, while the three

smaller panels to the right show the same data but with the y-axis representing the NO3/TN ratio rather than the NO3 load. The dark blue line represents the Phase 6 regression also shown in Figure 4-18 and Figure 4-20.

Table 4-10: Posterior parameter means and standard deviations

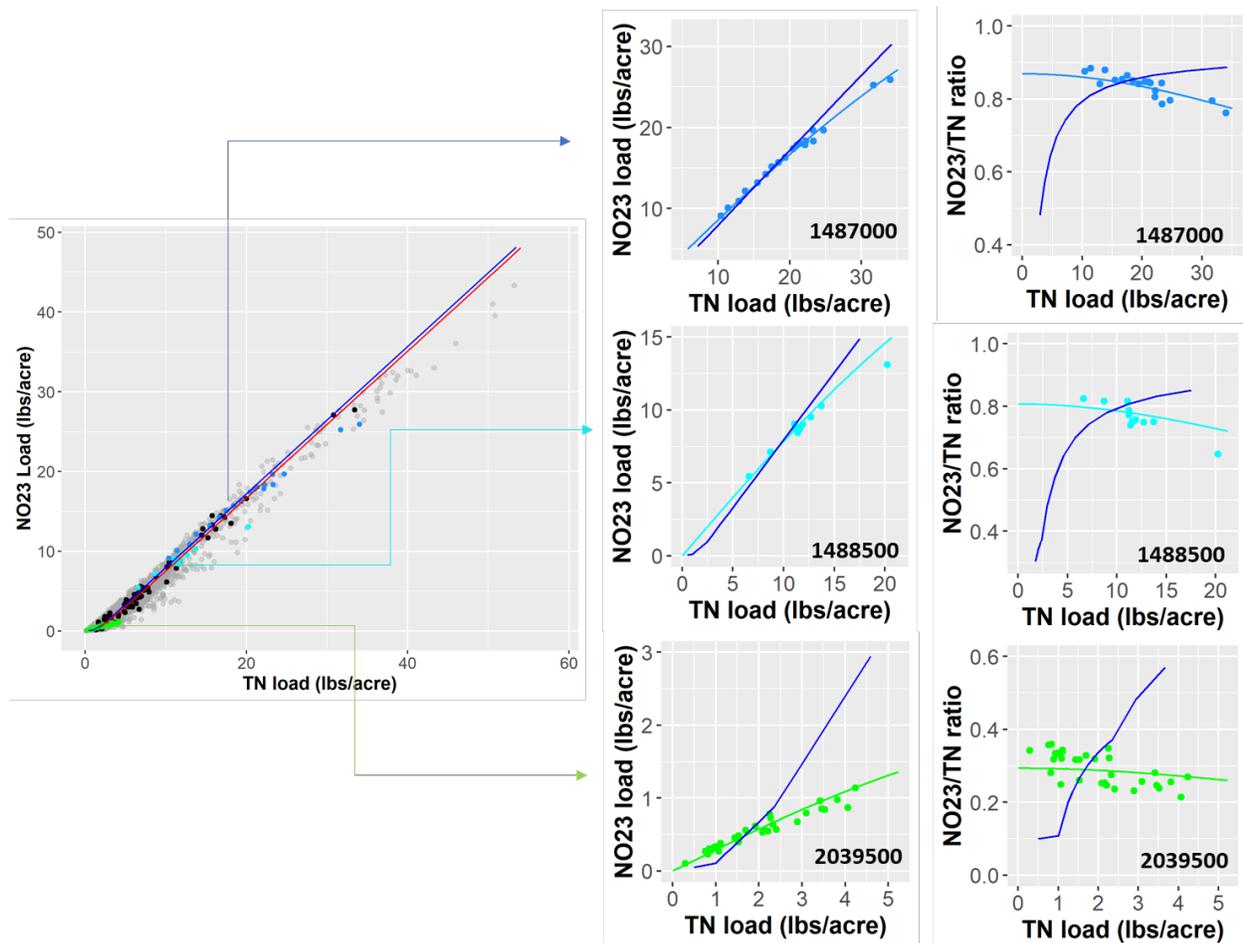| Parameter	Mean	SD
a0	-3.27	1.01
a1	3.15	0.11
b0	3.57	1.51
b1	3.26	0.15
σ	0.33	0.01
σα	2.83	0.14
σβ	2.78	0.21

Figure 4-22: Comparison between the Phase 6 regression (dark blue line) and the overall average regression obtained through hierarchical modeling (red line in main figure). The smaller panels to the right compare the Phase 6 regression (dark blue) to station-specific hierarchical regressions (light blue, cyan and green) for three example stations.

Table 4-11: Examples of predicted changes in the NO3/TN ratio as a result of changes in TN load mainly driven by inter-annual variability in hydrology vs. other factors (e.g., land-use, management practices, etc.) at three USGS nontidal stations spanning a broad range of average annual TN loads.

USGS Station ID	1487000	1488500	2039500
USGS Station Name	Nanticoke River near Bridgeville	Marshyhope Creek near Adamsville	Appomattox River at Farmville
Land Use	46% agricultural; 2% pasture; 10% developed; 42% natural/forested	50% agricultural; 2% pasture; 7% developed; 41% natural/forested	7% agricultural; 10% pasture; 5% developed; 78% natural/forested
$\overline{TN}$ (lbs/acre)	20.02	11.83	1.97
$\overline{NO3/TN}$	0.834	0.780	0.289
NO3/TN for 5% increase in TN due to hydrology	0.831	0.774	0.289
NO3/TN for 10% increase in TN due to hydrology	0.828	0.771	0.288
NO3/TN for 5% decrease in TN due to hydrology	0.838	0.780	0.290
NO3/TN for 10% decrease in TN due to hydrology	0.841	0.783	0.290
NO3/TN for 5% increase in TN due to non- hydrology factors	0.838	0.784	0.309
NO3/TN for 10% increase in TN due to non- hydrology factors	0.842	0.790	0.329
NO3/TN for 5% decrease in TN due to non- hydrology factors	0.830	0.770	0.267
NO3/TN for 10% decrease in TN due to non- hydrology factors	0.825	0.762	0.244

4.7.2 Groundwater Lag

Groundwater lag times are an important part of the Phase 6 dynamic simulation model but are not simulated in the Phase 6 CAST. CBP management scenarios are run without lag time and are meant to represent the long-term loading based on a static set of management practices. Lag scenarios in the dynamic model are only used for calibration and for specific lag time studies. Given that the CBP 2019-2021 climate assessment is using the CBP management scenarios

methodology that excludes lag time, the change in lag time due to climate change will be ignored for the 2019 assessment.

However, some discussion of the potential effects of lag time is helpful if the CBP would like to consider lag scenarios or the effects on calibration. Groundwater systems are expected to be impacted by climate change. Studies, summarized in Lall, et al. 2018, have found that climate change will have an effect on human uses of groundwater and also on the timing and amount of recharge. Konikow, 2015, in a nationwide study, found long-term depletion in the coastal plain of the Chesapeake region.

The equation found in figure 10-30 of the CAST documentation (CBP 2017) (reproduced here as Figure 4-23, left panel) establishes a relationship between groundwater age and the ratio of water table depth and recharge based on a MODFLOW model of the Potomac. The relationship was used to estimate groundwater age for all non-coastal plain segments the in the Chesapeake Bay watershed in the Phase 6 dynamic model. Using the equation from figure XXX, it is be possible to estimate the change in groundwater age from a climate-change induced change in recharge rate. Figure 4-23, right panel shows the changes in groundwater age based on a 1 inch per year recharge increase.

The regression model for estimating groundwater age
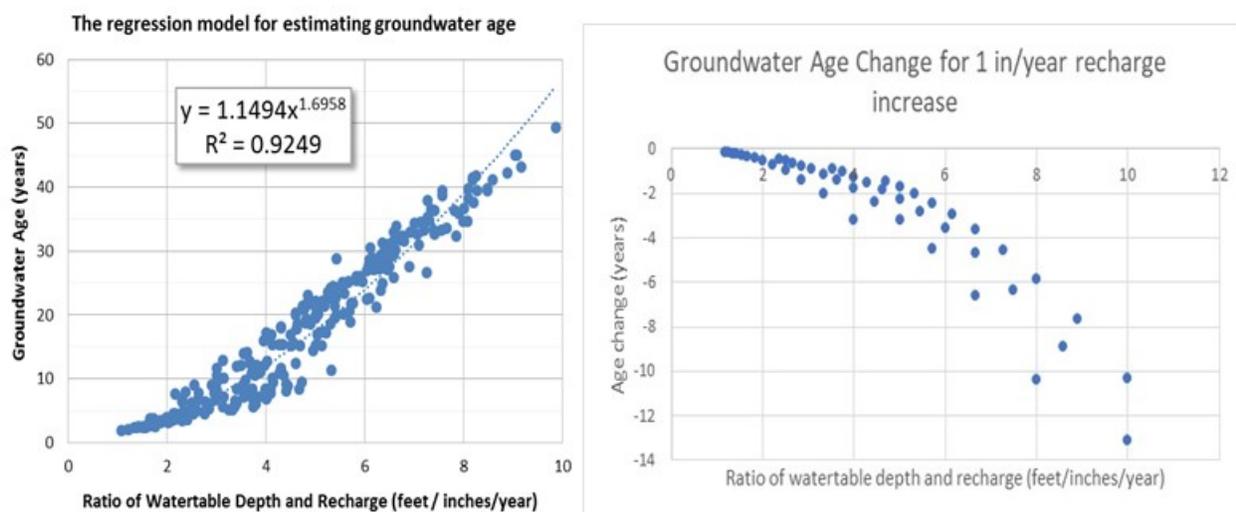
$$y = 1.1494x^{1.6958}$$
$$R^2 = 0.9249$$

Figure 4-23: Left panel: Groundwater age as a function of the ratio between water table depth and recharge rate [Adapted from Sanford (2015)]. Right Panel: change in groundwater age from a 1 inch per year increase in recharge based on the relationship in the left panel

In the coastal plain, figure 10-32 of the CAST documentation (reproduced here as Figure 4-24) found that recharge was a minor portion of the second principle component rather than a major influence. The weights for the 4 most important PCs are shown. Lithological, physiographic, and geological attributes are the main determinant of groundwater age in the Chesapeake Coastal Plain above recharge rate.
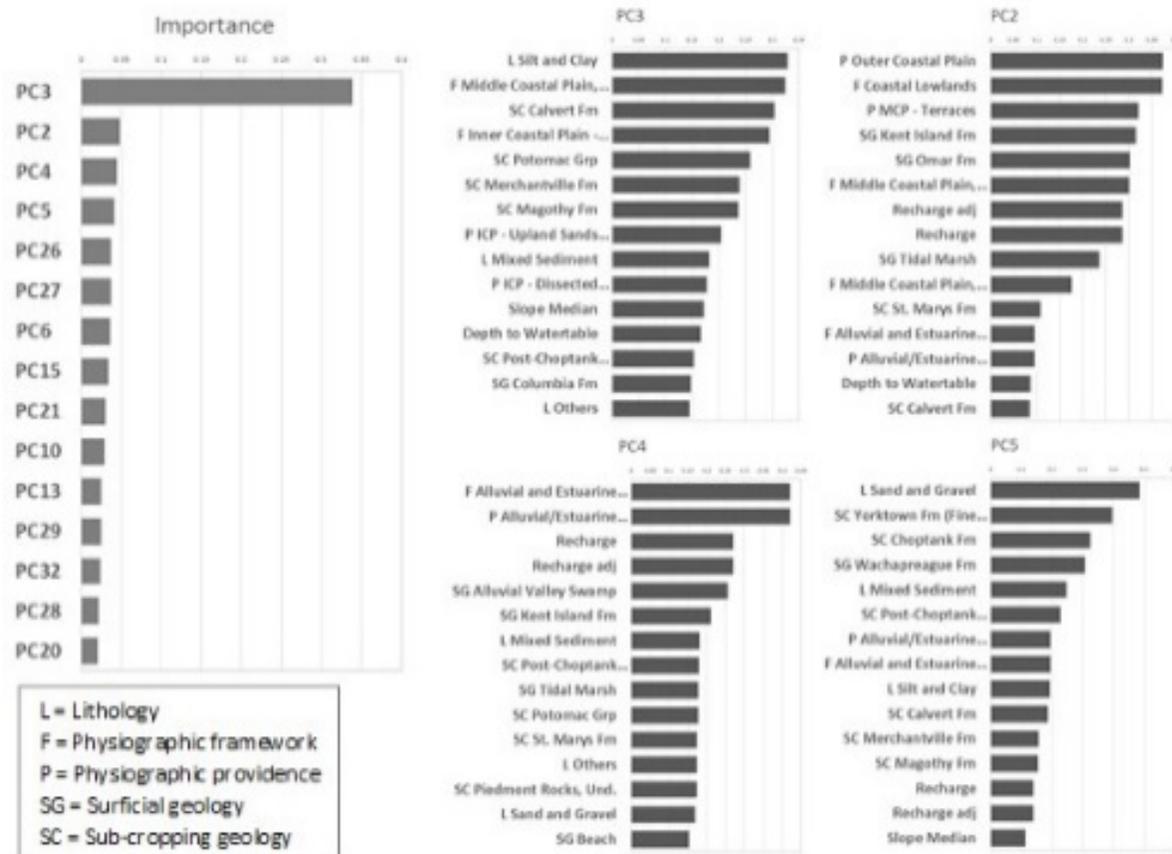
Figure 4-24: Left: Importance of the Principle components (PCs) in the statistical model for explaining the groundwater age in the Chesapeake Coastal Plain. Right: The weights of the watershed attributes in the principle components.

Both of these analyses were aimed at estimating the spatial variability of groundwater lag times and are not necessarily representative of change in lag over time as climate changes. The lack of consistency between the two approaches also causes some concern given that application of the methods may lead to a smaller change in the non-coastal plain regions based on the analysis method rather than real differences that may exist.

4.7.3   Land to water and stream to river effects

Figure 4-25 shows the structure of the time-averaged model for nutrients. The processes represented correspond to separable scales and physical domains. The output of the model is the amount of nitrogen or phosphorus delivered to tidal waters from a given land use or loading source in a land-river segment. The structure is discussed in more depth in Section 1 of the Phase 6 Watershed Model documentation.
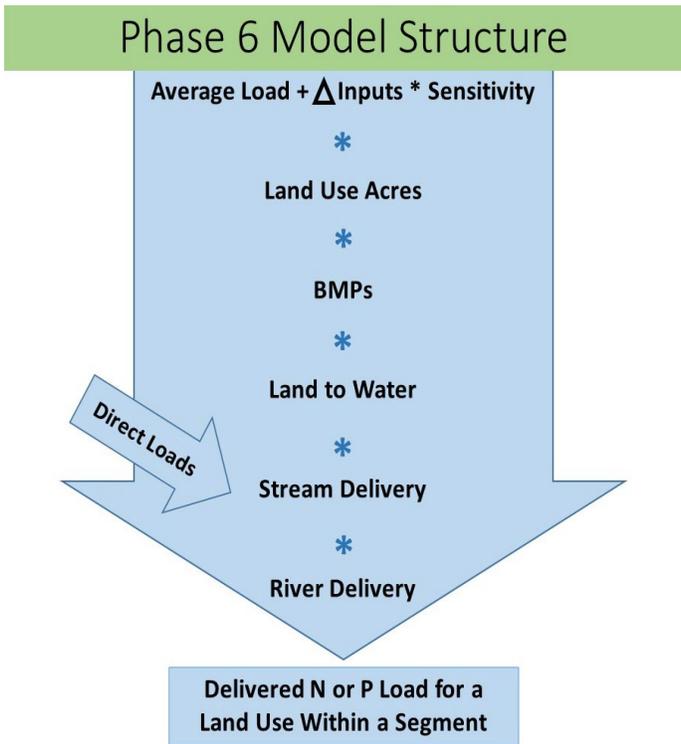
Phase 6 Model Structure

Average Load + Δ Inputs * Sensitivity

*

Land Use Acres

*

BMPs

*

Land to Water

Direct Loads

*

Stream Delivery

*

River Delivery

Delivered N or P Load for a
Land Use Within a Segment

Figure 4-25: Phase 6 Watershed Model Structure

The top line in Figure 4-25 (average loads, inputs, and sensitivities) represents the loads exported from a land use to a stream in a land segment taking into account local applications but not local watershed conditions. Land Use Acres and BMP factors account for local extent of the land use and modifications of the loads due to installed management practices.

The Phase 6 model accounts for the effect of landscape and riverine properties on load delivery by a series of factors which are applied after management is considered. Land to Water factors account for spatial differences in loads due to physical watershed characteristics. Stream Delivery and River Delivery factors are applied to account for nutrient and sediment processes in waterways. Streams are defined as having an average flow less than 100 cfs with rivers being larger.

Sections 4.4 and 4.5 of this document describe modeled and monitored responses of nitrogen and phosphorus, respectively to climate variables. In the discussion of nitrogen response to climate change in Section 4.4, the literature cited refers to studies that are conducted at the watershed scale. These studies include landscape delivery and the effects of small streams. Therefore, it would not be appropriate to apply an additional effect of climate change to the land-to-water or stream-to-river factors for nitrogen. Section 7 of the Phase 6 Watershed Model documentation describes an increasing nitrogen delivery with groundwater recharge and wetter soils which is consistent with the work cited in Section 4.4. Riverine processes are simulated directly in HSPF as described in Section 10 of the Phase 6 Watershed Model documentation. The effects of temperature on biological and chemical processes are simulated through temperature-corrected dynamic modeling. Stream scour is positively related to shear stress, which is in turn positively related to flow. Table 4-12 summarizes the information on the simulation of landscape process adjustment to climate change for nitrogen.

Table 4-12: Climate effects on nitrogen transport

Land use category	Land to water	Stream delivery	River delivery
Agricultural	Captured in literature review and analysis		Simulated in HSPF
Developed	Captured in literature review and analysis		Simulated in HSPF
Natural	Captured in literature review and analysis		Simulated in HSPF

As described in 4.5.1, change in agricultural and natural phosphorus loads due to climate change rest on the modeled response to the stormflow and sediment washoff. The responses to stormflow and sediment washoff were developed in the Phase 6 Watershed Model to account for spatial differences but can be applied to climate since there were initially developed through modeling of changes in these variables through time. Changes in these values due to climate change will be incorporated in the calculation of loads and will therefore account for climate-related changes in the land to water delivery. The climate effects on phosphorus delivery on developed in Section 4.5.1.1 similarly accounts for changes in phosphorus delivery due to changes in delivery through the landscape.

The analysis of climate effects on phosphorus transport in agricultural and natural areas includes only landscape processes and not stream processes. Similarly, the analysis of change in developed land rests on end-of-pipe values and would not include stream delivery effects. The Phase 6 simulation includes a direct simulation of rivers that will respond to higher flows with higher amounts of scour, however this effect is not simulated in smaller rivers. Currently the CBP has no way to address climate change effects on streams for phosphorus. It is still the case however, that streams will be simulated as increasing or decreasing their bed and bank loads relative to the change in upstream load for any scenario. Table 4-13 summarizes the information on the simulation of landscape process adjustment to climate change for phosphorus.

Table 4-13: Climate effects on phosphorus transport

Land use category	Land to water	Stream delivery	River delivery
Agricultural	Already represented in sensitivities	Not adjusted for climate	Simulated in HSPF
Developed	Added based on literature and analysis	Not adjusted for climate	Simulated in HSPF
Natural	Already represented in sensitivities	Not adjusted for climate	Simulated in HSPF

4.8   Climate Scenario Model Results

Phase 6 Watershed Model was used for assessing the impact of climate change on the delivery of flow, nutrients, and sediment. In this assessment, Watershed Implementation Plan Phase 2 (WIP2) Level of Effort scenario was used as the reference scenario for quantifying the impacts of climate change. The estimated change in delivery presented in this section represent anticipated change in watershed response between the 1991-2000 climatology and a future year. Therefore, in reference to 1991-2000, specific scenarios consist of climatic change over a 30-year period for the 2025 scenario and 55 years for the 2050 scenario.

Table 4-14: List of climate change scenarios run and corresponding inputs.

Year	No.	Scenario description	Rainfall	Volume to Intensity	Temperature	CO2
Year 2025	01	Rainfall sensitivity scenario	Extrapolation of 88-year historic trend	Equally between intensity deciles	N/A	N/A

	02	Rainfall sensitivity scenario	Extrapolation of 88-year historic trend	Based on observed trends	N/A	N/A
	03	Temperature sensitivity scenario	N/A	N/A	RCP 4.5 31-member ensemble median (P50)	N/A
	04	CO2 level sensitivity scenario	N/A	N/A	N/A	Change from 363 to 427 ppm
	05	Integrated scenario	Extrapolation of 88-year historic trend	Based on observed trends	RCP 4.5 31-member ensemble median (P50)	Change from 363 to 427 ppm
	06	Integrated scenario	Extrapolation of 88-year historic trend	Based on observed trends	RCP 4.5 31-member ensemble median (P50) – *Hamon Method*	Change from 363 to 427 ppm
	07	Integrated scenario uncertainty	Extrapolation of 88-year historic trend	Based on observed trends	RCP 4.5 10 percentile bound of 31-member ensemble (P10)	Change from 363 to 427 ppm
	08	Integrated scenario uncertainty	Extrapolation of 88-year historic trend	Based on observed trends	RCP 4.5 90 percentile bound of 31-member ensemble (P90)	Change from 363 to 427 ppm
Year 2050	09	Rainfall sensitivity scenario	31-member ensemble median (P50) of RCP 4.5	Equally between intensity deciles	N/A	N/A
	10	Rainfall sensitivity scenario	RCP 4.5 31-member ensemble median (P50)	Based on observed trends	N/A	N/A
	11	Temperature sensitivity scenario	N/A	N/A	RCP 4.5 31-member ensemble median (P50)	N/A
	12	CO2 level sensitivity scenario	N/A	N/A	N/A	Change from 363 to 487 ppm
	13	Integrated scenario	RCP 4.5 31-member ensemble median (P50)	Based on observed trends	RCP 4.5 31-member ensemble median (P50)	Change from 363 to 427 ppm
	14	Integrated scenario	RCP 4.5 31-member ensemble median (P50)	Based on observed trends	RCP 4.5 31-member ensemble median (P50) – *Hamon Method*	Change from 363 to 427 ppm
	15	Integrated scenario uncertainty	RCP 4.5 10 percentile bound of 31-member ensemble (P10)	Based on observed trends	RCP 4.5 10 percentile bound of 31-member ensemble (P10)	Change from 363 to 427 ppm
	16	Integrated scenario uncertainty	RCP 4.5 90 percentile bound	Based on observed trends	RCP 4.5 90 percentile bound of 31-member ensemble (P10)	Change from 363 to 427 ppm

			of 31-member ensemble (P10)			

4.8.1 Effect of rainfall intensity

As described in Section 2.1.5, two different approaches for the changes in rainfall intensity were evaluated in this assessment. In the first approach, the increase in rainfall volume was equally divided amongst the intensity deciles. Whereas in the second approach a large portion of increase was preferentially applied to the rainfall events in the highest decile. For the preferential approach, the proportion for dividing rainfall volume into the intensity deciles were based on Groisman et al. (2004) as shown in the Figure 2-7 that uses observed rainfall data for assessing the change. The latter will result in larger increase in intensity for the higher intensity events. Figure 4-26 shows the simulated changes flow, nitrogen, phosphorus and sediment deliveries. The results for both 2025 and 2050 are shown. As anticipated, for the same change in rainfall volume the simulated flow was slightly higher for the preferential approach, where rainfall volume was divided based on observed intensity trends. Although the differences in simulated flow are almost similar, the resulting changes in nitrogen, phosphorus, and sediment are significant. That response is due to higher delivery of particulate matter with higher intensity events. For the rest of the assessment the approach of increasing rainfall the most in the highest deciles for dividing rainfall volume into rainfall events was used because it is based on observations. It was also corroborated by the analysis of some of the daily climate projection dataset obtained using Bias Correction Constructed Analogues for the Chesapeake Bay region.
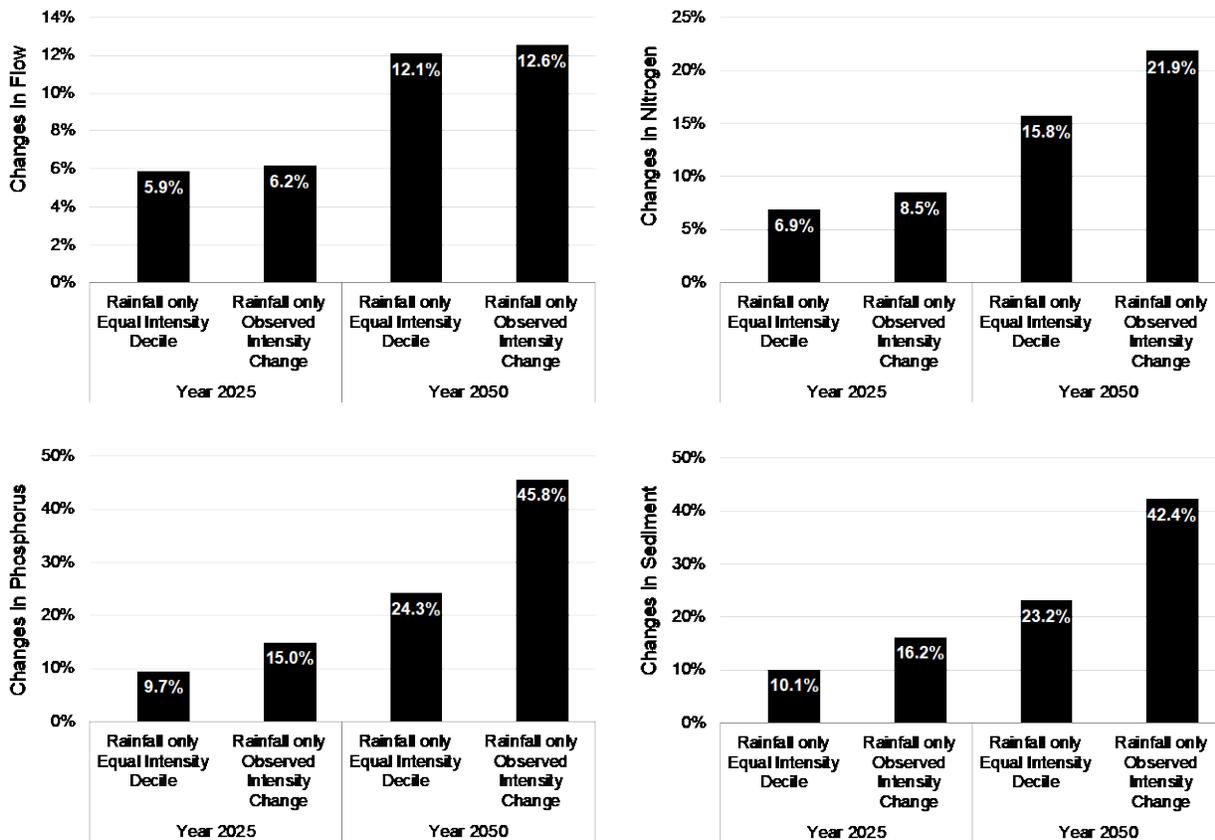

Figure 4-26: Changes in flow, nitrogen, phosphorus, and sediment are shown for the two different methods applied to projected changes in rainfall volume for the year 2025 and 2050.

4.8.2 Climate Change Sensitivity Scenarios

The impact of three climate change drivers incorporated in this climate change assessment were separately analyzed as sensitivity scenarios. The objective of these sensitivity scenarios was to develop better understanding of the watershed response by quantify the relative impact of these climatic drivers on the simulated changes flow, nutrients, and sediment transport. Changes in the delivery of flow, nitrogen, phosphorus, and sediment to the Chesapeake Bay are shown in the Figure 4-27. The results show that for both year 2025 and 2050 the changes in rainfall was the major driver of changes resulting in increased delivery of nutrients and sediment. Temperature and corresponding potential evapotranspiration resulted in a decreased delivery of loads as anticipated and were a close second in terms of impact. The impact of elevated CO_2 levels was relatively minor increases in delivery.
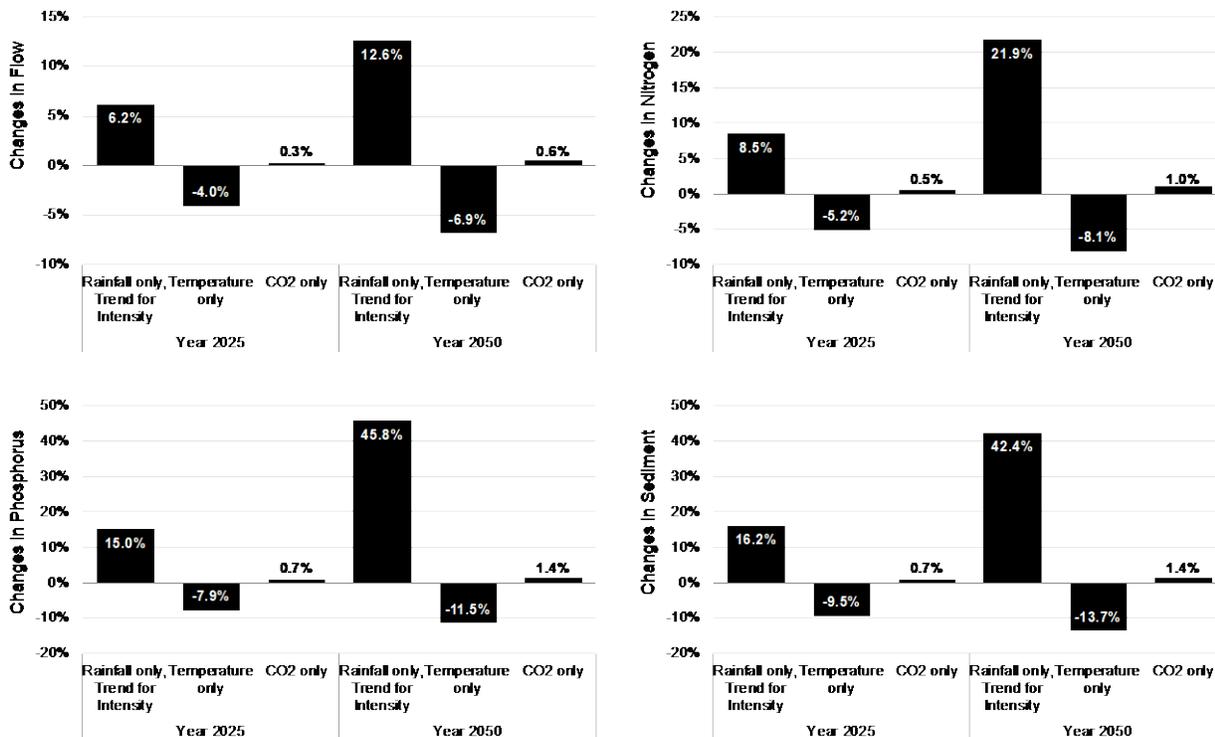

Figure 4-27: Relative impact of projected changes in rainfall, temperature, and CO2 levels were analyzed for the year 2025 and 2050. The changes in the delivery of flow, nutrients, and sediment are shown.

4.8.3 Integrated 2025 and 2050 Scenarios

With the integrated climate change scenarios, the combined impact of rainfall, temperature, and CO2 level were simulated. The integrated scenarios for 2025 and 2050 resulted in increased delivery of flow, nitrogen, phosphorus, and sediment. That is consistent with responses seen for both 2025 and 2050 climate change sensitivity scenarios in the previous section, where the rainfall change dominated the watershed response as compared to changes in temperature and CO2 level. For year 2025, delivery of flow increased by 2.3 percent, nitrogen by 2.4 percent, phosphorus by 3.1 percent, and sediment by 3.3 percent (Figure 4-28). For year 2050, delivery of flow increased by 6.0 percent, nitrogen by 8.3 percent, phosphorus by 15.3 percent, and sediment by 16.2 percent (Figure 4-28).
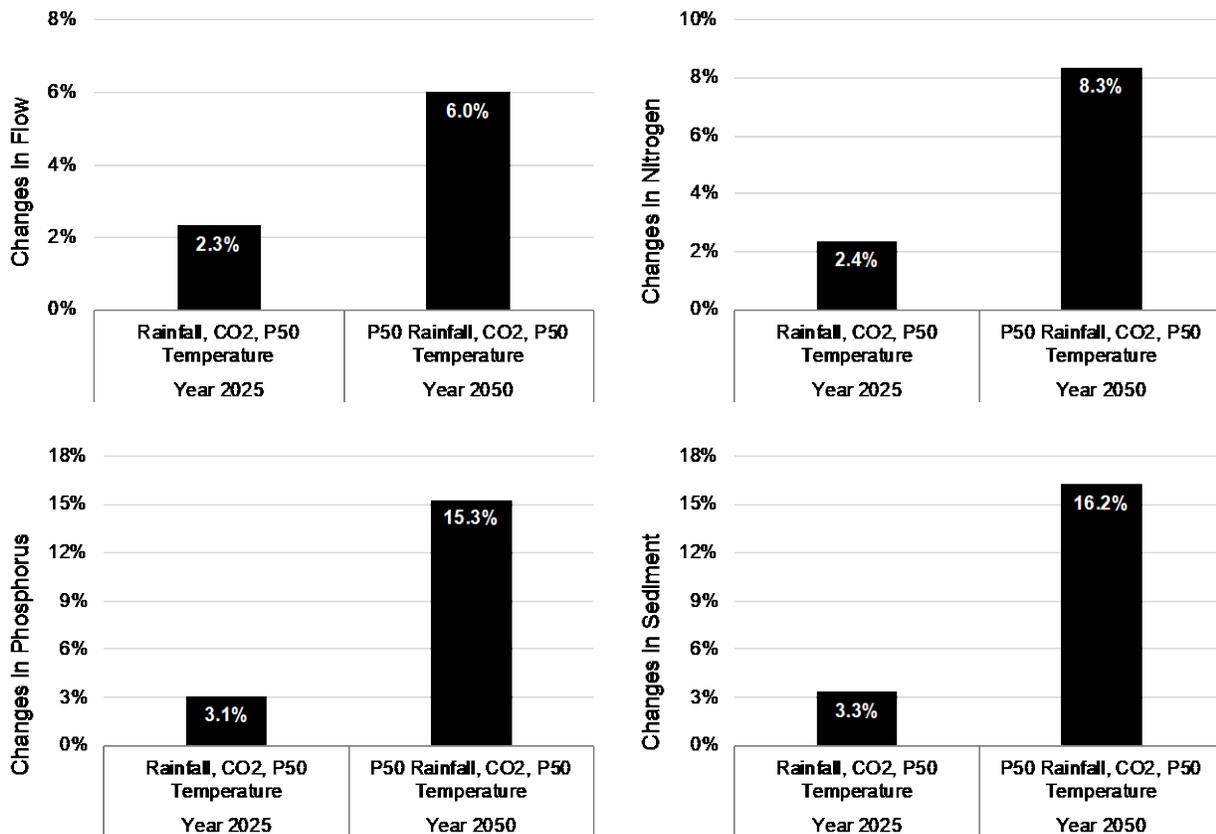
Figure 4-28: Simulated changes in the delivery of flow, nutrients, and sediment to the Chesapeake Bay for year 2025 and 2050 climate change scenarios are shown. For year 2025, rainfall projection from 88-year trends analysis, and temperature using RCP 4.5 31-member ensemble median were used. For year 2050, both rainfall and temperature using RCP 4.5 31-member ensemble median were used.

4.8.4   Changes for the Major Basins

Figure 4-29 shows simulated responses for the major river basins in the watershed. It was shown in the previous section that the increase in watershed delivery for flow, nutrients, and sediment for 2050 was higher than 2025. That behavior is also seen in the simulated responses for the major basins. However, it is noted the model simulation reveal some interesting behavioral differences in the river basin response. For example, the James River basin (JAM) had the lowest percent increase in flow in the 2025 climate changes assessment, but for 2050 it has the largest percent increase in flow. Similarly, percent increase in nitrogen delivery was lowest for James (JAM) in 2025, but it has 3rd largest percent increase for 2050. Similar behavior is seen in phosphorus and sediment response. Such responses are the result of interplay between estimated changes in rainfall (volume and intensity) and temperature that are simulated by the Phase 6 Watershed Model. For example, James River basin had some of the smallest increases in rainfall volume for 2025, but for 2050 it had higher increases in rainfall as compared to rest of the watershed. Temperature increase on the other hand was higher for 2050 but had a similar spatial distribution. As a result, large increase rainfall volume for 2050 in James resulted in a net increase in flow.
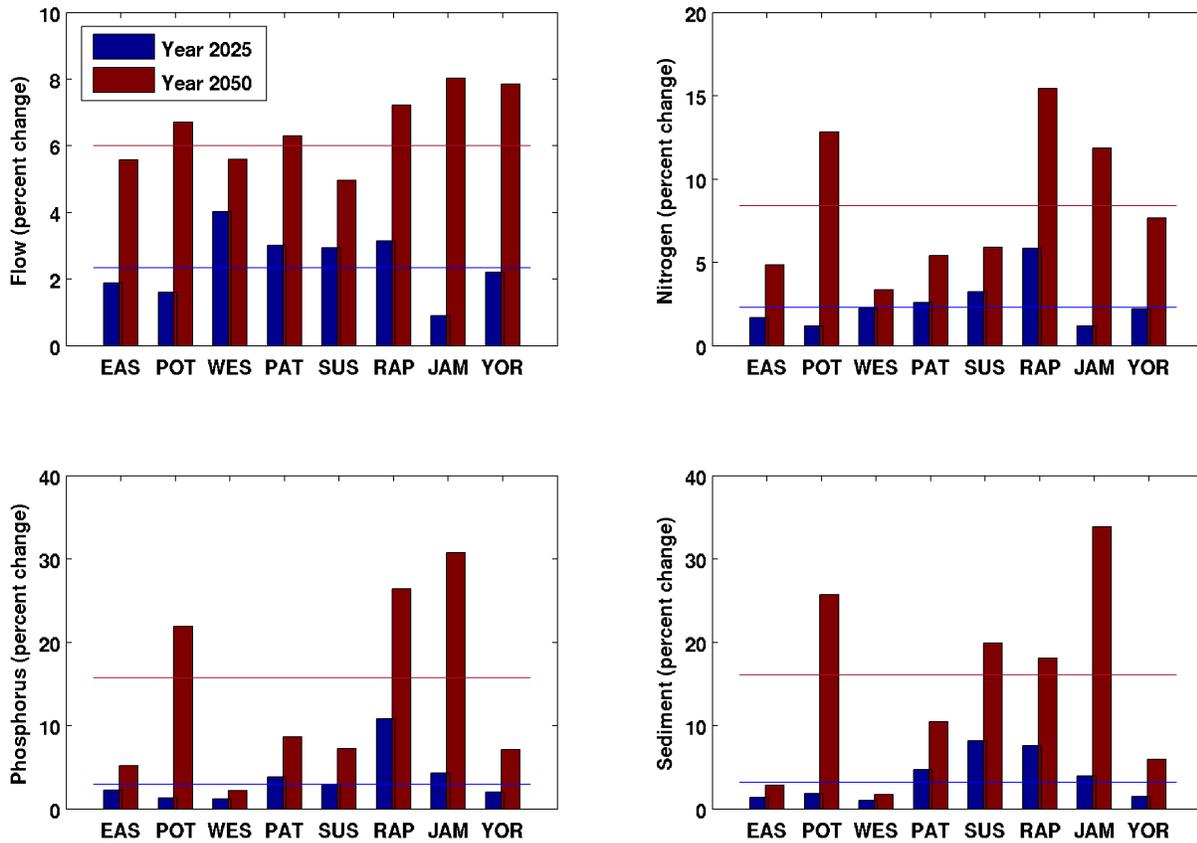
Figure 4-29: Average annual change in flow, nitrogen, phosphorus, and sediment for the major river basins – Eastern Shore (EAS), Potomac (POT), Western Shore (WES), Patuxent (PAT), Susquehanna (SUS), Rappahannock (RAP), James (JAM), York (YOR) are shown. The lines show the change for the entire watershed.

The differences in flow, nutrient, and sediment response to climate change between basins is substantial reflecting regional differences in precipitation change and PET change shown in Figure 2-15 and Figure 2-18. It is difficult to visually reconcile Figure 2-15 and Figure 2-18 with Figure 4-29 and so an analysis was performed to investigate the relative strength of the precipitation effect and the PET effect and to validate the model response to expected changes. Figure 4-30 shows the results of a multiple linear regression predicting percent change in flow for each land segment using percent change in precipitation and percent change in PET as predictors. The equation in the caption shows that flow increases as precipitation increases and that flow increases as PET decreases, which are both expected results. Precipitation is a considerably stronger predictor of flow with higher absolute coefficient. The R^2 reported in the caption and visual inspection of the figure indicate that the model fit is good.
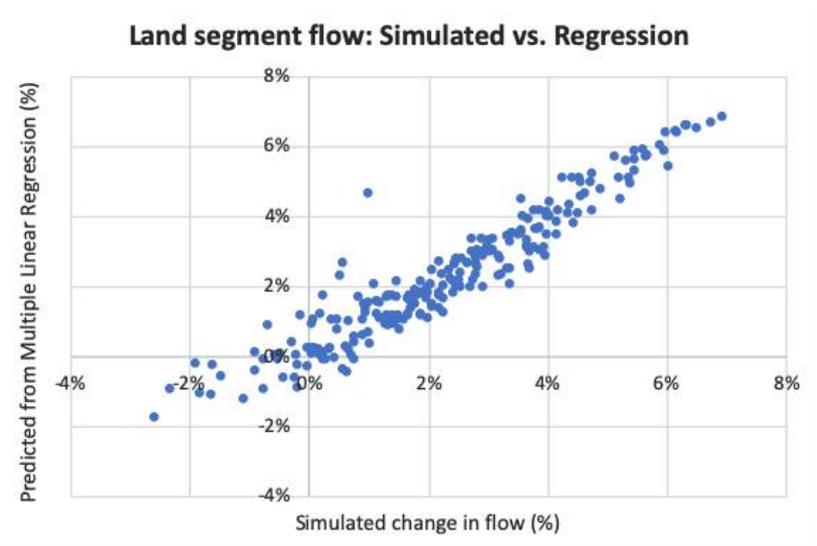
Figure 4-30: Multiple linear regression results plotted against model results by land segment. Percent flow change = 1.87 x Percent rainfall change −1.04 x Percent PET change. The regression model returned a R^2 of 0.95

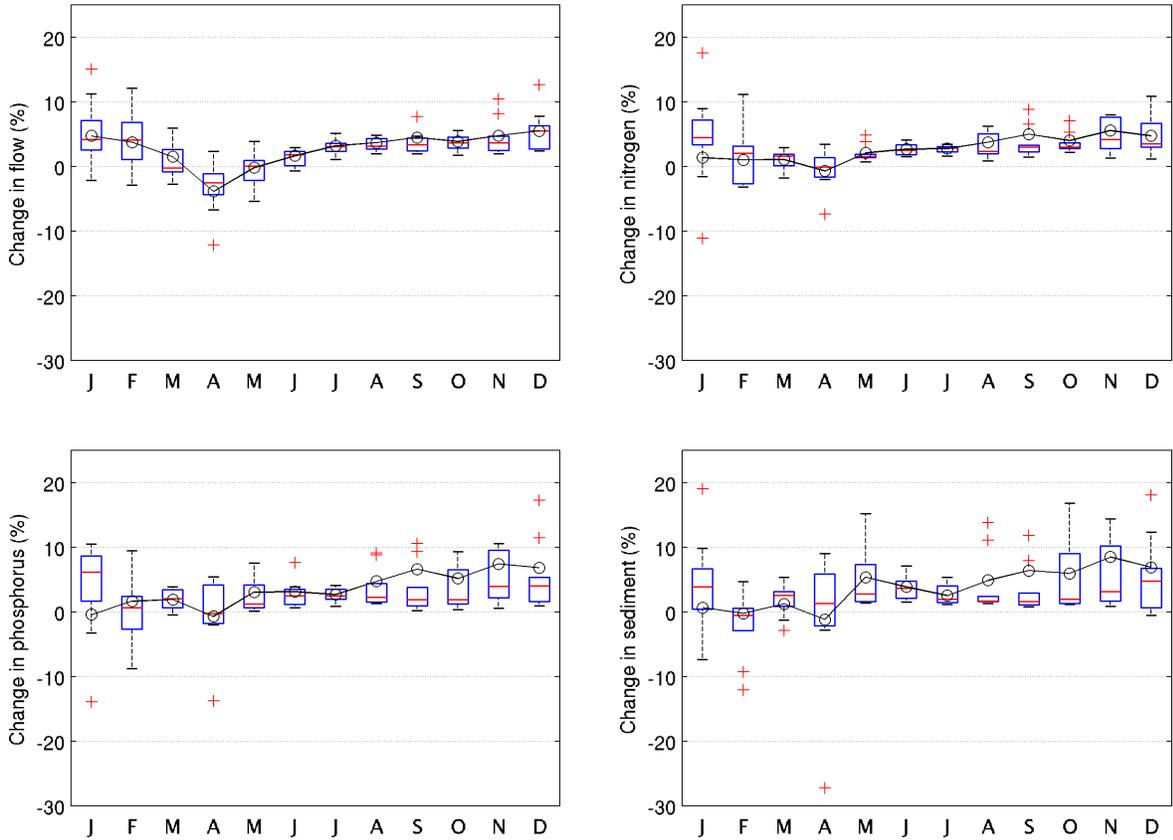### 4.8.5   Seasonal Changes for the Watershed

Figure 4-31: Simulated changes in flow, nutrients, and sediment are shown for year 2025 are shown. Box and whiskers show interannual variability, whereas the solid lines show average annual change.
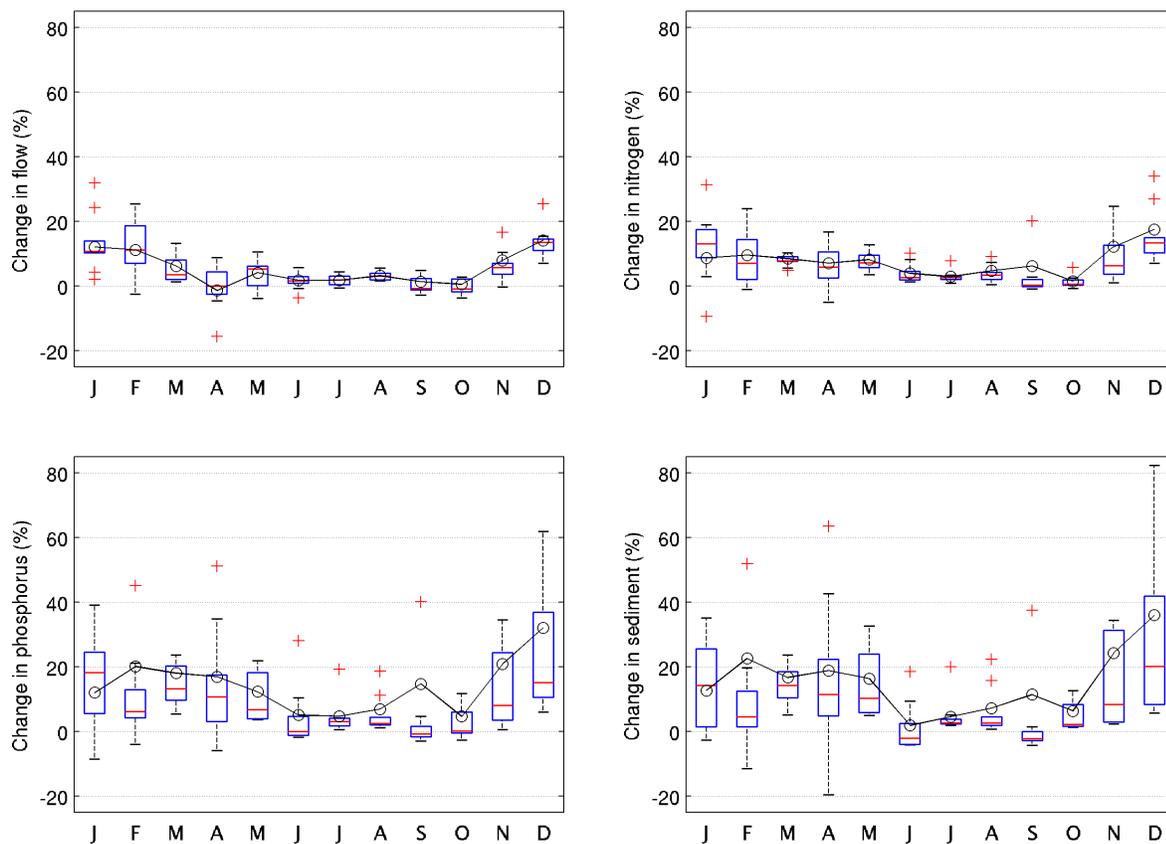

Figure 4-32: Simulated changes in flow, nutrients, and sediment are shown for year 2050 are shown. Box and whiskers show interannual variability, whereas the solid lines show average annual change.

4.8.6   Uncertainty Quantification

There are a number of uncertainties involved in the assessment of climate change impacts on hydrology and water quality. Some of those are (a) uncertainties in the global circulation models, (b) assumptions for the initial conditions in the GCMs and well documented issues of "model drift", (c) the downscaling methods for climate projections, (d) the time-disaggregation of monthly projections to daily or hourly time-steps for use with the watershed model simulation, (e) the methods for the estimation of potential evapotranspiration, and (f) the parameter uncertainty of the Phase 6 Watershed Model calibration. The technical aspects of the implementations are based on the recommendations of the Chesapeake Bay Program's Modeling Workgroup, the Climate Resiliency Workgroup, and the Scientific and Technical Advisory Committee workshop (Johnson et al. 2016).

The uncertainties arising from the climate change inputs used in the assessment were investigated. The 31 downscaled projections for a given period often have differences in the future projections. In the ensemble analysis, all of the models and the corresponding downscaled data were given same weight,

100

equivalent to an assumption of equal likelihood for any one of them to represent the likely future. The central tendency of the samples was characterized using the ensemble-median values of the dataset. To quantify the uncertainty 10th percentile and 90th percentile bounds of the projections were used.

The setup for uncertainty assessments for 2025 and 2050 were made slightly differently. For year 2025, since the projections for the rainfall was derived from the extrapolation of the long-term observations, only uncertainties due to temperature projections were assessed. For year 2050 scenario, uncertainties in both rainfall and temperature projections were used. And in this case, there are several possible ways the combination of rainfall and temperature can be used in the uncertainty assessment. The combinations for projected changes as "high precipitation – high temperature" and "low precipitation – low temperature" were selected to capture a conservative range for the uncertainty. It is acknowledged that this combination does not capture full range of possible impacts.

As shown in Table 4-15 the range of uncertainties around the 2025 are narrower than 2050. The wider uncertainty for the year 2050 is due to higher variability in the rainfall projections (Figure 4-33), as compared to 2025 where only variability in temperature projections were considered. The 2025 uncertainty assessment suggests change over average 10 year can be anywhere for – flow between no change to 4.8percent increase, nitrogen between 0.6 percent decrease to 6.9 percent increase, phosphorus between 1.6 percent decrease and 11.6 increase, and sediment between 1.8 percent decrease and 13.1 percent increase. The 2050 uncertainty assessment suggests change over average 10 year can be anywhere for – flow between no change to 4.8 percent increase, nitrogen between 0.6 percent decrease to 6.9 percent increase, phosphorus between 1.6 percent decrease and 11.6 increase, and sediment between 1.8 percent decrease and 13.1 percent increase.

Table 4-15: Uncertainty estimates for the climate change scenarios for the year 2025 and 2050. Change shown are difference in average annual delivery over the 10-year period.
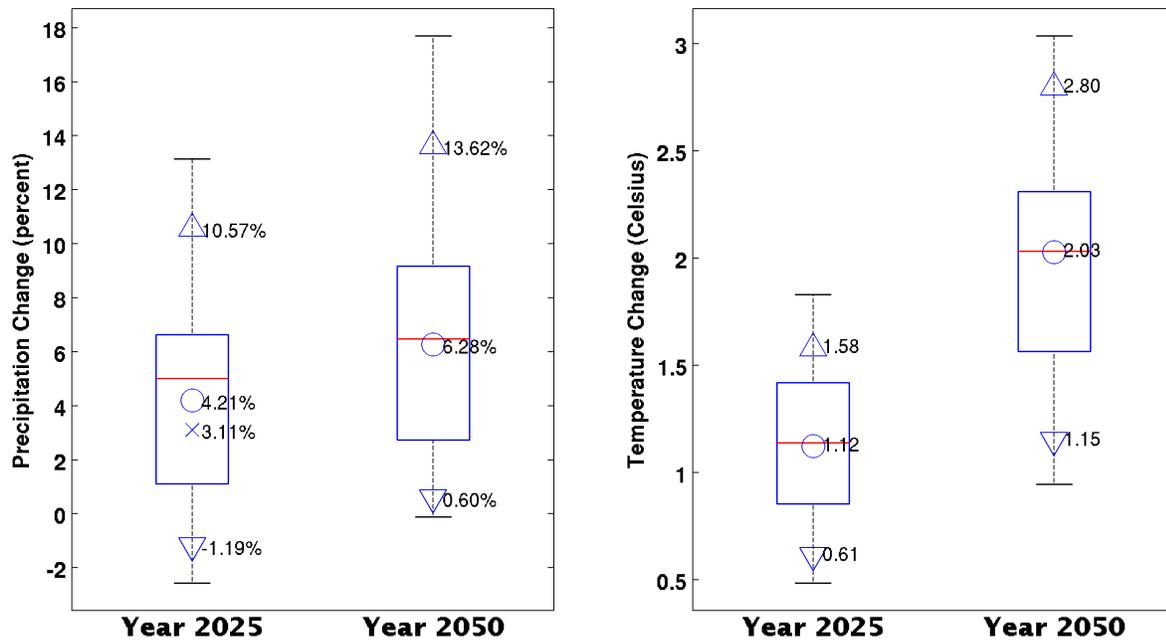
Figure 4-33: Summary of annual RCP4.5 annual rainfall and temperature change for the Chesapeake Bay watershed are shown. Then range for 10th percentile (P10), ensemble median (P50), and 90th percentile (P90) are shown. The estimated change in rainfall volume based on the extrapolation of long-term trends are also shown (with marker symbol x).

The method used for estimating the potential evapotranspiration is an important source of uncertainty. In this assessment two methods were included for quantifying its impact on the delivery of flow, nutrients and sediment. As discussed earlier, for the same delta increase in temperature, Hamon methods estimates higher changes in potential evapotranspiration as compared to Hargreaves Samani. As anticipated higher increase in potential evapotranspiration results in relatively drier conditions and lower delivery of flow and sediment (Figure 4-34).
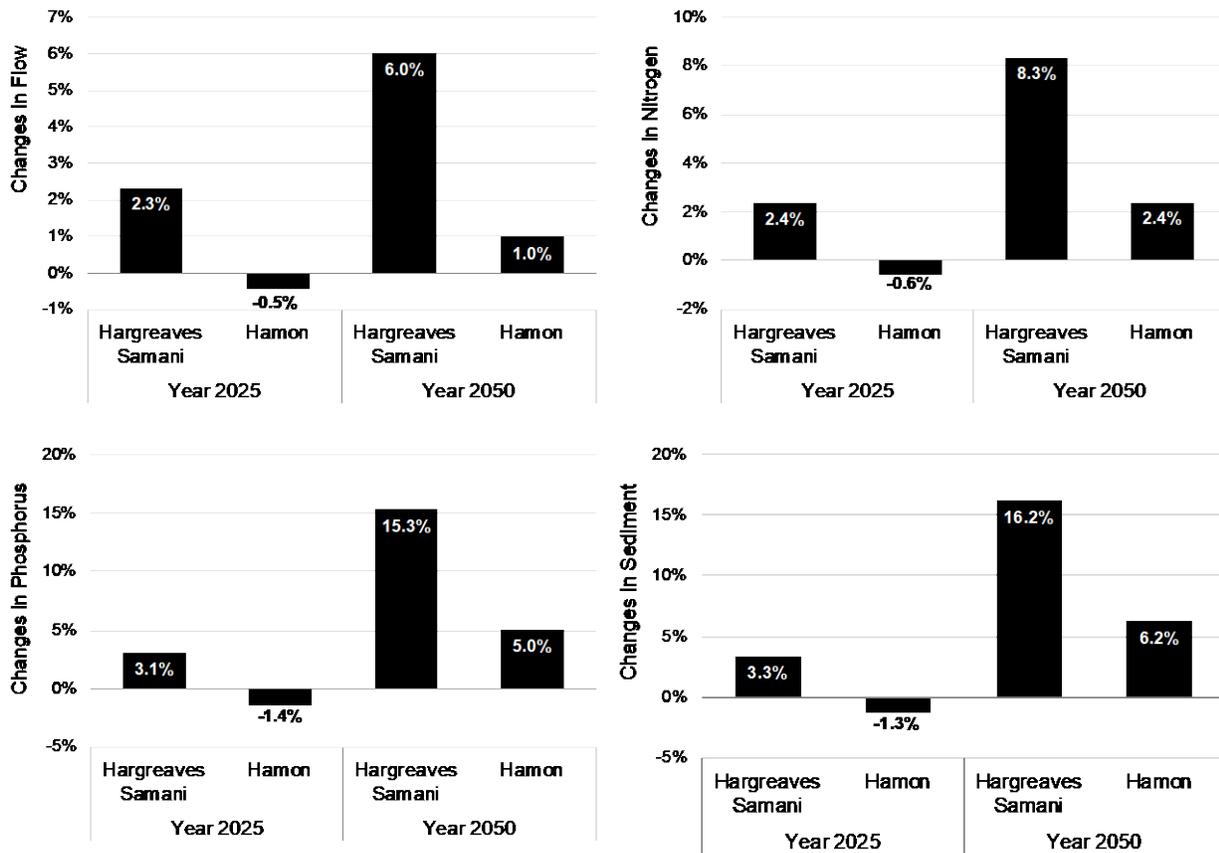
Figure 4-34: Uncertainty due to selection method for estimating potential evapotranspiration for 2025 and 2050 are shown. The uncertainties get higher with increase in temperature.

5 Estuarine Water Quality and Sediment Transport Model Results

The guidance for increasing levels of regional sea level rise based upon global tide gauge rates and regional land subsidence rates came from the CRWG. Specifically, the CRWG recommended that sea level rise projections for 2025 be based on long-term observations at Sewells Point, VA (0.17 m) and that a range be used for 2050 (0.3 - 0.8 m) be applied in the WQSTM. The approximate median of the 2050 range (0.5 m) was used for initial simulations. Temperatures for riverine inflow were provided by the Phase 6 Watershed Model. Air temperatures were consistent with the Watershed Model for each scenario. Changes in temperatures for the open boundary at the Bay mouth were estimated as a function to changes in air temperature. Tidal wetland loss was estimated by the GIS analysis of data from Sea Level Affecting Marshes Model (SLAMM).

5.1 Inputs

5.1.1 Wetland losses and gains

Tidal wetlands have a complex effect on dissolved oxygen in tidal waters. Wetlands attenuate nutrients, but also cyclically release organics which can depress local dissolved oxygen. As described in Cerco and Noel, 2019, wetlands area and change in wetland area were calculated using the Sea Level Affecting Marshes Model (SLAMM) (WPC 2018). The SLAMM results were

initially generated for a study of the effects of sea level rise on coastal habitats in the Chesapeake Bay region (Glick et al. 2008). Geographic information system (GIS) files of wetlands areas adjoining the Chesapeake Bay under base conditions and sea level rise scenarios from Glick et al. 2008 are publicly available and were processed and provided to the CBP by Dr. Lora Harris of the University of Maryland Center for Environmental Science through a master's thesis effort (Bryan 2014). Bryan 2014 extracted the tidal wetland extent for 1996 base conditions and sea level rise conditions from the complete SLAMM results as part of a study of nitrogen removal by Chesapeake Bay tidal wetlands. SLAMM considers the effects of sea level rise only and does not have components that simulates the changes in wetlands that may be due to changes in temperature or salinity. Developed land, defined as National Land Cover Data developed land with greater than 25% impervious, had some modeled resistance to wetland transgression. SLAMM results may be superseded by updated wetlands modeling being undertaken by the USGS over the next few years.

As discussed in Section 5.1.3 sea surface level is predicted to rise by 22cm by 2025, 31 cm by 2035, 42 cm by 2045 and 53 cm by 2050 compared to 1995. These sea level rise magnitudes were used to project tidal wetland acreage for future scenarios. The total baywide wetland acreage for the 1995 base and each scenario is shown in (Figure 5-1). Based on the 1996 condition which was used in the calibration run, wetland acreage will increase about 2% by 2025, which is equivalent to an increase of about 3000 hectares in the entire Bay. Wetland acreage will
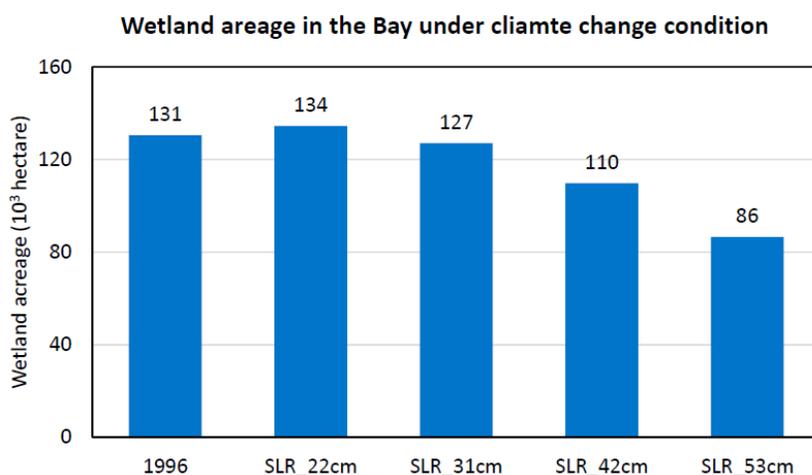

Figure 5-1: Projection of tidal wetland acreage in the Bay under climate change condition by SLAMM (Sea Level Affecting Marsh Model). 1996 is the base scenario; SLR_22cm: 22 cm sea level rise by 2025; SLR_31cm: 31 cm sea level rise by 2035; SLR_42cm: 42 cm sea level rise by 2045; SLR_53cm: 53 cm sea level rise by 2055.

decrease beyond 2025, by 3% in 2035 with 31 cm sea level rise, by 16% in 2045 with 42 cm sea level rise and by as much as 34% in 2055 with 53 cm sea level rise, which is equivalent to a decrease of 45,000 hectares in the entire Bay by 2055. The SLAMM scenarios were for different levels of sea level rise by the year 2100 and might underestimate wetland loss from more rapid sea level rise.

When analyzed by basin, half of the total wetland acreage is located in the Maryland Lower Eastern Shore basin, which is south of the Little Choptank River, extending to the Maryland state line, including the Honga River, the Nanticoke River, Fishing Bay, the Wicomico River, Tangier

Sound, the Manokin River, the Big Annemessex River and the Pocomoke River. This basin is one of the most vulnerable to sea level rise, with 50% of the tidal wetland projected to be lost by 2055, amounting to 31,000 hectares and 69% of tidal wetland loss in the entire Bay. Maryland Western Shore, Rappahannock, and Virginia Eastern Shore are also vulnerable to sea level rise with tidal wetland losses amounting to over 50%. On the other hand, there is projected to be a gain of tidal wetland coverage under climate change conditions in the

Figure 5-2: Projection of tidal wetland acreage in each basin under climate change condition by SLAMM. 1996 is the base scenario; SLR_22cm: 22 cm sea level rise by 2025; SLR_31cm: 31 cm sea level rise by 2035; SLR_42cm: 42 cm sea level rise by 2045; SLR_53cm: 53 cm sea level rise by 2055.

Maryland Middle Eastern Shore Basin (essentially the Choptank and Little Choptank basins), with an increase of 55% (4,000 hectares) by 2055. The James Basin is initially projected to see a significant increase of 21% in 2035, followed by losses so that the projection for 2055 is only 5% greater than 1996.

5.1.2   Wind effects

The effects of wind on DO aeration and distribution in the Chesapeake Bay are a result of both wind attributes and Bay properties. Variations in wind can alter vertical mixing as well as both along-channel and cross-channel circulation (Scully et al. 2005). Changes not only in wind speed but also in wind direction can modify DO, and these two attributes have the potential to modify DO in different ways (Scully, 2010). It has also been found, through a series of simulations using previous versions of the CBP partnership's WQSTM, that the bathymetry of the Bay plays a significant role in modulating the effect of wind on DO concentration (Wang et al. 2016a). Given the complexity and variability of the Bay's geometry, the potential effects of wind will differ from segment to segment as a function of the local geometry.

Wind speed is the primary metric for wind to influence mixing, circulation and ultimately DO in the Bay. Regardless of which direction it is blowing and how favorable the bathymetry is towards contributing to the wind effect, a slow wind speed, e.g., a few centimeters per second, cannot have a significant effect on the physics and biogeochemistry of the Bay. Wang et al. (2016b) reported sensitivity analyses of hypoxic volume to changes in wind speed and found that anoxic volume (DO < 0.2 mg/l) has a very minor response to wind forcing of 2 meters per second for 2 days (Figure 5-3). Only wind speeds greater than 4 meters per second have substantial influence on DO in the bottom of the Bay. Note that wind events of 2 days duration are relatively rare, and shorter wind durations will have less impact on the Bay.
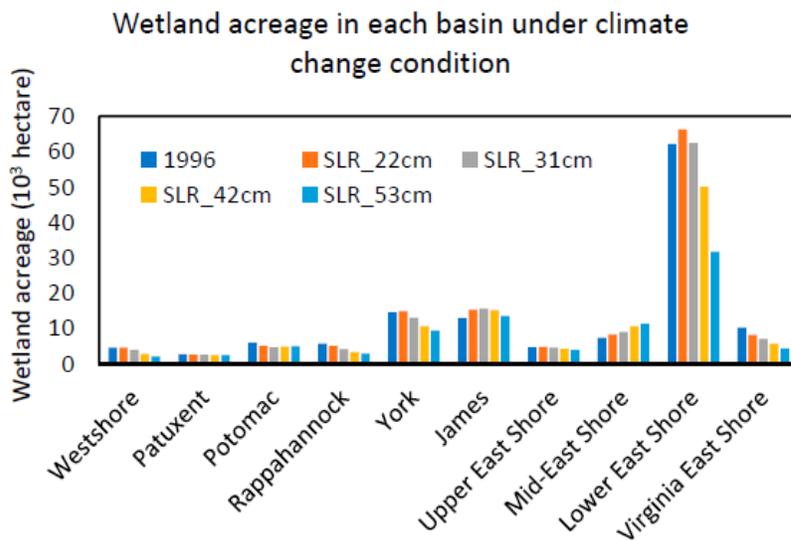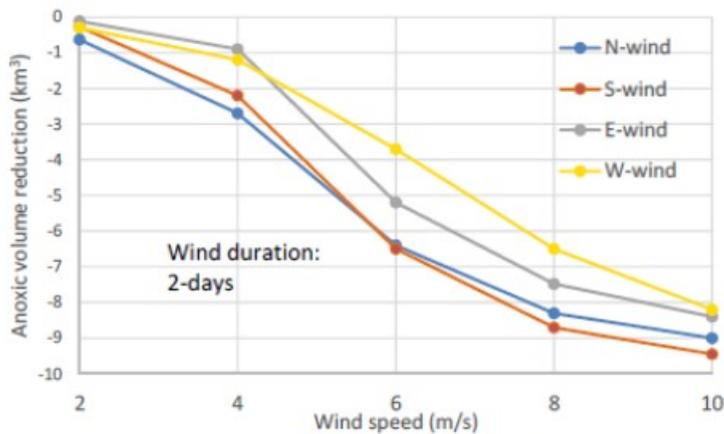
Figure 5-3: Peak anoxia volume reduction in the mainstem Bay, from a no-wind condition to 2-days duration of wind, from the four cardinal directions and at five speeds.

Maria Herrmann of Penn State University has assessed wind speeds under future modeled climate change conditions within the framework of the Chesapeake Hypoxia Analysis and

Table 5-1: Global Climate Models (GCMs) included in the downscaling analysis of wind speed in Chesapeake Bay (Maria Herrmann, personal communication, April 16, 2019).

Model Name	Model Country	Model Agency	Atmosphere Resolution(Lon x Lat)	Ensemble Used
bcc-csm1-1	China	Beijing Climate Center, China Meteorological Administration	2.8 deg x 2.8 deg	r1i1p1
bcc-csm1-1-m	China	Beijing Climate Center, China Meteorological Administration	1.12 deg x 1.12 deg	r1i1p1
BNU-ESM	China	College of Global Change and Earth System Science, Beijing Normal University, China	2.8 deg x 2.8 deg	r1i1p1
CanESM2	Canada	Canadian Centre for Climate Modeling and Analysis	2.8 deg x 2.8 deg	r1i1p1
CCSM4	USA	National Center of Atmospheric Research, USA	1.25 deg x 0.94 deg	r6i1p1
CNRM-CM5	France	National Centre of Meteorological Research, France	1.4 deg x 1.4 deg	r1i1p1
CSIRO-Mk3-6-0	Australia	Commonwealth Scientific and Industrial Research Organization/Queensland Climate Change Centre of Excellence, Australia	1.8 deg x 1.8 deg	r1i1p1
GFDL-ESM2M	USA	NOAA Geophysical Fluid Dynamics Laboratory, USA	2.5 deg x 2.0 deg	r1i1p1
GFDL-ESM2G	USA	NOAA Geophysical Fluid Dynamics Laboratory, USA	2.5 deg x 2.0 deg	r1i1p1
HadGEM2-ES	United Kingdom	Met Office Hadley Center, UK	1.88 deg x 1.25 deg	r1i1p1
HadGEM2-CC	United Kingdom	Met Office Hadley Center, UK	1.88 deg x 1.25 deg	r1i1p1
inmcm4	Russia	Institute for Numerical Mathematics, Russia	2.0 deg x 1.5 deg	r1i1p1
IPSL-CM5A-LR	France	Institut Pierre Simon Laplace, France	3.75 deg x 1.8 deg	r1i1p1
IPSL-CM5A-MR	France	Institut Pierre Simon Laplace, France	2.5 deg x 1.25 deg	r1i1p1
IPSL-CM5B-LR	France	Institut Pierre Simon Laplace, France	2.75 deg x 1.8 deg	r1i1p1
MIROC5	Japan	Atmosphere and Ocean Research Institute (The University of Tokyo), National Institute for Environmental Studies,and Japan Agency for Marine-Earth Science and Technology	1.4 deg x 1.4 deg	r1i1p1
MIROC-ESM	Japan	Japan Agency for Marine-Earth Science and Technology, Atmosphere and Ocean Research Institute (The University of Tokyo), and National Institute for Environmental Studies	2.8 deg x 2.8 deg	r1i1p1
MIROC-ESM-CHEM	Japan	Japan Agency for Marine-Earth Science and Technology, Atmosphere and Ocean Research Institute (The University of Tokyo), and National Institute for Environmental Studies	2.8 deg x 2.8 deg	r1i1p1
MRI-CGCM3	Japan	Meteorological Research Institute, Japan	1.1 deg x 1.1 deg	r1i1p1
NorESM1-M	Norway	Norwegian Climate Center, Norway	2.5 deg x 1.9 deg	r1i1p1

Modeling Program (CHAMP). To generate projections at the Bay scale, the analysis used the downscaling method of MACA, Multivariate Adaptive Constructed Analogs, which is a statistical method for downscaling Global Climate Model (GCM) simulation results from their native coarse resolution to a higher spatial resolution. Twenty GCMs were included in the downscaling analysis, including 2 from the NOAA Geophysical Fluid Dynamics Laboratory and 1 from the USA National Center for Atmospheric Research (Table 5-1).

The downscaling analysis was conducted on a monthly basis (Figure 5-4). Winter months from January through March show greater variability, with more outliers than in the summer months from July through September. In particular changes in July and August wind speed are very small. In other months, the median changes in wind speed, under projected climate change conditions, are mostly a few centimeters per second.
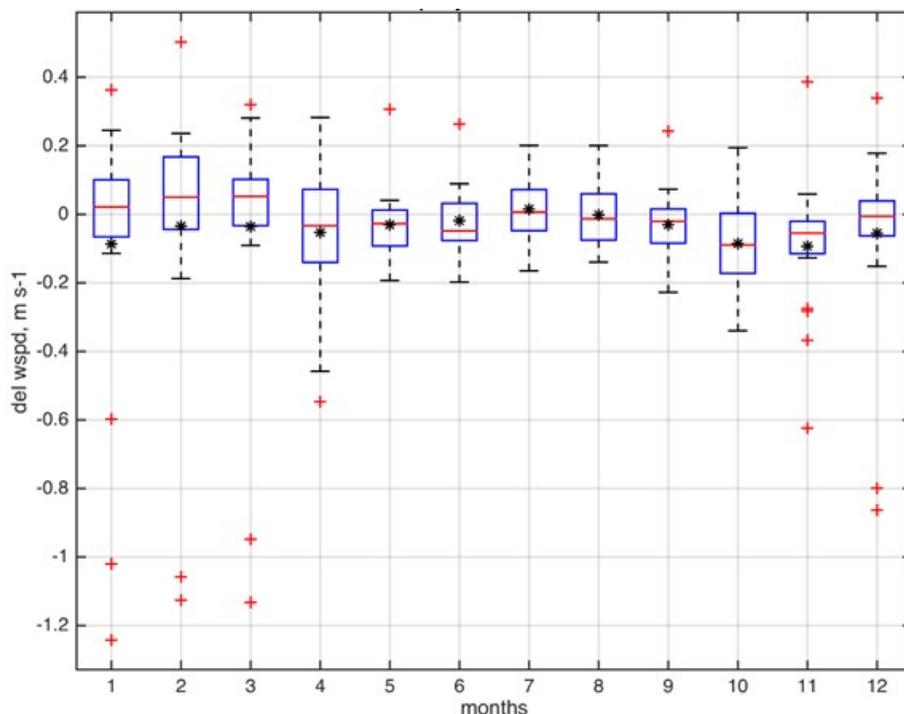

Figure 5-4: Results of wind speed downscaling analysis from 20 Global Climate Change Models (GCMs) to the Chesapeake Bay local scale for the year 2050 using the Multivariate Adaptive Constructed Analogs (MACA) method (Maria Herrmann, personal communication, April 16, 2019)

As mentioned above, modeling sensitivity analysis show that wind speeds below 2 meters per second have a small influence on anoxia volume in the Bay. Significant change in anoxia volume requires wind forcing greater than 4 meters per second. Based on these sensitivity results using the Chesapeake Bay partnership model, wind speed changes under future climate conditions, up to the year 2050, are approximately 2 orders of magnitude lower than what is needed to have a significant impact on bottom DO in the Bay. Given this large difference, it is unlikely that the Chesapeake Bay partnership model will show significant water quality effects of weak changes in wind speed. Additionally, the uncertainties of the change in wind speed are greater than the mean during the summer months. Consequently, further assessment of the climate effects on wind in our assessment of climate change impact on water quality in the Bay is not being pursued.

5.1.3   Sea level rise

Sea level rise is a major element in the climate change array of factors affecting water quality and ecosystem function in the Bay. Sea level rise can alter the gravitational circulation, stratification, saltwater intrusion, and DO advection fluxes. Robust projection of the magnitude of sea level rise contributes to the correctness and reliability of water quality assessment under future climate

change conditions. Two methods of sea level rise projection for the Bay area were assessed: The quadratic function method and the probabilistic projection method.

Boon and Mitchel (2015) fitted a quadratic function to tidal gauge data and successfully projected sea level rise magnitude up to 2055 at a large number of North America tidal gauge sites. The quadratic function is shown in Equation 5-1. Readers are referred to Boon and Mitchel (2015) for detailed description of the method.

Equation 5-1: Quadratic sea level rise equation

$$h = \beta_0 + \beta_1 t + \frac{1}{2}\beta_2 t^2 + \varepsilon$$

where:
h = sea surface level
t = time in years relative to the reference point
β_0 = intercept, i.e. the sea surface level at the reference point
β_1 = rate of sea level rise (m·yr^{-1})
β_2 = acceleration rate of sea level rise (m·yr^{-2})
ε = error of the prediction or the residual between the quadratic function projection and the observation data.

The tidal gauge site of Sewells Point, Norfolk, VA is located at the entrance of the Chesapeake Bay. The Climate Resiliency Workgroup recommended using data at this site to drive the estuarine partnership model for the assessment of climate change impact on water quality in the Bay. Sea surface level data over 50 years from 1969 to the present are available, which provides a sound basis for model fitting and projection (Figure 5.1.3.1). With data from 2018 included and 1992 as the reference point when the sea surface level is assumed at 0, the fitted sea level rise rate β_1 is 5.2 mm·yr^{-1} and the acceleration rate β_2 is 0.12 mm·yr^{-2}. Note that the sea level rise rate at Sewells Point is more than double the global ocean surface level rise of about 2 mm·yr^{-1}. A linear function fitting is comparable with the quadratic function with a coefficient of determination R^2 0.51 versus 0.52 of the quadratic function. However, the linear function does not take the acceleration of sea level rise into account. It can be seen in Figure 5-5 that the residuals of the linear function are consistently positive at the starting and ending periods and more often negative in the central period of the data, indicating that the linear function cannot adequately predict sea level rise for a long period of time within which the acceleration of sea level rise is significant. No trend in the distribution of the residuals of the quadratic function prediction (Figure 5-6) can be determined by inspection over the 50 years of data. The ability of the quadratic function in predicting the acceleration of sea level rise make it appropriate to predict sea level rise into the near future.
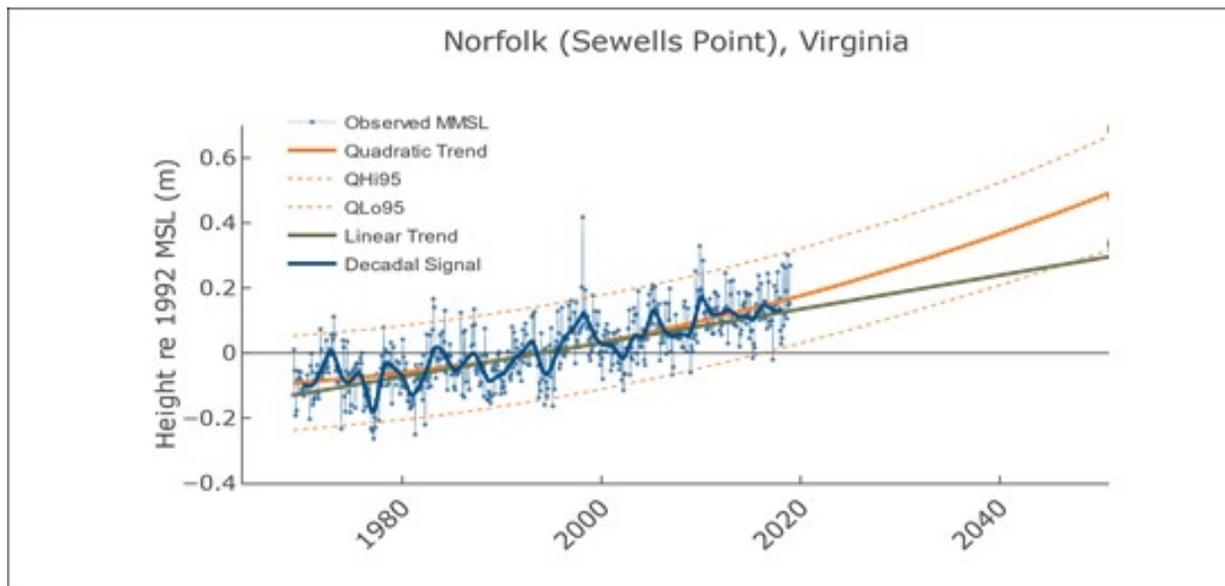
Figure 5-5: Quadratic function fitting and projection at Sewells Point, Norfolk, VA. The red solid line is the fitted quadratic function, the dashed lines are the 95% confidence interval and the black line is the fitted linear function as a comparison. (modified from Boon and Mitchel, https://www.vims.edu/research/products/slrc/localities/nova/index.php).
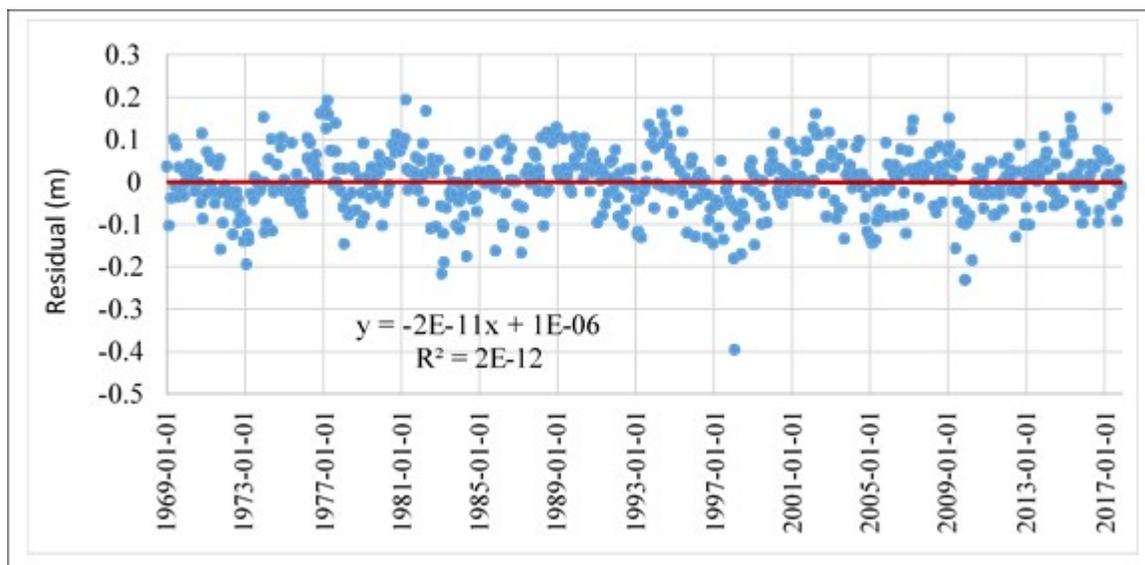

Figure 5-6: Residuals between quadratic method and observations and Sewell's Point, VA

The probabilistic method, known as the K14 method (Kopp et al. 2014), combines the IPCC projection of global seal level rise based on projections from GCMs with local tidal gauge data through a Gaussian process model for prediction at the local scale (Figure 5-7). Glacier and ice cap (GIC), ice sheet melt, oceanographic processes, local land water storage and local non-climatic background are all taken into account for sea level rise projection at local tidal gauge sites. Detailed information can be found in the original reference (Kopp et al. 2014).
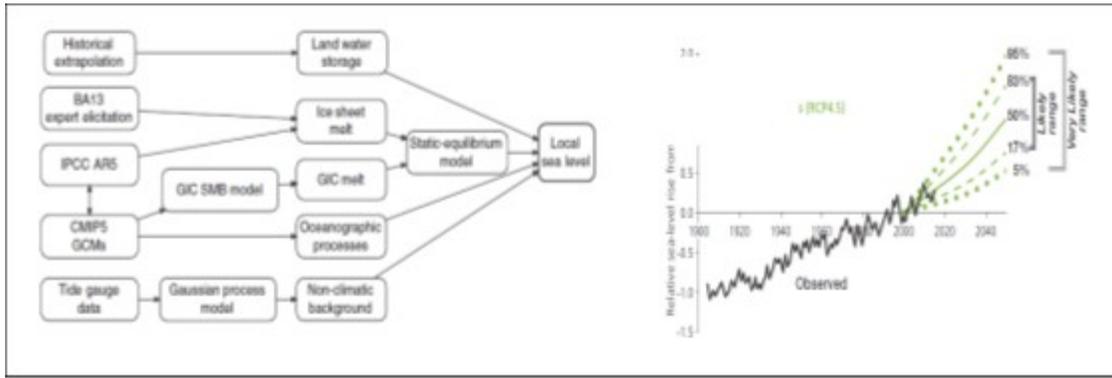
Figure 5-7: Probabilistic projection of future sea surface level at tide-gauge sites Sewells Point (Kopp et al. 2014, Boesch et al. 2018). BA13: Bamber and Aspinall [2013]. GIC: glacier and ice cap. SMB: surface mass balance.

The two projections at the Sewells Point are quite similar (Figure 5-8, left panel). Using 1995 as the reference point, the central year of the standard hydrology period used in the Chesapeake Bay Program, sea surface level will rise 0.22 m by 2025 based on the Quadratic Function projection and by 0.23 m based on the K14 projection, with a difference of 4.5%. The difference between the two methods are all within 5% up to 2055: 0.31 m versus 0.32 m by 2035, 0.42 m versus 0.41 m by 2045, 0.48 m versus 0.46m by 2050, and 0.54 m versus 0.52 m by 2055, respectively. It can be seen that the Quadratic Function projection is slightly lower than the K14 projection till 2035 and slightly higher after. *Based on the recommendation of the Climate Resiliency Workgroup, the CBP will use the average of the two methods for the analysis of climate change impacts on water quality in the Bay (Figure 5-8, right panel): 0.22 m for 2025, 0.31 m for 2035, 0.42 m for 2045 and 0.53 m for 2055, respectively*. The sea level rise numbers for 2050 are displayed in Figure 5.1.3.4 to facilitate comparison with other applications, but the Bay Program does not plan to do an assessment for 2050, rather every decade from 2025 through 2055.
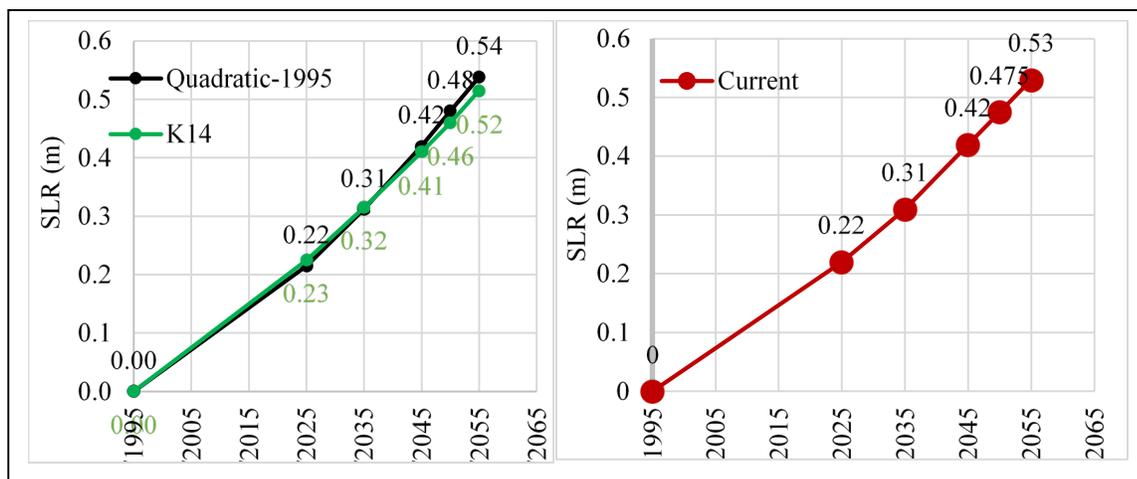

Figure 5-8: Projection of sea level rise by 2025, 2035, 2045 and 2055 as compared to 1995 using the probabilistic method (K14) and the Quadratic Function (left panel) and the average between the two (right panel) which are the final numbers that the Climate Resiliency Working Group recommended to use for assessing climate change impact on water quality in the Bay.

5.1.4 Temperature and Salinity at the Ocean Open Boundary

The oceanic open boundary conditions represent an additional forcing of the CBP partnership model. As with other model forcings, robust estimation of climatic changes at the ocean

110

boundary is important for producing a reliable assessment of projected water quality impacts in the Bay. An assessment of historical changes in sea surface temperature and modeled air temperature changes provides a relationship between air and ocean temperatures that is then applied across seasons and depths at the ocean boundary. The results of a modeling study relating salinity to sea level rise is applied do the ocean boundary.

5.1.4.1 Observed Ocean Temperature Change

Regional temperature changes are happening in the context of a global ocean that has been warming, as evidenced by global sea surface temperature (SST) increases of approximately 0.13 °F per decade from 1990 to 2015, which is equivalent to 0.072 °C increase per decade (Figure 5-9, left panel). However, SST trends vary over space and time, and there is evidence that global warming has tended to accelerate in recent decades as compared to temperature changes in the early 20th century. The National Oceanic and Atmospheric Administration (NOAA) conducted a comprehensive analysis of historical temperature trends for coastal waters of the United States, and the Northeast Continental Shelf ranging from Maine to Maryland constituted a part of the investigation (Dupigny-Giroux et al. 2018). Results for this region showed that SST from 1982 to 2016 increased by 0.6 °F per decade on average, which is equivalent to 0.33 °C increase per decade, more than 4 times the rate of the global SST increase (Figure 5-9, right panel).
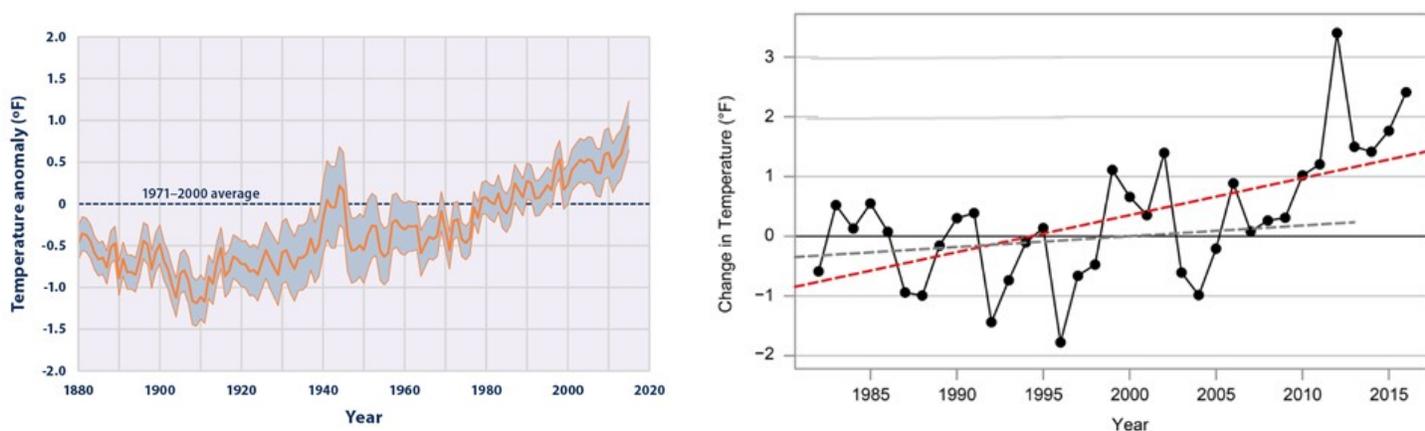

Figure 5-9: Left Panel: Average global sea surface temperature from 1880 to 2015 (from U.S.EPA, 2016b). Right Panel: Annual average sea surface temperature (SST) anomaly from the 1982–2011 average (plotted data and red line) over the period 1982–2016, on the Northeast Continental Shelf of USA (Dupigny-Giroux et al., 2018).

Thomas et al. (2017) conducted a similar historical trend analysis on the northeast continental shelf of the United States using SST data from 1982 to 2014, with a region extending from the Nova Scotian Shelf in the north to Cape Hatteras in the south. The authors were able to analyze the data separately for each major basin: Nova Scotian Shelf, Gulf of Maine and the Mid-Atlantic Bight. They found that SST has a faster pace of increase in the northern region than in the southern region. Over the 33 years of analyzed data, SST increased approximately 0.6 °C per decade on the Nova Scotian Shelf, 0.4 °C in the Gulf of Maine and about 0.3 °C in the Mid-Atlantic Bight. These numbers are in coherence with the NOAA analysis presented earlier, i.e., 0.33 °C per decade, while also fully including both the Gulf of Maine and the Mid-Atlantic Bight. The agreement between these two large-scale comprehensive analyses provides mutual support for

the findings, and consequently, these results provide a sound basis for our specification of temperature at the WQSTM's ocean boundary in the CBP climate change assessment.

These results provide a reliable reference for our determination of the Chesapeake Bay model ocean boundary condition. Our simulation is based on the standard hydrology period from 1991 to 2000, with 1995 being the central reference year, which is close to the central reference year of the NOAA investigation, which was 1996. The first period for the climate change assessment is a three-decade span from 1995 to 2025. Based on the NOAA trend analysis, SST will increase 1.0 °C from 1995 to 2025. The data in the NOAA analysis continued until 2016, which is only 9 years earlier than our target year. As in the Phase 6 Watershed Model simulation, observational data are preferred over GCM projections for 2025, because this target year is considered to be the near future relative to the most recent available observations.

5.1.4.2   *Modeled air temperature change*

Heat flux forcing for the WQSTM is computed from air temperature observations at the U.S. Naval Air Station located at the Patuxent River mouth (38.28N; -76.40W). For climate change application, a downscaling analysis of 31 GCMs was carried out to county scale using the Bias Corrected and Spatially Disaggregated method (BCSD; See Table 2-1 and Section 2.1.3 for details). The Naval Air Station is located at the boundary between the Maryland counties of St. Mary's and Calvert, and downscaled air temperature change for future climate conditions averaged between the two counties is used for the ICM forcing. Figure 5-10 displays the monthly air temperature change from 1995 to projections for 2025, with an annual average change of 1.058 ℃. To reproduce the surface water temperature change observed in the Mid-Atlantic Bight, the air temperature change was multiplied by a factor of 0.9 to produce the ocean boundary condition; this yielded a surface water temperature change of 0.95 ℃ over 30 years. This water temperature change at the ocean open boundary is the average between the two large scale analyses of historic data presented earlier (Dupigny-Giroux et al. 2018 and Thomas et al. 2017).
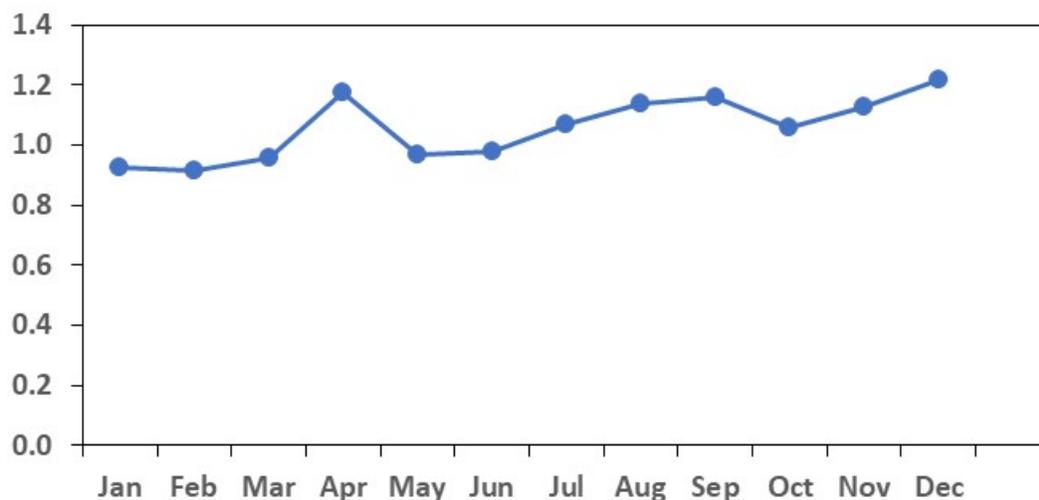

Figure 5-10: Air temperature change from 1995 to 2025 projected from downscaling analysis of 31 GCMs to the St Mary's and Calvert counties, with an annual average of 1.058 ℃ (data from climate models as described in Section 2.1)

5.1.4.3   Generation of the ocean boundary temperature

Water temperature below the surface was modified in proportion to the ratio of water temperature at depth and the surface water temperature:

Equation 5-2: Relationship between water temperature at depth and air temperature

$$\Delta T_{water} = 0.9 \bullet \Delta T_{air} \bullet T_{water} / T_{surface}$$

Where
T_{water} = water temperature
$T_{surface}$ = surface water temperature
ΔT_{air} = air temperature change under climate change conditions from downscaled GCM ensemble projection,
ΔT_{water} = water temperature change at the ocean open boundary under climate change conditions.

An example is given in Figure 5-11 for September 1, 1993. Air temperature change from 1995 to 2025 is 1.16 ℃ for September based on the downscaled GCM ensemble projection, leading to a change in surface water temperature of 1.04 ℃ (0.9*1.16 ℃). The observed surface water temperature at the ocean boundary is 22.3 ℃ and the modified temperature for 2025 is 23.34 ℃ (22.3+1.04 ℃). The observed bottom temperature is 21.3 ℃, which leads to a change in bottom water temperature of 0.996 ℃ (0.9*1.16*21.3/22.3 ℃) and a resulting modified bottom temperature for 2025 of 22.30 ℃.

The advantage of linking water temperature change to air temperature change is that it facilitates the generation of projections for other climate change scenarios, i.e., 2035, 2045 and 2055, that the Bay Program is charged to evaluate. Moreover, the acceleration of air temperature warming, which is included in the GCM simulations, propagates into the water column boundary condition values and is thus taken into account. The same coefficient (0.9) between air and water temperature change will therefore be used for the above future periods of time.
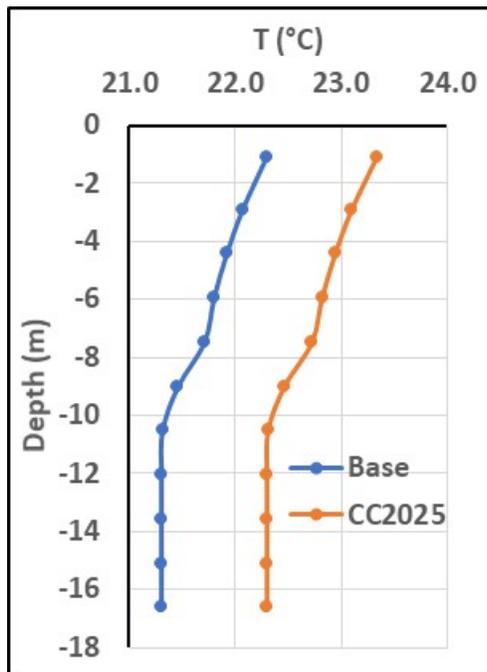
Figure 5-11: Example of modified vertical temperature profile (orange line) from the calibration conditions (blue line) at the ocean open boundary in September 1, 1993 under 2025 climate change conditions.

5.1.4.4   Salinity Changes at the Open Boundary

Salinity at the Bay mouth where the simulation boundary is located can increase with sea level rise and changes in oceanic circulation. Saba et al. (2016) conducted a high-resolution model projection (10 km, versus 100 km in IPCC GCMs; IPCC, 2013) under future climate change conditions for the Northwest Atlantic. They reported salinity increases under future climate change conditions due to the retreat of the Labrador Current, the northerly shifting of the Gulf Stream, the weakening of the Atlantic Meridional Overturning Circulation (AMOC), and an increase of Warm Slope Water entering the Northwest Atlantic Shelf.

Hong and Shen (2012) conducted a modeling analysis of sea level rise impact on salinity in the Chesapeake Bay (Figure 5.1.4.5). In their analysis, the model domain extended offshore, therefore the simulated salinity change can provide guidance for our specification of salinity change at the CBP model's open boundary. At the entrance of the Bay where the WQSTM ocean open boundary is located, salinity increased approximately 0.4 psu with a 0.5 m sea level rise. Assuming a linear relationship between sea level rise and salinity change at the entrance of the Bay, as indicated by the previous study, specification of salinity change at the ocean open boundary can be determined as:

Equation 5-3: Salinity changes as a function of sea level rise.

$$\Delta S = 0.4 \Delta \zeta / 0.5$$

where
ΔS = salinity change at the ocean open boundary,
$\Delta \zeta$ = sea surface level rise (m).

Based on the Climate Resiliency Working Group's recommendation, sea surface level is projected to rise 0.22 m by 2025, 0.31 m by 2035, 0.42 m by 2045 and 0.53 m by 2055, which will lead to a

salinity increase at the ocean open boundary of 0.18, 0.25, 0.34 and 0.42 psu, respectively. As shown in Figure 5-12, no significant stratification of salinity changes was projected at the boundary, and therefore a constant salinity change was specified over the entire water column.
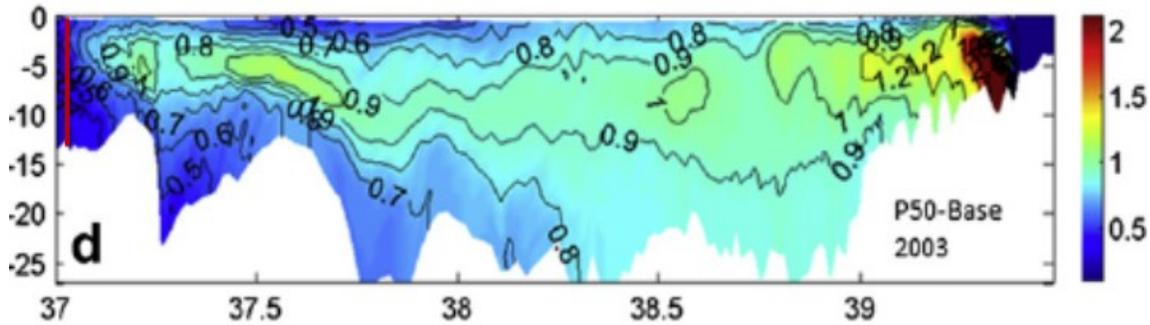

Figure 5-12: Longitudinal (x-axis) and depth (m; y-axis) distribution of projected salinity changes in Chesapeake Bay after a sea surface level rise of 0.5 m. A vertical red line indicates the entrance of the Bay where the ICM ocean open boundary is located, where the ICM ocean open boundary is located, where there is a 0.4 psu increase (from Hong and Shen, 2012)

Before adding the salinity change, salinity was re-interpolated to the new, sea-level rise expanded grid based on the new depth of each layer (Figure 5-13) such that the base salinity at each depth remained the same even though the depth of the cell centroids had changed.
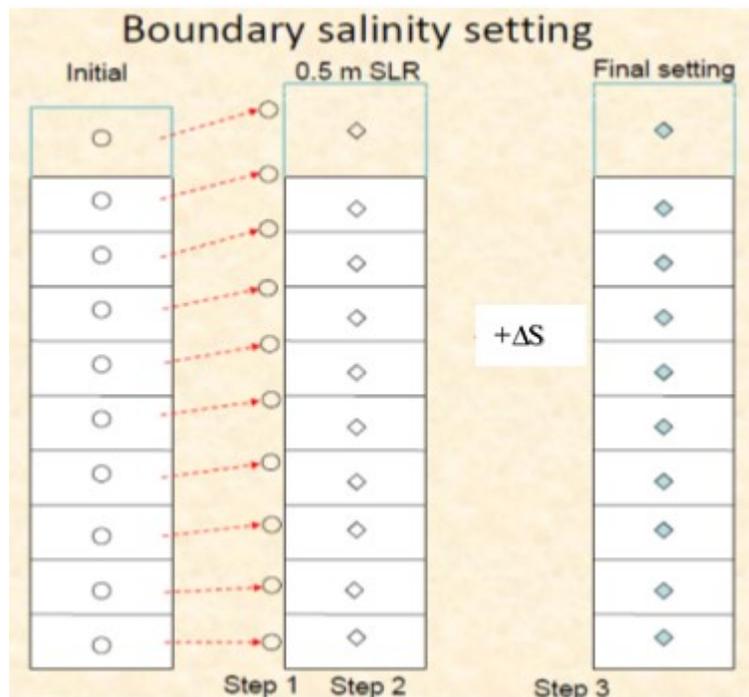

Figure 5-13: Interpolation of salinity to the new grid before adding the salinity change (ΔS) at the ocean open boundary.

5.1.5   Loads from flooding

Researchers have begun to measure the nutrient loads from the drawback of floodwater inundation. It is expected that climate change will make inundation events more frequent and more widespread, increasing the loads from this source. Initial results from the Lafayette river indicate that a single event can equal the expected nutrient loads from a year's worth or runoff,

according to news reports. The work is currently unpublished and so there is not sufficient information available to estimate a load or how that may change due to climate change at this time. However, it was requested by CBP partners to include this short section acknowledging flooding drawback loads in the anticipation that research will progress over the next several years.

5.2   Growth and Respiration Curve Modification

Water temperature increase is one of the projected effects of climate change on the ocean and coastal embayments, such as the Chesapeake Bay. Increased phytoplankton production, which can be driven by eutrophication as well as higher temperatures, leads to greater amounts of organic material, oxygen demand, and ultimately hypoxia in the Bay. As such, an adequate simulated response of phytoplankton growth and respiration to temperature increase is essential for a robust assessment of the climate change impact on water quality in the Bay.

5.2.1   Growth Curve Modification

The response of phytoplankton growth rate to temperature increase is usually expressed as the Q10 coefficient, which is the growth rate increase over a 10°C temperature increase. The value of this coefficient can differ from species to species and from region to region. Lomas et al. (2002) carried out an extensive study of the temperature effect on phytoplankton growth rate and microbial processes in the Chesapeake Bay and found values of Q10 ranging from 1.7 to 3.4. A Q10 of 2, which means that phytoplankton growth rate will double over 10 °C increase in water temperature, is commonly used in the literature and particularly in the modeling community (Eppley, 1972; Tian et al. 2014). Irby et al. (2018) used a Q10 of 2.1 in their modeling study of potential climate change impacts in Chesapeake Bay.

The CBP partnership's estuarine water quality sediment transport model (WQSTM) was calibrated for the period 1991 to 2000, the standard hydrology period used in the Chesapeake Bay TMDL. The phytoplankton growth curves used in the calibration were appropriate for temperatures observed in the Bay during that period. At the STAC workshop "Chesapeake Bay Program Climate Change Modeling 2.0" held on September 24-25, 2018, it was recommended to revise the temperature-related coefficients for phytoplankton growth and respiration to adequately reflect phytoplankton assemblage characteristics over the range of water temperatures expected in the Bay due to climate change.

In the ICM model, the response of phytoplankton growth rate to temperature increase is formulated in Equation 5-4:

Equation 5-4: Phytoplankton growth rate

$$g(T) = g_{max}e^{-K1 \cdot (T - Topt)^2} \quad \text{when T≤Topt}$$
$$ = g_{max}e^{-K2 \cdot (Topt - T)^2} \quad \text{when T>Topt}$$

Where:
g(T) = growth rate as a function of temperature (g C (g chl)$^{-1}$day^{-1})
g_{max} = theoretical maximum growth rate (g C (g chl)$^{-1}$day^{-1})
T = temperature (°C)

T_{opt} = optimal temperature for algal growth (℃)
K_1 = effect of temperature below T_{opt} on growth (℃$^{-2}$)
K_2 = effect of temperature above T_{opt} on growth (℃$^{-2}$)

Parameter values are listed in Table 5.2.1. There are three groups of phytoplankton in the model: cyanobacteria, diatoms, and green algae. These terms represent integrated phytoplankton groups rather than phytoplankton species. The cyanobacteria group represents fresh water species in the tidal fresh zone of the tributaries, diatoms represent transitional groups in the spring, and green algae represent all other species that succeed diatoms in the summer and fall. Initially, the optimal temperatures (Topt) was set to 29 ℃ for cyanobacteria and 25 ℃ for green algae, temperatures over which growth for these phytoplankton groups would decrease or remain static. With these optimal temperature values, the model can underestimate the impact of climate change on phytoplankton production and ultimately dissolved oxygen.

As recommended from the STAC workshop, the optimal temperatures for cyanobacteria and green algae are both revised to 37 ℃, a value that it is unlikely water temperature will reach even under climate change conditions (Table 5-2). The optimal temperature for diatoms was kept the same as in the calibration run because it is a transitional group in spring and succeeded by green algae. Diatoms are known to be a cold-water species, and theoretically it is poorly understood how they will respond to water temperature increases. The optimal temperature for diatoms in the model only affects the timing of when the diatom group is succeeded by other species, and not the total primary production and ultimately oxygen demand, which is the purpose of our assessment.

Once the optimal temperatures were revised, the theoretical maximum growth rate and the exponential coefficient were altered in such a way that the simulated growth rate is comparable with the original calibration during the growth season from 10 to 30 ℃ for cyanobacteria and from 10 to 25 ℃ for green algae (Figure 5-14). Given the equation of phytoplankton growth with respect to temperature presented above, the simulated growth rate is not linear with temperature change and, as such, the simulated Q10 is not a constant. The simulated Q10 for green algae is 2.02 from 5 to 15 ℃ and 1.92 from 10 to 20 ℃. This group is the dominant group in the main stem of the Bay and the robustness of its simulation is the most relevant to water quality simulation. Cyanobacteria is treated as a warm species in the tidal fresh zone in the model with higher optimal temperature up to 29 ℃ in the calibration. The simulated Q10 after the revision is 2.02 from 20 to 30 ℃ and 2.5 from 15 to 25 ℃. All these numbers show that the revised model has an adequate response of phytoplankton growth to temperature increase and thus is suitable for climate change simulation.

Table 5-2: Coefficients of phytoplankton growth and respiration response to temperature increase. g_{max}: Theoretical maximum growth rate of phytoplankton (g C (g chl)$^{-1}$day^{-1}), T_{opt}: Theoretical optimal temperature; K_1: Exponential coefficient for phytoplankton growth increase with temperature increase below T_{opt}, K_2: Exponential coefficient for phytoplankton growth decrease with temperature increase above T_{opt}, K_r: Exponential coefficient for phytoplankton respiration response to temperature increase (Carl Cerco, personal communication, March 29, 2019)

Coefficient	Cyanobacteria			Diatom			Green Algae		
	Calibration	Revision		Calibration	Revision		Calibration	Revision	
g_{max}	200	250		300	300		450	600	
T_{opt} (℃)	29	37		16	16		25	37	
K_1	0.005	0.0022		0.0018	0.0018		0.0035	0.0013	

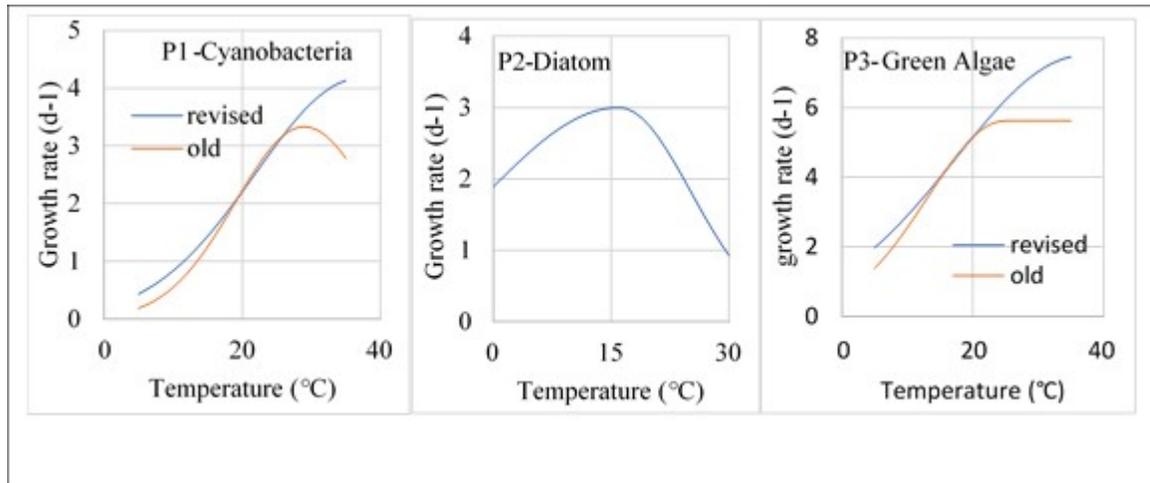| K_2 | 0.004 | 0.0 | 0.0022 | 0.002 | 0 | 0 |
| K_r | 0.0322 | 0.069 | 0.0322 | 0.069 | 0.0322 | 0.069 |

Figure 5-14: .

Phytoplankton growth curve in function of water temperature (Red line: Original calibration curve; Blue: Revised curve for climate change assessment; From Cerco and Noel, 2019)

5.2.2 Respiration Curve Modification

Base phytoplankton respiration is a complex formulation that varies spatially. The temperature dependence of the respiration is represented in Equation 5-5:

Equation 5-5: phytoplankton respiration multiplier

$$f(T) = e^{k_r(T - T_0)}$$

where:
f(T) = multiplier to the respiration rate (dimensionless),
k_r = exponential coefficient of response to temperature change (°C^{-1}),
T = temperature (°C),
T_0 = reference temperature at which respiration rate is equal to the base rate.

In the calibration, k_r was assigned a value of 0.0322, which leads to a Q10 of 1.38. This is relatively low as compared to the values reported for the Chesapeake Bay and in the literature (Lomas et al. 2002). For the climate change anlysis, k_r was revised to 0.069, yielding a Q10 of 2, in coherence with the literature and what is reported in Chesapeake Bay. The original and revised curves are shown in Figure 5-15.
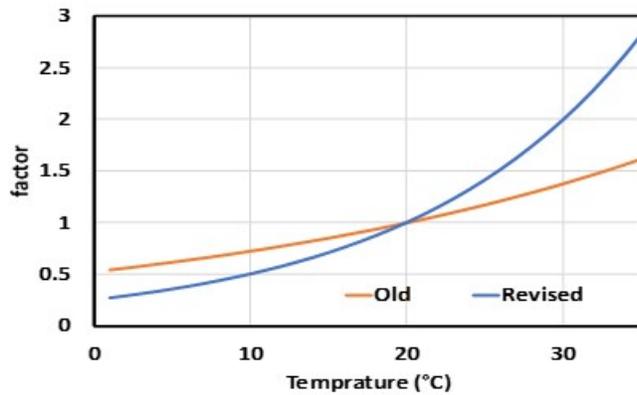
Figure 5-15: Response of phytoplankton respiration rate to temperature increase. The orange line is the calibration and the blue line is the revised curve for climate change application.

Analysis of model performance and expert opinion of the modeling workgroup found that the modification of the respiration was not warranted and so k_r maintains a value of 0.0322.

5.2.3   Test of Calibration

The temperature parameter values were modified after the calibration for the climate change application. A key question is whether these modifications significantly altered the calibration in such a way that simulation drifts away from the data. To address this question, a simulation was conducted with all forcing files and parameter values the same as in the calibration except the modified temperature parameters as shown in Table 5-2, and its results were compared with the results of the original calibration run. Mean difference (MD) and absolute mean difference (AMD), calculated as shown in Equation 5-6 were computed for both runs across the array of state variables used routinely during the calibration (Cerco and Noel, 2019):

Equation 5-6: Calibration metrics for the WQSTM

$$MD = \frac{\sum_{i=1}^{N}(P_i - O_i)}{N}$$

$$AMD = \frac{\sum_{i=1}^{N}|P_i - O_i|}{N}$$

Where:
P = prediction
O = observation
N = number of observations.

Time-series data comparison and whisker box plots of bottom DO at the central station CB4.2C are given as an example in Figure 5-16, followed by AMD and MD plots for DO (Figure 5-17), chlorophyll (Figure 5-18), total nitrogen (TN) (Figure 5-19) and total phosphorus (TP) (Figure 5-20). On the time-series plot of bottom DO at CB4.2C, the two simulations are superimposed on each other (Figure 5-16 left panel). Both simulations match well with the data in terms of magnitude, seasonal variation, and hypoxia events with DO < 2 mg/l during the summer season. Similarity between the two solutions dominates on the whisker plots in term of the median, the first and the fourth quartiles and even the extrema (Figure 5-16 right panel). The new solution with modified temperature-related parameter values even show some slightly better results as

compared to the original calibration solution, with the simulated median closer to the data median, such as in 1991, 1994, and 1997.
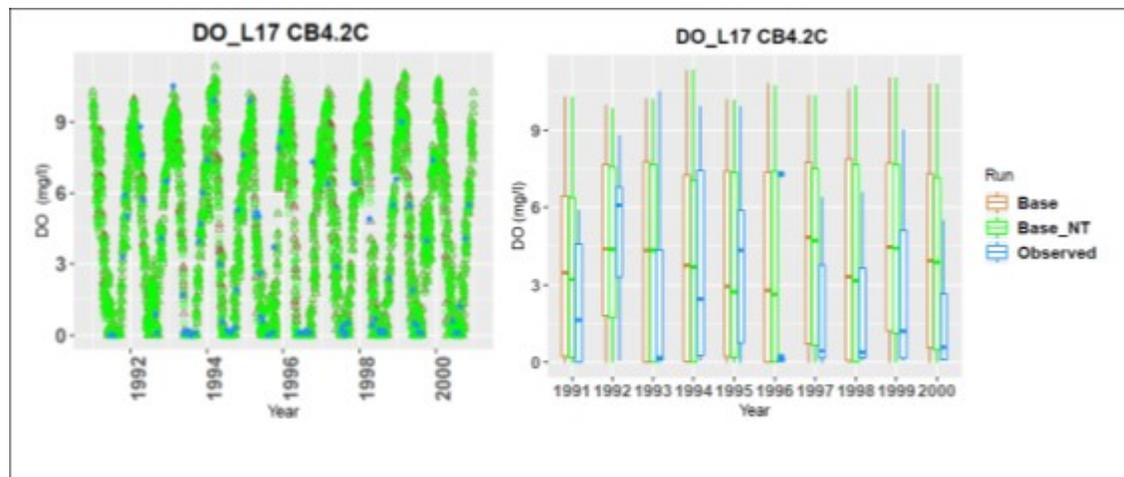

Figure 5-16: Bottom DO at the central Station CB4.2C in segment CB4MH (Base: Calibration run; Base_NT: Simulation with revised parameter values for the phytoplankton growth function and respiration rate with temperature).

In terms of AMD and MD of DO in the entire water column, the new solution with modified temperature parameter values generated slightly lower AMD in the main stem than the original calibration, but slightly higher in the tributaries (Figure 5-17, left panel). Nonetheless, all differences are within 5% of the original solution. The MD plot shows that both solutions slightly underestimate DO in the Eastern Shore and overestimate DO in the tributaries on the western shore, with the best solution for the main stem of the Bay resulting in the smallest MD over all the tributaries.
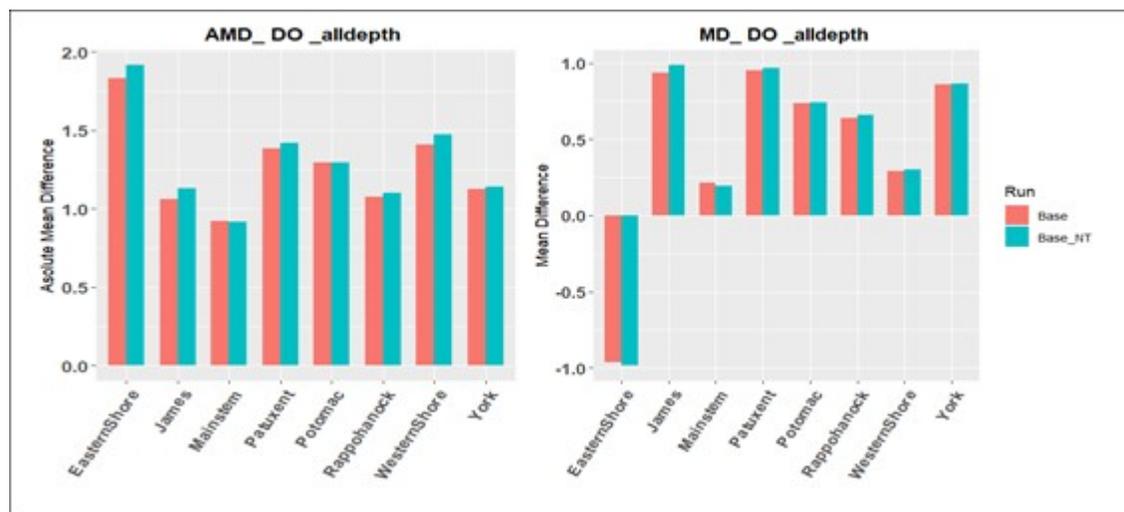

Figure 5-17: Absolute mean difference AMD (left panel) and mean difference MD (right panel) between simulation and data of DO in the major tributaries and the main stem of the Bay (Base: Calibration run; Base_NT: Simulation with revised parameter values for the phytoplankton growth and respiration functions with temperature).

The chlorophyll results are quite similar between the two solutions in the main stem (Figure 5-18), and the AMD of the new solution with the modified temperature parameter values is slightly higher than the original calibration solution in most of the tributaries. The differences are mostly below 15% of the original solution. Usually chlorophyll has greater variability in space,

time and in the vertical profile than DO, which can help to explain its larger AMD than DO. Both model solutions underestimate chlorophyll in the James River and on the Western Shore, but tend to slightly overestimate chlorophyll concentration in other tributaries. Similarity is even more apparent for total nitrogen (TN) and total phosphorus (TP) between the two model solutions (Figure 5-19 and Figure 5-20). For TN and TP, AMD is practically identical between the two model simulations in the main stem of the Bay, the James, Potomac, Rappahannock and the York rivers. The new solution has a slightly higher AMD than the original simulation in the western and eastern shore and in the Patuxent River, but the differences are minimal. Given the high similarity between the two model runs, the modification of the parameter values controlling phytoplankton growth and respiration rate to temperature increase did not significantly alter the calibration, and these parameter values can lead to adequate simulation of phytoplankton response to temperature under future climate change conditions.
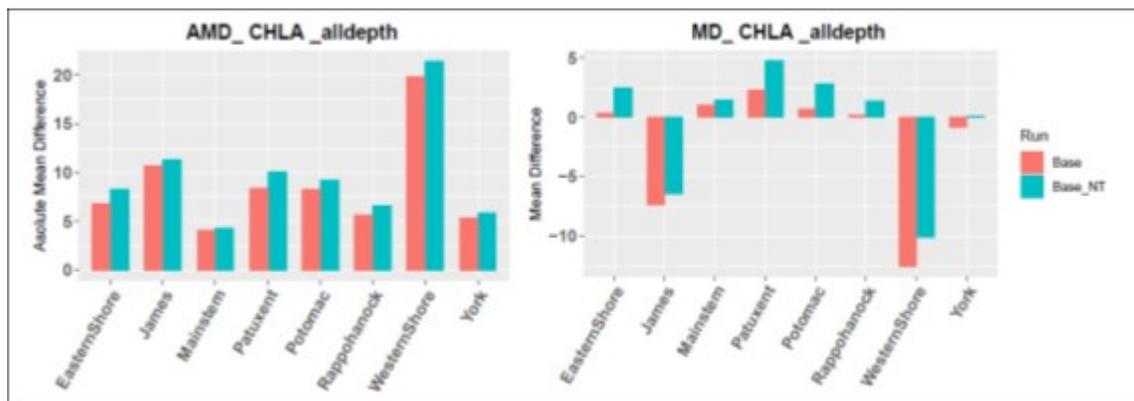

Figure 5-18: Absolute mean difference AMD (left panel) and mean difference MD (right panel) between simulation and data of chlorophyll in the main tributaries and the main stem of the Bay (Base: Calibration run; Base_NT: Simulation with revised parameter values for the phytoplankton growth and respiration functions with temperature).
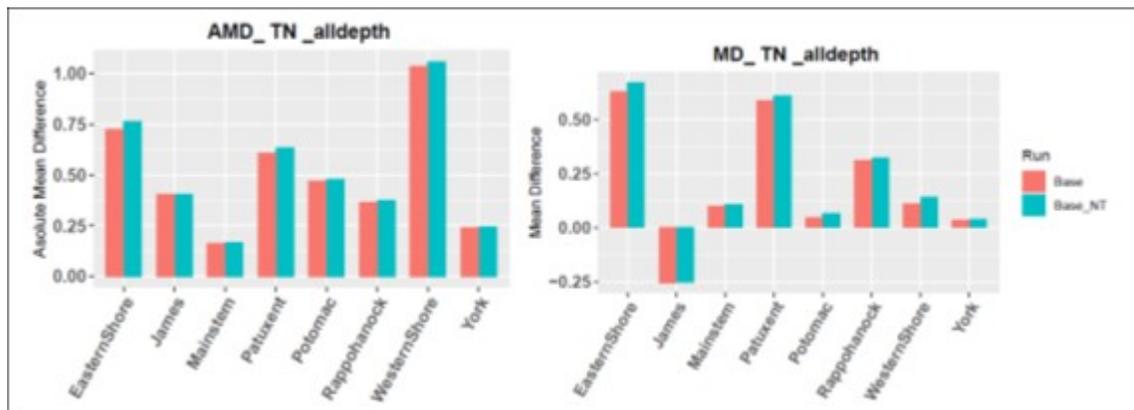

Figure 5-19: Absolute mean difference AMD (left panel) and mean difference MD (right panel) between simulation and data of total nitrogen TN in the main tributaries and the main stem of the Bay (Base: Calibration run; Base_NT: Simulation with revised parameter values for the phytoplankton growth and respiration functions with temperature).
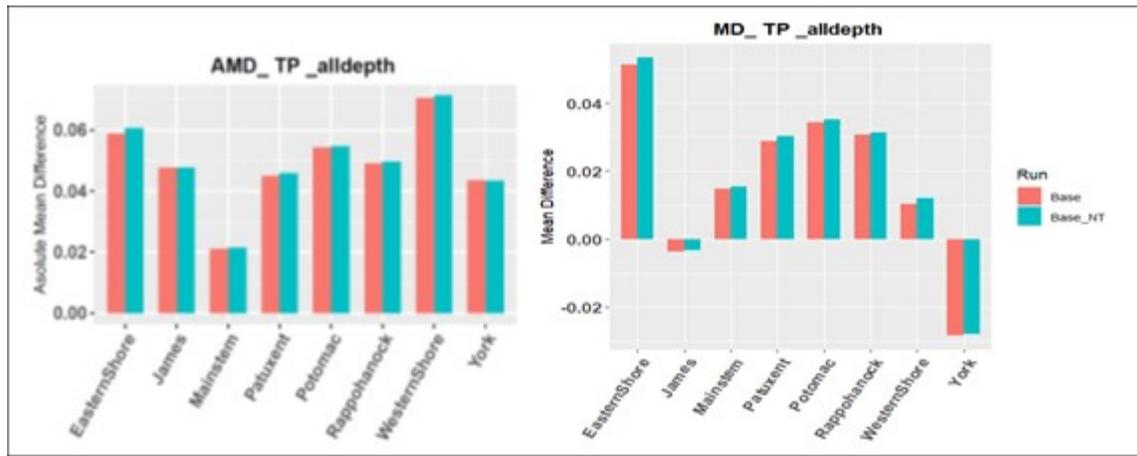
Figure 5-20: Absolute mean difference AMD (left panel) and mean difference MD (right panel) between simulation and data of total phosphorus TP in the main tributaries and the main stem of the Bay (Base: Calibration run; Base_NT: Simulation with revised parameter values for the phytoplankton growth and respiration functions with temperature).

5.3   Validation of model response

5.3.1   Reasonable response to Sea Level Rise

Clear and unambiguous validation of the effect of sea level rise on dissolved oxygen is impossible because of the absence of observational data. There is, however, the opportunity to compare the WQSTM results to the results of other models with equivalent sea level rise (SLR) projections, as well as to evaluate them relative to what would be expected with theory. A model intercomparison was conducted by Pierre St-Laurent under the direction of Dr. Marjorie Friedrichs at the Virginia Institute of Marine Science for the impacts of SLR on hypoxia over the period 1991-1995. Four scenarios were considered: a base case with historical sea levels and cases where the sea level is raised by 0.17m, 0.50m, and 1.00m (roughly representative of years 2025, 2050, and 2100, respectively). All aspects other than the sea level (e.g., atmospheric conditions, oceanic temperatures, and salinity) were kept the same across the four scenarios. Four Chesapeake Bay models (covering a spectrum of model resolutions, boundary conditions, and numerical algorithms) were considered: WQSTM/CH3D-ICM, ChesROMS-ECB, UMCES-ROMS-RCA, and SCHISM-ICM.

The four numerical models reproduced historical observations (1991-1995) of salinity, water temperature, and dissolved oxygen (DO) with comparable skill but with different biases. Despite these differences the models exhibited considerable agreement regarding the effects of SLR on salinity and temperature. SLR increases salinity throughout the Bay and in all seasons. The salinity increase is apparent throughout the water column but is largest in the upper 10m and in shallow areas (with bottom depths <10m). The increase is quasi-linear with SLR and reaches +1.5psu in the scenario of +1.00m (consistent with earlier studies; Hong & Shen 2012). In a departure from the three other models, CH3D-ICM suggested increases in salinity that were 2-3 times smaller (+0.1-0.2 psu versus +0.2-0.3 psu with SLR = +0.17 m).

SLR produced both cooler and warmer water temperatures depending on the time of the year. All four models exhibited the same seasonal pattern where SLR produces warmer conditions in the

winter months (November-January) and cooler conditions in the summer months (May-July;Figure 5-21). This seasonal pattern was amplified quasi-linearly by SLR and reached +/-0.5°C in the case SLR=+1.00m. Such temperature anomalies were apparent throughout the Bay, with the shallow areas being affected first followed by the deeper channels.
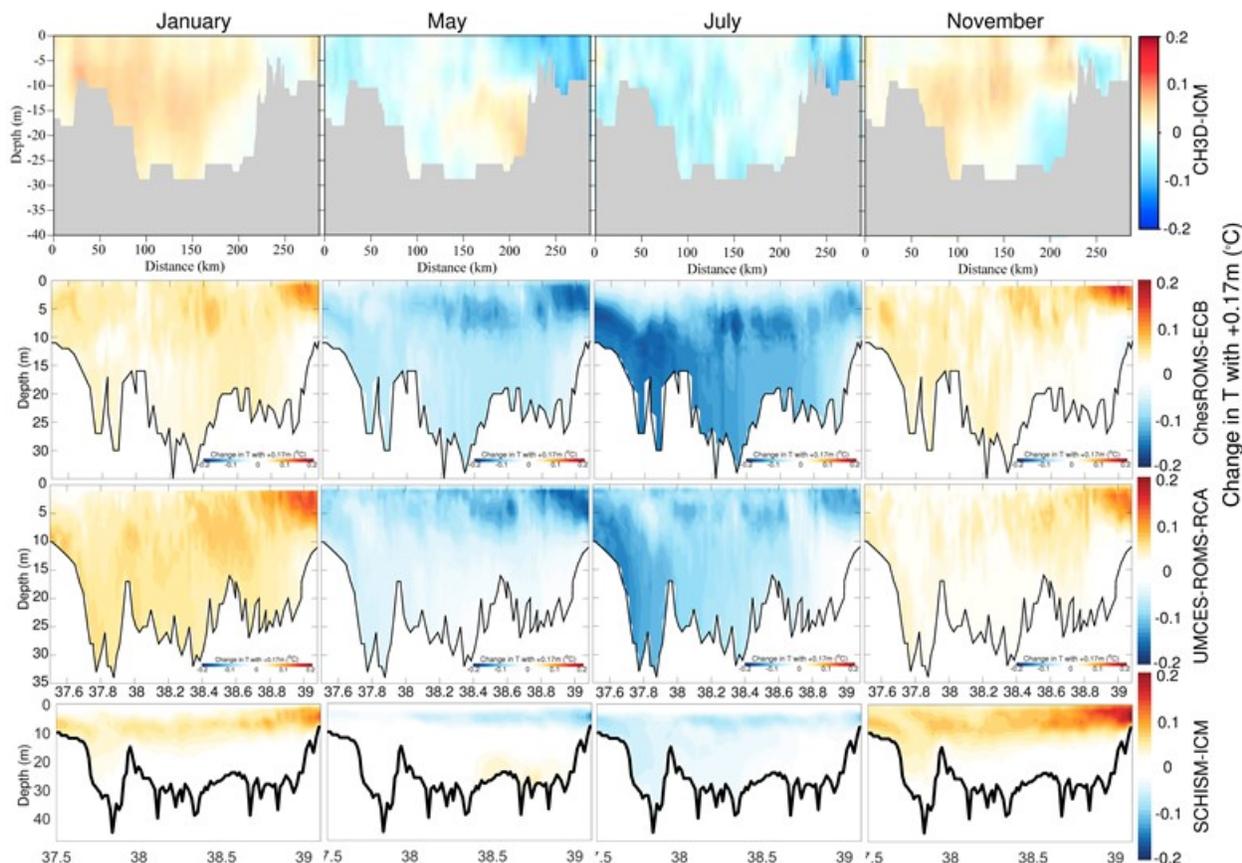

Figure 5-21:Change in water temperature along a transect of the Bay from south to north in response to an increase in sea level of 0.17m. The figure is a monthly climatology for the months of January, May, July, and November of years 1991-1995. Each row represents one of the four models considered.

SLR produced both increases and decreases in DO concentrations depending on the time of the year and the areas of the Bay. All four models exhibited some increases in DO concentrations in the bottom layer of the Bay's thalweg (a channel 25-30m deep aligned south-north that follows the main stem of the Bay) where hypoxia/anoxia is most prevalent (Figure 5-22). This improvement in bottom DO tended to be concentrated in the summer season and increased quasi-linearly with SLR. However, the absolute magnitude and duration of this improvement in summertime bottom DO varied substantially between the four models. CH3D-ICM exhibited the largest improvement in bottom DO with year-long DO increases of +0.2mg/L in the scenario SLR=+0.50m. UMCES-ROMS-RCA exhibited the smallest improvements in bottom DO; positive DO anomalies were concentrated in May-July and replaced by negative DO anomalies after July (Figure 5-22).
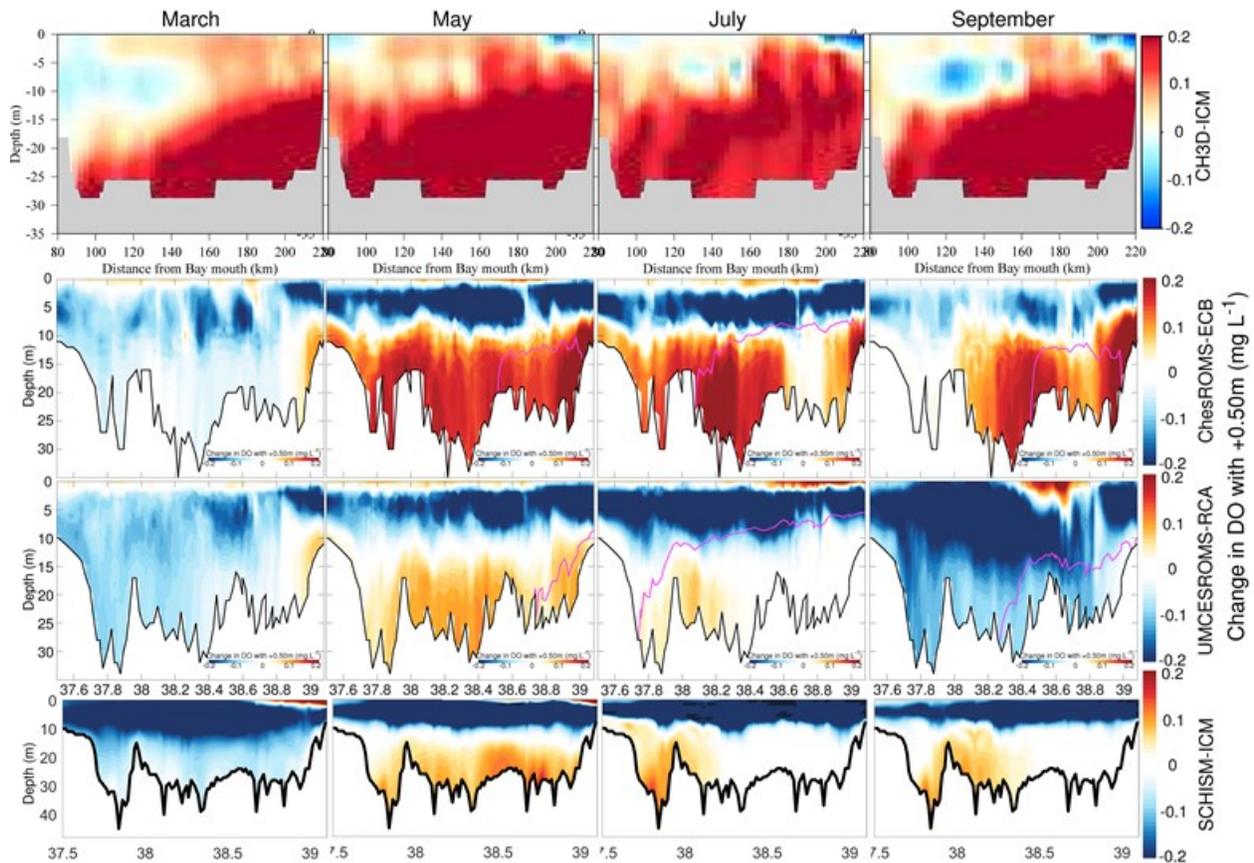
Figure 5-22: Change in dissolved oxygen concentrations in response to an increase in sea level of 0.50m. The figure is a monthly climatology for the months of March, May, July and September of years 1991-1995. Each row represents one of the four models considered. The magenta line in rows 2,3 is the vertical boundary of the hypoxic volume (DO<2mg/L) in the reference simulation.

Changes in the solubility of oxygen could not explain the changes in summertime bottom DO simulated by the models. SLR increased salinity and cooled water temperatures in the summer, with these two changes affecting the saturation of DO in opposite ways. The two effects mostly cancelled each other in May-July and thus only explain a small fraction of the modeled changes in summer bottom DO. Other causal mechanisms were examined, notably a temperature-driven decrease in respiration rates or an increase in the physical ventilation of the bottom layer. The former mechanism was positively identified as the primary cause of the improvement in bottom DO in ChesROMS-ECB.

The upper part of the water column (top 10m) and the shallow areas of the Bay (bottom depths <10m) exhibited a decrease in DO concentrations with SLR (Figure 5-22) in all four models. This decrease grows quasi-linearly with SLR and in the summer was linked to the upward shift of the pycnocline/oxycline with SLR. It is also apparent that the vertical boundary of the hypoxic volume (DO<2m/L) often reaches into the top 10m during the month of July (Figure 5-22), especially for UMCES-ROMS-RCA. Therefore, a vertical expansion of this hypoxic volume and an improvement in bottom DO are two impacts of SLR that are not exclusive, emphasizing the need for consistent metrics when comparing model projections.

In conclusion, all four models exhibit some improvement in summer bottom DO in response to SLR and this improvement is approximately proportional to sea level rise. However, the magnitude and duration of this improvement varies substantially between the models (Figure

124

5-22). These variations are to be expected given the differences in the parameterization of biogeochemical processes and the differences in the magnitude of the "summer cooling" predicted by the models (Figure 5-21) that affects respiration rates, sediment oxygen demand, and ultimately oxygen concentrations.

Note: the preceding text was approved based on presentations of the material in St-Laurent, et al. 2019 prior to publication.

5.3.2   Reasonable Response to Temperature Change

Water temperature change is one of the key elements in determining the climate change impact on water quality in the Bay. Changes in water temperature not only affect water column stratification, but also biogeochemical rates and DO solubility. Robust simulation of water temperature change under climate change conditions is thus essential for reliable assessment of climate change impacts on water quality.

Substantial data on water temperature have been collected over the past 30 years by the CBP partnership. A comprehensive analysis of long-term temperature trends and vertical patterns was conducted (Figure 5-23). The analysis was performed station by station, at each depth with 1 m resolution, and for each month of the year. Regression slopes were determined for temperature change over 30 years for the summer season (July-September) and throughout the year. Considering the regression with depth as an approximation of the central tendency, the temperature change at the sea surface in summer is an increase of approximately 1.2 °C over 30 years and 1 °C at the bottom. The analysis based on data year-round results in lower estimates of temperature increases as compared to the summer data, with increases of about 0.7 °C at the surface and 0.6 °C at the bottom.

In order to assess the simulated water temperature change over 30 years, similar analysis was performed on the modeled
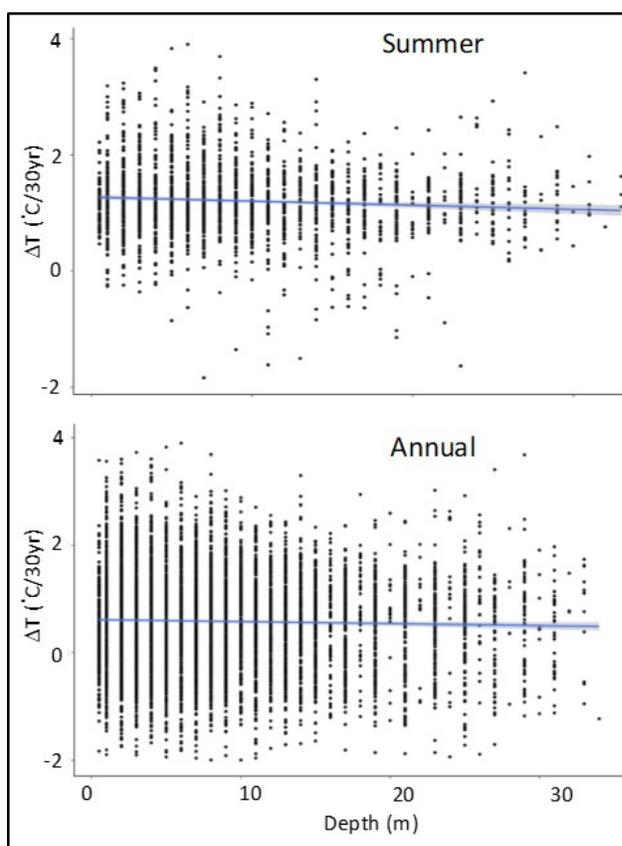
Figure 5-23: Water temperature change over 30 years (1986-2016) observed in Chesapeake Bay. Each dot is the regression slope for water temperature versus time at a specific station, depth and month, the blue line is the linear regression of temperature change with depth. The upper panel is July through September, and the lower panel is year-round.

results (Figure 5-24). For the base calibration case, a 10-year simulation was conducted for 1991 to 2000 with the central point at 1995. For the climate change scenario at 2025, which is 30 years apart from 1995, the model was run for a 10-year simulation using oceanographic and meteorological forcings from a downscaling analysis of 2025 projections from 31 the global circulation models described in Section 2. Increases in air temperature and net heat flux, changes in precipitation and river discharge, sea level rise, and an increase in sea water temperature at the open boundary constitute the major changes in the forcing files under climate change conditions as described in previous sections of this report. The monthly temperatures at each station and depth represent the average of the 10-year simulation. There are 728 observation stations within the simulation domain for which modeled results were extracted for the analysis. The first layer in the simulation grid is 2.13 meters (7
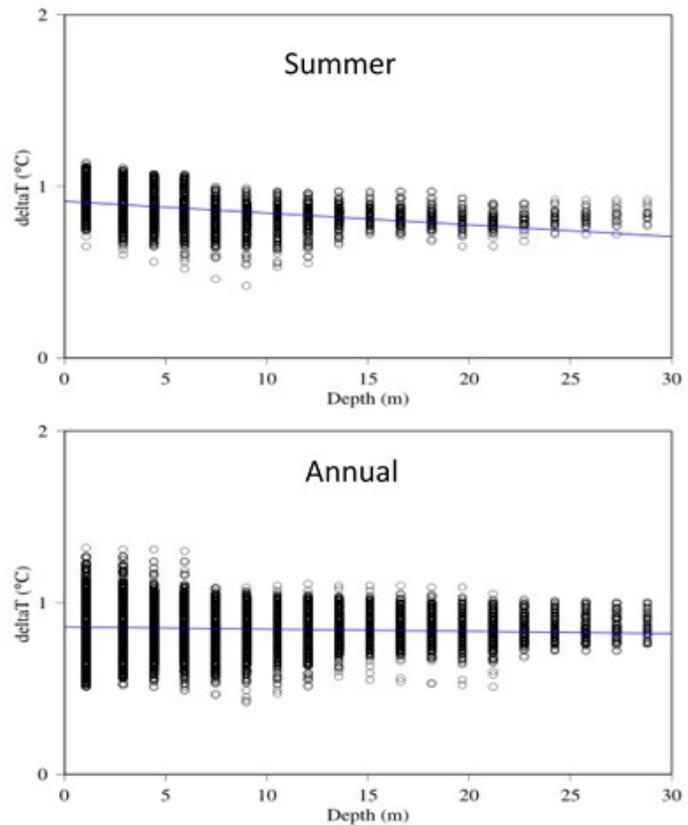

Figure 5-24:: Modeled water temperature change over 30 years (1995-2025) in the Chesapeake Bay. Each dot is the water temperature change at a specific station, depth and month. The blue line is the linear regression of temperature change with depth. The upper panel is July through September, and the lower panel is year-round.

feet) thick and all other layers below the surface are 1.524 m thick (5 feet). As such, the vertical resolution in the simulation results is coarser than the resolution of the observations (at each meter). Also, due to the lower horizontal resolution of the model, which is about 1 km, the depth of the model grid is cut at 30 m deep and does not extend to 35 meters as in the observations at certain stations.

A pattern similar to the observed trends is apparent in the simulation (Figure 5-24). For the summer period (July through September), the simulated temperature increase over 30 years is about 0.91 ℃ in the surface layer and 0.82 ℃ in the bottom layer. When considering year-round results, the simulated temperature increase is 0.86 ℃ over 30 years in the surface layer and 0.8 ℃ in the bottom layer. The modeled surface temperature increase in summer is somewhat lower than the number obtained from observations, but the predicted temperature increase over all seasons is slightly higher than the observations. Given that the model simulation has less spatial and temporal variability than the observations, the overall comparison between observed and simulated trends is plausible. There are two extensive studies on temperature change in the coastal area adjacent to Chesapeake Bay, and both reported a rate of temperature increase on the order of 0.3 ℃ per decade, which yields 0.9 ℃ increase over 30 years, similar to the modeled result (Thomas et al., 2017; Dupigny-Giroux et al., 2018).

A signal of the thermocline is apparent in the simulation profiles. At depths of 7 to 12 m, particularly in summer, the regression line is located above a majority of the individual slopes, whereas the regression line is primarily below most of the individual slopes in the bottom layers (Figure 5-24, upper panel). According to this pattern, 30-year water temperature increases were smaller in the pycnocline as compared to deeper waters. There are two major sources of heat to the Bay: the surface heat flux and at the open boundary. Due to the estuarine circulation, according to which surface water flows out of the bay and bottom water intrudes into the Bay from the coastal ocean, it is likely that the surface water temperature increase is essentially caused by increased in surface heat flux. In contrast, warming of the bottom water is more likely due to temperature increase in the coastal ocean. The pycnocline is a transitional zone where heat flux may be reduced due to limited vertical mixing.

As a specific example, the vertical profiles of simulated temperature and 30-year temperature change for Station CB4.3C, located along the thalweg in the upper Bay, are detailed in Figure 5-25. The individual and combined effects of climate change factors on Bay water temperatures were simulated by applying to the calibration run (Base): Increases in river discharge (Flow), surface heat flux (Heat), sea level rise (SLR) and all three combined (All). Temperature profiles of the base case, SRL, and Flow cases overlap (Figure 5-25, left panel), which means that changes in river

Figure 5-25: Temperature vertical profile in July (left panel) and temperature change over 30 years (right panel). Base: Calibration; Flow: River discharge projected for 2025 was applied; Heat: Heat flux increase projected for 2025 was applied; SLR: Sea level rise of 22cm from 1995 to 2025 was applied; All: All the above climate change factors were applied; s: Surface; b: Bottom; m: Mean over the water column.

discharge and sea surface level did not significantly alter water temperature at this station. Separately, the Heat and All cases also overlap with each other, indicating that heat flux is the primary factor in determining water temperature change under climate change conditions. A thermocline is visible from 5 to 12 meters. The right panel of Figure 5-25 illustrates the 30-year changes in water temperature in the difference scenarios. The Flow and SLR runs are practically identical and close to 0, indicating that these two factors had little impact on water temperature at this station in the central deep trench of the Bay. Nonetheless, the SLR run is slightly lower than the Flow run in the bottom layers, meaning that SLR may slightly decrease water temperature in the bottom layers. The two other runs, Heat and All, are quite similar as well. However, the All run generates temperature changes that are slightly lower than the Heat flux run at the bottom layers, which may reflect the effect of sea level rise at this station. In the All run, the surface water temperature increased 0.88 °C over 30 years, bottom water temperature by 0.8 °C with a water column average of 0.82 °C. Temperature change tended to decrease from the surface toward the pycnocline, in coherence with the observed temperature change slope profile in Figure 5-24.
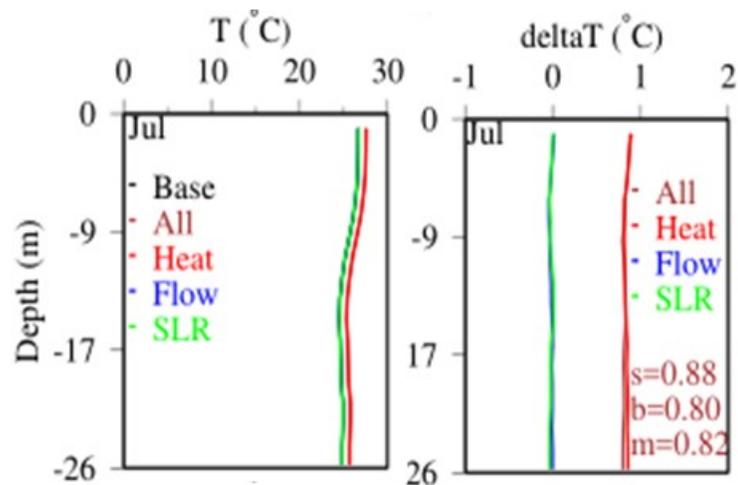
Figure 5-26 illustrates the monthly water temperature change over 30 years in both the surface and bottom water at Station CB4.3C, together with air temperature change predicted by GCM downscaling analysis. The downscaled air temperatures were used to compute heat flux change under climate change condition. Seasonal variations in water temperature change range from 0.7 to 1 ℃. These variations essentially follow the variations in the air temperature change, which tend to be higher in April and
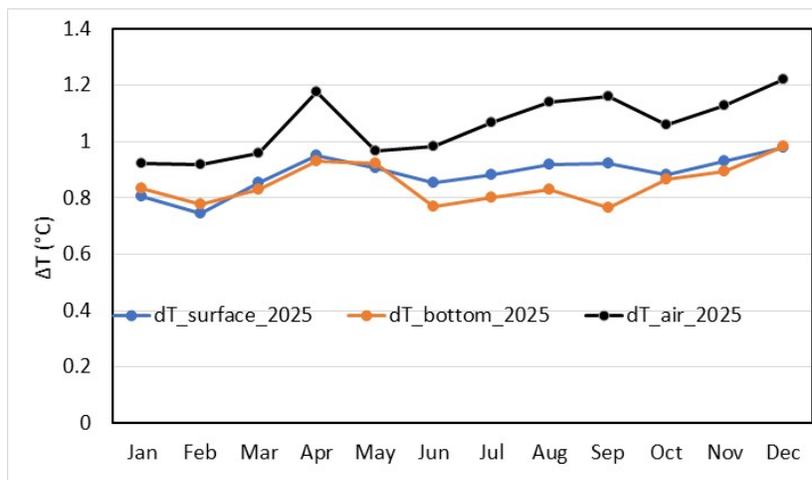

Figure 5-26: Monthly water temperature change from 1995 to 2025 in the surface layer (blue line) and bottom layer (orange line) predicted by the model at Station CB4.3C, together with air temperature change (black line) of downscaled GCMs ensemble prediction. The air temperature change was used to compute heat flux change in the climate change scenarios, and the simulated results are from the ("All") run with all climate change factors combined.

November-December. These months are typically transitional periods from and to winter. Thus, it appears that climate change affects air and water temperature more during the transitional periods than the rest of the year. There tends to be a slight delay between air and water temperature change. Air temperature change in May is relatively lower, but water temperature change remains relatively higher during the same period of time, most likely due to the high air temperature increase in April. The same phenomenon can be observed in January, following the high air temperature increase in December. In the vertical dimension, only during the strong stratification season of summer (June through September) did surface water temperature increase significantly more than bottom water temperature. During other periods of the year, water temperature changes are similar in the surface and bottom layers, indicating weak stratification and stronger vertical heat transfer in the water column.

Overall, the model predictions of water temperature change under climate change conditions are in reasonable agreement with the literature and observations. Although it is inevitable that discrepancies occur between simulation and observation, partly due to the large variation in the data, the model predictions are in reasonable agreement with the data in terms of magnitude and vertical patterns of temperature change under climate change conditions.

5.4   Two-Step Simulation Approach

Within the framework of the Chesapeake Bay TMDL, the approach of "Delta Change" of dissolved oxygen (DO) concentration has been taken for water quality criteria assessment of modeled nutrient management scenarios (EPA, 2010a). The WQSTM is calibrated to observed data but not unbiased relative to the data in each segment assessed. These biases would carry forward into all modeled scenarios of nutrient reduction and climate change. To account for these biases, the change in dissolved oxygen predicted by the WQSTM is applied to the observed data. These procedures are fully described in Appendix H of the TMDL documentation (EPA 2010a) and briefly discussed here.

Referring to Figure 5-27, the 1993-1995 observed oxygen data are evaluated through the criteria assessment procedures (EPA 2010b), independent of any results from the WQSTM. Consequently, the criteria assessment of the base condition related to the calibration scenario of the WQSTM is fully based on observed data. For management scenarios, a 'scenarioed' data set is created by copying the observed dataset and modifying each point by applying the relative oxygen change predicted by the model. Water quality model results are output on an hourly basis and a

Figure 5-27: Water quality criteria assessment procedure for nutrient management scenarios (OLS: Ordinary Least Square regression)

regression is performed for the specific month and depth corresponding to each individual sample. As such, approximately 720 paired data between the calibration and the nutrient management scenario are used for each regression specific to each datum of field observation. The regression function is then applied to its specific datum to project a modified datum. The scenarioed data are finally processed through the same water quality criteria assessment procedure as the observed data to obtain the water quality attainment status under the nutrient management conditions.
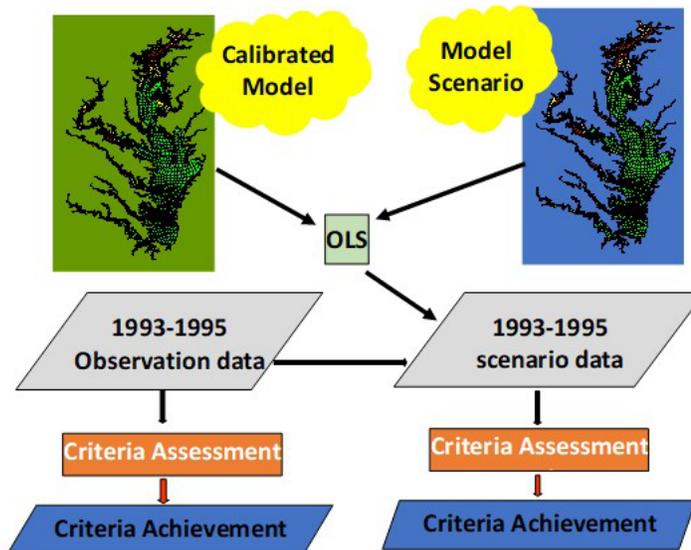
Management scenarios and the calibration run are simulated with the same physical forcings such as current, turbulence diffusivity, temperature, and salinity. Usually strong correlation between the calibration and management scenario exists so that the modified scenario data and

the consequent criteria assessment results are robust. However, a challenge arises for management scenarios under climate change conditions. Sea level rise, air-temperature increase, heat flux intensification, temperature and salinity changes at the open boundary, and changes in watershed inputs of water and heat all influence the simulated physics of the Bay, which cascades to the biological and water quality processes. For climate change scenarios, the physical model CH3D (Curvilinear Hydrodynamics Model in 3D) is first run with forcing under climate change conditions. A new hydrodynamic field is thus established, which differs from the calibration physics.
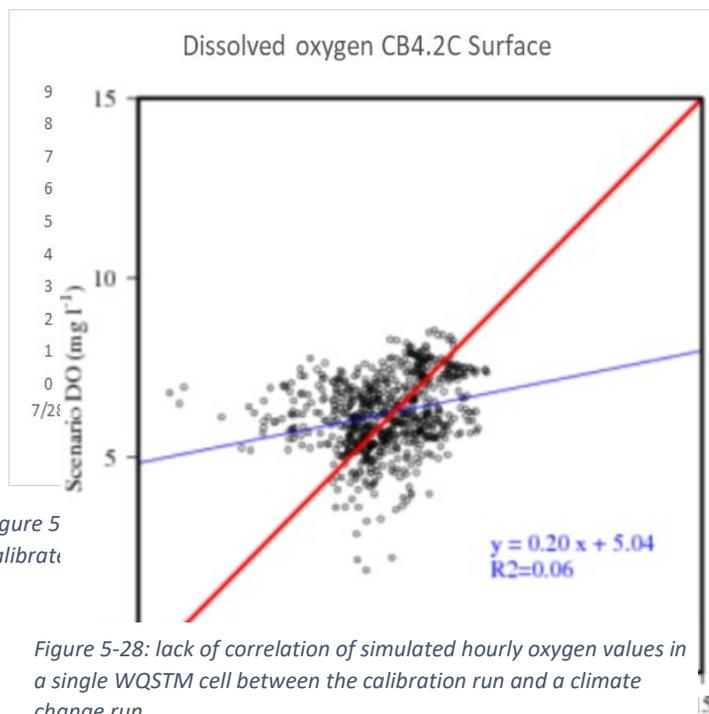

Figure 5-28: lack of correlation of simulated hourly oxygen values in a single WQSTM cell between the calibration run and a climate change run

For management scenarios under climate change conditions the newly established hydrodynamic field under climate change condition is used.

Figure 5-29 shows that temporal mismatches can occur under climate change conditions. The decrease in oxygen initially simulated on the evening of 7/29/1991 has moved to 7/28/1991 under climate change conditions. Accumulation of temporal mismatches over a simulated month can result in poor correlation between the calibration run and a climate change run, as shown in Figure 5-28. By inspecting the plot, it can be seen that climate change in this month caused a change in timing but did not have a large effect on the mean or variance of dissolved oxygen. Applying the regression would lead to a similar mean, but a much smaller variance.

The Modeling Workgroup of the Chesapeake Bay Program decided to use a two-step approach for water quality criteria assessment of climate change scenarios. The water quality model is run twice for each nutrient management scenario under climate change condition. The first water quality model is run with the physics under climate change conditions and nutrient loading of the calibration, called the "climate base scenario". The second run is conducted with both physics and nutrient loading under climate change condition. The first run is an intermediate solution to bridge the management scenario under climate change condition to the calibration. Figure 5-30 shows the two-step method. Observations are first modified for the effect of climate change using a method similar to quantile mapping, creating a set of climate modified observations. In the second step, the regressions are run between the climate base
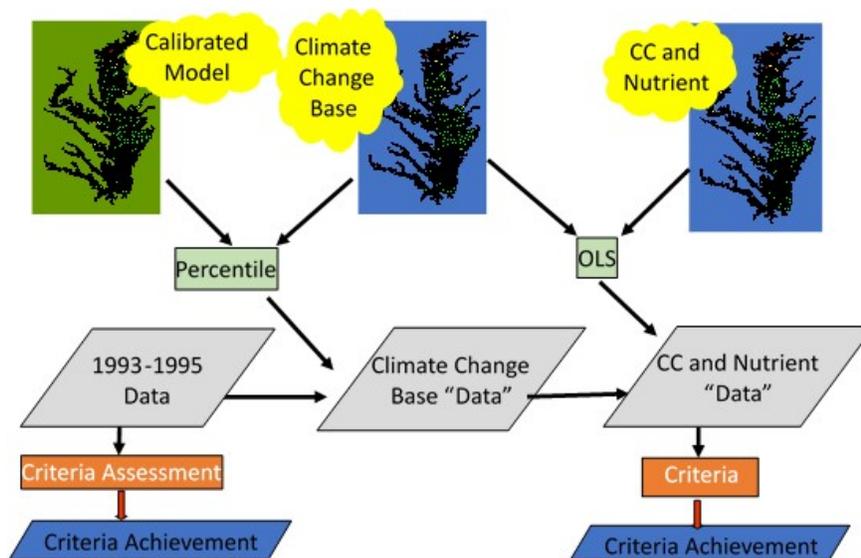

Figure 5-30: Two-step water quality criteria assessment procedure for management reduction scenarios under climate change condition (CC and Nutrient: Nutrient management scenario under climate change condition; OLS: Ordinary Least Square regression)

run and the climate nutrient run as in the standard CBP scenario analysis method.

The percentile method used to create the climate scenarioed data is a form of quantile mapping illustrated in Figure 5-31 The simulated results for each grid cell corresponding to a specific observation datum from both scenarios are ranked based on their percentile ranging from the lower to the higher end. The observation datum is then located in the percentile cumulative distribution curve. The difference of that percentile between the climate change base scenario and the calibration constitutes the delta change in DO concentration and is added to the observation datum to obtain a modified data set for the climate base scenario. The newly established data set for the climate change base scenario is then used as the starting data set for the criteria assessment of the nutrient management scenario under a climate change condition.
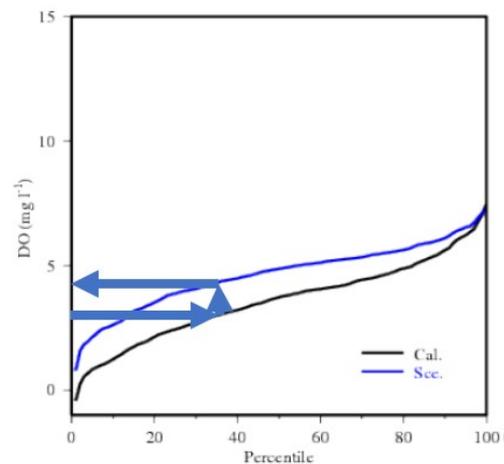

Figure 5-31; Percentile method to modify the observation data based on the difference between the climate base on and the calibration.

6 Findings and Partnership Decisions

6.1 Summary

The PSC met in March 2018 and agreed that the jurisdictions' Phase III WIPs would address climate change narratively and include numeric pollutant reduction loads due to 2025 climate change conditions. Specifically, the WIPs would include a narrative strategy describing the jurisdictions' current action plans and strategies to address an increase in nitrogen and phosphorus across the watershed as a result of climate change as well as changes in the tidal Chesapeake. The narrative included the initial estimates of climate change effects on dissolved oxygen standards equivalent to an increase of 9 million pounds of nitrogen and 0.5 million pounds of phosphorus across the watershed. As part of the same decision the PSC agreed to refine the climate modeling and assessment framework based on improved understanding of the science of the impacts of climate change. The partnership further committed to adopting revised numerical climate change targets by 2021 using updated versions of the CBP's modeling tools and incorporating those revised climate change estimates into 2022-2023 Milestones.

During 2019, the Modeling Workgroup oversaw improvements in the CBP's ability to simulate the effects of climate change as documented above. Based on input from STAC and the partnership, upgrades were made to model inputs and processes. Changes were made to model inputs of rainfall, air temperature, wetland area change, sea level rise, and ocean temperature and salinity. Watershed delivery of nitrogen, phosphorus, and sediment were modeled using improved processes to capture the effects of climate changes on watershed loads. The estuarine algal simulation was improved, and the model results were validated using multiple model comparisons and analysis of observed data.

Climate change was found to have a more detrimental effect on water close to the surface of the Bay compared to deeper water and the effect also varied spatially. However, an analysis showed that the current CBP models were not appropriately designed to assess designated uses

in shallow waters and that Open Water designated uses, while negatively affected, were still likely meeting water quality standards. There were also areas in the CB6MH and CB7MH segments of the Bay where the current open water designated use is applied throughout the water column (surface to bottom). In these areas, the models indicated that the non-attainment in the open water standard was isolated to areas below the pycnocline, an area typically held to the deep water or deep channel standard in mesohaline Bay segments. Modeling indicated that the deep water standard would be met in these areas of CB6 and CB7 under climate change conditions. The Modeling Workgroup recommended, and the WQGIT agreed, that Open Water designated uses not be considered for the current climate change allocation decisions. However, the partnership's Criteria Assessment Protocol Workgroup (CAPW) will evaluate climate change risks to current water quality standard criteria and designated uses, including the open water designated use for CB6MH and CB7MH, beginning this summer. Preliminary evaluations suggest that the expansion of the deep water designated use in these areas would be appropriate.

The WQGIT discussed climate allocation approaches at meetings from January through September, 2020. After consideration of many alternatives, the WQGIT recommended that the primary method of accounting for the effects of climate change should be to reduce loads in the areas where they are increasing due to climate change. The recommended reductions are to be included in milestones starting with 2022-2023 and additional implementation completed by 2025. Preliminary analysis suggests that the negative effects of climate change on dissolved oxygen water quality standards will increase in the future. The CBP will re-evaluate the effects of 2035 climate in 2025. The allocation method based on loads was approved by the Management Board on 10/15/2020 and the Principals' Staff Committee on 12/17/2020. Details of the decision are in section 6.7 below.

6.2   Estuarine Model Scenario Results

Climate change scenarios were run with modified inputs for the watershed and estuarine model for the years 2025, 2035, 2045, and 2055. The achievement of dissolved oxygen water quality standards was calculated for each run and designated use. Table 6-1 shows additional non-attainment that results from the application of climate change for the Deep Channel designated use. Note that for CB4MH deep channel the non-attainment roughly doubles from 2025 to 2035 and then doubles again by 3055. Other main bay segments are not pushed into additional non-attainment by climate change Table 6-2 shows the results, again in units of additional non-attainment, for the Deep Water designated use. Additional non-attainment is more widespread in Deep Water than in Deep Channel, but with lower percentage increases.

Table 6-1: Achievement of Deep Channel DO water quality standard (1mg/l instantaneous minimum) expressed as an incremental increase over the PSC agreed to 2025 planning targets

CB Segment	State	2025 Climate 2025 Land Use 204TN 14.0TP 1993-1995 DO Deep Channel	2035 Climate 2025 Land Use 208TN 14.6TP 1993-1995 DO Deep Channel	2045 Climate 2025 Land Use 212TN 15.4TP 1993-1995 DO Deep Channel	2055 Climate 2025 Land Use 220TN 16.7TP 1993-1995 DO Deep Channel
CB3MH	MD	0.00%	0.00%	0.00%	0.00%
CB4MH	MD	1.47%	3.15%	4.62%	7.31%
CB5MH	MD	0.00%	0.00%	0.00%	0.00%
CB5MH	VA	0.00%	0.00%	0.00%	0.00%
POTMH	MD	0.00%	0.00%	0.00%	0.00%
RPPMH	VA	0.00%	0.00%	0.00%	0.00%
ELIPH	VA	0.00%	0.00%	0.00%	0.00%
CHSMH	MD	0.01%	0.92%	1.08%	2.34%

Table 6-2: Achievement of Deep Water DO water quality standard (3 mg/l 30-day mean) epressed as an incremental increase over the PSC agreed to 2025 planning targets

CB Segment	State	2025 Climate 2025 Land Use 204TN, 14.0TP 1993-1995 DO Deep Water	2035 Climate 2025 Land Use 208TN, 14.6TP 1993-1995 DO Deep Water	2045 Climate 2025 Land Use 212TN, 15.4TP 1993-1995 DO Deep Water	2055 Climate 2025 Land Use 220TN, 16.7TP 1993-1995 DO Deep Water
CB3MH	MD	0.01%	0.15%	0.16%	0.21%
CB4MH	MD	0.94%	1.61%	2.00%	2.66%
CB5MH	MD	0.52%	1.01%	1.32%	1.66%
CB5MH	VA	0.00%	0.00%	0.00%	0.00%
CB6PH	VA	0.00%	0.00%	0.00%	0.00%
CB7PH	VA	0.00%	0.00%	0.00%	0.00%
PATMH	MD	0.01%	0.02%	0.42%	2.66%
MAGMH	MD	1.66%	1.66%	1.91%	1.91%
SOUMH	MD	0.00%	0.00%	0.00%	0.00%
SEVMH	MD	0.00%	0.00%	0.00%	0.00%
PAXMH	MD	0.00%	0.00%	0.00%	0.00%
POTMH	MD	0.03%	0.15%	0.56%	0.81%
RPPMH	VA	0.00%	0.24%	1.48%	1.85%
YRKPH	VA	0.00%	0.00%	0.00%	0.00%
ELIPH	VA	0.00%	0.00%	0.00%	0.00%
SBEMH	VA	0.00%	0.00%	0.44%	3.12%
CHSMH	MD	0.00%	0.00%	0.00%	0.00%

Table 6-3 contains results for non-attainment of Open Water dissolved oxygen water quality standards in main stem Bay and the mesohaline sections of large rivers where the WQSTM is most reliable for open water. Note that this table is not expressed as additional non-

attainment, but total non-attainment. CB6PH and CB7PH are the only segments where climate change causes significant increases in non-attainment through 2055. MOBPH (Mobjack Bay), and TANMH_VA (Tangier Sound in Virginia) both have very small increases by 2055, however these are adjacent to CB6PH and CB7PH and likely share some monitoring stations.

Table 6-3: non-attainment of open water DO water quality standard (5-5.5 mg/l 30-day mean), main bay and mesohaline regions only

Cbseg	Planning Target	2025	2035	2045	2055		Cbseg	Planning Target	2025	2035	2045	2055
CB1TF	0.00%	0.00%	0.00%	0.00%	0.00%		PAXMH	0.00%	0.00%	0.00%	0.00%	0.03%
CB2OH	0.00%	0.00%	0.00%	0.00%	0.00%		POTMH_MD	0.00%	0.00%	0.00%	0.00%	0.00%
CB3MH	0.00%	0.00%	0.00%	0.00%	0.00%		RPPMH	0.00%	0.00%	0.00%	0.00%	0.00%
CB4MH	0.00%	0.00%	0.00%	0.00%	0.00%		YRKPH	0.00%	0.00%	0.00%	0.00%	0.00%
CB5MH_MD	0.00%	0.00%	0.00%	0.00%	0.00%		MOBPH	0.00%	0.00%	0.01%	0.11%	0.16%
CB5MH_VA	0.00%	0.00%	0.00%	0.00%	0.00%		JMSPH	0.00%	0.00%	0.00%	0.00%	0.00%
CB6PH	0.03%	0.39%	0.71%	0.99%	1.29%							
CB7PH	0.32%	1.41%	2.11%	3.02%	4.19%		CHSMH	0.00%	0.00%	0.00%	0.00%	0.00%
CB8PH	0.00%	0.00%	0.00%	0.00%	0.00%		EASMH	0.00%	0.00%	0.00%	0.00%	0.00%
							CHOMH2	0.00%	0.00%	0.00%	0.00%	0.00%
							TANMH_MD	0.00%	0.00%	0.00%	0.00%	0.00%
							TANMH_VA	0.00%	0.00%	0.00%	0.00%	0.03%

6.3   Open Water designated uses

There was general agreement that the Open Water designated use is an important are to protect. The Open Water criteria are based on living resource needs for striped bass and other important species. Roughly two-thirds of the mainstem Bay volume and two-thirds of the tidal volume is designated as Open Water habitat and the portion of the Bay that people interact with the most.

It is also likely that Open Water and Shallow Open Water (less than 2 meters deep) may have increased impacts from future estimated temperature increases. However, Table 6-3 shows that only CB6PH and CB7PH are pushed into violation by the modeled effects of climate change in Open Water and it was determined that there were substantial questions about the appropriate Open Water boundary for these two segments. The MWG and WQGIT discussed Open Water violations during several meetings in 2020 and decided not to include Open Water violations in the current climate change allocations.

CB6PH and CB7PH are unique in that they are the only segments with Deep Water designated use where the Deep Water boundaries don't extend to the entire segment as shown in Figure 6-1. These boundaries were set in the 2003 Technical Support Document (U.S. EPA 2003). Quoting from the document: "The delineation of the boundary was determined by examining maps of contemporary dissolved oxygen concentration distributions and the anecdotal historical dissolved oxygen concentration data record." The preceding indicates that the boundaries may have been
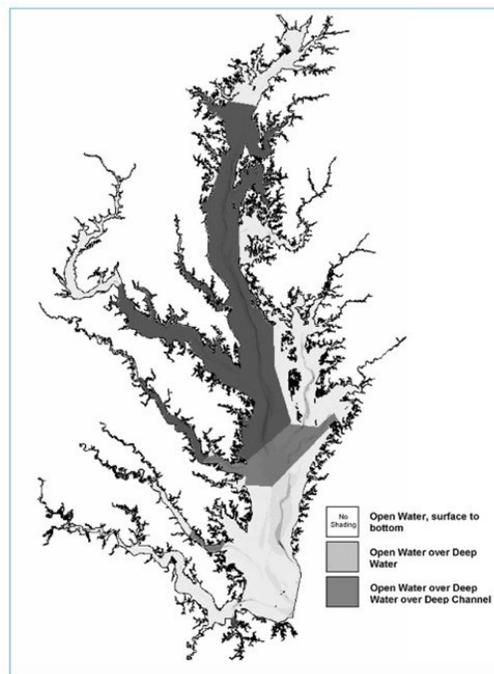

Figure 6-1: Dissolved oxygen designated use boundaries.

chosen based on best professional judgement. Further, in a 2004 addendum to the same document (U.S. EPA 2004), the Deep Water boundary for CB6PH was moved southward such that the 2003 Cap Load allocations produced non-attainment under 1% in Open Water. In other words, the CB6PH boundary was determined such that the Open Water designated use was right on the edge of non-attainment, rather than strictly looking at living resources needs.

To investigate whether the modeled violations were occurring in the surface mixed layer, an assessment was run where CB6PH and CB7PH had Deep Water for the entire area rather than just the northern portion. No violations of Deep Water or Open Water were found for climate change runs through 2055. The conclusion was that Open Water violations under climate change were occurring in sub-pycnocline waters and that the sub-pycnocline waters were not violating the Deep Water standard of 3 mg/l dissolved oxygen.

With this understanding, the MWG did not recommend using open water to drive climate change allocations in 2020. The Criteria Assessment Protocol Workgroup will be working on any changes to water quality standards assessment related to climate change in time for a re-evaluation of climate change effects in 2025.

Open Water DO nonattainment in shallow water requires additional investigation. Ultimately, an improved Bay Model simulation of shallow water is needed to better understand the climate effects on Open Water DO water quality standards in Chesapeake's shallow waters.

6.4   Violation Balancing

The MWG recommended and the WQGIT approved a method of climate change allocations whereby some areas of the bay will have higher non-attainment after climate change and allocated reductions and some areas will lower non-attainment compared to the modeled values used in setting the 2018 Phase III WIP planning targets. The rule was adopted that the total volume-weighted violation in the standard set of segments used to set TMDL allocations would remain the same. This method is illustrated in Figure 6-2.
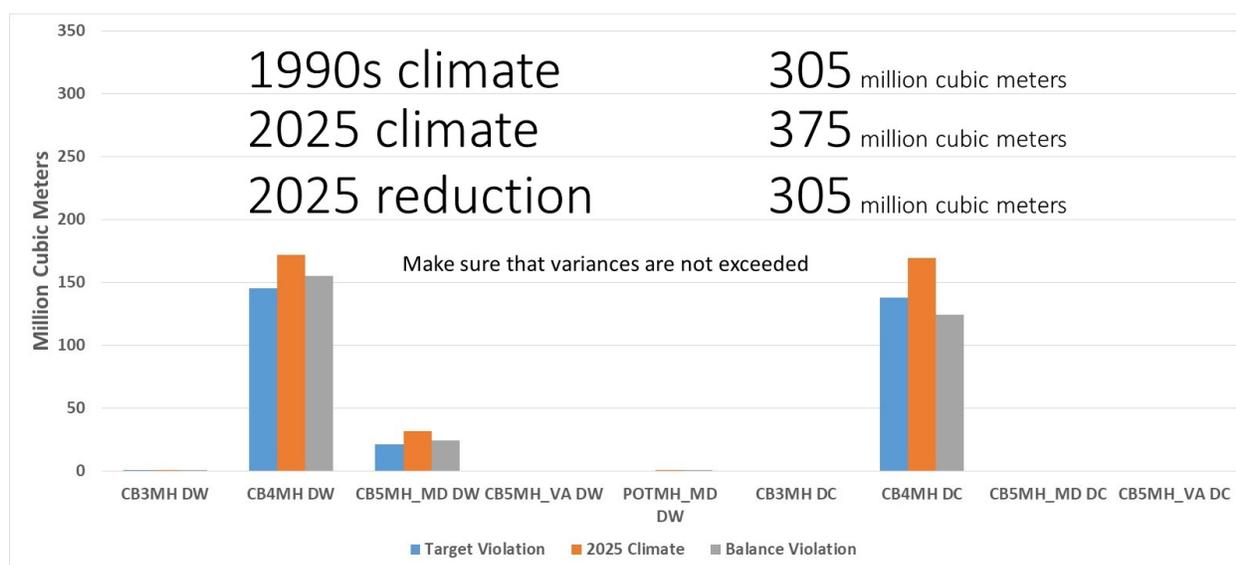

Figure 6-2: Illustration of violation balancing method

The planning targets agreed to be the PSC in 2018 resulted in a modeled violation rate of 5.09% for CB4MH Deep Water. Multiplying the violation percentage by the 2854 million cubic meter average volume of CB4MH Deep Water gives a volume of 145 million cubic meters of water in violation as shown by the blue bar in Figure 6-2 above. Values for other Deep Water and Deep Channel designated uses are calculated resulting in a total allowable volume of 305 million cubic meters. Climate change is then applied to the watershed and estuarine models and a new violation volume of 375 million cubic meters is estimated as shown in the orange bars. Finally, a watershed load reduction scenario is run that results in the same overall violation volume of 305 million cubic meters, although with different volumes in most designated uses compared to the 2018 planning targets.

6.5   Climate Allocation Options

Over the first half of 2020, the WQGIT considered alternatives for allocating the nutrient reductions to counter the effect of climate change on dissolved oxygen in the deep water and deep channel designated uses in the Chesapeake Bay. All options met the same volume-weighted average non-attainment as the PSC-agreed 2025 Phase III WIP planning targets based on 1990s climate. Further, all modeled non-attainment levels are within current or proposed variances. Regardless of the allocation option that is chosen, jurisdictions have the flexibility to meet the allocated climate change load reductions using whatever combination of point source or non-point source actions they deem appropriate. Jurisdictions may also exchange reductions between basins and nutrients, subject to appropriate basin-to-basin and nitrogen-to-phosphorus exchange ratios.

6.5.1   Year

The WQGIT reviewed modeling scenarios that showed increasing level of nutrient reduction effort necessary as climate change intensifies from 2025 through 2055. The WQGIT considered the options of 2025 and 2035 for the target years for climate change effects and for implementation. In keeping with the PSC direction, the WQGIT decided to continue with accounting for climate effects between 1995 and 2025 and incorporating additional reductions by 2025. The WQGIT also decided that the current estimates of 2035 climate change effects should be documented in a narrative in the 2022-2023 milestones and that the partnership should continue to refine the climate modeling and assessment framework to update the 2035 estimates in 2025. This approach mirrors the March 2018 PSC approved approach for the initial 2025 climate change estimates.

6.5.2   Allocation chart method

The allocation chart method was used in the 2010 TMDL and the 2017 Phase III WIP planning target calculations. The nitrogen allocation curve used in 2017 and 2018 is shown in Figure 6-3.
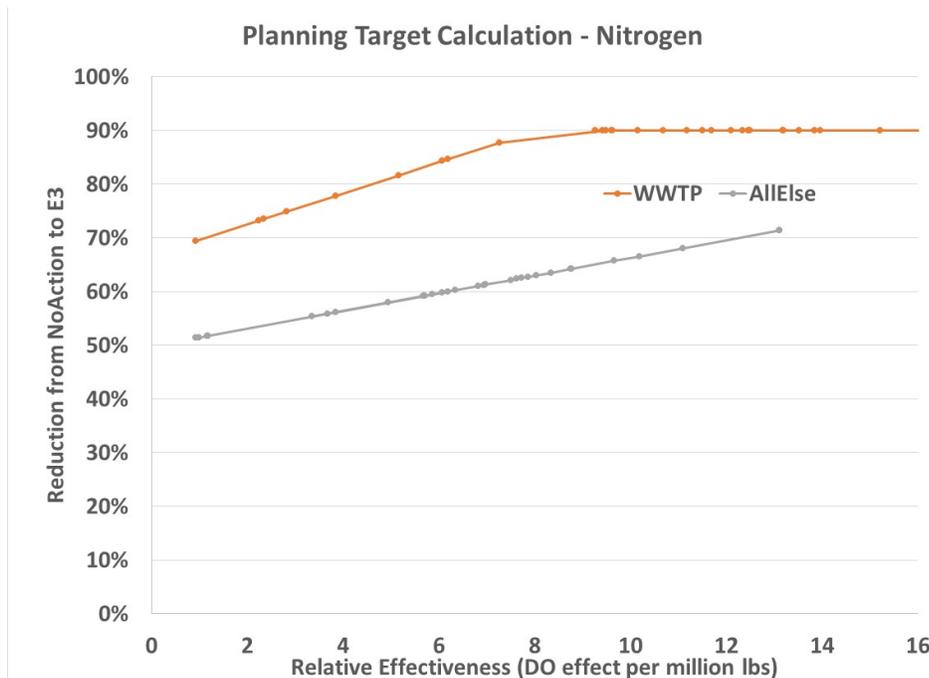
Figure 6-3:Nitrogen allocation curve used in the Phase III WIP planning targets

The horizontal axis is the relative effectiveness of a state-basin in ug/l increase in dissolved oxygen per million pounds of reduction. A state-basin with a score of 10 can achieve twice the oxygen effect with the same reduction effort compared to a state-basin with a score of 5. The vertical axis is the fraction of possible reductions that state-basin is expected to implement. A 0% score on this axis indicates the state-basin could remove all existing management actions and a 100% score would mean that the state-basin would need to implement the maximum possible management actions. More information on the allocation curve and relative effectiveness is available in the TMDL documentation (U.S. EPA 2010a).

An allocation curve is a statement of policy, not a description of a physical relationship. The orange line represents the CBP partnership policy that state-basins containing point sources are responsible for load reductions equivalent to 90% of what is possible if they are in the upper half of effectiveness values and responsible for load reductions equivalent to 67% of what is possible for a relative effectiveness score of zero. The grey 'all else' line represents the CBP partnership policy that the most effective basin should be responsible for a level of effort 20 percentage points higher than the least effective basin. The intercept of the 'all else' or 'non-WWTP' line is placed at the level of reduction where water quality standards are met.

The climate allocations presented to the WQGIT, MB, and PSC in 2017 were calculated by raising the intercept of the 'all else' line to counteract the effects of climate change, but this was simply an example method that was not part of any partnership deliberation. However, the WQGIT considered the option of increasing the 'all else' line as a viable allocation option.

6.5.2.1   *Consideration of Wastewater Treatment*

The WQGIT considered additional allocation options that used the TMDL allocation chart but included various changes to the wastewater treatment line. The wastewater treatment line in the original TMDL allocation chart had the loads from wastewater plants in the more effective basins

set a 4.5mg/l (90%) for nitrogen and those in the least effective basins moving toward an intercept at 8 mg/l (67%). Several scenarios were proposed and analyzed including:

- Moving the WWTP and non-WWTP lines by the same amount
- Moving the upper part of the WWTP line from 4.5 mg/l TN to 4 mg/l TN and from 0.22 mg/l TP to 0.18 mg/l TP and raising the non-WWTP line for any remaining load
- Moving the intercept of the WWTP line from 8 mg/l TN to 6 mg/l TN and from 0.54 mg/l TP to 0.364 mg/l TP and raising the non-WWTP line for any remaining load

These alternatives to the allocation approach resulted in options referred to as 'NPS+PS', '6 and 4.5', '6 and 4', and '8 and 4', each with a 'Watershed Loads First' and 'Allocate All' option. At the July 2020 WQGIT meeting, consensus was reached to exclude the '6 and 4.5' and '6 and 4' scenarios.

6.5.3 Jurisdictional Watershed Loads method

Climate change between 1995 and 2025 has generally increased total rainfall, the intensity of rainfall, and temperature-driven evapotranspiration in the watershed. Some of the improvements made since late 2017 in the CBP's ability to simulate the effects of climate change have allowed for improved geographic resolution in the resulting watershed loads. In most areas of the watershed, the total rainfall increase is larger than the evapotranspiration increase which leads to an increase in flow and resulting increase in nitrogen (Figure 6-4). The increase in water balance and the increase in rainfall intensity lead to an increase in phosphorus for all parts of the watershed. It was determined through modeling scenarios that if the individual jurisdictions were to reduce nitrogen and phosphorus loads by the amount of the climate-related increase in watershed loads estimated through 2025, water quality standards in the deep water and deep channel designated uses in the Chesapeake Bay would be met at a level consistent with the 2017 planning target decision. As a result, no additional allocation, beyond the watershed-based load increases estimated for each jurisdiction, would be

Figure 6-4: Change in nitrogen delivery to tidal waters due to climate change between 1995 and 2025

needed. However, the estimate for 2035 (and beyond) climate change would need allocation beyond the jurisdictional watershed loads. This alternative is referred to as 'Watershed Loads First' or 'L1st' and would also require the selection of an alternative allocation approach for 2035 and beyond.
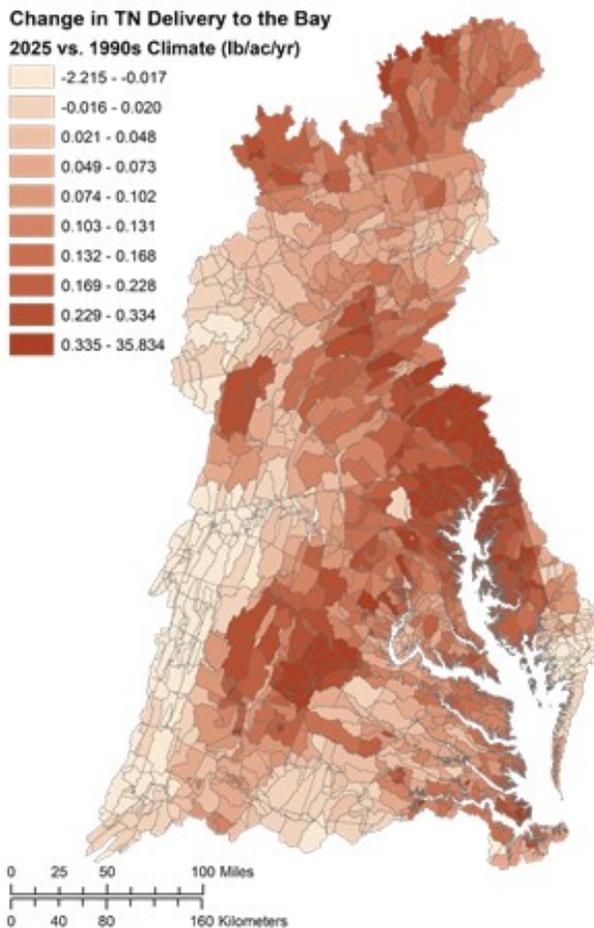
6.6   Proposed Adjustments to Watershed Loads First Allocation Method

The WQGIT expressed interest in the reduction of climate change-induced loads for each jurisdiction using the 'watershed loads first' method. It was noted that New York had a much larger proportional (to planning targets) increase than other jurisdictions using this allocation approach. New York's allocation was also a larger increase than the initial value presented to the PSC in December 2017. It was further noted that West Virginia had a negative load increase estimated due to climate change. The adjustment proposed, for the 2025 climate decision only, is for New York to be allocated 0.3 million pounds less nitrogen than their science-based watershed load increase due to climate change (returning to a value similar to the initial estimate in 2017). To make up for the 0.3 million pounds nitrogen adjustment policy, West Virginia would surrender their negative load increase to have no change in their nitrogen load. All other jurisdictions would make up the difference by increasing their allocated reductions equal to 108% of their science-based watershed load climate increase. This change will only be made to the nitrogen allocations for 2025 climate change. All jurisdictions' phosphorus allocations would remain unchanged from the science-based watershed loads first option.

Table 6-4: : Proposed additional reductions beyond the Phase III Planning Targets to account for the effects of climate change in million pounds per year. "Dec 2017 PSC" are the climate adjustments considered by the PSC in December 2017, prior to model adjustments. "L1st Climate increase" are the 2025 watershed load increases due to climate change. "Adjusted L1st Proposed" are the proposed final adjustments to nitrogen loads to account for NY increases compared to the December 2017 PSC loads.

State	TN			TP		
	Dec 2017 PSC	L1st Climate increase	Adjusted L1st Proposed	Dec 2017 PSC	L1st Climate increase	Adjusted L1st Proposed
DC	0.006	0.006	0.007	0.001	0.001	0.001
DE	0.397	0.036	0.039	0.006	0.003	0.003
MD	2.194	1.061	1.142	0.117	0.111	0.111
NY	0.400	**0.699**	0.399	0.015	0.044	0.044
PA	4.135	1.683	1.811	0.143	0.095	0.095
VA	1.722	1.476	1.589	0.187	0.337	0.337
WV	0.236	**-0.054**	0.000	0.017	0.009	0.009
Total	9.089	4.908	4.986	0.485	0.599	0.599

6.7   Decisions and Timeline

March 2018   PSC requests additional modeling and consideration of
                      climate change

October 2019   Modeling Workgroup approves modeling tools for
                      climate change

February 2020   WQGIT agreed to use the updated climate model when
                      assessing the allocation options

April 2020   WQGIT agrees to not include CB6MH and CB7MH in
                      climate calculations

July 2020   WQGIT agrees to include adjustments for 2025 climate
                      and reassess 2035 climate during the year 2025

August 2020   WQGIT considered Watershed loads first with a special
                      case for NY

September 10, 2020   WQGIT Consensus on 2025 Watershed loads first with a
                      special case for NY September 28, 2020   WQGIT
                      Consensus on 2035 narrative

October 15, 2020   Management Board reaches consensus on the following statements.
Approved statements are final decisions and do not need to be considered by the PSC.
Endorsed statements are recommended by the management board for approval by the PSC

Management Board Final Approved Statements 10/15/2020

1. Accept updated models for use in re-evaluating climate change for 2025 and 2035.

2. Exclude model estimated non-attainment in shallow open water from the climate
    change allocation.

3. Exclude model estimated non-attainment in open water in CB6 and CB7 from the
    climate change allocation.

4. Criteria Assessment Protocol (CAP) Workgroup will evaluate climate change risks to
    current water quality standard criteria and designated uses, including the open water
    designated use for CB6MH and CB7MH. A review of historical monitoring in these areas
    shows pycnoclines exist annually, justifying the Deep Channel designated use is
    appropriate in the area.

5. 2025 climate change estimate will consider main Bay DW/DC and ensure additional non-
    attainment returns to 2017 Planning Target levels and within existing variances.

Management Board Final Statements Endorsed to the PSC 10/15/2020

6. Jurisdictions will be expected to account for additional nutrient and sediment pollutant loads due to 2025 climate change conditions in a Phase III WIP addendum and/or 2-year milestones beginning in 2022.

7. Adopted the loads in Table 6-4, this document.

8. Include a narrative in the Milestones that describe the current understanding of 2035 climate change conditions, to the effect that "Preliminary estimates for the climate impact through 2035 suggest a doubling of the 2025 load effect, suggesting that the effect of climate change on our ability to meet the Bay's water quality standards is an ongoing concern." Specific language for the narrative to be developed by the WQGIT.

9. Continue efforts to improve understanding of the science and refine estimates of pollutant load changes due to 2035 climate change conditions.

   a) Develop a better understanding of the BMP responses, including new or other emerging BMPs, to climate change conditions.

   b) Compare the current 2025 climate change assumptions with measured climate conditions through 2024.

      i. To include rainfall volume, intensity, and distribution, air temperature, hydrology, water temperature, sea level rise, and changes in bay stratification and circulation.

   c) Consider the efficacy of using projections from measured trends versus downscaled global climate model data for revised 2035 estimates.

   d) Improve understanding and simulation of climate change impacts to open water designated use in shallow waters.

10. In 2025, the Partnership will consider results of updated methods, techniques, and studies and revisit existing estimated loads due to climate change to determine if any updates to those 2035 load estimates are needed.

December 17 2020   PSC meeting. The Principals' Staff Committee met on to discuss the climate change final decision. They approved the following:

o The 2020 update to the 2025 climate load allocations based on the latest modeling assessment.
o Jurisdictions are expected to account for additional nutrient and sediment pollutant loads due to 2025 climate change conditions in a Phase III WIP addendum and/or 2-year milestones beginning in 2022.
o Jurisdictions are expected to include a narrative in the 2022-2023 Milestones that describe the current understanding of 2035 climate change conditions,

- o In 2025, the Partnership will consider results of updated methods, techniques, and studies and revisit existing estimated loads due to climate change to determine if any updates to those 2035 load estimates are needed.

6.8   Final planning target adjustments for 2025

Table 6-5: Final jurisdiction-basin planning targets for the 2017 Midpoint Assessment.

StateBasin	2018 Planning Targets approved by PSC		2019 Planning Targets with Exchanges and Sediment			2020 Climate Adjustments		2020 Planning Targets with Climate reductions	
	Nitrogen	Phosphorus	Nitrogen	Phosphorus	Sediment	Nitrogen	Phosphorus	Nitrogen	Phosphorus
DC Potomac	2.42	0.130	2.42	0.130	41.9	0.01	0.001	2.42	0.129
DE Eastern Shore	4.55	0.108	4.55	0.108	26.7	0.04	0.003	4.51	0.105
MD Eastern Shore	15.21	1.286	15.60	1.290	2903.4	0.37	0.032	15.23	1.258
MD Patuxent	3.21	0.301	3.21	0.300	437.7	0.11	0.019	3.09	0.281
MD Potomac	15.30	1.092	15.80	1.090	1928.0	0.21	0.033	15.59	1.057
MD Susquehanna	1.18	0.053	1.60	0.050	113.8	0.14	0.007	1.46	0.043
MD Western Shore	10.89	0.948	9.63	0.950	2959.9	0.31	0.020	9.32	0.929
NY Susquehanna	11.53	0.587	11.53	0.587	532.7	0.40	0.044	11.13	0.543
PA Eastern Shore	0.45	0.025	0.46	0.022	27.4	0.05	0.005	0.41	0.017
PA Potomac	6.11	0.357	6.14	0.338	295.5	0.04	0.008	6.11	0.330
PA Susquehanna	66.59	2.661	66.87	2.544	1838.2	1.72	0.082	65.14	2.462
PA Western Shore	0.02	0.001	0.02	0.001	0.3	0.00	0.000	0.02	0.001
VA Eastern Shore	1.43	0.164	1.83	0.152	473.3	0.01	0.000	1.82	0.152
VA James	25.92	2.731	21.81	2.241	2015.2	0.30	0.143	21.51	2.097
VA Potomac	16.00	1.892	16.51	1.823	1929.7	0.56	0.073	15.95	1.750
VA Rappahannock	6.85	0.849	7.09	0.819	1505.1	0.54	0.102	6.54	0.717
VA York	5.52	0.556	5.71	0.548	949.1	0.17	0.018	5.54	0.530
WV James	0.04	0.005	0.05	0.006	13.0	0.00	0.000	0.05	0.006
WV Potomac	8.18	0.427	8.18	0.427	595.9	0.00	0.008	8.18	0.418

Table 6-5 contains the jurisdiction-basin planning targets for the 2017 Midpoint Assessment. The 2018 planning targets approved by the PSC were modified through exchanges documented in the phase III WIPs. Climate adjustments were made as detailed in this document to lower the planning targets for use starting with the 2022-2023 milestones.

7   References

Abatzoglou, J.T. and T.J. Brown 2011. A comparison of statistical downscaling methods suited for wildfire applications. International Journal of Climatology 32: 772-780.

Arheimer, B., J. Andréasson, S. Fogelberg, H. Johnsson, C. B. Pers, K. Persson. 2005. Climate Change Impact on Water Quality: Model Results from Southern Sweden. Ambio 34 (7): 559-566.

Alamdari, N., D.J. Sample, P. Steinberg, A.C. Ross, Z.M. Easton. 2017. Assessing the effects of climate change on water quantity and quality in an urban watershed using a calibrated stormwater model. Water 9 (7): 464.

Bash, J. O., Cooter, E. J., Dennis, R. W., Walker, J. T., & Pleim, J. E. (2013). Evaluation of a regional air-quality model with bi-directional NH3 exchange coupled to an agro-ecosystem model. Biogeosciences, 10, 1635-1645. https://doi.org/10.5194/bg-10-1635-2013

Boesch, D.F., W.C. Boicourt, R.I. Cullather, T. Ezer, G.E. Galloway, Jr., Z.P. Johnson, K.H. Kilbourne, M.L. Kirwan, R.E. Kopp, S. Land, M. Li, W. Nardin, C.K. Sommerfield, W.V. Sweet. 2018. Sea-level Rise: Projections for Maryland 2018, 27 pp. University of Maryland Center for Environmental Science, Cambridge, MD.

Boon, J.D. and M. Mitchell 2015. Nonlinear Change in Sea Level Observed at North American Tide Stations. Journal of Coastal Research, 31(6):1295-1305.

Bosch, N.S., Evans, M.A., Scavia, D. and Allan, J.D., 2014. Interacting effects of climate change and agricultural BMPs on nutrient runoff entering Lake Erie. Journal of Great Lakes Research, 40(3), pp.581-589.

Brown, D. G., C. Polsky, P. Bolstad, S. D. Brody, D. Hulse, R. Kroh, T. R. Loveland, and A. Thomson, 2014: Ch. 13: Land Use and Land Cover Change. Climate Change Impacts in the United States: The Third National Climate Assessment, J. M. Melillo, Terese (T.C.) Richmond, and G. W. Yohe, Eds., U.S. Global Change Research Program, 318-332. doi:10.7930/J05Q4T1Q. http://nca2014.globalchange.gov/report/sectors/land-use-and-land-cover-change (accessed 6/14/2019)

Bryan, J. 2014. Effects of Sea Level Rise on Tidal Marshes. Master's thesis, University of Maryland, College Park.

Butcher, J.B., T.E. Johnson, D. Nover, and S. Sarkar. 2014 Incorporating the effects of increased atmospheric CO2 in watershed model projections of climate change impacts. Journal of hydrology 513:322-334, http://dx.doi.org/10.1016/j.jhydrol.2014.03.073

Campbell, P.C., Bash, J.O., Nolte, C.G., Spero, T.L., Cooter, E.J., Hinson, K., Linker, L.C., 2019. Projections of Atmospheric Nitrogen Deposition to the Chesapeake Bay Watershed. Journal of Geophysical Research: Biogeosciences, In Review.

Cerco, C.F. and M.R. Noel, 2019. The 2017 Chesapeake Bay Water Quality and Sediment Transport Model: A Report to the US Environmental Protection Agency Chesapeake Bay Program May 2019 Annapolis, 108 pp.

Chanat, J.G and G. Yang, 2018. Exploring Drivers of Regional Water-Quality Change Using Differential Spatially Referenced Regression—A Pilot Study in the Chesapeake Bay Watershed. Water Resources Research. 54:10, October 2018. https://doi.org/10.1029/2017WR022403.

Chesapeake Bay Program, 2016. Climate Resiliency Workgroup. Recommendations on Incorporating Climate-Related Data Inputs and Assessments: Selection of Sea Level Rise Scenarios and Tidal Marsh Change Models. August 2016. https://www.chesapeakebay.net/channel_files/24216/crwg_mid_point_assessment_climate_data_recommendations_final_080516.pdf Last accessed 4/2019.

Chesapeake Bay Program, 2017. Chesapeake Assessment and Scenario Tool (CAST) Version 2017d. Chesapeake Bay Program Office, http://cast.chesapeakebay.net/ Last accessed 4/2019.

Chesapeake Executive Council, 2014. Chesapeake Bay Watershed Agreement. June 16, 2014.

Cressie, N., C.A. Calder, J.S. Clark, J.M. Ver Hoef, C.K. Wikle. 2009. Accounting for uncertainty in ecological analysis: the strengths and limitations of hierarchical statistical modeling. Ecological Applications 19: 553–570.

De Gouw, J.A., Parrish, D.D., Frost, G.J., & Trainer, M. (2014). Reduced emissions of CO_2, NOx, and SO_2 from U.S. power pants owing to a switch from coal to natural gas with combined cycle technology, Earth's Future, 2, 75-82. https://doi.org/10.1002/2013EF000196

Deryng, D., Elliott, J., Folberth, C., Müller, C., Pugh, T. A. M., Boote, K. J., et al. (2016). Regional disparities in the beneficial effects of rising CO_2 concentrations on crop water productivity. Nat. Clim. Change 6, 786–790. doi: 10.1038/nclimate2995

DiPasquale, N., 2014. EPA-CBPO Response to STAC report re: climate change April 22, 2014. US EPA Chesapeake Bay Program Office. http://www.chesapeake.org/pubs/319_DiPasquale2014.pdf last accessed 4/2019.

Dupigny-Giroux, L.A., E.L. Mecray, M.D. Lemcke-Stampone, G.A. Hodgkins, E.E. Lentz, K.E. Mills, E.D. Lane, R. Miller, D.Y. Hollinger, W.D. Solecki, G.A. Wellenius, P.E. Sheffield, A.B. MacDonald, and C. Caldwell, 2018: Northeast. In Impacts, Risks, and Adaptation in the United States: Fourth National Climate Assessment, Volume II [Reidmiller, D.R., C.W. Avery, D.R. Easterling, K.E. Kunkel, K.L.M. Lewis, T.K. Maycock, and B.C. Stewart (eds.)]. U.S. Global Change Research Program, Washington, DC, USA. doi : 10.7930/NCA4.2018.CH1.

Eppley, R.W., 1972. Temperature and phytoplankton growth in the sea. Fish. Bull. 70, 1063–1085.

Fischbach J.R., R.J. Lempert, E. Molina-Perez, A.A. Tariq, M.L. Finucane, F. Hoss. 2015. Managing Water Quality in the Face of Uncertainty: A Robust Decision Making Demonstration for EPA's National Water Program. Santa Monica, CA: RAND Corporation.

Gammas, Matthew; Mérel, Pierre; Ortiz-Bobea, Ariel. "Negative Impacts of Climate Change on Cereal Yields: Statistical Evidence from France" Environmental Research Letters. 12 (2017): 054007

Gelman, A., J. Hill. 2007. Data analysis using regression and multilevel/hierarchical models. Cambridge University Press, New York.

Glick, P., J. Clough, and B. Nunley. 2008. Sea-Level Rise and Coastal Habitats in the Chesapeake Bay Region. National Wildlife Federation. https://www.nwf.org/~/media/PDFs/Global-Warming/Reports/SeaLevelRiseandCoastalHabitats_ChesapeakeRegion.ashx .

Gowda, P., J.L. Steiner, C. Olson, M. Boggess, T. Farrigan, and M.A. Grusak, 2018: Agriculture and Rural Communities. In Impacts, Risks, and Adaptation in the United States: Fourth National Climate Assessment, Volume II [Reidmiller, D.R., C.W. Avery, D.R. Easterling, K.E. Kunkel, K.L.M. Lewis, T.K. Maycock, and B.C. Stewart (eds.)]. U.S. Global Change Research Program, Washington, DC, USA, pp. 391–437. doi: 10.7930/NCA4.2018.CH10 (accessed 6/21/2019)

Grimm, N., Chapin, F., Bierwagen, B., Gonzalez, P., Groffman, P., Luo, Y., Melton, F., Nadelhoffer, K., Pairis, A., Raymond, P., Schimel, J., Williamson, C. 2013. The impacts of climate change on ecosystem structure and function. Frontiers in Ecology and the Environment. 2013; 11(9): 474–482, doi:10.1890/120282

Grimm, J.W., and J.A. Lynch. 2000. Enhanced wet deposition estimates for the Chesapeake Bay watershed using modeled precipitation inputs. DNR Chesapeake Bay and Tidewater Programs CBWP-MANTA-AD-99-2.

Grimm, J.W., and J.A. Lynch. 2005. Improved daily precipitation nitrate and ammonium concentration models for the Chesapeake Bay Watershed. Environmental Pollution 135(2005):445–455.

Grimm, J.W., 2017. Extension of Ammonium and Nitrate Wet-Fall Deposition Models for the Chesapeake Bay Watershed. Report prepared for United States Environmental Protection Agency, Chesapeake Bay Program and the Pennsylvania Department of Environmental Protection, 63 pp.

Hatfield, J., G. Takle, R. Grotjahn, P. Holden, R. C. Izaurralde, T. Mader, E. Marshall, and D. Liverman, 2014: Ch. 6: Agriculture. Climate Change Impacts in the United States: The Third National Climate Assessment, J. M. Melillo, Terese (T.C.) Richmond, and G. W. Yohe, Eds.,

U.S. Global Change Research Program, 150-174. doi:10.7930/J02Z13FR.
http://nca2014.globalchange.gov/report/sectors/agriculture (accessed 6/21/2019)

Hong, B. and J. Shen 2012. Responses of estuarine salinity and transport processes to potential future sea-level rise in the Chesapeake Bay. Estuarine, Coastal and Shelf Science 104-105: 33-45

IPCC, 2013: Summary for Policymakers. In: Climate Change 2013: The Physical Science Basis. Contribution of Working Group I to the Fifth Assessment Report of the Intergovernmental Panel on Climate Change [Stocker, T.F., D. Qin, G.-K. Plattner, M. Tignor, S.K. Allen, J. Boschung, A. Nauels, Y. Xia, V. Bex and P.M. Midgley (eds.)]. Cambridge University Press, Cambridge, United Kingdom and New York, NY, USA.

Irby, I.D., A.M. Marjorie Friedrichs, D. Fei, and K.E. Hinson 2018. The competing impacts of climate change and nutrient reductions on dissolved oxygen in Chesapeake Bay. Biogeosciences, 15, 2649–2668.

Johnson, Z., M. Bennett, L. Linker, S. Julius, R. Najjar, M. Mitchell, D. Montali, R. Dixon. 2016. The Development of Climate Projections for Use in Chesapeake Bay Program Assessments. STAC Publication Number 16-006, Edgewater, MD. 52 pp. http://www.chesapeake.org/pubs/360_Johnson2016.pdf last accessed 4/2019.

Konikow, L. F., 2015: Long-term groundwater depletion in the United States. Groundwater, 53 (1), 2–9. doi:10.1111/gwat.12306

Kopp R.E., R.M. DeConto, D.A. Bader, C.C. Hay, R.M. Horton, S. Kulp, M. Oppenheimer, D. Pollard, and B.H. Strauss 2014. Evolving Understanding of Antarctic Ice-Sheet Physics and Ambiguity in Probabilistic Sea-Level Projections. Earth's Future 2, 383-406

Kutta, E. and Hubbart, J.A., 2019. Observed climatic changes in West Virginia and opportunities for agriculture. Regional Environmental Change, 19(4), pp.1087-1099

Lall, U., T. Johnson, P. Colohan, A. Aghakouchak, C. Brown, G. McCabe, R. Pulwarty, and A. Sankarasubramanian, 2018: Water. In Impacts, Risks, and Adaptation in the United States: Fourth National Climate Assessment, Volume II [Reidmiller, D.R., C.W. Avery, D.R. Easterling, K.E. Kunkel, K.L.M. Lewis, T.K. Maycock, and B.C. Stewart (eds.)]. U.S. Global Change Research Program, Washington, DC, USA, pp. 145–173. doi: 10.7930/NCA4.2018.CH3

Li, Y., Schichtel, B. A., Walker, J. T., Schwede, D. B., Chen, X., Lehmann, C. M. B., et al. (2016b). Increasing importance of deposition of reduced nitrogen in the United States. Proc. Natl. Acad. Sci. U.S.A., 113 (21), 5874-5879. https://doi.org/10.1073/pnas.1525736113

Linker, L.C., G.W. Shenk, P. Wang, K.J. Hopkins, S. Pokharel. 2002. A Short History of Chesapeake Bay Modeling and the Next Generation of Watershed and Estuarine Models

Proceedings of the Water Environment Federation, Watershed 2002 , pp. 569-582(14) Water Environment Federation. Alexandria, VA.

Lomas, M. W., Gilbert, P. M., Shiah, F. K., and Smith, E. M.: Microbial processes and temperature in Chesapeake Bay: current relationships and potential impacts of regional warming, Glo. Change Biol., 8, 51–70, 2002.

Moshtaghi, B., M.H. Niksokhan, F. Ghazban, S. Dalilsafaee. 2018. Assessing the impacts of climate change on the quantity and quality of agricultural runoff (case study: Golgol River Basin). Irrigation and Drainage 67 (Suppl. 2): 17-28.

Munson, K.M., R.M. Vogel, J.L. Durant. 2018. Climate sensitivity of phosphorus loadings to an urban stream. Journal of the American Water Resources Association 54 (2): 527-542.

Office of the President. 2009. Executive Order: Chesapeake Bay Protection and Restoration. Office of the President, Washington, DC

Plummer, M. 2015. rjags: Bayesian Graphical Models using MCMC. R package version 3-15.

Plummer, M. 2003. JAGS: A program for analysis of Bayesian graphical models using Gibbs sampling. Proc. 3rd Int. Work. Distrib. Stat. Comput. 124: 1–8.

Pyke, C., 2012. STAC Letter to the Chesapeake Bay Program Management Board re: Adapting to Climate Change in the Chesapeake Bay, June, 2012. STAC. http://www.chesapeake.org/pubs/288_Pyke2012.pdf last accessed 4/2019.

Pyke, C., M. Bennett, R. Najjar, M. Raub, K. Sellner, S. Stiles, D. Wardrop. (2012). Adapting to Climate Change in the Chesapeake Bay: A STAC workshop to monitor progress in addressing climate change across the Chesapeake Bay Watershed (CRC# STAC 12-01). STAC. http://www.chesapeake.org/pubs/287_Pyke2012.pdf last accessed 4/2019.

Pyke, C.R., R.G. Najjar, M.B. Adams, D. Breitburg, M. Kemp, C. Hershner, R. Howarth, M. Mulholland, M. Paolisso, D. Secor, K. Sellner, D. Wardrop, and R. Wood. 2008. Climate Change and the Chesapeake Bay: State-of-the-Science Review and Recommendations. Chesapeake Bay Program Science and Technical Advisory Committee, Annapolis, MD. http://www.chesapeake.org/pubs/Pubs/climchangereport.pdf last accessed 4/2019

Pyke C., M.P. Warren, T. Johnson, J.Jr. LaGro, J. Scharfenberg, P. Groth, R. Freed, W. Schroeer, E. Main. 2011. Assessment of low impact development for managing stormwater with changing precipitation due to climate change. Landscape and Urban Planning 103: 166-173.

Qian, S.S., Z. Shen. 2007. Ecological applications of multilevel analysis of variance. Ecology 88: 2489–2495.

R Core Team, 2015. R: A language and environment for statistical computing.

Rice, K.C., Douglas L. Moyer, and Aaron L. Mills, 2017. Riverine discharges to Chesapeake Bay: Analysis of long-term (1927 - 2014) records and implications for future flows in the Chesapeake Bay basin *JEM* 204 (2017) 246-254

Saba, Vincent S., Stephen M Griffies, Whit G Anderson, Michael Winton, M A Alexander, Thomas L Delworth, J A Hare, Matthew J Harrison, Anthony Rosati, Gabriel A Vecchi, and Rong Zhang 2016. Enhanced warming of the northwest Atlantic Ocean under climate change. Journal of Geophysical Research, 121(1), DOI:10.1002/2015JC011346.

Sanford, W. E., Pope J. P., Selnick, D. L., and Stumvoll, R. F., 2012, Simulation of groundwater flow in the shallow aquifer system of the Delmarva Peninsula, Maryland and Delaware: USGS Open-File Report 2012-1140, 58 p.

Scott, D., J. Harvey, R. Alexander, G. Schwarz. 2007. Dominance of organic nitrogen from headwater streams to large rivers across the conterminous United States. Global Biogeochemical Cycles 21 (1).

Scully M.E., C. Friedrichs and J. Brubaker 2005. Control of estuarine stratification and mixing by wind-induced straining of the estuarine density field. Estuaries 28: 321-326.

Scully M.E. 2010. The importance of climate variability to wind-driven modulation of hypoxia in Chesapeake Bay. Journal of Physical Oceanography 40: 1435-1440.

Sponseller, R.A., J. Temnerud, K. Bishop, H. Laudon. 2014. Patterns and drivers of riverine nitrogen (N) across alpine, subarctic, and boreal Sweden. Biogeochemistry 120: 105-120.

St-Laurent, P., M.A.M. Friedrichs, M. Li, W. Ni, 2019. Impacts of sea level rise on hypoxia in the Chesapeake Bay: A model intercomparison, Report to Virginia Tech and the Chesapeake Bay Program, October 2019, 34 pp.

STAC Report to the Executive Council 2011. http://www.chesapeake.org/pubs/162_E.C.Krome1990.pdf last accessed 4/2019.

Staver, K., P. Kleinman, S. Ator, A. Buda, Q. Ketterings, J.T. Sims, and J. Meisinger. 2014. A review of agricultural P-dynamics in the Chesapeake Bay Watershed Model. STAC Publication Number 14-005, Edgewater, MD. 20 pp.

Stow, C.A., E.C. Lamon, S.S. Qian, P.A. Soranno, K.H. Reckhow. 2009. Bayesian Hierarchical/Multilevel Models for Inference and Prediction Using Cross-System Lake Data, in: Miao, S., Carstenn, S., Nungesser, M. (Eds.), Real World Ecology: Large-Scale and Long-Term Case Studies and Methods. Springer New York, New York, pp. 111–136.

Thomas, A.C., A.J. Pershing, K.D. Friedland, J.A. Nye, K.E. Mills, M.A. Alexander‖, N.R. Record, R. Weatherbee and M.E. Henderson 2017 Seasonal trends and phenology shifts in sea surface

temperature on the North American northeastern continental shelf. Elem Sci Anth, 5: 48, DOI: https://doi.org/10.1525/elementa.240

Tong, S.T.Y., A.J. Lie. 2006. Modelling the hydrologic effects of land-use and climate changes. International Journal of Risk Assessment and Management 6: 344-368.

Tian, R., Chen, C., Qi, J., Ji, R., Beardsley, R. C., and Davis, C. 2014. Model study of nutrient and phytoplankton dynamics in the Gulf of Maine: patterns and drivers for seasonal and interannual variability. ICES Journal of Marine Science, doi: 10.1093/icesjms/fsu090.

Wainger, L., 2016. STAC Letter to CBP re: Climate Change Workshop Report. STAC. http://www.chesapeake.org/pubs/361_Wainger2016.pdf last accessed 4/2019.

Wang, P., H. Wang, L. Linker, R. Tian 2016a. Effects of cross-channel bathymetry and wind direction on destratification and hypoxia reduction in the Chesapeake Bay. Estuarine, Coastal and Shelf Science 178: 168-188.

Wang, P., H. Wang, L. Linker, K. Hinson 2016b. Influence of Wind Strength and Duration on Relative Hypoxia Reductions by Opposite Wind Directions in an Estuary with an Asymmetric Channel. Journal of Marine Science and Engineering 4, 62; doi:10.3390/jmse4030062.STAC, 2011.

Woznicki, Sean A. and A. Pouyan Nejadhashemi, 2011. Sensitivity Analysis of Best Management Practices Under Climate Change Scenarios. Journal of the American Water Resources Association(JAWRA) 48(1): 90–112.DOI: 10.1111/j.1752-1688.2011.00598.x

WPC (Warren Pinnacle Consulting). 2018. SLAMM: Sea Level Affecting Marshes Model. Warren Pinnacle Consulting Inc., Waitsfield, VT. http://warrenpinnacle.com/prof/SLAMM/.

U.S. Department of Agriculture-National Agricultural Statistics Service. Census. 2012 Census of Agriculture. Volume 1, Geographic Area Series (CD ROM). Washington, D.C.: USDA. 2014.

U.S. EPA (U.S. Environmental Protection Agency). 2003. Technical Support Document for Identification of Chesapeake Bay Designated Uses and Attainability. EPA 903-R-03-004. October 2003. 319pp. https://www.chesapeakebay.net/content/publications/cbp_13218.pdf

U.S. EPA (U.S. Environmental Protection Agency). 2004. Technical Support Document for Identification of Chesapeake Bay Designated Uses and Attainability. 2004 addendum. EPA 903-R-03-004. October 2004. 75pp. https://www.chesapeakebay.net/content/publications/cbp_13270.pdf

U.S. EPA (U.S. Environmental Protection Agency). 2010a. Chesapeake Bay Total Maximum Daily Load for Nitrogen, Phosphorus, and Sediment. USEPA, Philadelphia, PA

<http://www.epa.gov/chesapeake-bay-tmdl/chesapeake-bay-tmdl-document>. Accessed 1/8/2016

U.S. Environmental Protection Agency. 2010b. Ambient Water Quality Criteria for Dissolved Oxygen, Water Clarity and Chlorophyll a for the Chesapeake Bay and Its Tidal Tributaries: 2010 Technical Support for Criteria Assessment Protocols Addendum. May 2010. EPA 903-R-10-002. CBP/TRS 301-10. U.S. Environmental Protection Agency, Region 3 Chesapeake Bay Program Office, Annapolis, MD. http://www.chesapeakebay.net/content/publications/cbp_51366.pdf

U.S. EPA (Environmental Protection Agency). (2013) Watershed modeling to assess the sensitivity of streamflow, nutrient, and sediment loads to potential climate change and urban development in 20 U.S. watersheds. National Center for Environmental Assessment, Washington, DC; EPA/600/R-12/058F. Available from the National Technical Information Service, Alexandria, VA, and online at http://www.epa.gov/ncea

U.S. EPA. 2016a. Climate change indicators in the United States. www.epa.gov/climate-indicators; https://www.epa.gov/sites/production/files/2016-08/documents/climate_indicators_2016.pdf

U.S. EPA. 2016b. "Climate Change Indicators: Sea Surface Temperature." Accessed August 16, 2019 https://www.epa.gov/climate-indicators/climate-change-indicators-sea-surface-temperature.

U.S. EPA. 2016c. Emissions Inventory for Air Quality Modeling Technical Support Document: Heavy-Duty Vehicle Greenhouse Gas Phase 2 Final Rule, EPA-420-R-008, August 2016. https://nepis.epa.gov/Exe/ZyPDF.cgi/P100PKEE.PDF?Dockey=P100PKEE.PDF

Xiang Z. 2017. Hydrologic response of a suburban watershed to climate models. Master Thesis, University of Maryland, College Park, MD.